

**MINISTRY OF HIGHER EDUCATION  
AND SCIENTIFIC RESEARCH  
UNIVERSITY OF BAGHDAD  
COLLEGE OF SCIENCE**



**MINERALOGY, PETROGRAPHY AND  
GEOCHEMISTRY OF IRON-RICH SEDIMENTS  
IN BENA VI AREA-NORTHERN IRAQ**

**A THESIS  
SUBMITTED TO THE COLLEGE OF SCIENCE  
UNIVERSITY OF BAGHDAD  
IN PARTIAL FULFILLMENT OF THE REQUIRMENT  
FOR THE DEGREE OF MASTER OF SCIENCE IN  
GEOLOGY**

**BY  
ALI TAHA YASSIN  
B.Sc. IN GEOLOGY (1995)**

**SUPERVISED BY  
Asst. Prof. MUDHAFAR M. MAHMOUD, PH.D.**

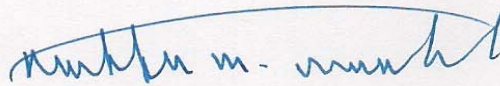
**2009**

**1430H**

## The supervisor certification

I certify that this thesis ( **MINERALOGY, PETROGRAPHY AND GEOCHEMISTRY OF IRON-RICH SEDIMENTS IN BENA VI AREA-NORTHERN IRAQ** ), was prepared under my supervision at the Department of Geology, College of Science, University of Baghdad, in partial fulfillment of the requirements for the degree of Master of Science in Geology (Petrology and Mineralogy).

**Signature:**



**Name:** Dr. *Mudhafar M. Mahmoud*

**Scientific title:** *Assistant professor*

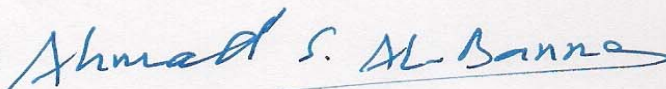
**Address:** *University of Baghdad- College of Science*

**Date:** *19/7/2009*

### **Recommendation of the head of committee of postgraduate studies in the Department of Geology**

In view of the available recommendation I forward this thesis for debate by the examining committee.

**Signature:**



**Name:** Dr. *Ahmad Shehab Al-Banna*

**Scientific title:** *professor*

**Address:** *University of Baghdad (Head of the Department of Geology)*

**Date:** *19/7/2009*

## Committee certification

We certify that we have read this thesis entitled ( **MINERALOGY, PETROGRAPHY AND GEOCHEMISTRY OF IRON-RICH SEDIMENTS IN BENA VI AREA-NORTHERN IRAQ** ), and as the examination committee examined the student in its content, and in our opinion it is adequate for award of the degree of Master of Science in Geology (Petrology and Mineralogy).

Signature: *H. R. Habib*

Name: Dr. Habib R. Habib  
Scientific title: Professor  
Address: University of Baghdad  
Date: 19/7/2009

Signature: *M. A. Basi*

Name: Dr. Muzahim A. Basi  
Scientific title: Asst. Professor  
Address: University of Wasit  
Date: 19/7/2009

Signature: *Ayten Hadi Ali*

Name: Dr. Ayten Hadi Ali  
Scientific title: Asst. Professor  
Address: University of Baghdad  
Date: 19/7/2009

Signature: *Mudhafar M. Mahmoud*

Name: Dr. Mudhafar M. Mahmoud  
Scientific title: Asst. Professor  
Address: University of Baghdad  
Date: 19/7/2009

Approved by the deanery of the College of Science

Signature: *Khalid S. Al-Mukhtar*

Name: Dr. Khalid S. Al-Mukhtar  
Scientific title: Professor  
Address: University of Baghdad (Dean of the College of Science)  
Date:

## ***Dedicated to:***

***The departed soul of my father...***

***My mother...***

***My family (my brothers and sisters)...***

***My wife...***

***And to my son (Taha) and my daughter (Mariam).***

## Acknowledgments

First and foremost, I would like to gratefully acknowledge the help, support and encouragement of my advisor Dr. Mudhafar M. Mahmoud. I am extremely thankful for his endless effort and with completing and revising the thesis to provide invaluable assistance and inspired ideas. It was my luck to work with him.

I would like to thank the Council of the College of Science and the Department of Geology at University of Baghdad for all the supports to prepare this study.

I am greatly indebted to the State Company of Geological Survey and Mining for offering me the opportunity to study for the master level with special thanks to the D.G. Dr. Khaldoun S. Al-Bassam .

I feel I should like to express my gratitude to Dr. Ali K. K. Nassir for his criticism and aid during this research, and also to Dr. Ali Ghiara, Dr. Ayten H. Ali, Dr. Ahmed Al-Shakiri and Dr. Salih M. Awadh for their comments and help during laboratory work and references.

I should extend my gratefulness to Mr. Gaudon for his guidance, motivations and endless supports during the lab. work at Ecole de Mines (CMGD)/Ales /France and also to all friends, research assistants, technicians and all staffs at this research center for their help and friendship.

Special thanks has to be directed to Dr. Yawooz Kettanah/ university of Dalhousi/Canada for his scientific advices during this project, and to Dr. Eike Gierth / Clausthal university of Technology for his help in Ore Microscopy study by oil immersion, and also to Dr. David Alderton /London university for the invaluable discussions. Many thanks to Mr. Mazin M. Mustafa for assistance to perform the chemical analyses for some samples in SNIM/Mauritania and to Mr. Varoujan K. Sissakian, Dr. Saffa F. Fouad, Dr. Rafea Z. Jassim, Dr. Adil Al-Kaaby, Dr. Mudher Q., Dr. Thair Jirjees Benni, Mrs. Wafaa Philip, Mrs. Loma A.A., and all my colleagues at the State Company of Geological Survey for their various support during my study.

At the end, thanks to my family (especially my big brother Mr. Hassan Taha Yassin) for their encouragement, support and patience.

## Abstract

Benavi Iron- Rich Sediments (IRS) is located about (20) km (N-NW) of Amadia district in Duhok Governorate - Northern Iraq. It occurs as an elongated E-W body within Jurassic-Cretaceous sequences and extends about (2) km. The true thickness of IRS outcrop ranges (2.5-12.8m) enclosed within highly fractured carbonate beds. Forty eight samples were collected from ten sections represent the whole IRS body. The sampling was systematic according to variations in color, hardness, texture and iron content.

Mineralogical study using instrumentations: XRD, SEM, EDS, TGA and FTIR showed that Benavi IRS composed of mineral assemblages: carbonates (calcite, siderite, ankerite), iron oxides/hydroxides (hematite, goethite, limonite, magnetite), sulphides (pyrite, arsenopyrite), silicates (kaolinite, chamosite, glauconite, quartz ) and apatite. Calcite is the main mineral in IRS which is mostly impure containing  $Mg^{+2}$  and  $Fe^{+2}$ . Siderite and ankerite are minor.

The main iron minerals are hematite and goethite; the former is higher at the upper part of Benavi IRS outcrop (that looks more reddish in the field), and is mostly poor in (Al) content which probably originated by dehydration of primary Al- poor goethite. Contrarily, the later is higher at the middle part (that looks more yellowish in the field). Two different goethites are coexisting; they differ in crystallization and Al content. Most Al-poor goethite (primary) probably altered to Al-poor hematite. Al-rich goethite (secondary) produced by goethitization of pyrite, siderite and chamosite under surface weathering circumstances. Kaolinite and chamosite are the main clay minerals in IRS whereas glauconite is trace. Arsenopyrite is confirmed by EDS, and it is found restricted at the base of Benavi IRS outcrop that looks dark grey in the field associated with chamosite, pyrite, phosphates and glauconite.

Petrographic study showed that IRS is related to algal-bioclastic- packstone host rocks suffered from many diagenetic processes. Iron oxides have replaced

completely or partially the calcareous structures produced deposits of unusual content. Chamosite mostly occurs around impregnation fossils by iron oxides.

Ore microscopy and BSE study showed that most ore textures of Benavi IRS formed by replacement processes which are: rim, zonal, inclusions, vein and idiomorphic. Porous texture produced by dehydration of goethite is common, oolitic texture is present as well as boxwork texture of microplaty hematite grains. Euhedral magnetite crystals are observed in many samples.

Pyrite is unevenly distributed throughout this body, which occurs in euhedral massive, and framboidal forms. The euhedral pyrite crystals are produced by evolution of framboidal pyrite texture, where the main steps of this evolution are recognized. Pseudomorph goethite and magnetite framboids formed by oxidation of pyrite framboids are also common.

Geochemical analyses showed that  $\text{Fe}_2\text{O}_3$  ranges (3.28-33.9%) with an average of (20.44%), which is considered as low-grade ironstones. Benavi IRS is characterized by high content of CaO, L.O.I,  $\text{P}_2\text{O}_5$ , MgO, Cr, V and low content of Ni, Cu, Zn, Mn,  $\text{TiO}_2$ ,  $\text{Al}_2\text{O}_3$ ,  $\text{SiO}_2$ ; in comparison with Gaara and Hussainiyat and most international ironstones.

The very strong negative correlation between CaO and  $\text{Fe}_2\text{O}_3$  attributed to the replacement of calcareous components by iron minerals suggesting epigenetic ores form by the diagenetic replacements of carbonate rocks, and the negative correlations of CaO with  $\text{SiO}_2$ ,  $\text{Al}_2\text{O}_3$ ,  $\text{P}_2\text{O}_5$ , Co, Ni and Zn revealed the high effect of diagenetic processes.

The discrimination diagrams based on ( $\text{TiO}_2$  vs.  $\text{Al}_2\text{O}_3$ ) and [Zn-Ni-Co] support the sedimentary origin corroborated by high As in pyrite, low Zn, Pb, Cu, Mn/Fe ratio and high content of Cr &  $\text{P}_2\text{O}_5$ . Furthermore, a bivariate plot of (Si vs. Al) showed that Benavi IRS is of diagenetic origin.

The discrimination diagram of  $[(\text{FeO}+\text{MnO})-\text{Fe}_2\text{O}_3-\text{SiO}_2]$  and the average of [Zn+Pb+Cu+Ni+Co] in addition to high Cr content promote to classify Benavi IRS as one of Phanerozoic ironstones.

# Contents

## Chapter one: Introduction

1-1	Preface.....	1
1-2	Location .....	2
1-3	Aims of the study.....	3
1-4	Previous works.....	3
1-5	Regional tectonic setting .....	6
1-5-1	Northern Ora Thrust Zone.....	8
1-5-2	The relationship between mineralization & Regional tectonic setting.....	8
1-6	Structure, morphology and climate of Benavi .....	10
1-7	Stratigraphy of Benavi area .....	10

## Chapter two: Research methodology

2-1	Preface.....	14
2-2	Field work.....	14
2-3	Laboratory work.....	21
2-3-1	Transmitted light microscopy.....	22
2-3-2	Reflected light microscopy (Ore Microscopy).....	22
2-3-3	X-Ray Diffractometry (XRD).....	23
2-3-4	Fourier Transform Infrared spectrometry (FTIR).....	23
2-3-5	Scanning Electron Microscopy (SEM).....	24
2-3-6	Energy Dispersive Spectrometry (EDS) .....	24
2-3-7	Thermal Gravimetric Analyses (TGA).....	25

## Chapter three: Mineralogy

3-1	Preface.....	26
3-2	X-Ray Diffraction Study (XRD).....	26
3-2-1	Carbonate minerals identification.....	31
3-2-2	Iron oxides/hydroxide identification.....	33
3-2-2-1	Hematite.....	33
3-2-2-2	Goethite.....	34
3-2-2-3	Magnetite.....	35
3-2-3	Silicate minerals identification.....	37
3-2-3-1	Chlorite (chamosite).....	37
3-2-3-2	Kaolinite.....	37
3-2-3-3	Sepiolite.....	38
3-2-3-4	Glaucanite.....	39
3-2-3-5	Quartz.....	39
3-2-4	Phosphate mineral identification.....	39
3-3	Scanning Electron Microscopy (SEM&EDS).....	40
3-4	Thermal Gravimetric Analysis (TGA).....	46

3-4-1 Thermal behavior of IRS carbonates.....	47
3-4-2 Thermal behavior of Iron oxides /hydroxides.....	47
3-4-3 Thermal behavior of silicates.....	49
3-4-4 Thermal behavior of phosphates.....	49
3-5 Fourier Transform Infrared Spectroscopy (FTIR).....	55
3-6 Discussion.....	57

## Chapter four: Petrography

4-1 Preface.....	59
4-2 Country rocks.....	62
4-3 Host rocks (IRS) classification and petrography.....	62
4-3-1 (IRS) classification.....	62
4-3-2 IRS petrography.....	63
4-4 Diagenetic processes.....	64
4-4-1 Iron oxides replacement .....	64
4-4-2 Glauconitization .....	65
4-4-3 Phosphatization .....	65
4-4-4 Chamosite formation and sideritization .....	66
4-4-5 Pyritization .....	66
4-4-6 Silicification .....	67
4-4-7 Cementation .....	68
4-4-8 Neomorphism .....	68
4-4-9 Dolomitization .....	69
4-4-10 Dedolomitization .....	69
4-4-11 Compaction .....	69
4-5 Ore petrography.....	70
4-5-1 General description.....	70
4-5-2 Ore textures.....	72
4-6 Framboids evolution.....	74
4-7 Discussion.....	76

## Chapter five: Geochemistry

5-1 Preface.....	102
5-2 Precision and accuracy of analysis.....	106
5-2-1 Precision.....	106
5-2-2 Accuracy.....	106
5-3 Correlation coefficient.....	107
5-4 Benavi IRS Geochemistry.....	107
5-4-1 Geochemistry of major elements.....	107
5-4-1-1 SiO <sub>2</sub> .....	107
5-4-1-2 Fe <sub>2</sub> O <sub>3</sub> & FeO.....	108
5-4-1-3 Al <sub>2</sub> O <sub>3</sub> .....	111
5-4-1-4 TiO <sub>2</sub> .....	112
5-4-1-5 CaO.....	112

5-4-1-6 MgO.....	113
5-4-1-7 L.O.I.....	114
5-4-1-8 Na <sub>2</sub> O.....	115
5-4-1-9 K <sub>2</sub> O.....	115
5-4-1-10 P <sub>2</sub> O <sub>5</sub> .....	116
5-4-2 Geochemistry of Trace elements.....	117
5-4-2-1 S .....	117
5-4-2-2 Mn .....	118
5-4-2-3 Zn.....	119
5-4-2-4 Co.....	121
5-4-2-5 Ni.....	121
5-4-2-6 Cr.....	122
5-4-2-7 As .....	124
5-4-2-8 V .....	126
5-4-3 Mn/Fe .....	126
5-5 Factor analysis.....	128
5-6 Cluster analysis.....	130
5-7 Geochemical criteria in classification & genesis.....	131
5-8 Discussion.....	135

## Chapter Six: Conclusions and recommendations

6-1 Conclusions.....	137
6-2 Recommendations.....	140

<b>References</b> .....	141
-------------------------	-----

## Appendices

Appendix1 :	Certificate.
Appendix2 :	Details of studied sections & field description for all samples.
Appendix3 :	Clarifying the procedure of peak area calculations for each mineral.
Appendix4 :	BSE images and EDS analyses of (15) samples (clarified in 22 figures).
Appendix5 :	A- Bulk chemical analyses of major (wt%) and trace elements ( ppm ) of Benavi IRS, (GEOSURV). B- Bulk chemical analyses of some of trace elements in (ppm) and Mn /Fe ratios, of Benavi IRS, (GEOSURV). C-Bulk chemical analyses of major oxides (wt%) and trace elements ( ppm) with Mn/Fe ratios of Benavi IRS, ( SNIM).
Appendix6 :	A-Precision at confidence level of 95% &63%, B- Accuracy.
Appendix7 :	Correlation coefficients of major & trace elements of Benavi IRS .
Appendix8 :	Chemical analyses of many local & international ironstones ( for comparison).
Appendix9 :	A-Factor analyses based on chemical analyses (28 samples). B- R-Mode cluster analysis of Benavi IRS samples.

## List of Figures

Page

Figure (1-1): Location map of the Benavi IRS.....	2
Figure (1.2): Tectonic map of Iraq showing the location of Benavi IRS. ....	7
Figure (1-3): Mineralogical map of Iraq showing mineral occurrences of Northern Ora Thrust Zone and Benavi IRS .....	9
Figure (2-1): Sampling according to color.... & iron content.....	15
Figure (2-2): Topographic map & Satellite image show the continuity of IRS.....	16
Figure (2-3): One of the best outcrops of Benavi IRS.....	17
Figure (2-4): Parallal , cross & vertical veinlets filled with iron oxides .....	18
Figure (2-5): The hematite grains at the surface of Benavi IRS .....	19
Figure (2-6): The abounding vegetation & high covered features in IRS area.....	19
Figure (2-7): The general direction of beds in the study area .....	20
Figure (2-8): FTIR instrument type IFS 66 / 2004.....	23
Figure (2-9): SEM Type/ FP 2032-11 / Q U A NTA 200 F E G .....	24
Figure (2-10): TGA analyzer type Pyris series 1 TGA .....	25
Figure (3-1): Relative abundance of minerals of ( 4 )of the studied sections ..	27
Figure (3-2): XRD patterns of BN1 section samples as: A-bulk sample not treated, B-after acetic acid treatment and C- after heat treatment.....	28
Figure (3-3): XRD patterns of BN5 section samples as: A-bulk samples not treated, B-after acetic acid treatment and C- after heat treatment.....	29
Figure (3-4): XRD patterns for some of treated samples.....	30
Figure (3-5): The shift between real & theoretical peaks of (104) of calcite.....	32
Figure (3-6): (FWHM) of (110) and (104) peaks in hematite .....	34
Figure (3-7): A: d-space( theoretical and real) of (111) goethite ,B:XRD pattern of a sample picked from brown vein shown in Figure (2-4-C).....	37
Figure (3-8): BSE image and elemental map which confirm the presence of arsenopyrite in the base of IRS, sample no. (BN8/2).....	41
Figure (3-9): Elemental map, BSE image and EDS analysis of site 3 of the sample BN1/4 show ankerite, pyrite, chamosite and quartz.....	42
Figure (3-10): TGA curves for some of treated & untreated samples .....	50
Figure (3-11): FTIR spectra of samples of the sections: A-BN1&B-BN5 .....	56
Figure (4-1): 3-D Pie charts based upon point counting results .....	61
Figure (4-2): BSE images for euhedral , framboids & massive pyrite .....	75
Figure (4-3): BSE images clarify the textural evolution of framboids pyrite to euhedral pyrite morphology in IRS samples ).....	75
Figure (5-1): Bar charts of the average of major & trace elements (geosurv).....	103
Figure (5-2): Vertical variations of major and trace elements along BN1, BN2, BN5 and BN6 sections of Benavi IRS ,(geosurv).....	104
Figure (5-3): SEM view of mineralized bacteria in Benavi IRS.....	109
Figure (5-4): Histograms illustrating the distribution style of major elements of Benavi IRS :A-SiO <sub>2</sub> % , B-Fe <sub>2</sub> O <sub>3</sub> % , C-Al <sub>2</sub> O <sub>3</sub> % , D-TiO <sub>2</sub> % , E-CaO % , F-MgO% , G-L.O.I % , H-Na <sub>2</sub> O % , I-K <sub>2</sub> O% and J-P <sub>2</sub> O <sub>5</sub> % ....	110
Figure (5-5): EDS elemental transverse shows P2O5 positively relates with iron oxides in Benavi IRS.....	117

Figure (5-6): Histograms illustrating the distribution style of Trace elements and FeO of Benavi IRS: A-FeO%, B-Log S ppm, C-Mn ppm, D-Zn ppm, E-Co ppm, F-Ni ppm, G-Cr ppm & H-V ppm.....	120
Figure (5-7): BSE image and EDS analyses showing chromium associated with clays (mostly with chamosite) in Benavi IRS .....	123
Figure (5-8): BSE images and EDS analyses showing arsenic content in : A-arsenopyrite , B-euhedral pyrite , C-massive pyrite , D-goethite (after goethitization of massive pyrite ) , E-framboidal pyrite ,F-goethite (after goethitization of framboidal pyrite ).....	125
Figure (5-9): BSE images and EDS analyses showing Venadium association with clay minerals and iron oxides/hydroxides.....	127
Figure (5-10) : (FeO+MnO)-Fe <sub>2</sub> O <sub>3</sub> -SiO <sub>2</sub> Diagram.....	131
Figure (5-11) : TiO <sub>2</sub> vs. Al <sub>2</sub> O <sub>3</sub> Diagram.....	132
Figure (5-12): Zn-Ni-Co Diagram.....	133
Figure (5-13): Si vs. Al Diagram.....	134

## List of Tables

Table (1-1): Stratigraphic succession of Benavi area (Al-Hasni ,1973).....	11
Table (2-1): Shows all studied samples with technique of study.....	21
Table (3-1): Mineralogical interpretation for all the spectra of EDS analyses .....	43
Table (3-2): Results of TGA analyses derived from TGA curves .....	52
Table (4-1): Point counting results of thin sections .....	60
Table (4-2): Textural classification of iron rich sediments .....	63

## List of Plates

Plate (4-1).....	79
Plate (4-2).....	81
Plate (4-3).....	83
Plate (4-4).....	85
Plate (4-5).....	87
Plate (4-6).....	89
Plate (4-7).....	91
Plate (4-8).....	93
Plate (4-9).....	95
Plate (4-10).....	97
Plate (4-11).....	99
Plate (4-12).....	101

# *Chapter One*

## *Introduction*

## **1-1 Preface:**

Sedimentary iron ores can broadly be considered as occurring in three major classes: bog iron ores, ironstones and banded iron formations (Vaughan and Craig, 1981).

Banded iron formations belong to Precambrian age, whereas ironstones to Phanerozoic age (Pettijhon, 1975). Phanerozoic sedimentary ironstones are usually thin sequences which were deposited in shallow marine or non-marine environments (Young and Taylor, 1989).

The mineralogy of ironstones is comparatively simple, oxides and hydroxides of iron along with siderite and chamosite make up almost all of the iron bearing species.

Pyrite may be present as fine particles or as replacement of fossil fragments, glauconite is common in associated rocks; other minerals commonly found are calcite, phosphates, kaolinite, quartz and sometimes amorphous silica (Maynard, 1983).

Practically, iron is present in all sedimentary rocks to the extent of few percent but less commonly it forms ironstones and iron formations where the iron content exceeds 15% (James, 1966). The behavior of iron and precipitation of its minerals are strongly controlled by the chemistry of the surface or diagenetic environment (Tucker, 1981).

The deposits and occurrences of iron ores in Iraq are located in the mountain folded zone of the country (Asnawa, Mishau, Benavi...) and in the platform area western desert (Gaara and Hussainiyat), (Etabi, 1982).

Benavi iron ore deposits, one of these occurrences, is an elongated E-W body hosted in ferruginous-carbonaceous breccias horizon occurring in Jurassic-Cretaceous sequences (Chaikin, 1970). Initially, this ore body was believed to be sedimentary iron ore deposit related to shallow-marine high-energy in origin (Geozavod, 1981).

**This research to our knowledge is the first academic study tackling the mineralogy, petrography and geochemistry of Benavi iron ore deposits; and the name of Benavi Iron-Rich Sediments (IRS) is adopted in this thesis instead of Benavi iron ore deposits, that we found more appropriate.**

1-2 Location:

Benavi Iron-Rich Sediments (IRS) lies about one kilometer (S-SW) of the Benavi village which is about (19-20) kilometers (N-NW) of Amadia district in Duhok governorate - northern Iraq (Fig 1-1), the limits of Benavi IRS are shown as below:

Easting	0354836 (UTM)	0356256 (UTM)
	43° 21' 48.2" (DMS)	43° 22' 45.9" (DMS)
Northing	4122880 (UTM)	4122770 (UTM)
	37° 14' 28.2" (DMS)	37° 14' 25.4" (DMS)

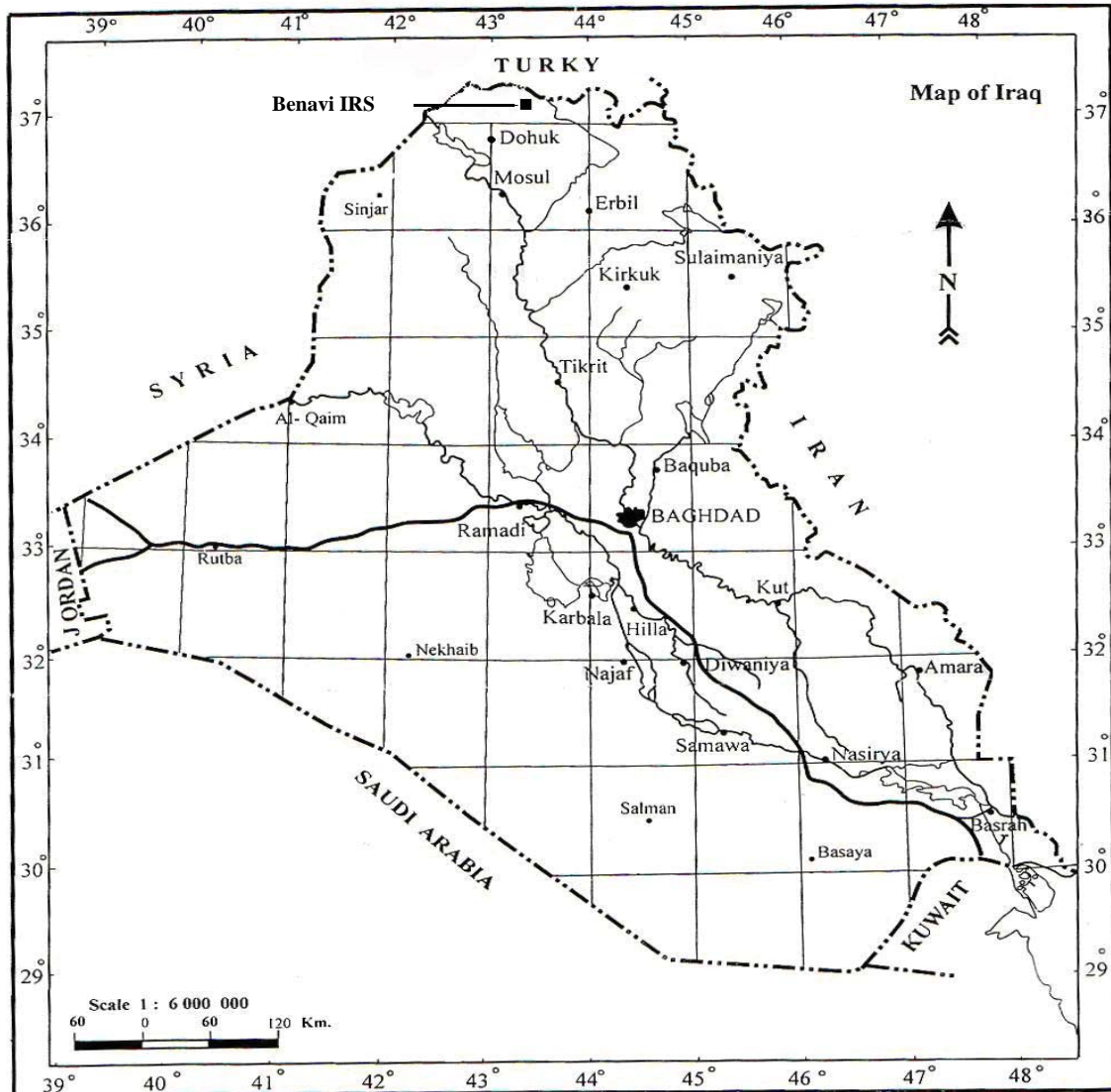


Figure (1-1): Location map of Benavi IRS.

### **1-3 Aims of the study:**

This research aimed at covering the following aspects:

- a- To carry out a mineralogical and geochemical investigation of Benavi IRS, and this would be represent a necessary step for future exploitation of this deposit.
- b- To study the relation between the different minerals, their structures, textures and other characteristics under the microscope (this may throw some light on the origin of this deposit).
- c- To illustrate the relationship between the mineralization and the host rocks as well as their mutual interactions.

### **1-4 Previous works:**

Although the north parts of Iraq represent the most interesting areas, as far as the metallic mineralization is concerned; they have been poorly studied compared with other parts of the country. The geological work started in the early fifties and was carried out by British geologists mainly concerned with the general geology of the area, stratigraphy, structure...etc; and with a general study of some ore deposits based on the examination of hand specimens and a few chemical analyses only. The next geological work in this area took place in 1961 which has been carried out by Russian geologists and was a relatively for a short period (Al-Bassam, 1972).

It has been found that applied studies covering this area were very limited, no bore-holes were drilled to investigate the extensions of Bnavi IRS; in addition, there is a lack of academic studies especially those regarding mineralization. However, occurrences of sedimentary iron ores near Benavi and Hadiena villages are mentioned by:

- 1- Wetzel (1950) showed that Hadiena formation consists of angular fragments of hematite in matrix of ferruginous limestone in the type locality south of Hadiena in Amadia district, northern Iraq.

2- Mc Carthy (1955) described Benavi IRS as a ferruginous grit horizon, (5-6 m thick) extending for more than (1 km) and occurs in the Chia Gara series of Hadiena and Benavi villages.

3- Boukhtoyarov and Yevlentyev (1962) described the horizon as hematitic sandstones (6 m) in thickness.

4-Chaikin (1970) subdivided Benavi IRS to three beds:

A-Basal portion consists of dark gray limestone with clear fragmental texture; the ferruginization is represented by dispersed goethite and ovoids of hematite were recorded especially at its uppermost part.

B- Intermediate part which consists of hematitic carbonate rocks with reddish-lilac in appearance consisting of oval or rounded fragmentas and groundmass ( about 2.4-4 m thick), ovoids of hematite are most common than the previous part.

C-The uppermost part of the ore – bearing horizon with (5-6 m) thick characterized by grey sandy limestone and lilac –brown siliceous hematite fragments.

Chaikin also showed that the ore-bearing horizons are broken by sublongitudinal fractures. He mentioned too that the chemical composition of ores obtained from the base of the horizon is as follow:

SiO<sub>2</sub> 3.67%, Fe 18.82%, Fe<sub>2</sub>O<sub>3</sub> 21.48%, FeO 4.88%, Al<sub>2</sub>O<sub>3</sub> 0.77%,  
P 0.23%, S 0.07%, CaCO<sub>3</sub> 57.97%.

According to the latter, this ore deposit is a basal horizon for Cretaceous sediments, and it is related to the Neocomian transgression.

5- Vanecek (1970) showed that the IRS is a bed of fine grained limestone with hematite, the iron content is not very high, but due to the carbonate character of the ore and iron content (about 25-30%) that should be satisfactory for industrial use . They mentioned that Benavi IRS is the biggest one in Iraq and recommended to dig trenches at distances of (500 m) apart.

6- Buday and Vanecek (1971) mentioned that the whole ferruginous horizon is about (20-30 m) thick and exposed over a distance more than (1 km).

Their microscopic results reported that this small grained breccia consists mainly of calcite grains in ferruginous limestone matrix; they also mentioned that the mineralogical composition of the iron content and its origin is not yet clear.

7- Geozavod (1981) mentioned that a series of detrital ferruginous limestones with notable iron concentrations in the form of limonite, goethite or hematite lies in the Upper Cretaceous deposit of Hadiena formation between the villages of Benavi and Hadiena which is about (25m) thick, and also mentioned that the outcrop of ferruginous sediments are located on northern slopes of the Barush ridge within Hadiena formation for a length of (2.2 km) and with (E-W) orientation.

According to Geozavod examinations in their laboratory:

a- Chemical analyses of some samples gave the following results:

Sample no.	Fe%	Al <sub>2</sub> O <sub>3</sub>	MnO	CaCO <sub>3</sub>	P	SiO <sub>2</sub>	S
1	17.80	2.49	0.03	32.70	0.43	4.68	0.17
2	26.20	2.23	0.04	27.40	0.74	4.62	0.21
3	25.80	2.42	0.03	28.20	0.75	4.94	0.12
4	24.80	2.05	0.04	30.50	0.56	4.40	0.14

b- Ore microscopic examination of these ores revealed the presence of Limonite, Magnetite, Pyrite, hydro hematite, Quartz and Carbonate minerals.

c- Benavi iron ores are poor in iron content and sedimentary in its origin, formed in shallow water marine environment of high water energy.

## 1-5 Regional tectonic setting :

Jassim and Goff (2006) have modified Buday and Jassim (1987) tectonic classification of Iraq; where Iraq was divided to:

### I-Stable shelf

#### A-Rutba – Jazira zone

- 1- Rutba subzone
- 2- Jazira subzone

#### B- Salman zone

##### Salman subzone

#### C- Mesopotamian zone

- 1- Zubair Subzone
- 2- Tigirs subzone
- 3- Euphrates subzone

### II- Unstable shelf

#### A-Foothill zone

- 1- Makhul – Hamrin subzone ( Kirkuk Embayment )
- 2- Makhul –Hamrin subzone ( Mosul high )
- 3- Makhul – Hamrin subzone ( Sinjar basin )
- 4- Butmah – chemchemical subzone ( Mosul High )
- 5- Butmah – chemchemical subzone ( structurally lower blocks )

#### B – High folded zone

- 1- High folded zone
- 2- Imbricated zone
  - 1- Balambo – Tanjero zone
  - 2- Northern ( Ora ) Thrust zone

### III- Zagros Suture Zone

- 1- Qulqula –Khwakurk zone
- 2- Penjween Walsh zone
- 3- Shalair zone

**According to this classification, Benavi IRS is located in Northern Ora Thrust Zone (Fig 1-2).**

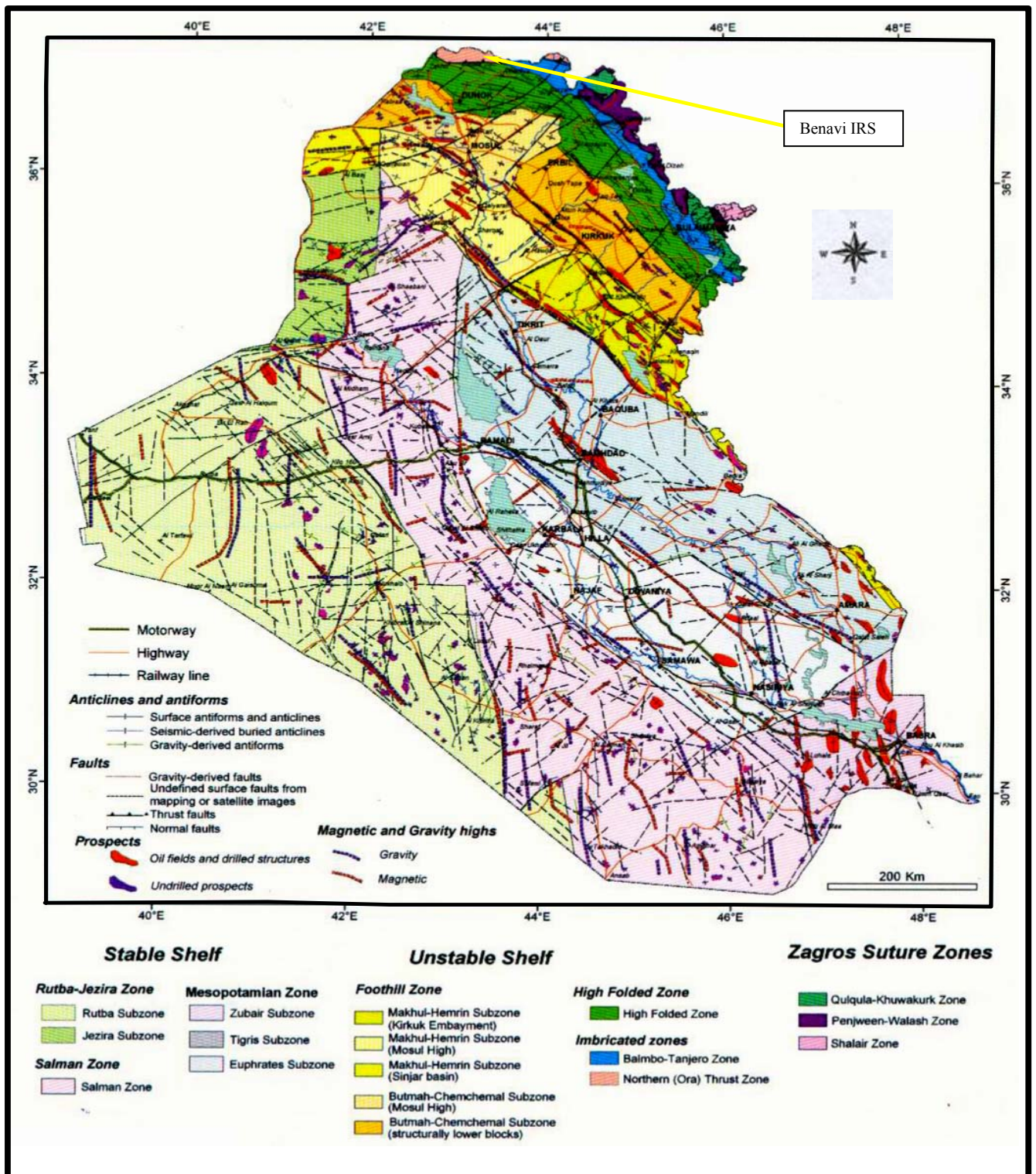


Figure (1.2): Tectonic Map of Iraq (after Jassim & Goff, 2006), showing location of Benavi IRS.

**1-5-1 Northern Ora Thrust Zone:**

The structural pattern in this zone is characterized by a relatively long, east-west trending anticlinorium with three dome shaped where the oldest Paleozoic rocks are cropping out. The southern limbs of the anticlinorium are the steeper ones. The northern flanks are less disrupted faults, the southern steeper flanks where the Jurassic – Cretaceous beds are concentrated and accompanied by conspicuous thrust fault (Buday and Jassim, 1987). Transversal faults occur too that are sinisterly strike- slip, (Mitchell, 1960).

**1-5-2 The relationship between mineralization& Regional tectonic setting:**

There is close relationship between the tectonic devisions and occurrences of mineral deposits in different regions of Iraq (AL-Bassam, 2004). Metallic mineralization is restricted to the New-Tethyan Suture Zones and is related to various phases of the plate tectonic history of the region. Low-temperature hydrothermal deposits occur in the Northern Thrust (Ora) Zone, including Pb-Zn, Ba, pyrite mineralization (e. g. the Serguza deposits). Placer and secondary deposits occur in the Balambo-Tanjero Zone and include some chromite placers and secondary Cu minerals in sedimentary clastics derived from the Qulqula –Khwakurk Zone. Magmatic Cr-Ni,Cu and Fe mineralization is associated with basic and ultrabasic igneous intrusives (e. g. Mawat Cr-Ni,Cu and Penjween Fe). Hydrothermal and strata-bound mineralization of Pb-Zn and Fe(e. g. Marapasta) and volcano-sedimentary deposits of Mn-Fe are associated with the Qulqula Group. The Arabian shelf units contain non-metalic minerals and industrial rocks. Laterite deposits occur in the western desert zone and comprise karst bauxite and ironstone,which are associated with kaolinitic clays, quartz-sand and heavy mineral bearing – sandstones, (Jassim&Goff, 2006). Northern Ora Thrust Zone is characterized by base metal occurrences in two districts, the western district NE of Zakho and the eastern district to the north of Amadia. Benavi IRS occurs in the eastern district of Northern Ora Thrust Zone, (Fig.1-3).

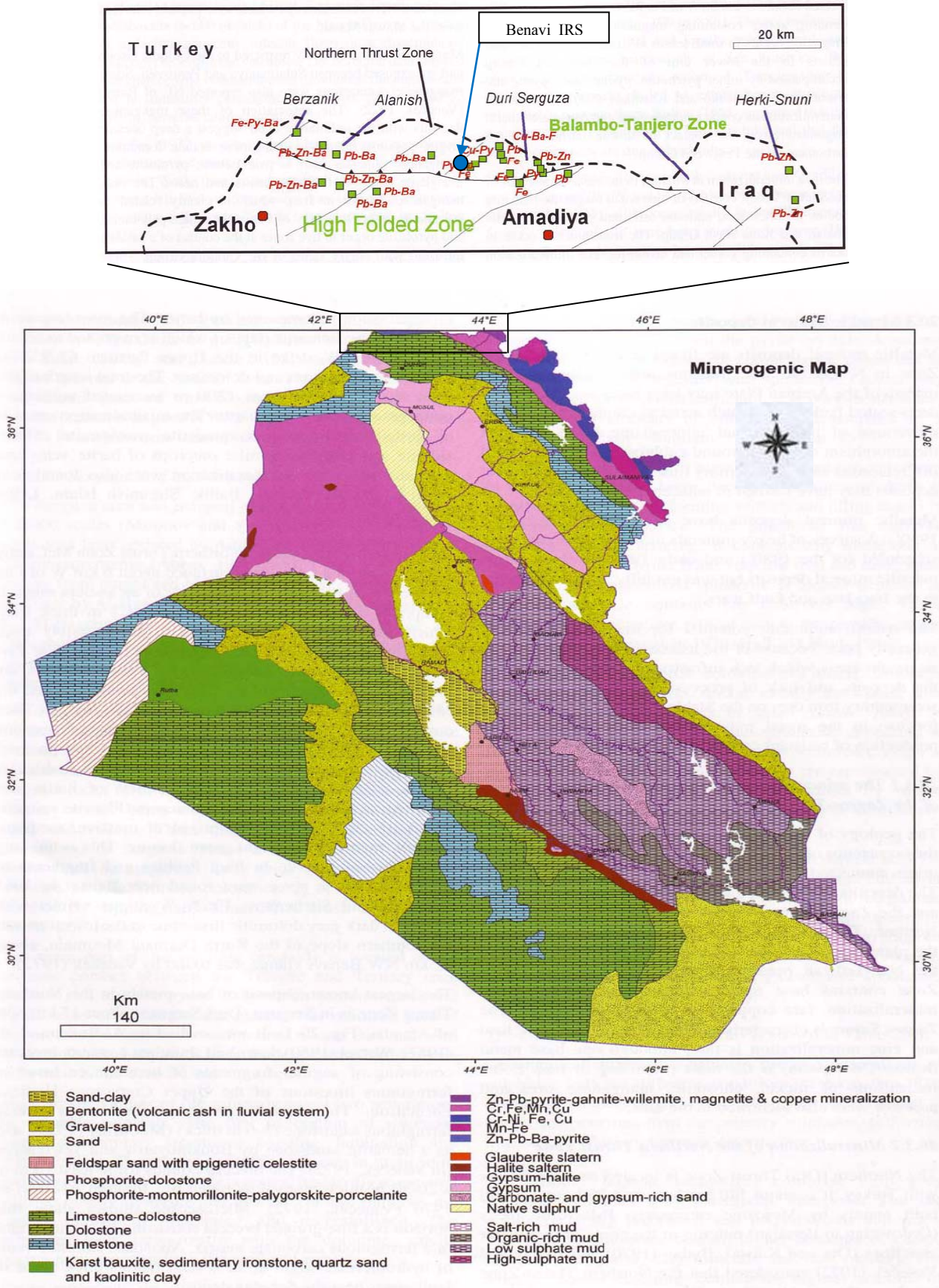


Figure (1-3): Minerogenic map of Iraq shows mineral occurrences of the Northern Ora Thrust Zone and Benavi IRS (after Jassim and Goff, 2006).

## 1-6 Structure, morphology and climate of Benavi area :

The most prominent structural feature in the study area is the Ora anticline, striking E-W and points with its steeper limb towards south, and the eastern parts of the Ora anticline lies beyond the Iraqi-Turkish border (Al-Rawi , 1978). To the south, the anticline is flanked by a large thrust fault striking in latitudinal direction from the greater Zab river to the Khabour valley in the west (AL-Hasni, 1973).

Morphologically, the studied area is one of three major mountain ranges in Amadia district. It is the highest area of this district and runs along the Turkish border in sublongitudinal direction, and the mountain range is separated by broad valleys which are with hilly ground dissected by numerous rivulets and streams. Plains could not be recognized in this area (AL-Hasni, 1973).

The climate is continental, hot in summer (temp. over 35°C) and cold in winter and the area becomes completely covered by snow. In spring time, the snow melts and heavy rain falls takes place; the investigated area is covered by trees, bushes and weeds.

The name of Benavi belongs to the abounding water eyes in this area and vegetation covers slopes and river valleys. Most of trees are Oak.

## 1-7 Stratigraphy of Benavi area:

The age relationship of the different rock units encountered in the area is illustrated in the stratigraphic column (Table 1-1).

### ❖ Paleozoic formations:

In the core of the E-W asymmetrical, Ora anticline exposes the Khabour quartzite, which is the oldest known formation in Iraq (Wetzel, 1950).

Paleozoic is characterized by two transgressions and by shallow water deposits ranging from clastic to organogenic sediments. Clastic materials prevail in the early Paleozoic and the beginning of the late Paleozoic, whereas the organogenic limestone predominates in late Paleozoic, (AL-Rawi, 1975).

Age	System	Series and stage	Formation
Mesozoic	Cretaceous	Maastrichtian	Aqra limestone
		Campanian(upper part)	Hadiena
	Jurassic	Late Berriasian	Chia Gara
		And middle Tithonian	Barsarine
		Kimeridgian	Naoklekan
		Callovian?- Early Kemeridgian	Sargelu
		Late Toarcian?- Bathonian	Sehkaniyan
		Pre-Toarcian?- Toarcian?	Sarki
	Triassic	Liassic	Kurrachina
		Late	Gelikhana Beduh shale
Middle		Mirgamir	
Early		Chaizairi Harur	
Palaeozoic	Permian		
	Early Carboniferous		
	Late Devonian?		
Palaeozoic	Ordovician		Ora shale Kaista
			Pirispiki red beds Khabour quartzite shale

Table (1-1): Stratigraphic succession of Benavi area (Al-Hasni ,1973).

**❖ Mesozoic formations:**

The color may be diagnostic for the different periods of the Mesozoic. The lower Triassic is characterized by typical yellowish color whereas middle and upper Triassic is composed of thick, grey, dolomite, limestone beds, and the dark colors prevail generally in the Jurassic formation (AL-Rawi, 1975) .

According to Mc carthy(1955) Benavi IRS occurs in Chia Gara formation of Hadiena area, as well as Hamza and Isaac (1971) mentioned that Benavi IRS outcrop extends over Chia Gara or Barsarin formations, whereas Wetzel (1950) and Geozavod (1981) mentioned that this outcrop is within Hadiena formation. However, more details for these formations are as follows:

**• Barsarin formation :**

The formation is composed of limestone or dolomitic limestone (Buday, 1980). The middle part of Barsarin formation is mostly aphanocrystalline limestone which is grey, massive rock, and the upper part of this formation consists of calcareous dolomite grey massive with yellowish brown weathered surface (AL-Hasni, 1973).

Fossils were not yet found , the age of the formation has determined using its position between the proved Early Kimmeridgian (Naokelekan formation ) and middle Tithonian (Chia Gara formation), (Buday, 1980).

**• Chia Gara formation :**

The formation was introduced by Wetzel (1950). The type locality lies on the Chia Gara anticline of the high folded zone, northern Iraq (Buday, 1980).

It is a thinly bedded grey to dark grey aphanocrystalline limestone interbedded with grey calcareous shale (AL-Hasni, 1973). The age of the formation is Middle Tithonian – Berriasian and there are still some debate concerning the relation of the formation to the underlying and overlying formations (Buday , 1980).

- **Hadiena formation:**

The formation was first defined by Wetzel in 1950 from the Hadiena area of the northern thrust zone, to the north west of Amadia district. The Hadiena formation consists of three divisions. The uppermost being the most typical one, the lower division consists of dolomitized limestone with vestiges of conglomeratic and fragmental elements. The middle division is composed of silty detrital calcareous marls and marly sandy limestone containing detrital hematitic, phosphatic and chert grains and the upper division, which is composed of conglomeratic and fragmental limestone consisting of angular fragments of hematite in matrix of ferruginous limestone (Buday, 1980).

In some areas, between the type locality and Benavi village, the lower and middle divisions are absent and the hematitic, brecciated and conglomeratic beds transgress over the Chia Gara or Barsarin formations (Hamza and Isaac, 1971).

Fossils are abundant in the middle and upper division but are totally lacked in the lower division (Buday, 1980). The age of the formation was determined as late Campanian with possible Maastrichtian at the extreme top.

The lower contact of the formation is unconformable. The formation overlies mostly the Chia Gara, but sometimes Barsarin or Naokelekan formations, such cases were observed in the field surveys around and to the east of Benavi and between Benavi and Maya village (Hamza and Isaac, 1971).

The upper contact of the formation is conformable and gradational, the overlying formation is a limestone – dolomitic considered to be the equivalent of the Aqra limestone formation (Bellen et al, 1959).

The formation is distributed on the area of the northern thrust zone only and the thickness of the formation in the type area amounts to (750m) (Buday, 1980).

# *Chapter Two*

## *Research Methodology*

## **2-1 Preface:**

There are three major tasks that have been carried out throughout this research:

1-Field work.

2- Laboratory works at Baghdad University / College of Science / Department of the Earth Sciences covered the petrographical study by using reflected and transmitted light microscopy . And at the laboratories of State Company of Geological Survey and Mining covered the chemical analyses for major and trace elements to the bulk samples and preparation of polished sections. Some samples (11 ones) were sent to SNIM laboratories in Mauritania for chemical analyses and ore microscopy by oil immersion, as well.

3-Detailed mineralogical investigations performed at the Ecole de mines laboratories in France – Ales by modern techniques available in this French research center such as SEM, EDS, FTIR, TGA and XRD (Appendix 1).

## **2-2 Field work:**

Benavi IRS was sampled by the author; (48) specimens were collected during field trip in September 2007. The true thickness of IRS outcrop ranges (2.5 -12.8 m). The sampling was systematic according to variations in color, hardness, texture, iron content ...etc as illustrated in Figure (2-1). All samples were described in details (Appendix 2), these samples were distributed in ten sections which represent the best outcrop sites of IRS (Fig 2-2) including country rocks, as well. All locations of these sections were determined by GPS (Type: GARMEN –XL-12).

Digital photos and movies for field observations were taken by digital camera. These observations showed that IRS is highly fractured as illustrated in Figure (2-3). Parallel and cross veinlets filled with iron oxides widespread throughout all this body with some of vertical veins (Fig. 2-4). The upper parts of IRS are more reddish in color because they contain higher amount of hematitic grains in distinct habit like granular texture (Figs.: 2-5&2-1-A); the middle part is more yellowish due to richness in limonite and goethite contents (Figs.: 2-1-B, 2-3-A&B), whereas the lower parts are

dark grey to black (Fig. 2-1-C). IRS is mostly covered by soil and characterized by abounding vegetation (Fig. 2-6). It is restricted within carbonate beds which dip ( $54^{\circ}$  -  $60^{\circ}$ ) and the general trend of the strike direction is E-W as illustrated in Figure (2-7).

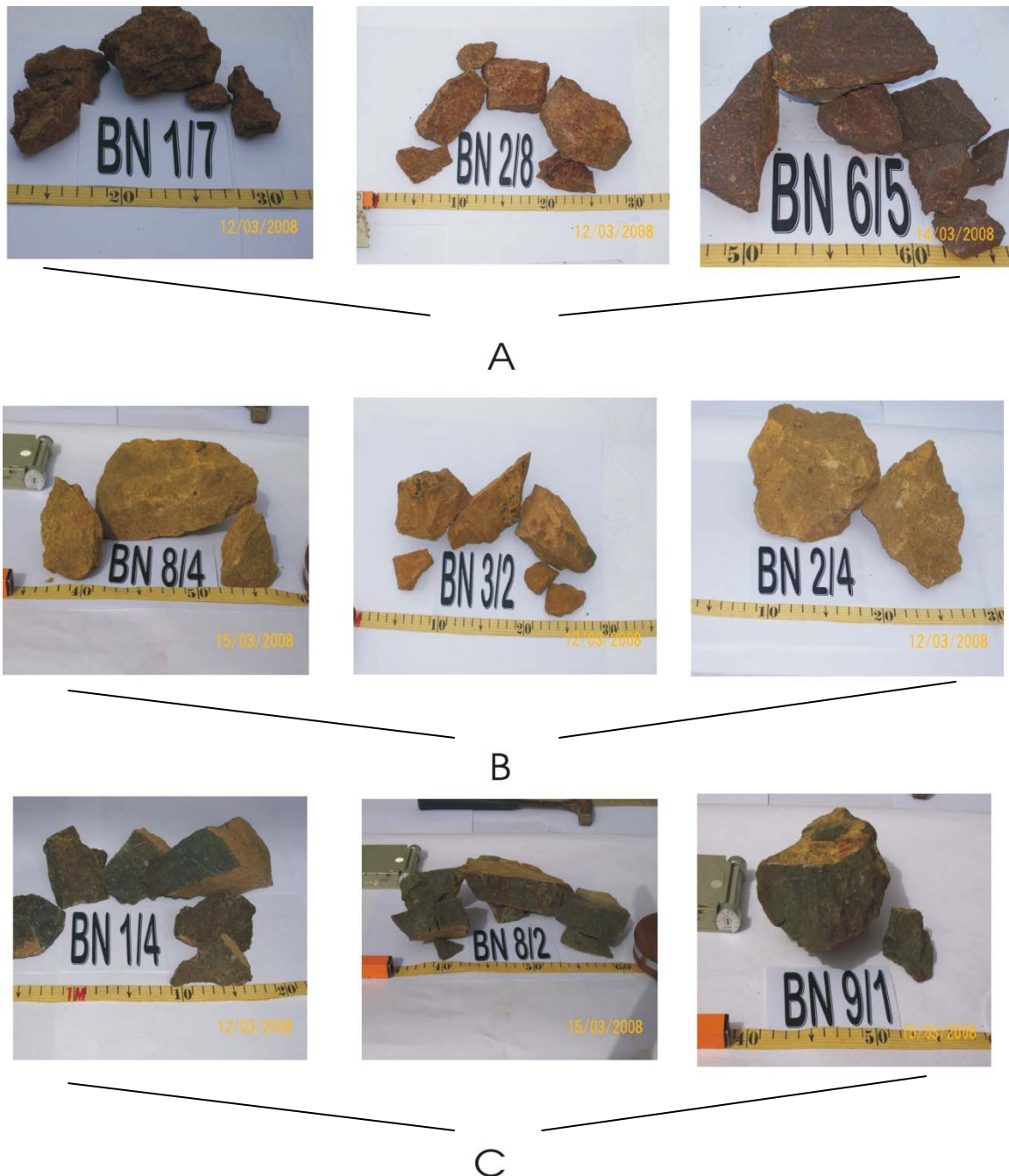


Figure (2-1): The sampling was according to variations in color and iron content: A-higher hematitic fragments content (more reddish, upper parts of IRS), B-higher goethite content (more yellowish, middle parts of IRS), and C- lower iron content (dark grey – black, at the base of IRS).

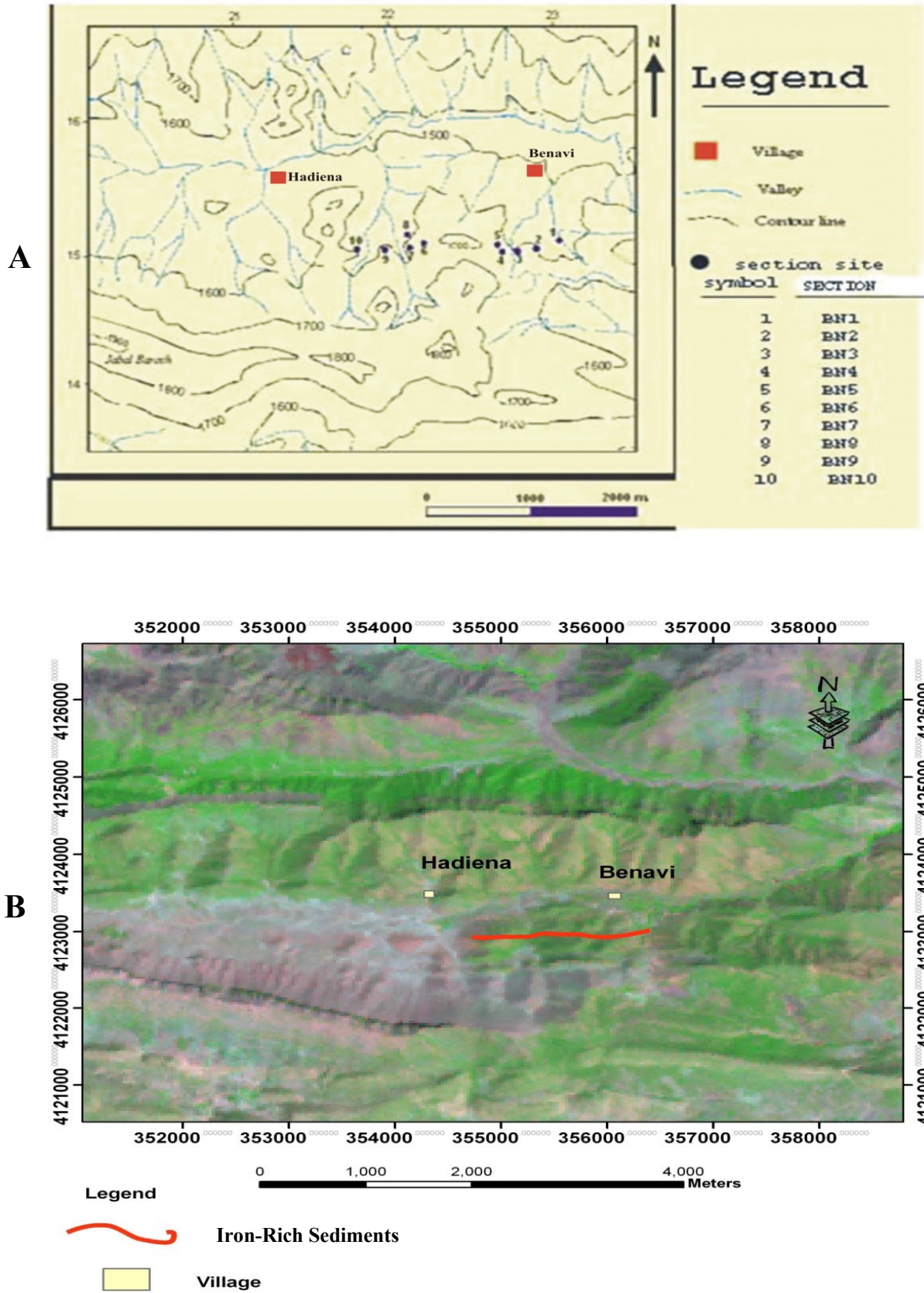


Figure (2-2): A: Topographic map showing locations of studied sections.

B: Satellite image showing the continuity of Benavi Iron- Rich Sediments.

A



B



Figure (2-3): A- One of the best outcrops of Benavi IRS shows the highly hematitic part at the top (reddish), and the more yellowish part in the middle due to limonite and goethite contents (Note the fractured feature). B- The fractured feature of Benavi IRS (middle part).



**A**



**B**



**C**

Figure (2-4): A: parallel veinlets filled with iron oxides (hematite).

B: cross veinlets filled with iron oxides (limonite and goethite).

C: vertical vein filled with secondary calcite crystals and iron oxides (limonite and goethite).



Figure (2-5): Showing the hematite grains exposed at the surface of Benavi IRS.



Figure (2-6): Showing the abounding vegetation related to the iron- rich horizon, (Note the highly covered feature). The row refers to the direction of the continuity of Benavi IRS (E-W).

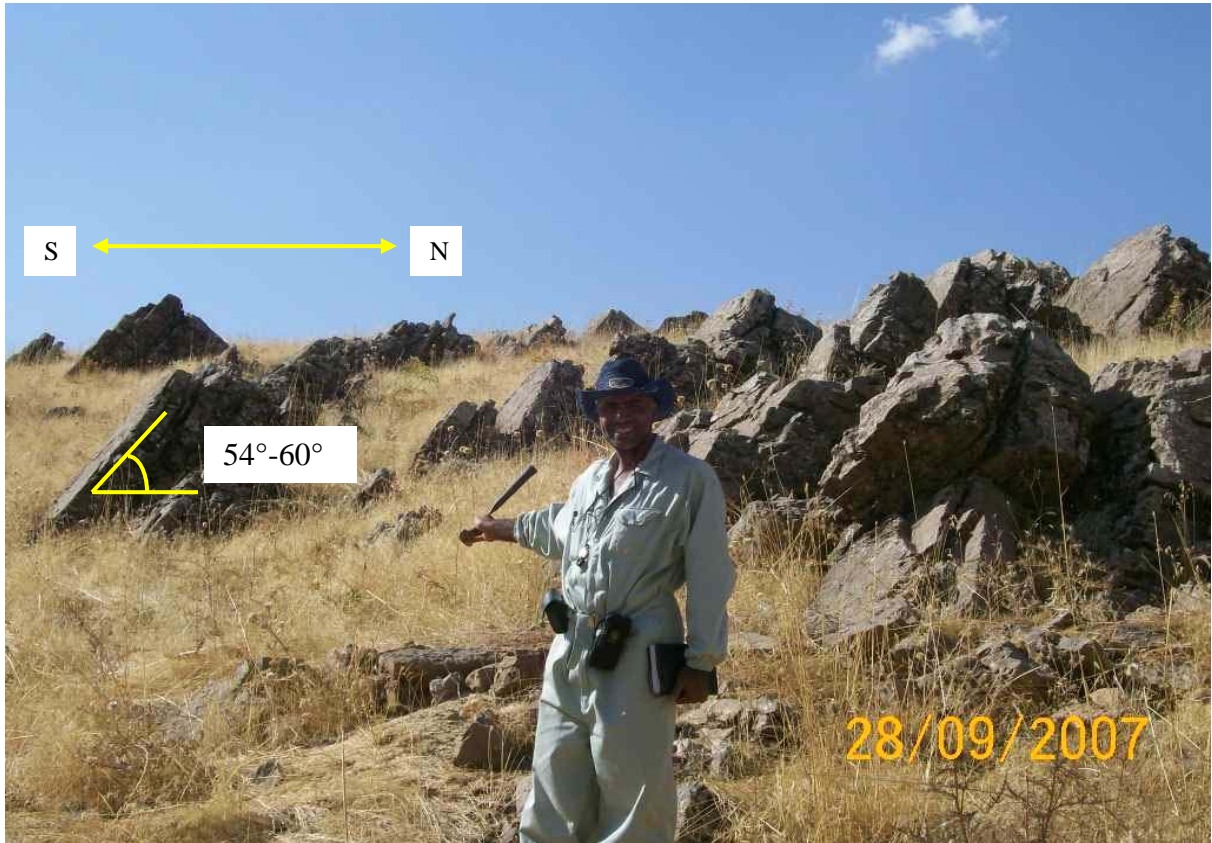


Figure (2-7): General trend of beds in the study area striking E-W.  
The dip amount ( $54^{\circ}$ - $60^{\circ}$ ) to the south.

### 2-3 Laboratory work:

(48) Samples represent the whole Benavi IRS and country rocks have been studied in detail by different mineralogical and geochemical techniques (Table 2-1).

	Sample Number	Thin	Polish	XRD	SEM	FTIR	TGA	EDS	chemical analyses for Bulk samples ( Geosurv )	chemical analyses for Bulk samples (SNIM)
1	BN1/1A	•								
2	BN1/1	•		•		•	•		•	
3	BN1/2	•								
4	BN1/3	•								
5	BN1/4	•	••	•	•	•	•	•	•	•
6	BN1/5	•	•	•	•	•		•	•	
7	BN1/6	•	•	•	•	•		•	•	
8	BN1/7	•		•		•			•	
9	BN1/8	•		•		•				
10	BN2/1	•								
11	BN2/2	•								
12	BN2/3	•								
13	BN2/4	•	••	•			•		•	•
14	BN2/5	•	••	•					•	•
15	BN2/6	•		•					•	
16	BN2/7	•	•	•	•		•	•	•	
17	BN2/8	•	••	•					•	•
18	BN2/9	•								
19	BN3/1	•								
20	BN3/2	•	•	•			•		•	
21	BN3/3	•								
22	BN3/4	•	•		•		•	•	•	
23	BN4/1	•	•						•	
24	BN4/2	•	•						•	
25	BN5/1	•		•		•			•	
26	BN5/2	•	••	•	•	•		•		•
27	BN5/3	•	••	•	•	•		•	•	•
28	BN5/4	•	••	•	•	•		•	•	•
29	BN5/5	•								
30	BN6/1	•								
31	BN6/2	•								
32	BN6/3	•		•					•	
33	BN6/4	•	••	•					•	•
34	BN6/5	•	••	•	•			•	•	•
35	BN7	•	•		•			•	•	
36	BN8/1A	•								
37	BN8/1	•								
38	BN8/2	•	•	•	•		•	•	•	
39	BN8/3	•	•		•			•		
40	BN8/4	•	•						•	
41	BN8/5	•			•			•	•	
42	BN8/6	•								
43	BN9/1	•	•	•					•	
44	BN9/2	•	•		•			•		
45	BN9/3	•	•						•	
46	BN10/1	•	••	•	•			•	•	•
47	BN10/2	•								
48	BN10/3	•	••						•	•
<b>sum</b>	<b>48</b>	<b>48</b>	<b>25</b>	<b>22</b>	<b>15</b>	<b>10</b>	<b>7</b>	<b>15</b>	<b>28</b>	<b>11</b>

Table (2-1): Shows all studied samples with technique of study, (•• Thin-polished sections and oil immersion).

**2-3-1 Transmitted light microscopy:**

(80) Of thin sections for (48) samples were prepared for petrographic examinations under transmitted light microscopy. Some samples have been cut in two directions perpendicular to each other. (58) Of them treated with Alizarin red solution to distinguish between calcite and dolomite according to (Friedman, 1959; Dickson, 1965), in this test, the color of calcite turned red-brown, whereas dolomite was not affected.

**2-3-2 Reflected light microscopy (Ore Microscopy):**

(25) Polished sections were prepared and examined under reflected light microscopy according to procedures described by (Vaughan and Craig, 1981).

The preparation of polished surface free from scratches, thermal and mechanical modification of the sample surface is essential for the examination, identification and textural interpretation of ore minerals under reflected light, necessity grinding and polishing of specimens.

The first stage was grinding to remove surface irregularities, reduce thickness, prepare a smooth surface for further work, and remove any zone of major deformation resulting from initial sample cutting. Each sample subjected to 400, 600, 800, 1000 mesh abrasive for (1) hour respectively.

The second stage was polishing of these specimens with diamond abrasives embedded in a napless cloth. The embedding permits the diamond grains to smoothen the surface without rolling and causing irregular scratching or gouging. (25  $\mu\text{m}$  , 15  $\mu\text{m}$  , 10  $\mu\text{m}$  and finally 2  $\mu\text{m}$  diamond abrasives ) have been used respectively.

Ore microscopic study using oil immersion for (11) samples performed in SNIM laboratories in Mauritania.

### 2-3-3 X-Ray Diffractometry (XRD):

(22) Untreated (bulk ) powder samples, followed by treating each one with acetic acid (0.3 molar ) at room temperature to dissolve calcite without affecting other minerals (Ostrom ,1961 ), then followed by heating each sample to 550°C (Thorez,1976). All these samples subjected to X-ray diffraction technique on a D8 DISCOVER SERIES 2 DOC-M88-E02055 / 2004 X-RAY DIFFRACTOMETER.

### 2-3-4 Fourier Transform Infrared spectrometry (FTIR):

Infrared spectroscopy is an important technique in chemistry and mineralogy. One can use the unique collection of absorption bands to confirm the identity of a pure compound or to detect the presence of specific impurities. This technique measures the absorption of various infrared light wavelengths by the material of interest.

Minerals contain covalent bonds absorb infrared radiation. The infrared region of the electromagnetic spectrum extends from the red end of the visible spectrum out to the microwave region. The spectral range of greatest use in mineral analysis is the mid – infrared region which covers the frequency range of 400 to 4000  $\text{cm}^{-1}$  (Connor et al, 2003). In this study, the infrared absorbance for (10) untreated samples (bulk) was measured using (IFS 66 /2004) instrument (Fig 2-8).



Figure (2-8): FTIR instrument type IFS 66 / 2004. In Ecole De Mines Lab. /Ales/France.

### 2-3- 5 Scanning Electron Microscopy (SEM):

SEM is a powerful technique applied in micro-imaging of a variety of surfaces. This technique can be used in exploring the surface structure to determine particle size and texture on that surface. The surface of a solid sample is scanned in a raster pattern with a beam of energetic electrons (Connor et al, 2003).

In this work, SEM was applied, using instrument of the type FP 2032-11 / QUANTA 200FEG (Fig 2-9) for the morphological characterization of the minerals and recognition of ore textures for selected samples as illustrated in Table (2-1).



Figure (2-9): Scanning electron microscope type FP 2032-11 / Q U A N T A 2 0 0 F E G.

Ecole De Mines Lab. /Ales/France.

### 2-3-6 Energy Dispersive Spectrometry (EDS):

EDS is a technique that can be applied in the determination of elemental composition of a surface. This technique makes use of X-rays emitted by elements with the surface that are initially excited by bombarding electrons.

The dimension of the interacting volume depends on the mean atomic number, density of the material, beam energy and the emitted X-ray energy.

X-ray maps of a surface are often quite valuable in revealing compositional variation across a sample (Connor et al, 2003).

EDS was used in this study to perform spot analysis of the elemental composition at different points on the solid surface, and to examine the distribution of the elements on the surface of the minerals via mapping analysis.

### **2-3-7 Thermal Gravimetric Analyses (TGA):**

(TGA) is a simple analytical technique that measures the weight loss (or weight gain) of a material as a function of temperature. Thermogravimetry analyses are among the standard methods of mineralogy. From reaction which occur in a mineral or other chemical substances during thermal treatment, the weight and energy changes can be identified and measured very clearly, weight loss which occur during dehydration (drying), structural water release, structural decomposition, carbonate decomposition, gas liberation, ...etc, and graphed versus temperature or time (Kloss, 1974).

In this study, (7) samples were chosen as bulk for this analysis, (5) of them after treated with acid using thermogravimetry analyzer type Perkin Elmer /Pyris series 1 TGA (Fig. 2-10 ).



Figure (2-10): TGA analyzer type Pyris series 1 TGA.

Ecole De Mines Lab. /Ales/France.

# *Chapter Three*

# *Mineralogy*

### **3-1 Preface:**

This chapter deals with analyzing the IRS samples using instrumentations of: X-Ray Diffraction (XRD), Scanning Electron Microscopy (SEM), Energy Dispersive Spectrometry (EDS), Thermal Gravimetric Analyses (TGA) and Fourier Transform Infrared spectrometry (FTIR). Identification of minerals of studied samples by their optical properties has been proved by investigating them in the aforementioned techniques.

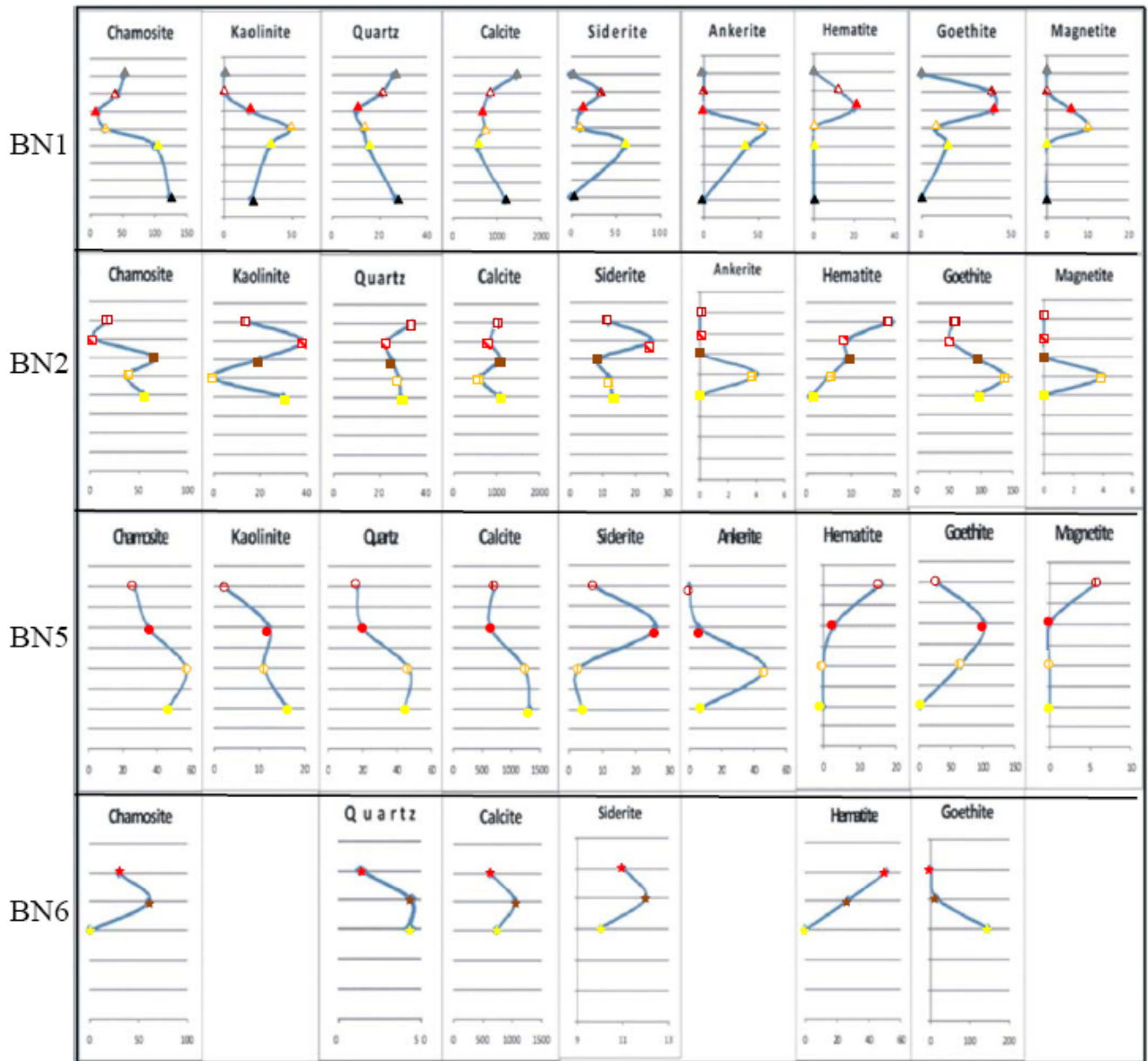
### **3-2 X-Ray Diffraction Study (XRD):**

Among all techniques available, (XRD) has been extensively used for qualitative identification and for quantitative estimation of mineral components in studied IRS samples.

The relative abundance of minerals for bulk samples of: BN1, BN2, BN5 and BN6 sections have been measured according to their peak area calculations using software program of D8 DISCOVER SERIES 2 DOC-M88-E02055 / 2004 X-RAY DIFFRACTOMETER, the results are shown in Figure( 3-1), the procedure of peak area calculations for each mineral are clarified in Appendix (3).

For more clear identification of minerals present in small quantities in IRS samples, some samples were carefully chosen to represent all IRS of Benavi to explore their mineralogical content.

These selected samples are : 10 samples of ( BN1 & BN5) sections as well as six samples (BN2/4,BN3/2,BN6/5,BN8/2,BN9/1 and BN10/1); they all were treated with acetic acid to dissolve the mineral calcite to remove its peaks in order to enhance the peaks of the other minerals (Ostrom, 1961); the same samples subjected to treatment by heating to 550°C to distinguish chlorite minerals from kaolinite (Thorez, 1976), the results are shown in the XRD patterns in Figures: (3-2), (3-3) and (3-4).



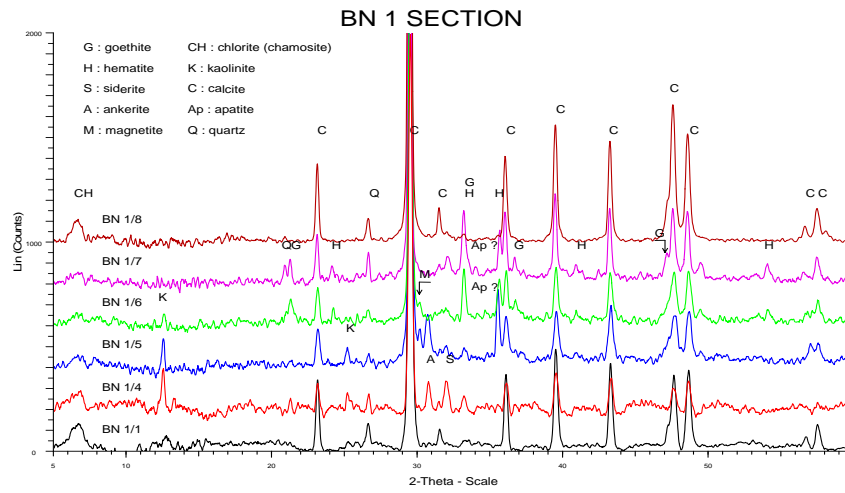
Legend:

BN1/8	▲	BN2/8	▣	BN5/4	○	BN6/5	★
BN1/7	▲	BN2/7	▣	BN5/3	●	BN6/4	★
BN1/6	▲	BN2/6	■	BN5/2	○	BN6/3	★
BN1/5	▲	BN2/5	▣	BN5/1	●		
BN1/4	▲	BN2/4	■				
BN1/1	▲						

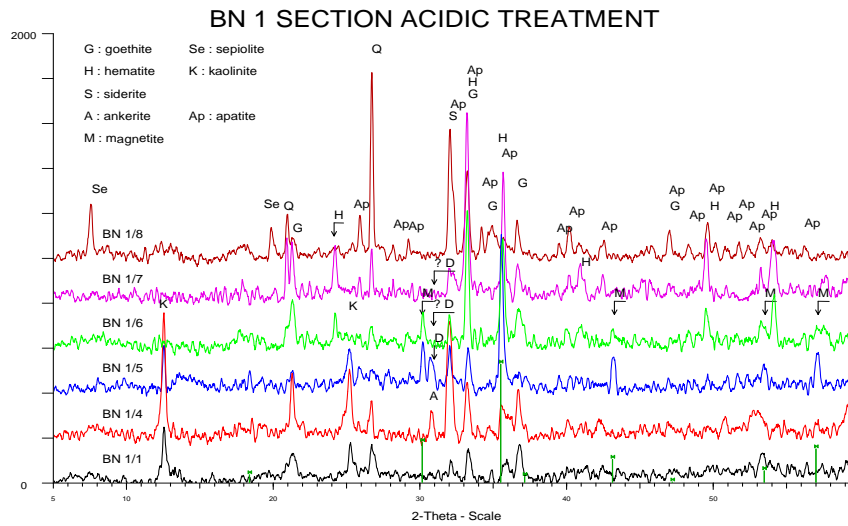
Where: X axis=Peak area value based on peak area calculations by software program of (D8 DISCOVER SERIES 2 DOC- M88-E02055 / 2004 X-Ray diffractometer).

Yaxis=Sites of the samples in the sections (see real scale in appendix 2).

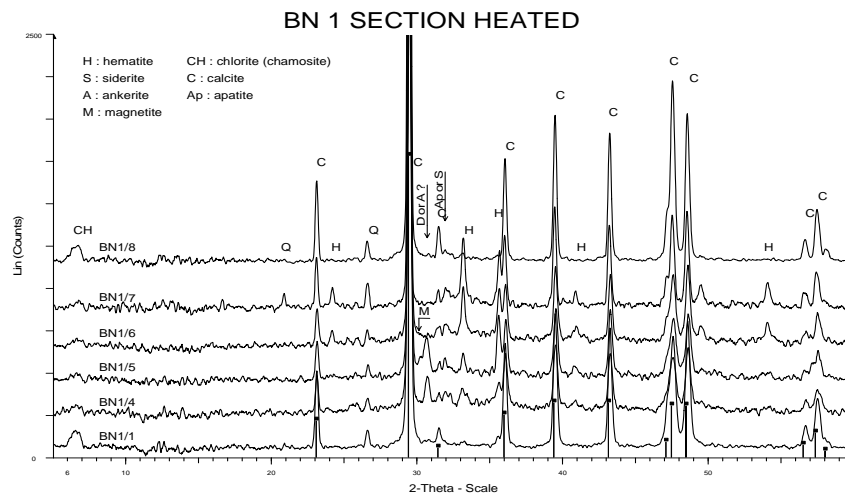
Figure (3-1): Relative abundance of minerals in samples of: BN1, BN2, BN5 and BN6 sections.



**A**

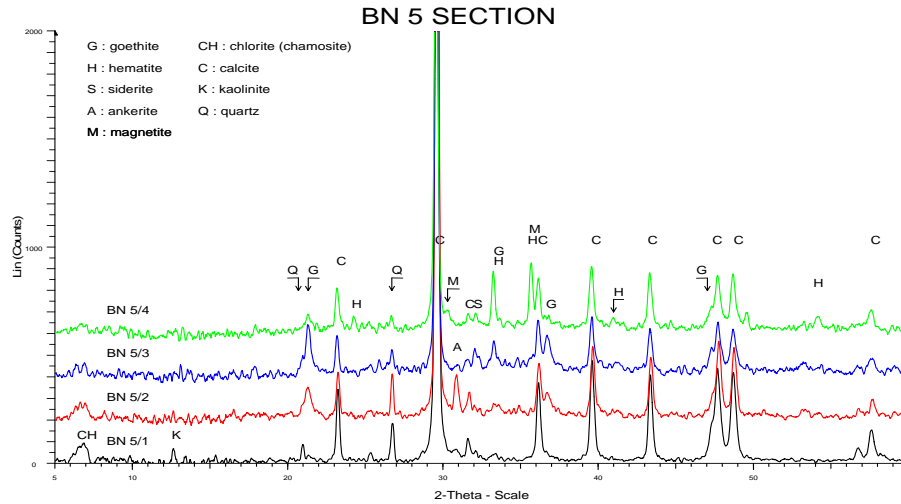


**B**

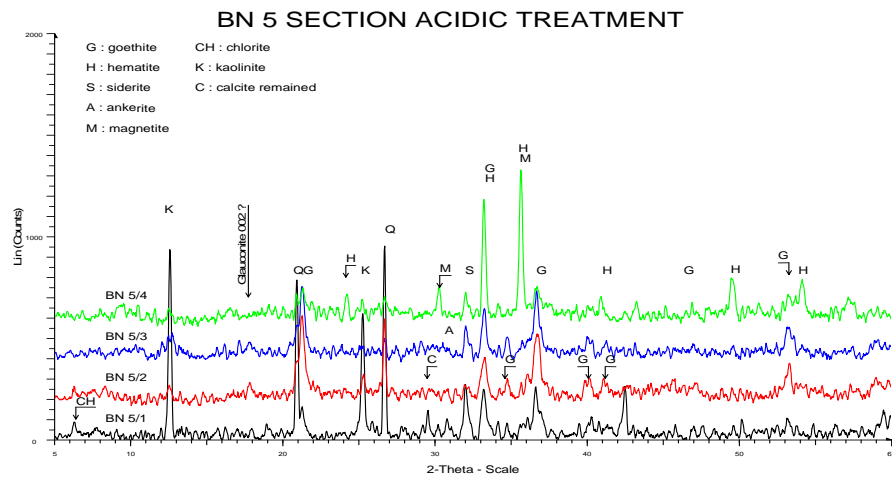


**C**

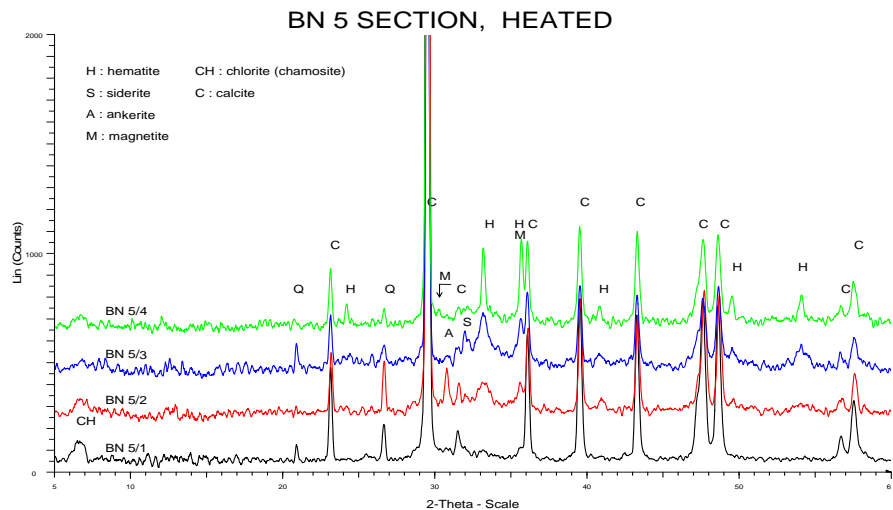
Figure (3-2): XRD patterns of BN1 section samples as: A-bulk sample not treated, B-after acetic acid treatment and C- after heat treatment.



**A**



**B**



**C**

Figure (3-3): XRD patterns of BN5 section samples as: A-bulk samples not treated, B-after acetic acid treatment and C- after heat treatment.

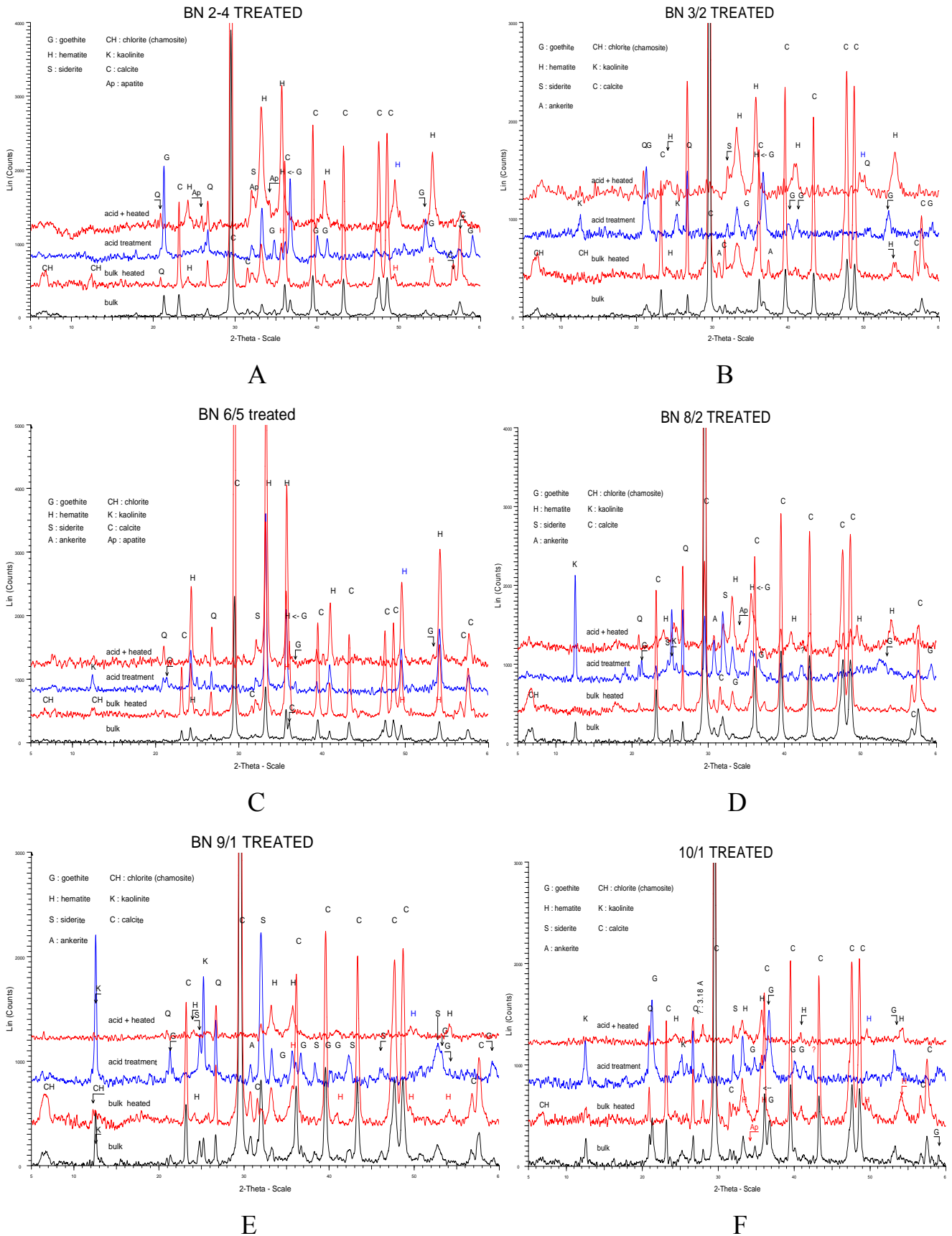


Figure (3-4): XRD patterns of treated samples: A- BN2/4, B -BN3/2, C-BN6/5, and D-BN8/2, E-BN9/1 and F-BN10/1.

### 3-2-1 Carbonate minerals identification:

Calcite, siderite, ankerite and dolomite of IRS were identified by XRD. Calcite is predominating whereas siderite and ankerite are minor, and dolomite is trace.

Calcite( $\text{CaCO}_3$ ) is the main mineral in all IRS samples which was identified by the (104) reflection:  $d=3.03\text{Å}$ ,  $2\theta=29.43^\circ$  as well as other less intense reflections. Shifts of the main real peaks values of calcite about the theoretical value in its d-space in all IRS samples[  $(104)_{\text{real}}=3:03\text{ Å}$  &  $3:025\text{ Å}$  and  $(104)_{\text{theoretical}}=3:035\text{ Å}$ ] gives the indication that there is no pure calcite in most studied samples and in some there is pure but in little amounts. This feature is clearly shown in samples of BN1 and BN5 sections Figure (3-5-A, B).

Impure calcite presence is most likely due to  $\text{Mg}^{+2}$  and  $\text{Fe}^{+2}$  substitutions in the space lattice of the calcite crystals, this is supported by EDS analysis which showed the presence of Mg and Fe in the calcite spectra (Ap.4-Figs. : (15)-A-spectrum 4, (17)-spectrum 6, (2)-A-spectra 3&4). Bricker (1971) mentioned that the skeleton of red algae consists of Mg-calcite crystals. Oldershaw and Scoffin (1967), as well mentioned that the different physicochemical parameters probably existed during the formation of second stage cement (increasing of temperature and pressure in addition to change in pH ) may have facilitated leaching of iron resulted conditions favorable for ferron calcite formation, where EDS also showed the presence of ferron calcite (Ap.4-Figs.: (20)-C- spectrum 2, (21)-B- spectrum 1, (18)- spectrum 4).

Siderite ( $\text{FeCO}_3$ ) is identified by the (104) reflection:  $d=2.79\text{ Å}$ . It is clear there is extremely little shift between theoretical main peak value of siderite ( $104:d=2.789\text{ Å}$ ) and the real peak value observed ( $d=2.79\text{ Å}$ ) (Appendix 3 - A).

Ankerite [  $\text{CaMg}_{0.27}\text{Fe}_{0.73}(\text{CO}_3)_2$  ] is also identified by the (104) reflection:  $d=2.90\text{ Å}$ . The theoretical and real peaks values are superimposed of ankerite in IRS samples (Appendix 3- B).

Dolomite was very difficult to distinguish by XRD technique because it is present in quite little amounts (not exceeding 5%); it was identified in only two samples: (BN1/6 and BN1/7) by the (104) reflection:  $d=2.89\text{ Å}$ .

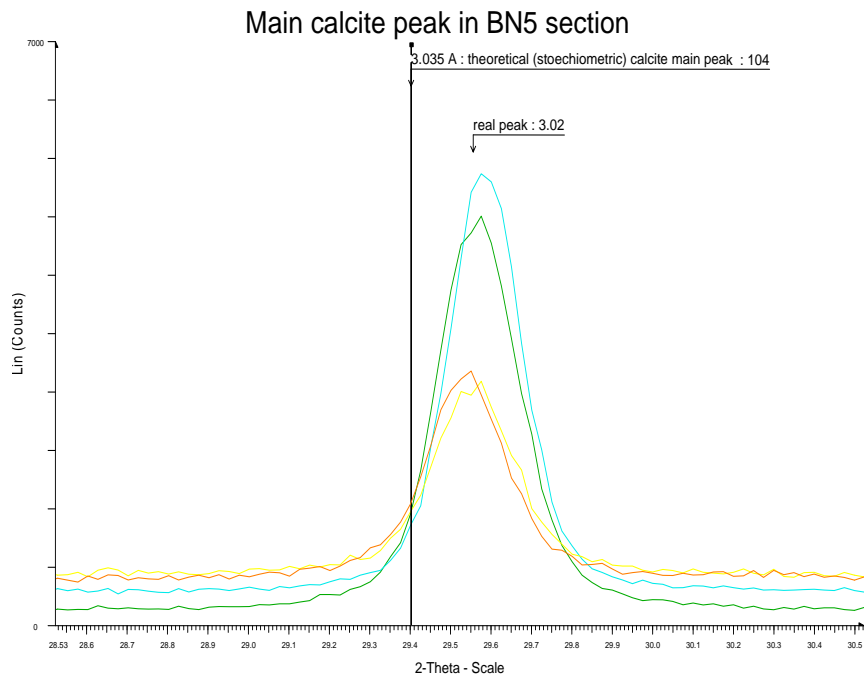
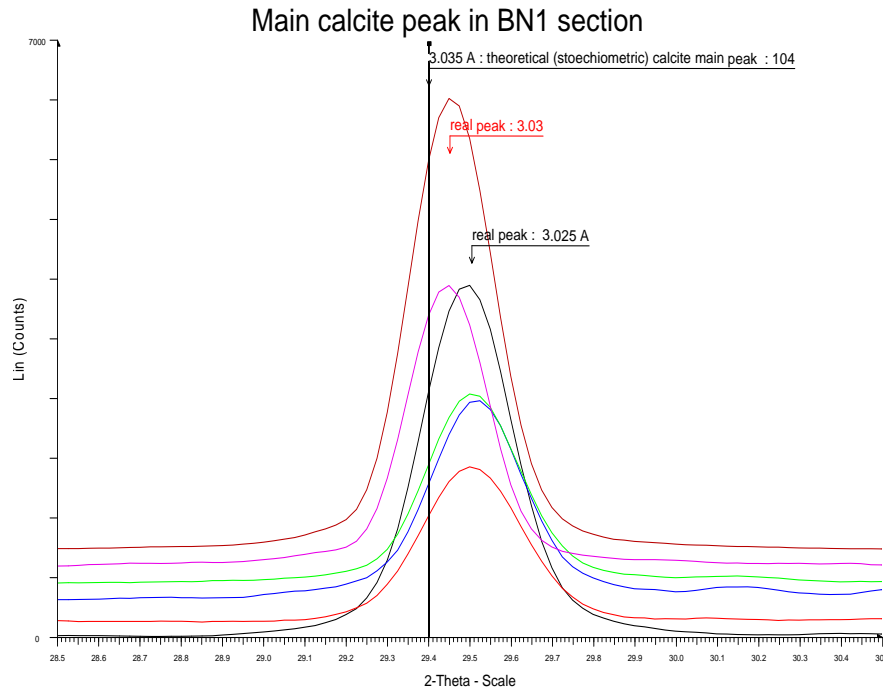


Figure (3-5): Shows the shift between the real and the theoretical peaks of (104) reflection,  
 A- Samples of BN1 section, B- Samples of BN5 section.

### 3-2-2 Iron oxides/hydroxides identification:

In general, iron oxides/ hydroxides are a group of minerals composed of Fe together with O and/or OH; they characterized by low solubility and thereby high stability, conspicuous colors and high surface area making them very effective sorbents for dissolved species. There are 17 known iron oxides/ hydroxides differing in composition, valence of Fe and most importantly in the crystal structure. Six of them are polymorph of (Fe O OH) & four of (Fe<sub>2</sub>O<sub>3</sub>). Nearly all the iron oxides/hydroxides are crystalline with the exception of ferrihydrite and schwertmannite which are poorly crystalline. The degree of crystal order is, however, variable and depends on the conditions under which the iron oxides/ hydroxides formed (Cornell and Schwertman, 2003 ).

XRD results showed the presence of hematite, magnetite and goethite in IRS samples whereas the other mentioned species were not detected.

#### 3-2-2-1 Hematite:

Hematite ( $\alpha$  Fe<sub>2</sub>O<sub>3</sub> ) is a blood red iron oxide found widespread in rocks and soils (like goethite, though, less common), its name comes from the Greek “haimtites” which means blood like. Hematite is very stable in an oxidizing environment but, it is unstable under reducing one because Fe<sup>+3</sup> can be reduced to Fe<sup>+2</sup> under reducing conditions. Hematite forms by dehydration of goethite through the removal of hydroxyl sheets and some of the oxygen in strips parallel to the c-axis to form water (Frost et al, 2003). In the studied samples, hematite is recognized by the X-ray peaks of the reflections: (104):  $d= 2.69\text{\AA}$  and (110):  $d=2.51\text{\AA}$ , the theoretical and real peaks values were fit. On the XRD the full width on half the maximum (FWHM) are measured. Measurements showed that (FWHM) for the reflection (104) is not doubled (not broader) than for the reflection plane (110), this indicates that there is no Al<sup>+3</sup> substitution occurred with Fe<sup>+3</sup> in the hematite lattice crystals (Al-Youzbaky, 1989), Figure (3-6). XRD results also showed hematite to increase upward in the studied sections, this does confirm field observations.

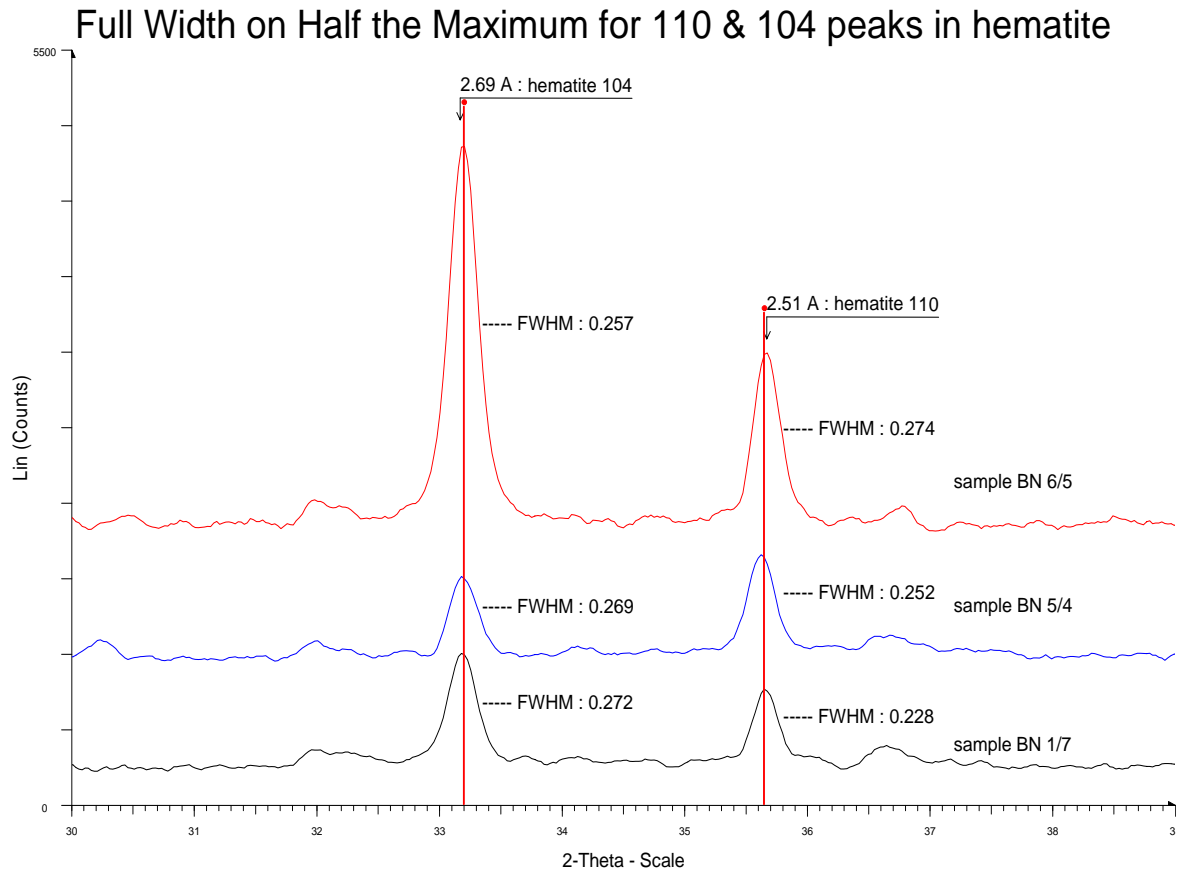


Figure (3-6): Showing (FWHM) of (110) and (104) peaks in hematite for some samples.

### 3-2-2-2 Goethite:

Goethite ( $\alpha$ -Fe O OH) is yellow suspended as particles in aqueous solutions, and it is one of the most stable iron oxides at ambient temperature. Goethite was named after the author scientist Johann Wolfgang von Goetha. It is one of the most common minerals in soil and rocks over broad climatic regions (Frost et al, 2003).

Goethite has been identified by the reflection (110):  $d = 4.18 \text{ \AA}$  which fits the theoretical value, (Appendix 3-C).

XRD results also showed that the real d-space values of (111) in goethite is less than the theoretical value ( $2.448 \text{ \AA}$ ) in most of IRS studied samples (Fig. 3-7-A); this mean  $\text{Al}^{+3}$  substitution with  $\text{Fe}^{+3}$ , probably occurred in the lattice of goethite because  $\text{Al}^{+3}$  is smaller than  $\text{Fe}^{+3}$  and this substitution caused the unit cell of goethite to shrink, consequently XRD to be shifted to higher  $2\theta$  angles (Al-Youzbaky, 1989).

XRD patterns show the abundance of goethite in samples that have been picked from the middle part of IRS (which appear yellow to yellowish brown color in fresh sample and in the field ) compared to samples picked from the upper parts of IRS (those look reddish brown to dark red in the fresh samples and in the field) (graphs of BN2/5, BN6/3, BN5/3, BN5/2, BN6/4). This means that the yellow color of this part is due to its goethite content.

All peaks of goethite disappeared on the XRD patterns of the samples treated by heating to (550 °c) because the dehydration or dehydroxylation of goethite to form hematite occurred (Brindely and Brown, 1980). The peaks of the latter are clearly shown in these patterns (Figs.: 3-2-C & 3-3-C).

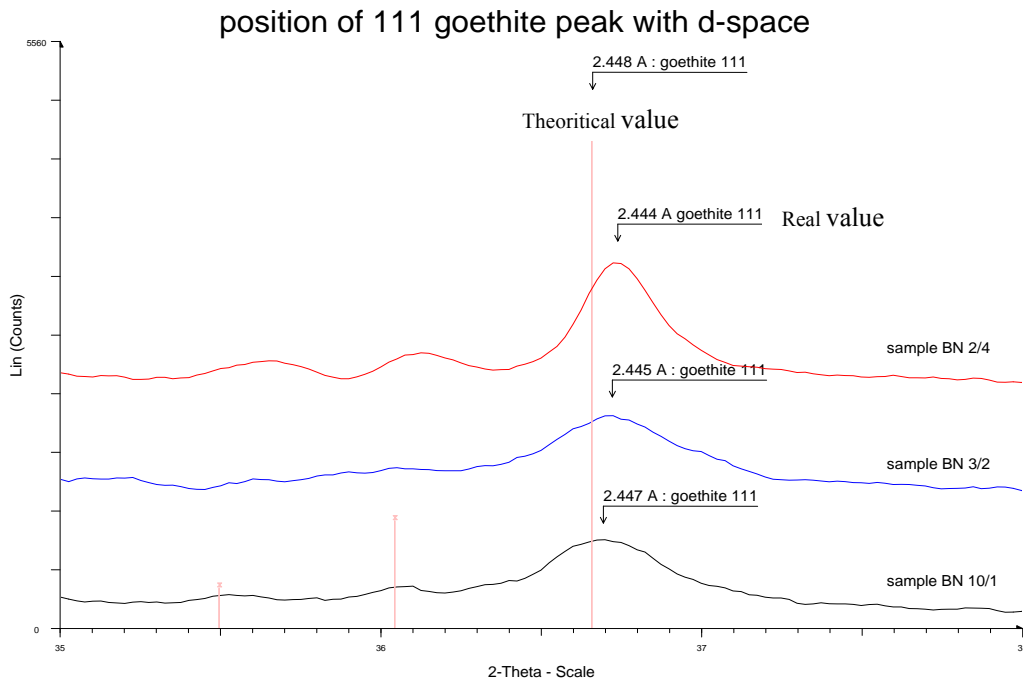
XRD analyses also showed that the brown veinlets which are spread in IRS outcrop mineralogically composed mainly of calcite with significant amount of Goethite (Fig. 3-7-B). Goethite content explains why these veinlets are yellowish brown to pale yellow in color.

### **3-2-2-3 Magnetite**

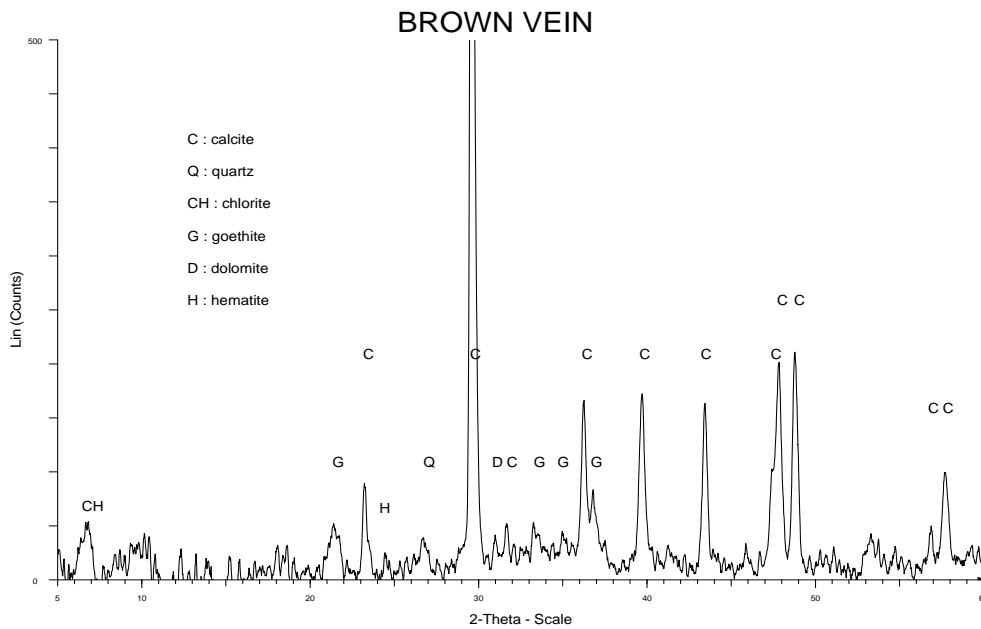
Magnetite ( $\text{Fe}_3\text{O}_4$ ) is a black, ferromagnetic mineral containing both  $\text{Fe}^{+2}$  &  $\text{Fe}^{+3}$ , the oxidation of magnetite yields maghemite which is also magnetic (Cornell and Schwertman, 2003).

This mineral was identified in some of the IRS samples by the reflections: (200):  $d= 2.96 \text{ \AA}$ , (400):  $d= 2.09 \text{ \AA}$  and (511):  $d=1.61 \text{ \AA}$ , (Appendix 3-D).

XRD outputs of the samples BN1/5, BN1/6, BN2/7 and BN5/4 show the presence of this mineral. This was verified by ore microscopy study (XRD confirmed the optical observations). Other samples probably contain magnetite but in such limited amounts to the content of being difficult to detect them by XRD technique.



**A**



**B**

Figure (3-7): A-d-space (theoretical and Real) of the plane (111) for goethite, B-XRD pattern of the sample picked from brown vein which is shown in Fig. (2-4- C).

### 3-2-3 Silicate minerals identification:

Chlorite (chamosite), kaolinite and quartz are the most common minerals among the silicate minerals group which were identified by XRD in many of the IRS samples.

XRD also showed the presence of sepiolite only in sample no. (BN1/8), this sample belongs to the overlying country rocks.

#### 3-2-3-1 Chlorite (chamosite):

Chlorite [chamosite,  $(\text{Fe}^{+2}, \text{Fe}^{+3} \text{Mg})_5 \text{Al} (\text{Si}_2\text{Al}) \text{O}_{10} (\text{OH})_8$  ], was determined based on the (002) reflection:  $d= 13.17 \text{ \AA}$ , (Appendix 3-E). The identification of the various forms of chlorite is very difficult and may be impossible unless chemical and optical data are available to supplement the X-ray analysis (Grim, 1968). Therefore, this reflection (002) with  $d= 13.17 \text{ \AA}$  identified as chamosite because it was clearly identified from the optical properties during the petrographical study.

Further, EDS analysis proved the presence of this mineral (Table 3-1 ) and the TGA analyses support this possibility too (Table 3-2).

Although, XRD confirmed the presence chlorite ( chamosite ) in most the Benavi IRS samples but it is present in low quantities.

#### 3-2-3-2 Kaolinite:

Kaolinite  $[\text{Al}_2 (\text{Si}_2\text{O}_5) (\text{OH})_4]$ , the identification of this mineral was based on its basal reflection (001):  $d= 7.14 \text{ \AA}$  (Appendix 3-F ).

The presence of chlorite minerals in the samples containing kaolinite usually makes confusion in the identification of these minerals; therefore, some tests are necessary for precise determinations. Chlorite has great solubility in acid; whereas kaolinite has good resistance for acid treatment. On the other hand when heated kaolinite tends to lose the crystalline character while chlorite only partially dehydrated causing increased intensity of the  $d=14 \text{ \AA}$  reflection (Grim, 1968). On this base, our samples were treated to identify these two minerals.

The results are shown in (Figure 3-4) exhibits peaks of kaolinite disappeared by heating due to the collapse of the crystallographic structure whereas the peak of chlorite (chamosite) stayed intact.

On the contrary, the XRD patterns of treated samples with acid: BN2/4, BN3/2, BN6/5, BN8/2 and BN10/1 showed disappearance of chlorite (chamosite) peaks whereas kaolinite peaks stayed intact.

### **3-2-3-3 Sepiolite:**

Sepiolite ( $\text{Si}_{12}\text{Mg}_8\text{O}_{30}(\text{OH})_4(\text{H}_2\text{O})_4 \cdot 8\text{H}_2\text{O}$ ), is one of the fibrous clay minerals which unlike other clays, is not a layered phyllosilicate. Its structure can be described as chain – like structure produces needle-like particles instead of plate like ones like other clays. These particles are arranged forming loosely packed and porous aggregates with an extensive capillary network which explains the high porosity of sepiolite and its light weight because of the large void space (Palau et al, 1997).

Sepiolite was identified by the (011) reflection:  $d=11.90 \text{ \AA}$  and (060):  $d= 4.45 \text{ \AA}$ . XRD results of acid- treated samples showed that this mineral occurs in the upper part of BN1 section in sample no.BN1/8 (Figure 3-2-B) which represents the overlying country rocks of the IRS.

The high neomorphism (recrystallization ) observed in the petrographical study is probably a good reason for sepiolite to form in this zone where the formation of this mineral is significant in constructing the recycling flux of Mg during recrystallization of carbonate sediments with high proportion of high Mg-calcite (Yan et al, 2005).

In the other side the neomorphism (recrystallization ) is high in IRS, but , no presence of sepiolite in this zone .

The absence of sepiolite in the IRS samples, may be attributed to the high content of iron which unite with Mg in the presence of carbonate to form ankerite causing depletion in Mg released from recrystallization of high-Mg calcite; this limited Mg is not enough to form sepiolite in the IRS.

**3-2-3-4 Glaucosite:**

$(K, Ca_{0.5}, Na)_{0.84}(Al_{0.47}Fe_{0.47}Fe_{0.19}Mg_{0.40})(Si_{3.65}Al_{0.35})O_{10}(OH)_2$ . This mineral is characterized by potassium content as well as its characteristic green color in plane polarized light under transmitted light microscopy.

Although the petrographical study and EDS analysis showed the presence of glaucosite in some samples, but its peak was very difficult to distinguish on the XRD sketch due to the low quantity of this mineral in the powder of studied samples (less than 5%). Exceptions of samples :( BN5/1, BN5/2 and BN5/3) where appearance of the glaucosite reflection (002):  $d=10.0 \text{ \AA}$  is detected very weak (Figure 3-3-B).

**3-2-3-5 Quartz ( $\alpha$ -SiO<sub>2</sub>):**

Sharp peaks of quartz reflect the good crystallinity of this mineral in the Benavi IRS samples. This coincides with the microscopic analyses which showed the presence of euhedral quartz (Plates: 4-5 A, B, C&D). Therefore, identification of quartz by XRD was very simple especially on the graphs of acid treated samples.

Quartz was identified by the reflections: (101):  $d=3.34 \text{ \AA}$  ( representing the highest intensity) and (100):  $d=4.26 \text{ \AA}$  . Peaks of quartz are quite clear in the patterns of samples: BN10/1, BN9/1, BN8/2, BN6/5, BN3/2 and BN2/4 (Figure 3-4).

**3-2-4 Phosphate mineral identification:**

Apatite (francolite ,  $CaF(Ca,C)_4[(P,C)(O,OH,F)_4 ]_3$  ), is the only one among phosphates group identified by XRD analysis in the IRS.

Although collophane was observed through microscopic investigation, but it was too difficult to be distinguished on the XRD technique because collophane is amorphous and has bad crystallinity character (Kerr, 1959). Some confusion was experienced of the apatite peak (211):  $d= 2.79 \text{ \AA}$  with the (104):  $d=2.79 \text{ \AA}$  belongs to the main peak of siderite. However, on heating samples, peaks of apatite were more easy distinguished, especially the reflections: (202):  $d=2.62 \text{ \AA}$  and (002): $d=3.44 \text{ \AA}$  (Appendix 3-G).

### 3-3 Scanning Electron Microscopy (SEM&EDS):

(15) Samples have been appropriately chosen from IRS as shown in Table (2-1); they were prepared by gold – coating to a thickness of 200 Å for SEM observations and EDS analyses. Identification of minerals by the other methods was confirmed by SEM and EDS techniques. Furthermore, minerals which are present in minor quantities and did not detect by XRD, they were easily identified by SEM & EDS such as, arsenopyrite, pyrite and glauconite.

This technique has the superiority to reveal the presence of arsenopyrite at the base of Benavi IRS. The only place where arsenopyrite has been reported in Iraq is marabasta Pb-Zn deposit in the Shalair zone of the Zagros suture. Marabasta deposit is of late Triassic- early Jurassic age (isotopic dating), composed of galena, sphalerite, pyrite, arsenopyrite, smithsonite and marcasite, it was later regionally metamorphosed (green schist facies) and some skarn minerals were developed such as magnetite, gahnite and willimnite, the deposit is strata –bound, probably of low temperature hydrothermal origin hosted in carbonate rocks. Finding arsenopyrite in Benavi IRS is very interesting (Al-bassam, 2008, personal communication).

Arsenopyrite (FeAsS) was identified by ore microscopic study (plate 4-8-F) and it was confirmed by EDS analyses (Fig. 3-8); therefore, this thesis is the first academic work proves the presence of arsenopyrite in Benavi IRS (more details are shown in this context in chapter five).

As well as, the elemental map was very useful in the identification of ankerite [ $\text{CaMg}_{0.27}\text{Fe}_{0.73}(\text{CO}_3)_2$ ] (Figure 3-9), which is very difficult to distinguish by other techniques, although it is identified by XRD and confirmed by EDS.

Table (3-1) and Appendix (4) show the results of SEM and EDS analyses of IRS samples where all spectra and BSE images are shown in Appendix (4) and the mineralogical identification and interpretation of each spectrum in Table (3-1).

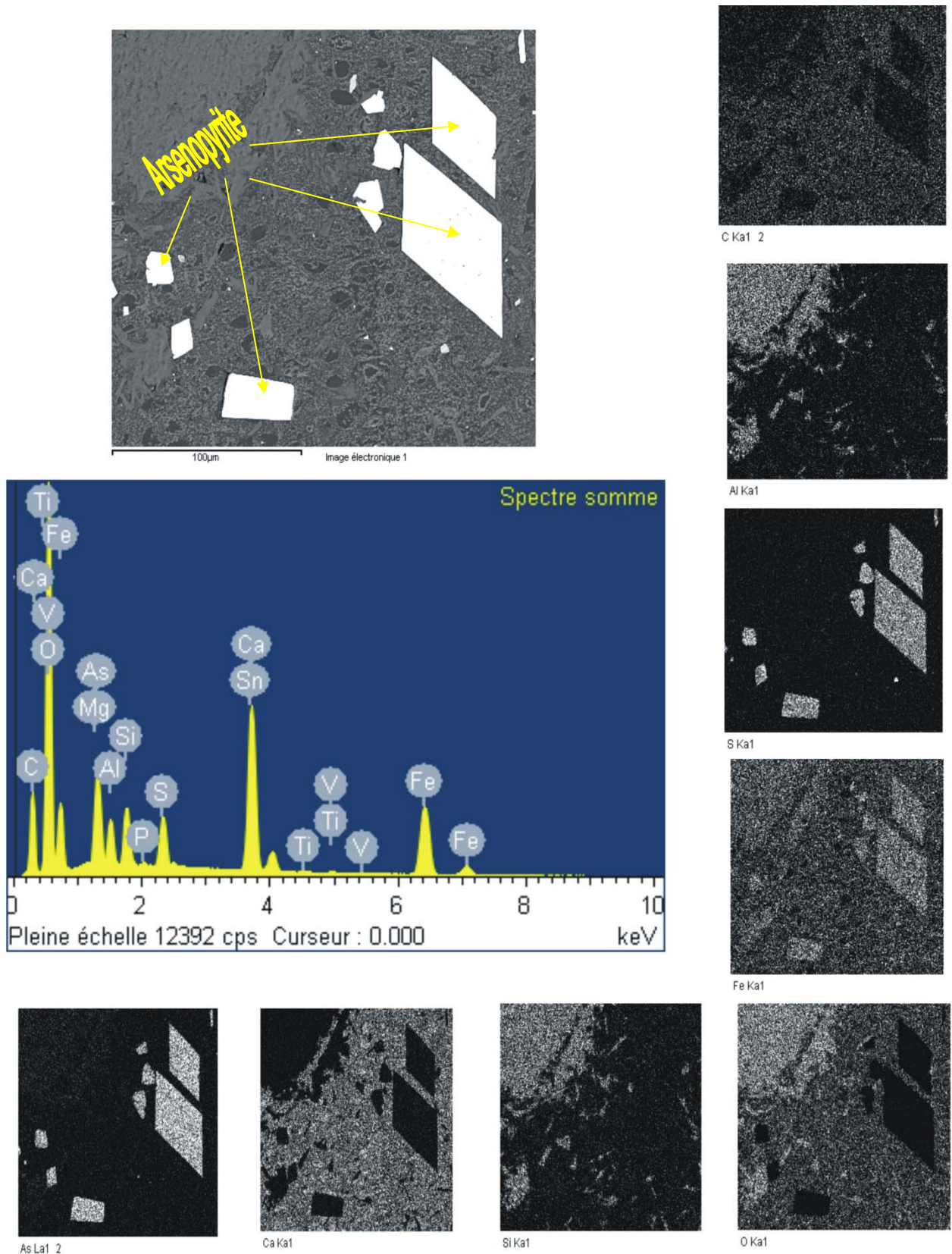
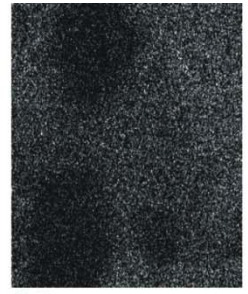
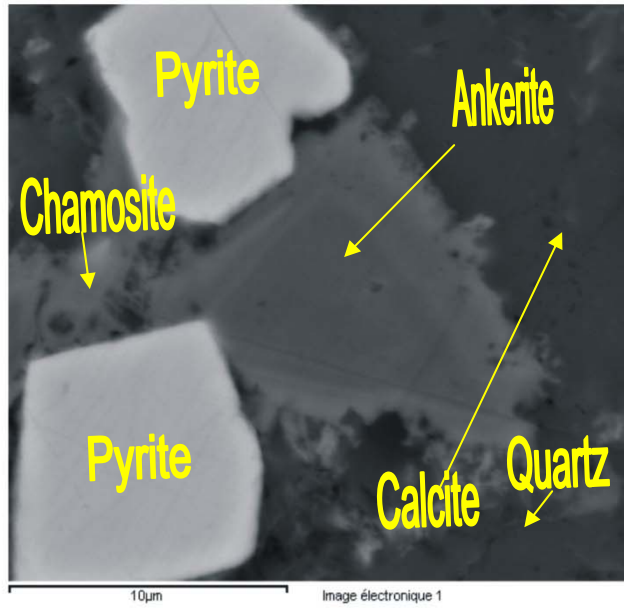


Figure (3-8): Elemental map, BSE image and EDS analysis that confirm the presence of arsenopyrite (FeAsS) at the base of Benavi IRS, sample no. ( BN8/2 ).



C Kα1\_2



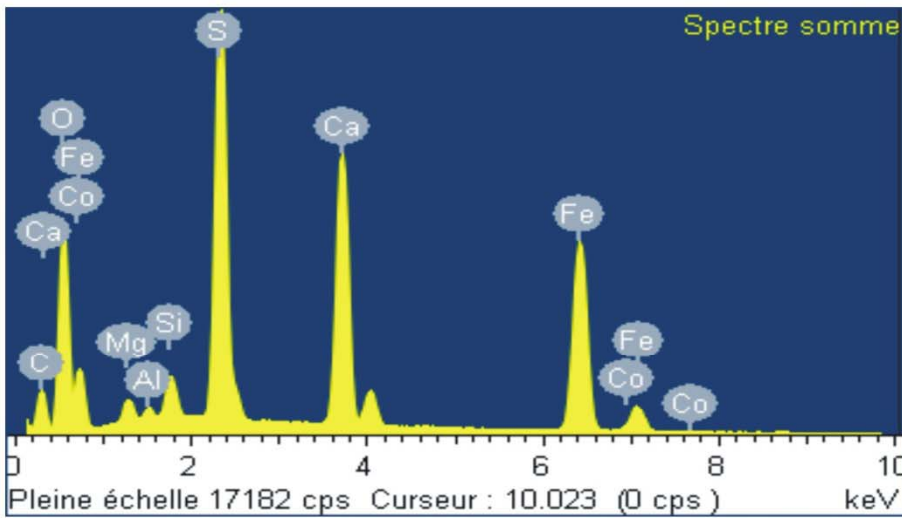
O Kα1



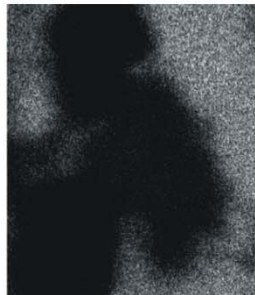
Mg Kα1\_2



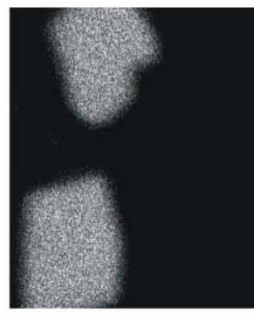
Al Kα1



Fe Kα1



Ca Kα1



S Kα1



Si Kα1

Figure (3-9): Elemental map, BSE image and EDS analysis of site 3 of the sample BN1/4 show ankerite, pyrite, chamosite, calcite and quartz.

Sample	Site /Figure no.	Spectrum	Mineralalogy
BN1/4	1/Ap.4-Fig.(1-A)  2/ Ap.4-Fig.(1-B)	1 2 1 2 3 4	Pyrite (dense framboidal pyrite). Pyrite (framboidal pyrite). Chamosite. Calcite (impure contain Fe&Mg). Chamosite. As the same of spectrum 2.
BN1/5	1/ Ap.4-Fig.(2-A)  2/ Ap.4-Fig.(2-B)	1 2 3 4  Elemental transverse	Goethite (Fe $\approx$ 59%, O $\approx$ 39.31%), occurs as veinlet. Magnetite (Fe $\approx$ 71.15%, O $\approx$ 27.69%). Calcite as groundmass & it is impure containing Fe & Mg. Calcite as inclusions within veinlets of goethite & it is also impure. Magnetite and goethite, respectively.
BN1/6	1/ Ap.4-Fig.(3)  2/ Ap.4-Fig.(4)	1 2 3 4 5 6 1 2 4 7 8 9	Calcite (bioclast). Calcite (bioclast) with trace of chamosite. Goethite and chamosite. Calcite is the main, phosphates, with a small amount of chamosite. Chamosite is the main, calcite, with a few amount of phosphates. Magnetite (Fe $\approx$ 70.76%, O $\approx$ 26.75%). Magnetite (Fe $\approx$ 70.0%, O $\approx$ 27.0%) with trace of kaolinite. Chamosite is the main with a few of calcite. Calcite (secondary calcite filled veinlets) & it is impure. Calcite is the main (impure contains Mg & Fe). Calcite is the main with significant amount of chamosite. Chamosite (main), significant amount of calcite & trace of glauconite.
BN2/7	1/ Ap.4-Fig.(5)  2 / Ap.4-Fig.(6)	1 2 3 4 1 2 3 4 7 8	Pure Calcite occurs as groundmass. Calcite is the main, chamosite, with trace of glauconite. Calcite is the main, chamosite and trace of phosphates. Magnetite (Fe $\approx$ 70.0%, O $\approx$ 27.0%). Chamosite occurs around bioclastic particle with trace of calcite. Magnetite (Fe $\approx$ 70.0%, O $\approx$ 26.76%) with trace of calcite. Calcite (impure contains Mg & Fe). Chamosite inside bioclastic particles with trace of calcite. Pure Calcite as a groundmass. Magnetite (Fe $\approx$ 70.0%, O $\approx$ 26.76%) with trace of calcite.

Table (3-1): Showing the mineralogical interpretation for the spectra of EDS analyses results of different sites in fifteen samples from IRS (Ap.4=Appendix 4).

Sample	Site /Figure no.	Spectrum	Mineralogy
BN2/7	3/ Ap.4-Fig.(7)	1	Goethite (Fe $\approx$ 54.51%, O $\approx$ 33.76%), few amount of : calcite , phosphates with trace of kaolinite.
		2	Impure calcite (contains Fe & Mg in its structur lattice).
		3	Magnetite (Fe $\approx$ 70.76%, O $\approx$ 28.37%) with trace of calcite & quartz.
		4	Calcite with trace of chamosite & trace of goethite and/or limonite.
		5	Chamosite is the main with trace of glauconite & very trace of calcite.
		6	As the same of spectrum 5 .
		7	Magnetite (Fe $\approx$ 70.80%, O $\approx$ 28.45%) with trace of quartz.
BN3/4	1/ Ap.4-Fig.(8)	1	The main mineral is calcite. Chamosite in significant amount with trace of glauconite.
		2	Calcite is the main , with very little amount of chamosite , and trace of glauconite probably is present.
		3	Mixing of: Goethite(main), chamosite , calcite and phosphates .
		4	Hematite (Fe $\approx$ 66.57%, O $\approx$ 30.99%), probably trace of kaolinite is present.
	1/ Ap.4-Fig.(9)	5	As the same of spectra 4.
		6	Calcite is the main with afew of chamosite & trace of glauconite .
		7	Calcite (ferron).
		8	As the same spectrum 6 in previous site.
		9	Calcite is the main with trace of chamosite.
		10	Hematite (Fe $\approx$ 64.31%, O $\approx$ 31.0%), with trace of chamosite.
		11	As the same of spectra 6 and 8.
		12	Calcite is main , with: phosphates, trace of: chamosite & pyrite.
2/Ap.4-Fig.(10-A)	1	Abundant fine grained of apatite associated with chamosite and trace of pyrite.	
	2	Hematite (Fe $\approx$ 64.31%, O $\approx$ 31.0%), with trace of : chamosite , phosphates and calcite.	
3/ Ap.4-Fig.(10-B)	1	Hematite (Fe $\approx$ 64.31%, O $\approx$ 31.0%), with trace of: kaolinite, phosphates and calcite.	
	2	Chamosite is the main with trace of calcite.	
4/ Ap.4-Fig.(11)	1	Calcite(impure).	
	2	Calcite is the main with trace of chamosite.	
	3	Hematite (Fe $\approx$ 64.31%, O $\approx$ 31.0%), with afew of chamosite.	
	4	Chamosite	
5/ Ap.4-Fig.(12)	1	Calcite.	
	2	Chamosite is main with trace of : glauconite and calcite.	
Table (3-1): continued.			

Sample	Site /Figure no.	Spectrum	Mineralogy
BN5/2	1/ Ap.4-Fig.(13-A)	1	Impure calcite contains Fe&Mg.
		2	Hematite (Fe $\approx$ 66.40%, O $\approx$ 30.39%) with trace of calcite&quartz.
		3	Impure Calcite with trace of chamosite .
BN6/5	1/ Ap.4-Fig.(13-B)	3	Goethite Fe $\approx$ 56.87%, O $\approx$ 32.27%( alteration of pyrite) & glauconite.
		4	Hematite (Fe $\approx$ 69.02%, O $\approx$ 29.42%), (dehydration of frambooids goethite which produced from alteration of pyrite frambooids ).
		5	Goethite (Fe $\approx$ 54.12 % O $\approx$ 35.55%), kaolinite & probably glauconite.
BN5/3	1/ Ap.4-Fig.(14)	1	Pyrite rich in arsenic.
		2	Goethite rich in arsenic too, produced by goethitization of pyrite.
		3	Phosphates (main) with trace of pyrite and calcite.
		4	Phosphates (main) with trace of calcite.
		5	As the same of spectrum 2.
BN5/4	1/ Ap.4-Fig.(15-A)	1	Magnetite (Fe $\approx$ 72.80%,O $\approx$ 28.45%) (oxidation of pyrite frambooids).
		2	Quartz (possibly authigenic in origin because they are euhedral and rich in inclusions from surrounding minerals such as carbonate and iron oxides with trace of calcite .
		3	Impure calcite with trace of quartz.
		4	Calcite (impure calcite contains Mg & Fe in its structure).
	2/ Ap.4-Fig.(15-B)	1	Phosphates (fine grained apatite) , with trace of kaolinite & calcite.
		2	Magnetite (Fe $\approx$ 71.70%,O $\approx$ 28.6%) , trace of phosphates & kaolinite.
		3	Magnetite (Fe $\approx$ 72.80%,O $\approx$ 28.45%),(oxidation of pyrite frambooids).
	3/ Ap.4-Fig.(16)	1	Magnetite (Fe $\approx$ 72.80%,O $\approx$ 28.45%),(oxidation of pyrite frambooids).
		2	As the same of spectrum 1.
		3	Siderite with trace of quartz.
4		Impure calcite (contain Mg and Fe in its structure lattice).	
BN7	1/ Ap.4-Fig.(17)	1	Goethite (Fe $\approx$ 56.60%,O $\approx$ 31.22%), with trace of: quartz & calcite.
		2	As the same of spectrum 1.
		3	Mg- calcite, probably with trace of dolomite, both as inclusions within veinlets of goethite.
		4	As the same of spectrum 3.
		5	Chamosite with trace of calcite.
		6	Impure calcite contains Fe&Mg.
BN8/3	1/ Ap.4-Fig.(18)	1	Hematite (Fe $\approx$ 66.04%, O $\approx$ 38.90%), with trace of:kaolinite & calcite.
		2	Chamosite with trace of : glauconite & calcite.
		3	Quartz.
		4	Ferron calcite.
BN8/5	1/ Ap.4-Fig.(19)	1	Hematite (Fe $\approx$ 67.64%, O $\approx$ 29.31%), with a trace of kaolinite.
		2	Goethite (Fe $\approx$ 51.98%,O $\approx$ 34.65%),with a few amounts of: calcite or /and siderite , phosphates and kaolinite besides trace of pyrite.
Table (3-1): continued.			

Sample	Site /Figure no.	Spectrum	Mineralogy
BN8/5	1/ Ap.4-Fig.(19)	3	Goethite (Fe $\approx$ 59.12%, O $\approx$ 32.59%) with a few amounts of: calcite or /and siderite , phosphates and kaolinite.
		4	Hematite (Fe $\approx$ 65.60%, O $\approx$ 30.02%) with trace of kaolinite.
		5	Goethite (Fe $\approx$ 57.63%, O $\approx$ 38.04%) with trace of :calcite and/or siderite, phosphates and kaolinite.
		6	Goethite (Fe $\approx$ 55.34%,O $\approx$ 31.35%) with significant amount of kaolinite.
		7	Impure calcite contains ( Mg &Fe) with trace of quartz.
BN9/2	1/ Ap.4-Fig.(20-A)	1	Quartz as the same of BN5/4 (site 1/ Fig.(15)-A-spectrum 2 ).
		2	Pure calcite (groundmass).
		3	Pure calcite (groundmass).
	2/ Ap.4-Fig.(20-B)	1	Calcite (as inclusions in quartz ) with a few of quartz.
		2	Pure quartz.
	3/ Ap.4-Fig.(20-C)	1	Pure quartz.
		2	Ferron calcite.
	4/ Ap.4-Fig.(21-A)	1	Goethite with a few of chamosite and trace of: phosphates &calcite.
		2	Chamosite with trace of calcite & phosphates.
		3	Chamosite with trace of calcite &phosphates.
5/ Ap.4-Fig.(21-B)	1	Impure calcite (ferron).	
	2	Siderite with a few of kaolinite.	
BN10/1	1/ Ap.4-Fig.(22)	1	Pyrite rich in arsenic.
		2	Goethite rich in arsenic too, as alteration after pyrite, with trace of quartz.
		3	Calcite is the main with a few of : phosphates, chamosite and trace of pyrite.
		4	Chamosite with trace of calcite.
		5	Pure calcite.

Table (3-1): continued.

### 3-4 Thermal Gravimetric Analysis (TGA):

Thermal gravimetric analyses (TGA) were performed using a Perkin Elmer Pyris-1 TGA, thermobalance operating under air conditions in alumina crucible containing around 10+/- 2 mg from the powder of studied sample. The runs were carried out under dynamic conditions at heating rate of 100°c/min from room temperature to (900 °c -1017 °c). Seven of the IRS samples have been chosen for TGA analysis.

Five of them were treated with acetic acid to dissolve calcite mineral (which present in high amount) to enhance thermally affected minerals present in few quantities facilitating their identification. Results of thermogravimetric analysis with interpretations are reported in (Table 3-2). This table content has been derived from TGA curves. These curves are shown in (Fig.3-10).

#### **3-4-1 Thermal behavior of IRS carbonates:**

Minerals of the carbonate group can be determined by their decomposition temperatures: 430 °c – 650 °c, 570 °c – 900 °c and 700 °c – 900 °c for siderite, ankerite and calcite, respectively. Pure calcite decomposes at very high temperatures (>1000 °c) (Kloss, 1974).

The difference in weight loss pre-acetic acid and post-acetic acid digestion that ranged (19.522% – 24.28%) indicates that carbonate minerals are the major components of the IRS samples. Furthermore, TGA results proved that impure calcite is predominant in IRS samples as the maximum decomposition temperature was up to 863 °c in sample BN3/4, whereas pure calcite decomposition temperature must be not less than 900 °c (Kloss, 1974). This was reasoned to the Mg<sup>+2</sup> and Fe<sup>+2</sup> within the structures of calcite that caused decrease of temperature decomposition of calcite below 863 °c, supported by XRD and EDS results which also showed that most of IRS calcite is impure (mostly containing Fe or Mg or both).

#### **3-4-2 Thermal behavior of Iron oxides /hydroxides:**

The principle thermal changes in iron oxides/ hydroxide are dehydroxylation and dehydration. The escaping water can be bound in minerals by two fundamentally different mechanism: by adsorption forces on surfaces of structure or by coordination forces around certain cations of the structures (crystal water). The temperature of the released OH-groups depend on the mineral structures where the same bonding may decomposes at higher temperatures if it is within a complex structure (Frost et al, 2003).

A steady weight loss of adsorbed water in IRS samples was observed over the ambient to 150 °c as indicated by TGA curves.

Goethite and hematite are the most common forms of the crystalline iron Oxides / hydroxide present in the IRS samples. As mentioned before, when samples heated, goethite altered to hematite. This alteration occurred by the removal of hydroxyl sheets and some of the oxygen in strips parallel to the c-axis to form water (Frost et al, 2003). TGA results showed that there is a wide range in thermal decomposition of goethite of IRS samples, from 263 °c (sample BN2/4) to 350 °c (sample BN3/2).

Usually the dehydroxylation of goethite to form hematite occurs between 260 °c to 400 °c depending upon the degree of crystallinity. Besides the degree of crystallization, the chemical composition also influences the dehydration of goethite, especially aluminium content.

The coexistence of two different goethite in sediments is not unusual. In some ironstones from Sulzbach-Rosenbeg-Bavaria; there are two goethites different in their degree of crystallization (at 262 °c and 370 °c ). This is analogous to the IRS studied samples, where the wide range of decomposition of goethite was observed and is probably due to the  $Al^{+3}$  content and the degree of crystallinity (Kloss, 1974).

Kampf and Schwertmann(1983) reported that the extent of  $Al^{+3}$  substitution in goethite is positively related to the surface weathering conditions and the increase in  $Al^{+3}$  substitution causes increase in stability of goethite.

The higher weight loss was observed in BN2/4, BN5/2 (Table3-2), this again agrees with the EDS and XRD results which showed the presence of goethite in these samples in significant amounts. The particular color of these samples (yellowish brown to yellow) due to goethite content.

The weight loss between 150 °c to 260 °c occurred probably due to the dehydration of limonite to form goethite at these temperatures.

**3-4-3 Thermal behavior of silicates:**

(TGA) results showed some evidences for the presence of: chlorite (chamosite), kaolinite and glauconite in IRS samples. Thermal analysis is quite suitable for classifying members of the chlorite group. Mg-chlorite decomposes at 860 °c , and with the increasing of Fe-content the decomposition temperature decreases from 860°C (Mg-chlorite free of iron) to less than 700°C in (pure Fe-chlorite) (chamosite), where the curves of dehydration and decomposition of the structure coincide, (Kloss, 1974).

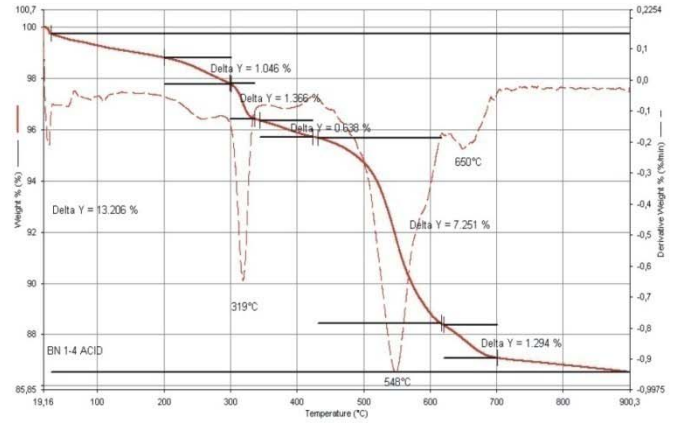
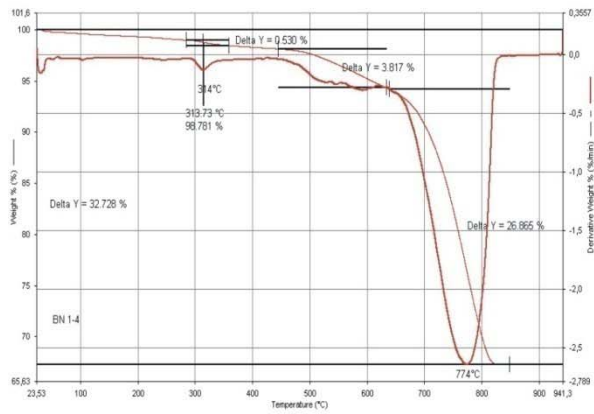
Weight loss values in untreated samples at temperatures >650 °c may be due to decomposition of chamosite besides the decomposition of other carbonate minerals.

The sorbed water in kaolinite is released at temperature up to 200 °c , whereas the dehydroxylation reaction of kaolinite occurs in temperature range ( 400 °c to 700 °c ) (Kloss, 1986). Thus, part of weight loss of the treated and untreated samples in IRS over 400 °c attributed to decomposition of kaolinite content.

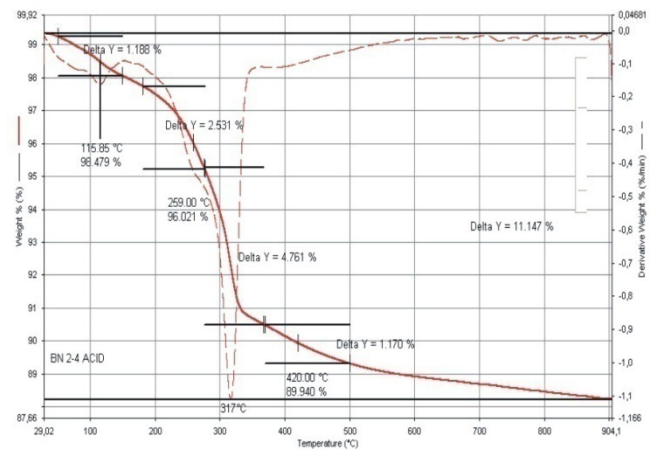
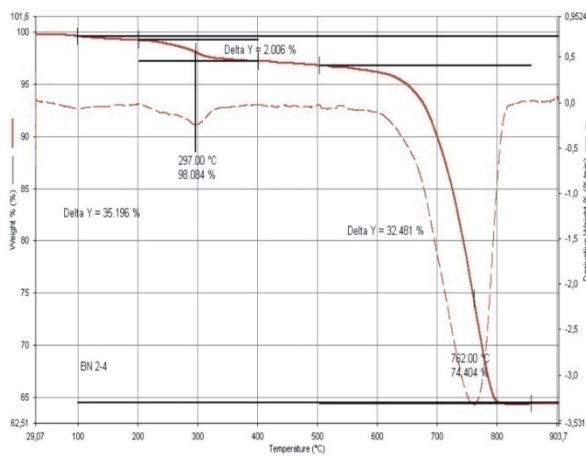
The decomposition of siderite in a mixture with kaolinite by TGA is inhibited by the superposition of their peaks in 500 °c - 600 °c range. If both minerals are present in the same sample, then superposition would form a single composite curve (Bayliss and Warne, 1972). Dehydroxylation of glauconite occurs between 500 °c to 630 °c , the same as with kaolinite, part of the weight loss in the studied samples (treated and non treated) at temperatures above 500 °c probably due to the decomposition of glauconite (Kloss, 1986).

**3-4-4 Thermal behavior of phosphates:**

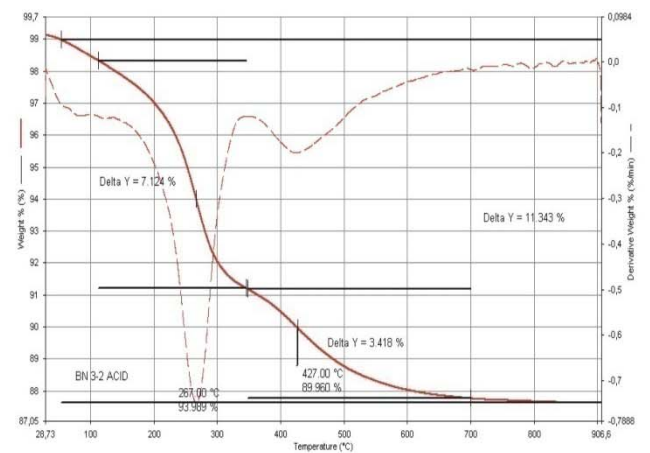
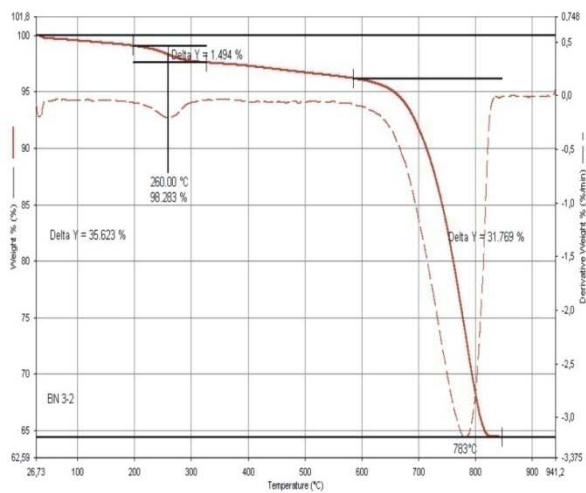
Melting of phosphates occurs between 500 °c to 800 °c (kloss, 1986). Curves of phosphates expressed in publications of ( Hausen and Aristarian, 1968 in Kloss, 1986), they mentioned that decomposition melting of phosphates group occurs between 630 °c to 802 °c . Based on above, part of the weight loss of studied samples between 500°C to 802 °c; is due to the decomposition of the structure of phosphate minerals present in these samples.



**A**

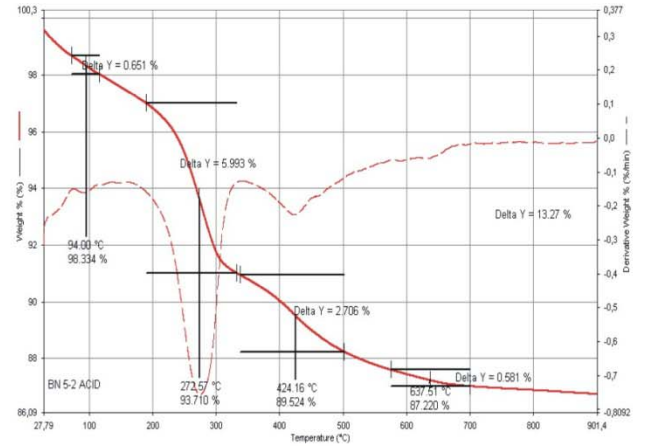
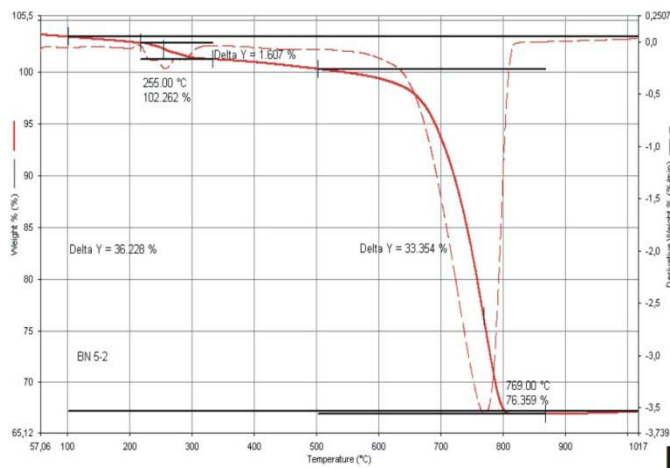


**B**

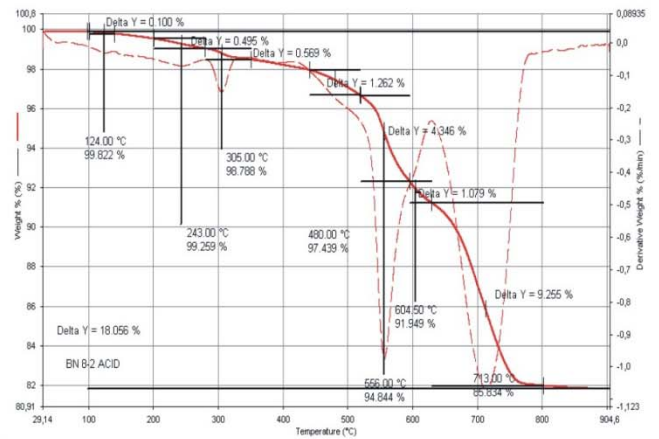
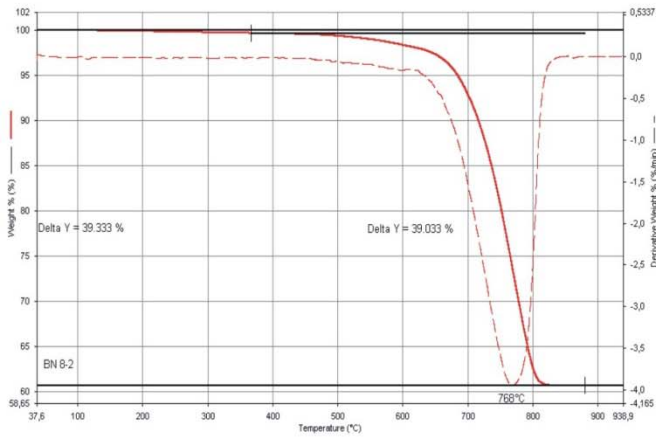


**C**

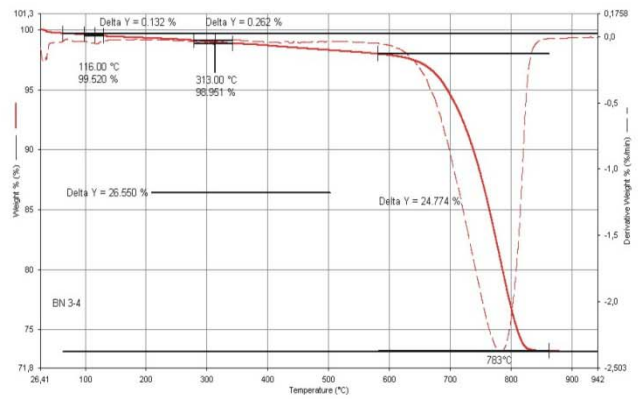
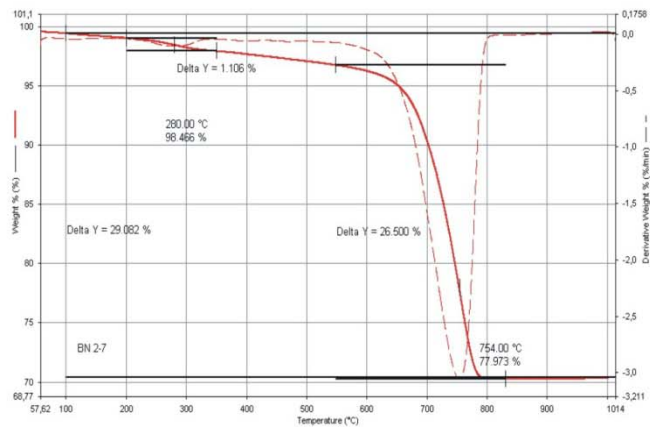
Figure (3-10): TGA curves of: A- Sample no.BN1/4 as untreated (left) and treated by acetic acid (right), B-Sample no.BN2/4 as untreated (left) and treated by acetic acid (right), C- Sample no.BN3/2as untreated (left) and treated by acetic acid (right).



D



E



F

Figure (3-10): Continued: TGA curves of the samples: D-Sample BN5/2 as untreated (left), treated by acetic acid (right), E-Sample BN8/2 as untreated (left), treated by acetic acid (right) and F-Sample no.BN2/7 untreated (left) and BN3/4 untreated (right).

Sample No.	Main Stages	Step	Temp/c□		Weight Loss Step %	Weight Loss All %	W.L.D T&N.T %	Interpretation
			From	To				
BN1/4	3	1	290	347	.0.530	32.728	19.522	Dehydroxolation (dhx.), of goethite to form hematite.
		2	440	638	3.817			At the beginning dhx. of kaolinite, then decomposition(dcm.) of siderite occurred, and dhx. of glauconite probably also occurred.
		3	650	842	26.865			dcm. of :impure calcite, chamosite , ankerite, and phosphates.
BN1/4 Acid	5	1	200	287	1.046	13.206		Dehydration of limonite(dhd.) to form goethite, and probably dhd .of poorly crystalline goethite occurred.
		2	288	345	1.366			Dhx. of goethite to form hematite.
		3	353	428	0.638			Dhx. of goethite differs in Al-content and its crystallinity than previous goethite.
		4	428	621	7.251			Dhx. of kaolinite and dcm. of siderite.
		5	622	708	1.294			dcm.or dhx of glauconite and dcm. of ankerite and phosphates.
BN2/4	2	1	201	346	20.006	35.196	24.049	At the beginning, dhd. of limonite to form goethite probably occurred, then dhx. of goethite to form hematite surly occurred.
		2	581	838	32.481			Dcm. of: impure calcite.siderite , ankerite, chamosite and phosphates.
BN2/4 Acid	4	1	50	150	1.188	11.147		Water adsorbed released.
		2	170	259	2.531			Dhd. of limonite to form goethite.
		3	263	363	4.761			Dhx. of goethite to form hematite.
		4	369	500	1.170			At the beginning, dhx. of goethite differs in Al-content and crystallinity than previous to form hematite, then dhx. of kaolinite.

Table (3-2): Shows the results of TGA analyses derived from TGA curves shown in Figure (3-10), (W.L. D for T&N.T: weight loss differentiation between treated and non treated samples).

Sample No.	Main Stages	Step	Temp/c□		Weight Loss Step %	Weight Loss All %	W.L.D T&N.T %	Interpretation
			From	To				
BN3/2	2	1	200	325	1.494	35.623	24.28	Dhd. of limonite to form goethite, then dhx. of goethite to form hematite.
		2	585	850	31.769			Dcm. of: impure calcite , siderite, ankerite, and chamosite.
BN3/2 Acid	2	1	313	348	1.24	11.343		Dhx. of goethite to form hematite .
		2	352	700	3.418			At the beginning, dhx. of goethite differs in Al-content than previous goethite to form hematite ,and after 400 C ° dcm. of: kaolinite occurred (first), then glauconit,siderite,ankerite and phosphates(later).
BN3/4	3	1	99	140	0.132			Water adsorbed release.
		2	295	335	0.262			Dhx. of goethite to form hematite.
		3	581	863	24.774			Dcm. of : impure calcite siderite ,ankerite ,chamosite ,glauconite ,chamosite and phosphates .
BN5/2	2	1	212	316	1.607	36.228	22.958	Dhd. of limonite to form goethite and then dhx. of goethite to form hematite.
		2	579	828	33.354			Nearly like step 2 in BN3/2.
BN5/2 Acid	4	1	65	96	0.651	13.27		Water adsorbed release.
		2	160	338	5.993			At the beginning, dhd. of limonite to form goethite, then dhx. of goethite to form hematite.
		3	348	520	2.706			At the beginning, dhx. of goethite differ in AL-content and crystallinity than previous occurred , and over 400 dcm. of kaolinite also occurred .
		4	600	700	0.581			Dcm. of siderite , ankerite and probably dhx. of glauconite and dcm. of Phosphates.

Table (3-2): continued.

Sample No.	Main Stages	Step	Temp/c□		Weight Loss Step %	Weight Loss All %	W.L.D T&N.T %	Interpretation
			From	To				
BN8/2	1	1	501	840	39.033	39.333	21.277	Dhx. of kaolinite at the beginning occurred, then dhx. of glauconite & chamosite, and dcm. of carbonates (siderite, ankerite and impure calcite) also probably occurred.
BN8/2 Acid	7	1	100	140	0.100	18.056		Adsorbed water released.
		2	199	278	0.495			Dhd. of limonite to form goethite.
		3	279	338	0.596			Dhx. of goethite to form hematite.
		4	422	516	1.262			Dhx. of kaolinite.
		5	519	600	4.346			Dcm. of siderite.
		6	600	630	1.079			Dhx. of glauconite.
		7	630	800	9.255			Dcm. of ankerite and phosphates.
BN2/7	2	1	216	331	1.106	29.082		At the beginning, the dhd. of goethite to form hematite probably occurred ,and later, dhd. of goethite differs in crystalinity than previous one to form hematite also occurred.
		2	564	809	26.500			Dcm. of impure calcite besides: chamosite, siderite, ankerite, phosphates and probably glauconite.

Table (3-2): continued.

### 3-5 Fourier Transform Infrared Spectroscopy (FTIR):

FTIR has been successfully used as an alternative to XRD in the analysis of sedimentary minerals where common minerals exhibit unique absorbance spectra in the mid-IR range, which extends from  $400\text{ cm}^{-1}$  to  $4000\text{ cm}^{-1}$  (Herron et al, 1997).

Ten samples of IRS belong to BN1 and BN5 sections have been chosen for FTIR analysis using instrument type IFS66 at resolution  $2\text{ cm}^{-1}$  (32 scan), the results are shown in (Fig. 3-11).

FTIR spectra of IRS were compared with FDM-FTIR spectra charts of minerals and inorganic components (Fiveash data management INC. 1997-2008). They also compared with spectra minerals charts in the atlas of infrared spectroscopy of minerals according to (Vandermarel and Beutelsparcher, 1976).

It is apparent that the spectra of IRS samples are characterized essentially by five main regions interpreted as follow:

The asymmetric internal stretching mode (C) as shown in (Fig.3-11) is characteristically broad for many carbonates in IRS samples (calcite, siderite and ankerite). The similarity in the structures of calcite group minerals is reflected in their infrared spectra (Haung and Kerr, 1980). However, infrared vibrations of calcite  $1422\text{ cm}^{-1}$  and  $712\text{ cm}^{-1}$  are clearly shown on the FTIR results graphs of Benavi IRS samples. Siderite characterized by large intensity at  $1800\text{ cm}^{-1}$  (Vandermarel and Beutelsparcher, 1976) clearly shown in (Fig. 3-11).

The slight variability in peak position, peak height and in full-width at half maximum for calcite bands indicates the replacement of  $\text{Mg}^{+2}$ ,  $\text{Fe}^{+2}$  and  $\text{Mn}^{+2}$  within calcite structure during substitution (Dubrawski and Channon, 1989). Furthermore, the significant frequency shifts in the vibrational bands of the calcite occur as a function of chemical composition; these shifts are due to cationic substitution reflecting the different ionic radii (Bottcher et al, 1992). Thus, FTIR results confirmed the presence of impure calcite in IRS samples in accordance with the results of XRD, EDS and TGA. The main spectra of goethite are observed at  $870\text{ cm}^{-1}$  which represent Fe-OH band (Al-youzbaky, 1989). Hematite was identified by the peaks at:

425, 463 & 600  $\text{cm}^{-1}$ . The main absorbance of phosphates in FTIR spectra is observed at 1035  $\text{cm}^{-1}$  (Wright and Schwarcz, 1996), and the range bands of phosphates are (1077  $\text{cm}^{-1}$  - 1160  $\text{cm}^{-1}$ ) were also observed (Arai and Sparks, 2001).

The chlorite spectra were determined at (1082  $\text{cm}^{-1}$  & 668  $\text{cm}^{-1}$ ). Quartz was also identified by: 798  $\text{cm}^{-1}$  & 779  $\text{cm}^{-1}$  doublet. Thus, the mineralogy of Benavi IRS samples identified in FTIR technique is consistent with that found by XRD.

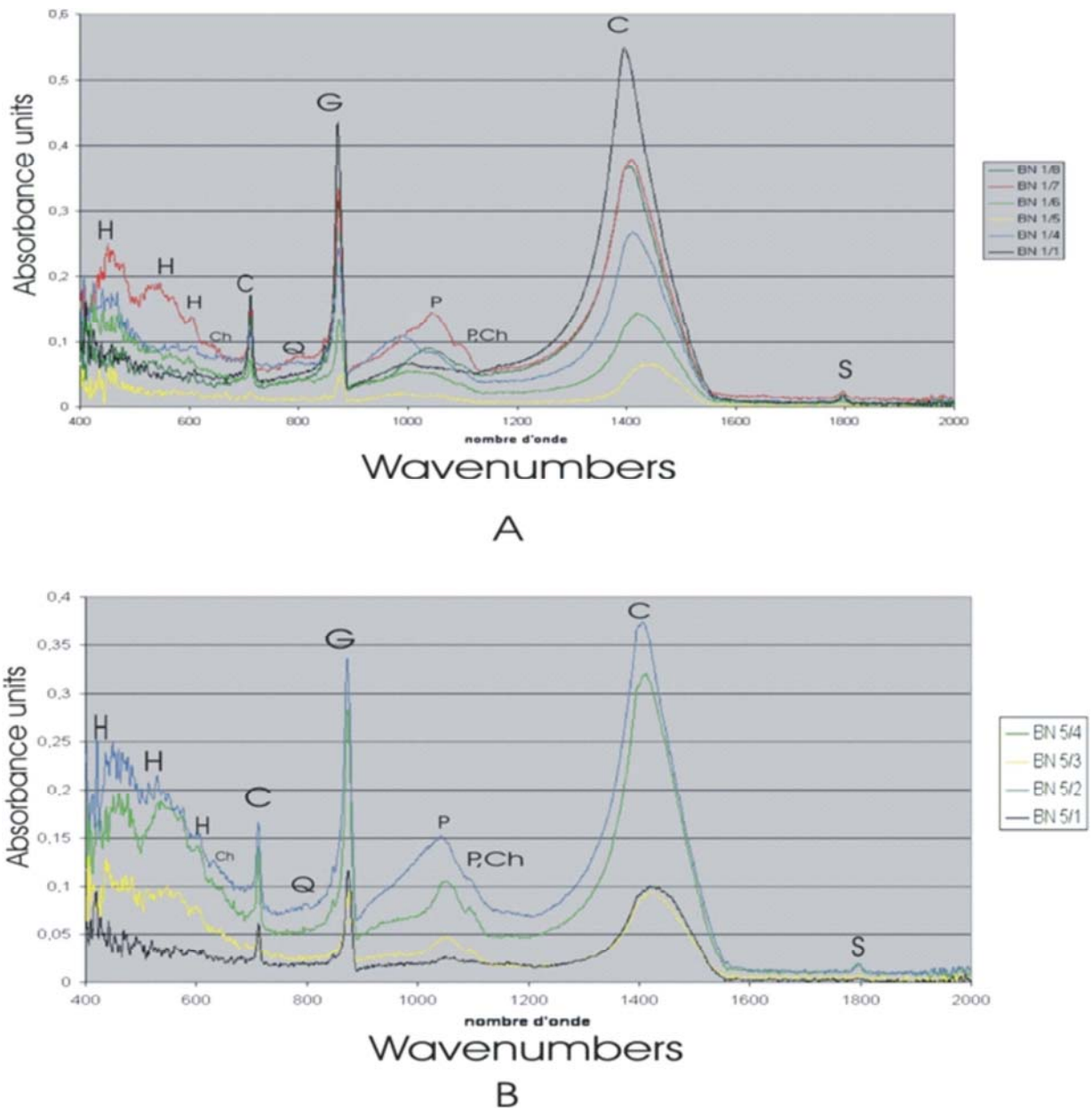


Figure (3-11): Shows FTIR spectra of IRS samples of the sections: A-BN1 & B-BN5.

Where: C= Calcite, G=Goethite, H=Hematite, Q=Quartz, P=Phosphates, Ch=Chlorite and S=Siderite.

### 3-6 Discussion:

Mineralogical study of Benavi IRS samples by XRD, SEM, EDS, TGA and FTIR techniques showed that these samples are mainly composed of mineral assemblages including: carbonates (calcite, siderite, ankerite), iron oxides/ hydroxides minerals (hematite, goethite and/or limonite, magnetite), sulphide iron minerals (pyrite & arsenopyrite), silicates minerals { kaolinite, chlorite(chamosite), glauconite, quartz } and apatite. Sepiolite is observed just in the overlying country rocks of IRS.

The relationship of these minerals throughout the IRS throws some light on the diagenetic history of IRS.

XRD results showed that there is negative relationship between calcite and iron oxides /hydroxides in the IRS. This is probably due to the loss of carbonate that took place during the oxidation of ferrous iron to ferric and release of  $H^+$  where the initial calcite had been dissolved and replacement of iron oxides/ hydroxides occurred. The later minerals probably undergone structural transformation when entering an anoxic environment. These transformations were investigated by many researchers where high specific surface area of iron oxides/ hydroxides act as important sorbents to dissolve species: particularly heavy metals, phosphates and arsenate, then under reduction conditions most of the adsorbed species released from iron oxides /hydroxides surfaces (Pedersen, 2006). This may give a clue about the presence of phosphate minerals in the IRS samples, as well as, the presence of arsenopyrite in the lower part of IRS in Benavi area.

The negative relationship between chamosite with: kaolinite and iron oxides/hydroxides may shade some light on the formation of chamosite from kaolinite and iron oxides/ hydroxides under reduced conditions (Gartner and Schellmann, 1965), where kaolinite may have recrystallized or transformed to chamosite under reducing conditions in the availability of  $Mg^{+2}$  and iron oxides (Mucke and Farshad, 2005).

On the other hand, the negative relationship observed between chamosite and iron oxides/ hydroxides is good evidence about oxidized chamosite to form goethite under weathering circumstances beyond exposure of IRS (Taylor, 1949).

XRD showed the presence of hematite poor in Al-content and also showed presence of goethite rich in Al-content, whereas TGA proved the presence of two types of goethite differ in Al content (rich & poor Al-goethite). The Al-poor hematite most probably originated by dehydration of primary Al-poor goethite in the absence of water or elevated temperatures.

In the other side, Al- rich goethite (secondary goethite) probably produced by the weathering processes which caused goethitization of chamosite and pyrite as well as probably siderite; this goethitization may have occurred after exposure of Benavi IRS where Kampf and Schwertmann (1983) reported that Al-substitution in goethite relates positively with surface weathering circumstances; SEM and EDS analyses clearly showed the goethitization of pyrite and chamosite. This yield interpretation to the source of present goethite in IRS and why the middle part of Benavi IRS looks yellow to yellowish brown in its color at present.

## *Chapter Four*

# *Petrography*

**4-1 Preface:**

In this study, we adopted the definition of "microfacies" after Flugel (1982) "Microfacies is the total of all the paleontological and sedimentological criteria which can be classified in thin section ", the system of classification that modified after Dunham (1962) and expanded by Embry and Klovan, (1971). This system is most widely used as it is based on the simplest textural classification (the particle fabric and the kind of particle binding during sedimentation). This textural classification is the first step to identify the lithofacies of the studied samples aiming at recognizing their original depositional environment.

According to this classification, limestones are divided in to three main textural groups: mud - supported (mudstone and wackstone), grain-supported (packstone and grainstone) and biologically bound during deposition (boundstone). Mudstones and wackstones contain less than 10 % grains; mud is still present in packstone which are grain-supported but totally lacked in grainstones.

Dunham classification provides a clue to the environmental energy during deposition; mudstone reflects low energy on the contrary of grainstone (Tucker, 1981).

This chapter depends upon the cumulative knowledge acquired through microscopic analyses of thin and polished sections, in addition to part of SEM observations which contributed to the identification of opaque minerals with their textural relationships supported by unique BSE images.

The point counting Punktfeld -method after Sander (1951) and improved by Chayes (1956) in (Flugel, 1982) was carried out for (36) thin sections represent the whole (IRS). The results are shown in Table (4-1), and in the 3-D Pie charts (Fig. 4-1) as well.

The petrographic study was focused on IRS details more than the country rocks that are poor in iron content.

Sample No.	Mineralogical Constituents %								Calcite Components %						Iron Oxides %		
									Groundmass		Allochems			Secondary Calcite (filled veinlets)	Intergranular and intragranular	Coated	Replacement
	Calcite	Dolomite	Siderite	Phosphate	Chamosite	Glaucanite	Iron oxides	Quartz	Spary	Micrite and Microspar	Lithoclast	Algae	Other Bioclasts				
BN1/1	93.4	-	1.0	2.0	-	-	3.6	-	22.0	2.6	-	56.6	9.6	2.6	0.6	1.0	2.0
BN1/2	88.0	1.0	3.0	1.0	-	-	5.0	2.0	25.0	2.0	-	50.0	10.0	1.0	0.4	1.0	3.6
BN1/3	60.0	-	2.0	1.0	-	9	27.0	1.0	23.0	-	3.0	30.0	4.0	-	3.0	4.0	20.0
BN1/4	55.6	-	1.4	9.0	8.0	1.4	22.6	2.0	24.3	-	10.0	16.3	5.0	-	10.0	2.0	10.6
BN1/5	52.6	-	2.0	6.0	3.0	1.0	34.0	1.4	14.0	1.0	2.0	24.0	10	1.6	6.0	6.0	22.0
BN1/6	67.0	-	3.0	-	-	-	30.0	-	18.0	2.0	-	40	6	1.0	6.0	6.0	18.0
BN1/7	62.5	-	3.0	-	-	-	34.5	-	24.5	-	2.0	29.5	3.5	3.0	5.0	4.5	25.0
BN2/3	80	-	1.0	4.0	-	0.5	14.0	0.5	37	-	-	41	2	-	1	8	5
BN2/4	60	-	2.0	2.0	-	1.5	34.5	-	31.5	-	-	28.5	-	-	-	2	32.5
BN2/5	78	-	1.0	1.0	-	1.0	19.0	-	16.0	1.0	10.0	26	18.0	7	5	3	11
BN2/7	52	-	3.0	4.0	-	-	41.0	-	38.0	0.0	0.0	12	2.0	0.0	-	6	35
BN2/8	80	-	-	-	-	2	18	-	34	-	17	22	4.0	3	-	6.5	11.5
BN3/1	74	-	-	-	-	1	22	3	27	1.0	10	29	6	1	1	14	7
BN3/2	64	-	-	-	-	1	35	-	20	-	-	32	12	-	3	6	26
BN3/3	63	0.5	0.5	1	-	1	33	1	19	-	-	27	15	2.0	2.0	3.0	28
BN4/1	58	-	0.6	0.3	-	2.6	35.6	2.9	18	2	8	20	9	1.0	-	11.6	24.0
BN4/2	53	-	-	-	-	4.0	42	1.0	21	1	10	17	4	-	19	8	15
BN5/1	76.0	2.0	9.0	4.0	-	1.0	5.0	3.0	30	-	2.0	38	5	1	-	2.0	3.0
BN5/2	35	0.5	18	2.5	-	3.0	41.0	-	10	1	3.0	11	10	-	26	4	11
BN5/3	41	0.5	19.5	2	-	1.5	34	1.5	11	2.0	0.5	15	12	0.5	15	2	17
BN5/4	49	-	4.0	1.5	-	1.5	43	1.0	21	2	-	24	2	-	5.0	10.0	28.0
BN5/5	50	-	4.0	1.0	-	4.0	41.0	-	20	-	1	20	9	-	9	9	23
BN6/2	89	-	1	0.5	-	1.5	4.0	4.0	30	1	3	26	25	4.0	-	-	4.0
BN6/4	57	-	3.0	-	-	1.0	38	1.0	17	2	0.5	30	7.5	-	4	12	22
BN6/5	49	-	7.0	1.0	-	-	40	3	15	1	-	25	8.0	-	14	12	14
BN7	66	-	-	-	-	-	34	-	26	1	1	28	10	-	2	6	26
BN8/2	65.5	-	2.1	5	8.7	-	16.2	2.5	15.7	-	-	36.7	13.2	-	7.5	5	3.7
BN8/3	64.6	-	-	-	0.6	2.6	30.6	1.6	31.0	-	-	27	6.6	-	1	5	24.6
BN8/4	51	0.3	1.0	-	-	6.7	39	2	25	1	1	17	7	-	2	4	33
BN8/5	53.7	-	3.0	1.0	-	1.0	39.7	1.6	19	1.0	2.0	27	3.7	1	11.2	5.5	23.0
BN9/1	74.5	-	-	2.5	6.0	1.5	14.5	1.0	23.5	0.5	3.0	40	7.5	-	1.5	0.5	12.5
BN9/2	55	-	4	2	1	2	35	1.0	20	-	5	20	10	-	4	5	26
BN9/3	60	4	1	-	-	2.0	32	1.0	20	-	2.0	25	12	1	2	7	23
BN10/1	49	-	3	3	1	4	36	4	18	-	3	23	5	-	16	11	9
BN10/2	57.5	-	1.0	-	-	-	39.5	2.0	20.5	-	-	30	7	-	10.5	9	20
BN10/3	53	-	1.0	-	-	-	44	2.0	17.5	-	-	30	5.5	-	5.0	9	30
Max.	93.4	4	19.5	9.0	8.7	9	44	4.0	38	2.6	17	56.6	25	7	26	14	35
Min.	35	0.3	0.5	0.5	0.6	0.5	3.6	0.5	10	0	0	11	2	0	0.4	0.5	2
Av.	62.2	1.4	4.0	2.6	4.1	2.4	29.0	1.9	22.3	1.3	4.6	27.9	8.4	2.0	7.0	6.0	18.0

Table (4-1): Point counting results of thin sections (Petrographic study) based on Punktfeld-method after Sander (1951) and improved by Chayes (1956) (in Flugel, 1982).

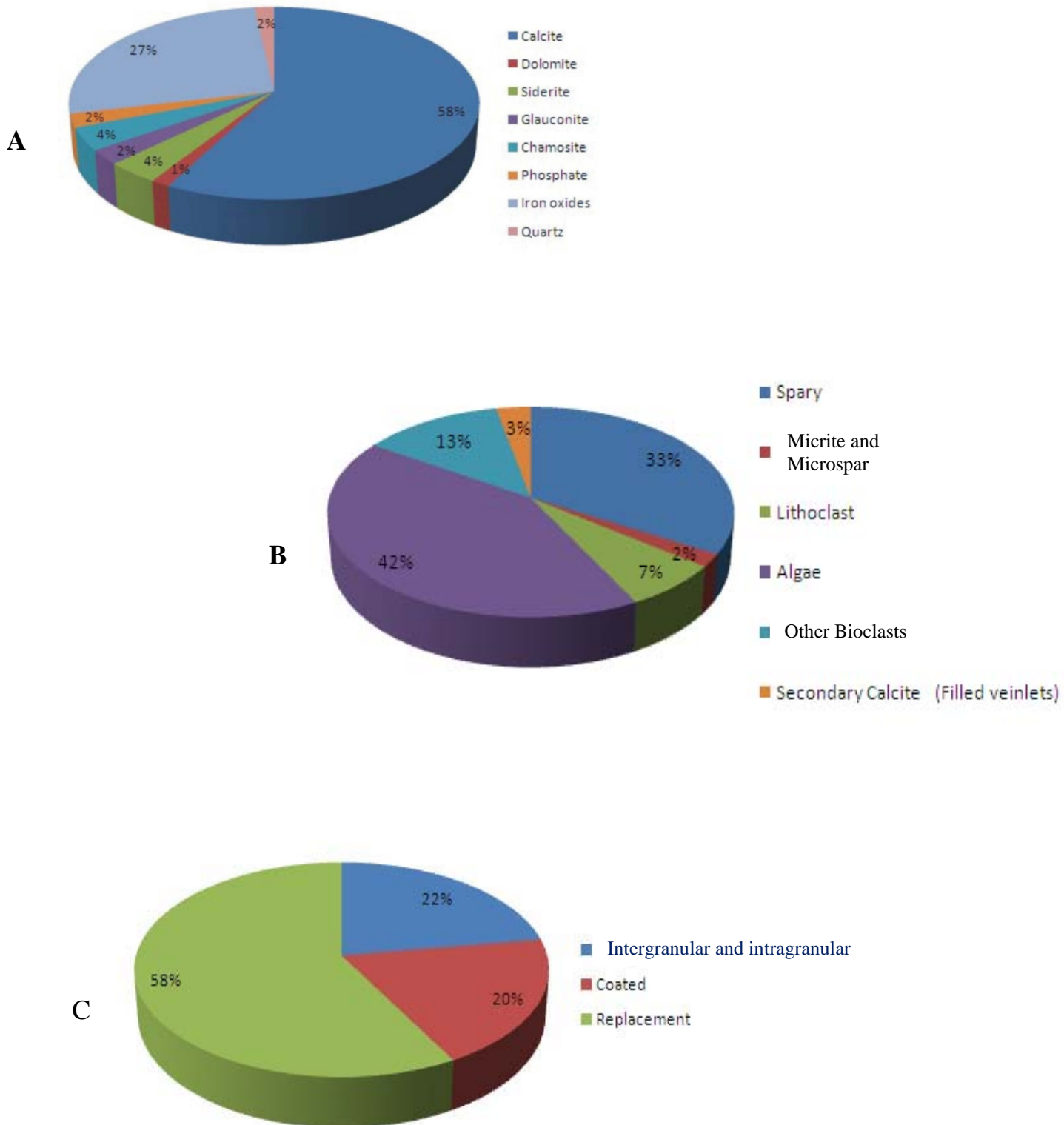


Figure (4-1): 3-D Pie charts based upon point counting results of Benavi IRS samples showing in: A- the general mineralogical constituents, B- calcite components, and C- iron oxides occurrences.

## **4-2 Country rocks:**

Country or surrounding rocks in this work refer to the iron-poor carbonate rocks which underlie and overlie IRS.

These country rocks can be classified to three main types:

1-Wackstone : characterized by the presence of stylolite (Plate 4-1-A ) . It outcrops under BN1 and BN2 sections at the eastern part of the IRS outcrop .This facies probably belongs to Chia Gara formation (Late Jurassic ) according to (Hamza and Isaac, 1971; Mc Carthy, 1955).

2-Dolostone: the outcrop of this facies appears under BN6 section and extends to the end of the lower western part of IRS outcrop. It is characterized by subhedral dolomite crystals (Plate 4-1-B); this facies is probably belongs to Barsarin formation (Late Jurassic), (Hamza and Isaac, 1971).

The wackstone and dolostone represent the country rocks which lie below IRS.

3- Bioclastic packstone: This facies overlies IRS and characterized by high neomorphism effect and the presence of rudist (Plate 4-1-C). Previous studies mentioned that Benavi IRS with the overlying rocks are belong to Hadiena formation (Late Cretaceous), (Wetzel, 1950; Chaickin, 1970; Buday and Vanecek, 1971; Geozavod, 1981).

## **4-3 Host rocks (IRS) classification and petrography:**

### **4-3-1 (IRS) classification:**

Actually, the reason we adopt Dunham classification is because the IRS (the ore body) is a limestone rich in iron contents. The microscopic analyses showed that the original facies of IRS is an algal- bioclastic - packstone according to the mentioned classification and the estimation by point counting results are shown in Table (4-1).

This facies suffered from many diagenetic processes, the explanations of which are mentioned later in (4-4) of this chapter.

Hallsworth and Knox (1999) mentioned that the iron rich sediments textural classification follows the textural limestone scheme. This classification scheme is summarized in Table (4-2); therefore and based on above, IRS of Benavi belongs to (iron- packstone).

Depositional texture recognisable					Depositional texture not recognisable
Contains matrix (silt and clay < 32 µm in diameter)			Lacks matrix	Components bound together by action of plants and animals in the position of growth	
Matrix-supported		Grain-supported			
> 75% matrix	< 75% matrix				
<b><u>iron-mudstone</u></b>	<b><u>iron-wackestone</u></b>	<b><u>iron-packstone</u></b>	<b><u>iron-grainstone</u></b>	<b><u>iron-boundstone</u></b>	<b>ironstone</b> (use qualifiers to describe crystal size)

Table (4-2): Shows textural classification of iron- rich sediments (ironstone), after Hallsworth and Knox (1999).

#### 4-3-2 (IRS) petrography:

The main petrographical constituents in IRS are allochems and spary calcite cement. The allochems composed of high amount of skeletal components including calcareous red algae and other bioclasts with very small amounts of non-skeletal components (lithoclasts, detrital minerals and clay ).

Calcareous red algae are very common in all IRS samples; they have skeletons composed of cryptocrystalline calcite (Tucker, 1981). Their size are measured with a range (0.11-1.68 mm), and regular cellular structure is present (Plate 4-1-D).

Bioclasts is less common compared with red algae including echinoderms, shell fragments with few amount of foraminifera. Echinoderms acts optically as a single crystal of calcite, consequently each element uniformly extinct under crossed nicols in a polarizing microscope. The uniform optical reaction of these skeleton elements is caused by the parallel arrangement of the c-axes of the calcite crystals which constitute the skeletal elements (Plate 4-1-E and F), (Flügel, 1982). Most of the studied samples contain echinoderms, their sizes range between 0.3 mm to 1.4 mm in diameter.

Shell fragments are less common, in comparison with echinoderms that range in size between 0.36 mm to 0.78 mm (Plate 4-1-G).

Foraminifera are observed in some samples and biserial type is more common than other foraminifera species (Plate 4-1-H). Sponge specules is also observed in some samples (Plate 4-1-I).

The groundmass of the studied samples is mainly composed of spary calcite cement crystals, and the sizes of calcite crystals range between 0.032 mm to 0.17 mm.

#### **4-4 Diagenetic processes:**

Diagenesis is a term used to define all the changes that occur in sediments during the interval between deposition and before the transition to metamorphism. These diagenetic changes may take place in the submarine, subaerial fresh water and subsurface environments (Larsen and Chilingar, 1979 ). Benavi IRS suffered from many diagenetic processes through its geological history. Replacements effects are the most common where the replacements processes have been observed in all IRS samples. the following are the main types of diagenetic processes which observed in studied samples.

##### **4-4-1 Iron oxides replacement:**

In general, the replacement includes two processes: dissolution of an original mineral and the cavities replaced by another one (Tucker, 1981)

Iron oxides replacement is the most important one among replacement processes occurred in the diagenetic history of IRS. Partial replacement of fossils by iron oxides is very common (Plate 4-2-A). Complete replacement is common too (Plate 4-2-B). Locally, iron oxides have replaced the calcareous structures produced deposits of higher than usual content. Iron oxides observed as coating of grains (Plate 4-2-C), filled pores (intragranular) (Plate 4-2-D), between grains (intergranular) (Plate 4-2-E), and replaces fossils especially red algae. Estimation of the percentage of each case was measured by point counting (Fig. 4-1-C).

The euhedral crystals of iron minerals are widely distributed in IRS range in size (0.02-0.94 mm), the morphology of these minerals includes: hexagonal (Plate 4-2-F), and cubic in shape (Plate 4-2-G), twin cubic shape is also present (Plate 4-2-H).

Selective dissolution for algae to iron oxides replacement has been observed in many of IRS samples, this reflects that the resistances of fossils present in IRS to dissolution was not the same (selley, 2007).

#### **4-4-2 Glauconitization:**

Glauconite occurs in very small amount at the base of IRS, especially in the following samples: BNI/4, BN1/5, BN3/4, BN9/1 and BN10/1 associated with pyrite, phosphates and chamosite. The presence of glauconite indicates submarine conditions in areas of low sedimentation rate in a confined environment (Odin and Matter, 1981). Plates (4-3-A, B, C) show the growth of glauconite inside fossils due to the prevailing of confined microenvironment.

#### **4-4-3 Phosphatization:**

Phosphate minerals are found in IRS samples but in minor amounts. Apatite and collophane were the two phosphates mineral recognized in the studied samples.

The first was distinguished by its habit as minute six-sided prismatic crystals with its parallal extinction (Plate 4-3- D); the size of apatite crystals ranges between 0.05 mm to 0.19 mm. Apatite is prominent in some iron ores (Kerr, 1959).

The second is distinguished by its massive form, which appears under plane polarized light (PPL) in light to dark brown in color, occasionally it was colorless, and by its isotropic characteristic under cross nicoles (XPL) (Kerr, 1959).

Partial phosphatization of fossils is common (Plate 4-3-E, F) and complete replacement are observed in many samples (4-3-G, H), some of original phosphatic bones are also present. The solubility of phosphates decreases with increasing temperature and pH. When these changes occur, phosphate tends to precipitate (selly, 2007). The vital circumstances of replacing calcite by phosphates are:

non- depositional environment, high carbonate components, marine solution rich in  $\text{Ca}^{+2}$ , pH more than 7 and high amount of phosphates ions ( Ali, 2007).

#### **4-4-4 Chamosite formation and sideritization:**

Microscopic analyses showed occurrences of chamosite and siderite in most IRS samples as shown in Table (4-1).

In Benavi IRS the chamosite occurs around grains which often forms the outer rim of completely or partially impregnation fossils by iron oxides, and it is distinguished by its pale green color under plane polarized light(Plate 4-4-A,B,C) .

Chamosite occurrence around fossils that are not affected by iron oxides replacement is also observed (Plate 4-4-D). The presence of chamosite as coating of impregnation fossils by iron oxides reveals that the paragenesis is probably; iron oxides replacement preceded chamosite formation through diagenetic history of IRS.

Siderite marked by interlocking rhombic grains characterized by brown stains around their borders and along cleavage cracks (Plate 4-4-E, F).

Carbonate iron sediments usually form when iron precipitates in the presence of dissolved carbonic acid or as a result of interaction of the primary sediments with organic matter in the course of diagenesis (Melnik, 1982).

Siderite is mostly widespread in sedimentary iron ores. The important feature of siderite is its extreme instability where it is clearly oxidized to form: goethite, hematite and other iron oxides/hydroxides minerals (Kholodov and Butuzova, 2004). Siderite also is a prominent mineral in the oolitic ironstones of England as associated with chamosite (Kerr, 1959).

#### **4-4-5 Pyritization:**

Pyrite occurs as euhedral or clusters of euhedral crystals. It is randomly distributed within the IRS. Pyritization is quite clear in samples: BN1/4, BN1/5, BN2/8, BN9/1, BN10/1 and BN5/4.

Pyritization indicates anoxic or dysaerobic environments (Berner ,1970). It may

be formed in diagenetic environments characterized by slow detrital addition, abundant organic matter and readily available sulfate maintain high sulfide activities (Curtis and Spears, 1968). Pyrite is the most common sulfide mineral in marine and lacustrine sediments where its formation takes place via sulfate reduction in anoxic sediments. The biologic process in low temperature sedimentary environment is the result of the oxidation of organic matter that occurs through bacterial reduction of sulfate and the production of hydrogen sulfide that reacts with iron from detritus or other sources to form amorphous monosulfide (FeS) precipitates.

Many experiments have shown that an oxidant is required to produce pyrite from precursor iron monosulfide (Neumann et al, 2005) where the major steps to form sedimentary pyrite are: bacterial sulfate reduction, reaction of H<sub>2</sub>S with iron minerals to form iron monosulfide and reaction of iron monosulfide with elemental sulfur to form pyrite (Berner, 1984). Postdepositional sulfidisation take place where the downward diffusion of H<sub>2</sub>S is balanced by upward migration of Fe<sup>+2</sup> which combined with sulfur to form pyrite (Neumann et al, 2005).

#### **4-4-6 Silicification:**

Selective replacement of fossils by silica was identified, where some bioclasts especially algae have been observed replaced by: euhedral quartz crystals that possibly authigenic in origin (Plate 4-5-A,B,C ,D), subhedral and anhedral quartz (Plate 4-5-E, F), and most probably chalcedony in part (Plate 4-5-G,H ).

The appropriate chemical conditions to dissolve calcite and precipitation of silica are supersaturated pores solutions by silica and decrease of pH and temperature (Blatt et al, 1972). The silicification can take place during early or late diagenesis (Tucker, 1981). The source of silica probably is endogenic from siliceous skelton debris including sponge spicules and radiolarian or the corrosion of quartz and clay minerals at high pH, when pH decreases precipitation of dissolved silica occurs; thus, this proces is produced by pH changes and decreases of temperature (Engelhardt, 1977).

**4-4-7 Cementation:**

Cementation is defined as a diagenetic process of cavity filling or open space filling through chemical precipitation of material from a solution on a free surface (Flügel, 1982).

The sparry calcite cement is distinguished based on calcite crystals morphology occupies the majority of the original pore space (Plates: 4-6-A&B).

**4-4-8 Neomorphism:**

This term introduced by Folk in 1965 for diagenetic processes in which older crystals are consumed and their places simultaneously occupied by new crystals of the same mineral or a polymorph.

Neomorphism includes inversion and recrystallization and refers to changes of morphology, size, and orientation of calcite crystals. It is a special form of replacement where the original and new minerals have the same chemical composition.

This feature is widespread in Benavi IRS and overlying country rocks (Plate 4-6-C) and (Plate 4-6-D), respectively.

In some samples, pyrite crystals have been observed as floats in the groundmass of sparry calcite cement. The intense affects of bioclasts by neomorphism processes probably give an interpretation for why these pyrite crystals look as floating grains (Plate 4-6-E, F, G, H). These Plates clarify how pyrite crystals released from the inside fossils to sparry calcite. Probably, this occurred by the intense phreatic meteoric diagenesis where these plates show fossils (algae) undergone from neomorphism and also show the microstructure of algae is still visible. This leads to the possibility of arranging events as follows:

Deposition → fossilization → pyritization (in reduced microenvironments inside fossils) → neomorphism (dissolution of calcareous fossils that recrystallized to sparry calcite where pyrite crystals present inside these fossils released gradually in to spar), (Bricker, 1971).

**4-4-9 Dolomitization:**

This diagenetic process is very limited in IRS samples. It is with difficulty observed in samples: BN1/2, BN3/3, BN5/1, BN5/2, BN5/3, BN8/4 and BN9/3 ( Plate 4-7-A ).

The presence of dolomite rhombs with silica, Plates( 4-7-B&C ) is interpreted to indicate that dolomitization preceded precipitation of silica as post depositional process ( Larsen and chilingar, 1979). The dolomitization is commonly the late phase of diagenetic history (Qureshi et al, 2005).

**4-4-10 Dedolomitization:**

This feature has been recognized in few samples (Plate 4-7-D). After dolomitization, the selective leaching for dolomite rhombohedron occurred and the pores partially filled by calcite druse (Evamy, 1967). This calcitization process is referred to dolomitization and predominantly takes place through contact with meteoric waters (Tucker, 1981).

According to De Groot (1967) dedolomitization can only take place at or near the earth's surface. This phenomenon is one of the late diagenetic processes (Dabbagh, 2006).

**4-4-11 Compaction:**

There are two types of compaction clearly observed in the studied samples:

A-Mechanical compaction: evidences for mechanical compaction are represented by sutured and corroded grains margins. Fractured and dislocated grains are also noticed (Plate 4-7-E).

B-Chemical compaction: chemical compaction and pressure dissolution of grains and sediments is a significant source of  $\text{CaCO}_3$  for burial cementation. Under conditions in which the pore fluid pressure is less than the lithostatic pressure there will be a preferential dissolution of quartz or calcite grains at high stress points where they touch and precipitate quartz and calcite cement in the adjacent interstices (Flugel, 1982).

The pressure solution structure in studied samples includes the following:

1-Condensed fabric: the surface between grains vary from having point and planar (Plate 4-7-F), interfering to sutured and corroded grain margins (Plate 4-7-G), depending upon the degree of dissolution and compaction (Flügel, 1982).

2-Stylolitization: Stylolites are the zones of discontinuity within rocks. In thin section, they have undulated to zigzag sutures; the stylolite transect the grains, rock fabric, cement and matrix indiscriminately. Irregular and low peaks amplitude stylolites (Trurnit, 1968 ) are observed in IRS and underlying country rocks samples, (Plate 4-7-H, I) respectively.

#### **4-5 Ore petrography:**

(25) Polished sections and (11) thin-polished sections were prepared of selected IRS samples, all these sections were studied under the microscope at polarized light; and the constituents and their intergrowths evaluated.

The following references are adopted for opaque minerals identification as well as ore textures: Edwards (1965), Ramdohr (1980 ), Vaughan and Craig (1981 ) and Spry & Gedlinske (1987). The results of ore microscopy study showed that there are few differences between the studied samples; the differences are given by the mineral content and the microstructures.

##### **4-5-1 General description:**

IRS samples mainly consist of bioclasts which are carbonates with varying contents of iron (Plate 4-8-A), they are frequently rimmed by limonite and the interstices and fissures are filled by hematite, limonite and calcite.

The pyrite preferably forms framboidal textures (Plate 4-8-B), which may be transformed to limonite or/and hematite in many samples (Plate 4-8-C); disseminated pyrite inside fossils is also present (Plate 4-8-D).

BN1/4 and BN8/2 samples appear as a relatively somehow different, these samples have a considerable high content of pyrite, it may reach some tens of  $\mu\text{m}$  in size or/and forming framboidal groupings of minute individuals (Plate 4-8-E), a significant amount

of idiomorphic magnetite is sometimes present. Euhedral crystals of arsenopyrite are also present. Arsenopyrite has been identified by its characteristic rhomb shape besides other optical properties (Vaughan and Craig, 1981) (Plate 4-8-F), it was found as a minor phase.

BN2/4 mainly consists of carbonate with biogenic structures, limonite is rather scarce, besides there are traces of framboidal pyrite, and calcite fills veinlets and interstices (Plate 4-8-G).

BN2/5 with high iron bioclasts, they are mainly cemented by limonite but also by some calcite. Traces of pyrite and rutile are present (Plate 4-8-H).

In BN2/8, besides the iron rich bioclasts, several hematite rich fragments are present, traces of magnetite were found (Plate 4-9-A).

BN5/2 also consists mainly of iron rich bioclasts, several idiomorphic aggregates of limonite are embedded there; there are framboidal pyrites altered to limonite (Plate 4-9-B).

BN5/3 showed bioclasts partially very rich in limonite and they are mainly cemented by limonite and to a lesser extent by calcite; some pseudomorph of limonite after idiomorphic pyrite (Plate 4-9-C). Also, relicts of pyrite embedded in goethite are present (Plate 4-9-D).

The bioclasts in BN5/4 are very rich in pseudomorphs of magnetite and hematite after framboidal pyrites (Plate 4-9-E, F), the cementing materials between the bioclasts are limonite and calcite. Many bioclasts in BN6/4 are rich in iron bearing carbonates, and they all are commonly rimmed by some hematite or limonite; the interstices are preferably filled by hematite and calcite (Plate 4-9-G).

Sample BN6/5, shows bioclasts moderately impregnated by hematite; it fills interstices too. The sample contains several fragments of magnetite (Plate 4-9-H).

In BN10/1, idiomorphic quartz is clearly shown, some framboidal pyrite frequently transformed to limonite and traces of rutile were detected at the polished section (Plate 4-10-A, B).

Samples: BN3/4, BN2/7, BN1/6, BN4/1, BN10/3, BN5/3, showed besides bioclasts with cementing hematite, they exhibit simple sedimentary texture: Alternating hematite rich and hematite poor carbonate layers with thicknesses between  $\sim 50\mu\text{m}$  &  $\sim 300\mu\text{m}$  (Gierth, 2008), (Plate 4-10-C). Some veinlets filled by calcite were observed in many of the IRS samples, they cut the structures of bioclasts that are coated by hematite (Plate 4-10-D). Significant amounts of magnetite were identified in samples: BN1/4, BN1/5, BN1/6, BN2/7, BN2/8, BN3/4, BN4/1, BN5/4, BN6/5 and BN10/3, distinguished by their moderate reflectivity, gray color and sometimes become duller and grayer (this may be attributed to the Mn content) (Ramdhor,1980), (Plate 4-10-E).

Euhedral pseudomorph magnetite after hematite, hexagonal in shape was also observed (Plate 4-10-F). Pseudomorph maghemite after magnetite was distinguished too by its bluish gray color, cubic habit and its isotropic behavior (Plate 4-10-G,H) (Vaughan and Craig, 1981). This mineral may be formed under certain conditions of oxidation from magnetite (Ramdohr, 1980). According to Alipour et al, (1995), maghemite is a common mineral in weathered profiles in arid, semi arid, sub tropical and tropical environments. The formation of maghemite has become attributed to aerial oxidation of magnetite.

#### **4-5-2 Ore textures:**

Ore microscopic study, as well as, BSE images showed that the most prominent ore textures observed in IRS samples are most likely produced by replacement processes. The replacement textures depend chiefly in their development on three features: cleavages, fractures and grain boundaries. Replacement is the result of a surface chemical reaction; there is a wide variety of replacement geometries like: inclusions, rim, zonal, idiomorphic ...so on, but they all appear to represent variations of the same processes (Vaughan and Craig, 1981). Many of these textures were observed in the studied samples like:

Rim texture (Plate 4-11-A), zonal texture (Plate 4-11-B), inclusions (Plate 4-11-C), and idiomorphic texture (Plate 4-11-D).

Inclusions are small particles of one mineral included in the material of another, this texture is observed predominant in some samples like: BN1/4, BN5/4 and BN8/2 which shows relics of pyrite inside goethite ( Plate 4-11-C and 4-9-D); this is probably produced by the alteration of pyrite to goethite through weathering (goethitization of pyrite ).

A vein replacement texture is observed as in (Plate 4-11-E, F), this generally a good evidence of their relative ages (Edwards, 1965). Porous texture is very common in most IRS samples (Plate 4-11-G, H); it is probably produced by dehydration of goethite to form hematite (Tobia, 1983). Oolitic texture is present (Plate 4-12-A); this texture is ubiquitous in the chamosite-bearing phanerozoic ironstones which are commonly known as minnete ores ( Bhattacharrya and Kakimoto, 1982).

BSE images showed a boxwork texture of hematite (Plate 4-12-B) where the microplaty hematite grains appear as thin plates ranging in size from 5 $\mu$ m to 10  $\mu$ m and are developed with no preferred orientation. Usually the orientation of microplaty hematite grains filled veinlets is as the orientation of these veinlets ( Plate 4-12-C &D), whereas the microplaty hematite filled pore space is randomly orientated (Plate 4-12-E).

Euhedral magnetite crystal up to 50  $\mu$ m was clearly observed embedded in carbonate matrix (Plate 4-12-F).

Framboidal texture of pyrite is very common and it is widely distributed in most Benavi IRS samples especially in samples: BN1/4, BN8/2, BN10/1 (Plate 4-8-B) (more details followed).

The goethite and magnetite framboidal texture is also present in many of IRS samples, they are possibly formed by the oxidation of original pyrite framboids (Wilkin and Barnes, 1997) (Plate 4-12-G&H).

#### 4-6 Framboids evolution:

BSE images showed that pyrite occurs as: euhedral crystals, framboids and massive forms (Fig .4-2-A, B, and D respectively). Goethitization of different pyrite forms is clearly observed in many IRS samples (Fig.4-2- C, D).

According to (Merinero et al, 2008), the euhedral pyrite is often a result from framboidal evolution and there is close spatial relationship between framboidal and euhedral pyrite that often observed in nature and suggest genetic relationship (Love, 1965; Love and Amstutz, 1966; Ostwald and England, 1977, 1979; Sawlowicz, 1987, 1993). Multi-faceted framboids with regular arrangement of microcrystals represent the link between these two morphologies (Sawlowicz, 1993). (Love and Amstutz, 1966) suggested the possibility of recrystallization from framboidal to single grain pyrite.

Sawlowicz (1993) developed this suggestion and proposed a continuous growth of microcrystals in the framboids (sometimes towards euhedral crystals).

Frias et al, (1997) defined a textural evolution pattern where framboids were progressively better faceted until they become euhedral in morphology.

In the studied samples of Benavi IRS, some intermediate steps of this pattern have been identified which is characterized by:

1-Irregular arrangement of pyrite microcrystals (before complete framboid formation), as shown in (Fig.4-3-A).

2- Spherical microcrystals packing to form complete framboids of pyrite, and gradually loss of framboidal texture (before transforming to euhedral crystals), (Fig.4-3-B).

3-Faces development to form euhedral texture crystal without internal framboidal texture, (Fig.4-3-C).

**This textural evolution proposed by (Merinero et al, 2008) is clearly shown in (Fig. 4-3).**

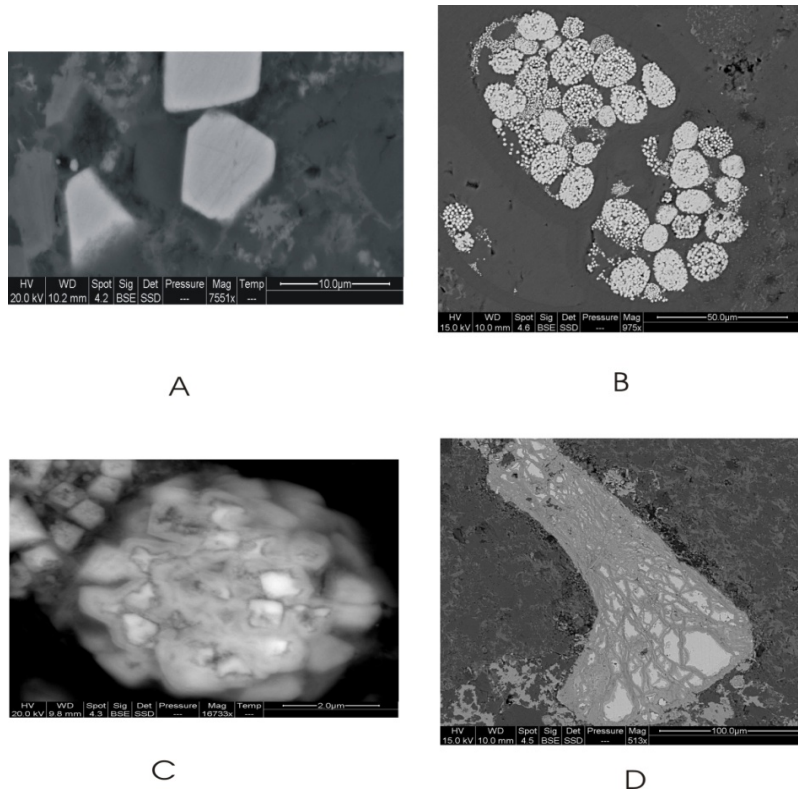


Figure (4-2): BSE images shows: A-Euhedral pyrite crystals, B-Framboids of pyrite crystals, C-Goethitization of pyrite framboids, and D-goethitization of massive pyrite.

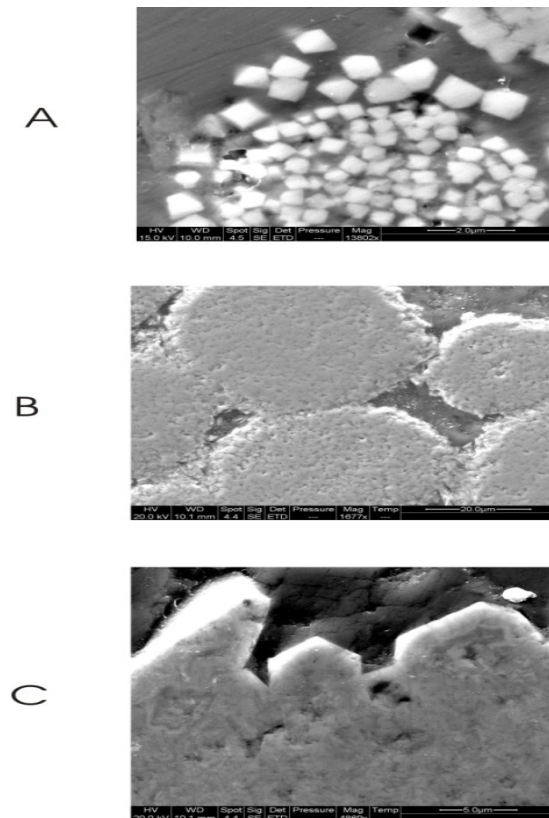


Figure (4-3): BSE images reveal the textural evolution of framboids pyrite to euhedral pyrite morphology in IRS samples after (Merinero et al, 2008): A-Irregular stage, B-Spherical stage (framboidal texture), and C- Euhedral texture after loss of internal framboidal texture.

#### 4-7 Discussion:

The petrographical observations of thin and ore polished sections have revealed the main stages of Benavi (IRS) formation.

The first stage is the deposition of algal- bioclastic - packstone under warm climate in shallow marine high energy. The fossils assemblages (algae, echinoderm ...) reflects this environment (Flügel, 1982). Presence of spary calcite cement also supports this opinion because a lack of micrite denotes high energy environment (Tucker, 1981).

Petrographical observations indicated that dissolution of fossils preceded the precipitation of iron oxides and sometimes there is selective dissolution occurred (Selley, 2007); where these observations showed that algae affected more than other particles by dissolution and replacement processes. During early diagenesis at shallow burial conditions, changes in oxidation fugacity can result in the precipitation of iron as goethite and hematite under oxidizing conditions (atmospheric effect). Probably slightly acidic solution rich in  $\text{Fe}^{+2}$  penetrated to this facies along fissures and fractures then reacted with the calcareous constituents and dissolved it partially and completely in parts where  $\text{Fe}^{+2}$  oxidized to  $\text{Fe}^{+3}$  and precipitate (Melnik, 1982). Oxidation of  $\text{Fe}^{+2}$  led to release of  $\text{H}^+$ ; the precipitation of  $\text{CaCO}_3$  would be inhibited during periods of iron minerals formation; otherwise these environments would be ideal for carbonates formation explaining the similarity in texture between iron formations and carbonates (Maynard, 1983). In this stage, bacteria may have played an important part in the formation of iron oxides (Stanton, 1972). The ferric oxides /hydroxides that formed in this stage are important predecessors to minerals formed later such as, magnetite that were produced during early diagenesis near the sediment/water interface (Johnson et al, 2008).

The presence of chamosite in most IRS samples contributes to understand the precisely of next stage where the formation of chamosite may have occurred after previous oxidized stage when Eh and pH changed. The reduction conditions are necessary for chamosite formation under marine conditions. The reduction of iron in diagenetic environments followed by de-hydration would favor transformation to

chamosite (Curtis and Spears, 1968), and also, chamosite may be formed from hydrated iron oxides and detrital clay minerals ( especially kaolinite ) during early stages of diagenesis in an iron rich environment (( Bhattacharrya and Kakimoto, 1982). Based on above and depending upon the petrographical observations that showed chamosite occurrences around impregnation fossils by iron oxides, this does confirm chamosite growth beyond iron oxides replacement after changing of initial redox conditions in diagenetic environment. For any reason sulphide activity in the diagenetic environment was low; the reaction between organic matter and ferric components would have likely created conditions favorable for siderite formation in the presence of  $Fe^{+2}$  and carbonate activity (Curtis and Spears, 1968). Sideritization of IRS observed in many samples may be attributed to this reason .

After the stage of chamosite and siderite formation and at more deep burial with conditions of intense compaction and increasing in sulphide activities, most iron components will tend to transform to pyrite (Neumann et al, 2005). Ore microscopic study proved the presence of pyrite throughout Benavi IRS, which raised the indication of the suffering of this body with its iron content from high reduction conditions, and the more highly affected part was at the base of IRS that looks dark color in the field.

Quartz, pyrite and glauconite which were observed in the IRS samples are authigenic in their origin formed post-depositionally (Listizin, 1972), and their presence is a good evidence for late diagenetic (Al-Ani, 2005).

The high neomorphism effect which was identified by transformation of fossils to spary calcite , and the presence of dolomitization, dedolomitization and silicification; probably represent the late stage of diagenetic history occurred beyond the exposure of IRS and country rocks above sea level, as conditions of phreatic & vadoze zone were prevailing, respectively (Longman, 1980); the transformation of: (pyrite , siderite and chamosite) to: (goethite ,limonite and hematite), as well as, dehydration of goethite to form hematite, and oxidation of magnetite to form maghmite, too, may be belong to this stage with its effects going on.

## Plate (4-1)

Plate (4-1-A): Photomicrograph showing wackstone facies which lies under eastern part of IRS with stylolite (st) feature, sample no. (BN1/1A), (5X), PPL.

Plate (4-1-B): Photomicrograph showing the dolostone which lies under the middle and western part of IRS, sample no. (BN8/1A), (5X), PPL.

Plate (4-1-C): Photomicrograph showing the bioclastic packstone facies (overlying contry rocks of IRS) , rudist (r) is present, sample no.(BN1/8) , (5X),PPL.

Plate (4-1-D): Photomicrograph showing calcareous red algae with it's fine cellular structure (cs), sample no. (BN2/3), (20X), PPL.

Plate (4-1-E): Photomicrograph showing presence of echinoderm (↑) in IRS samples, sample no. (BN4/3), (20X), PPL.

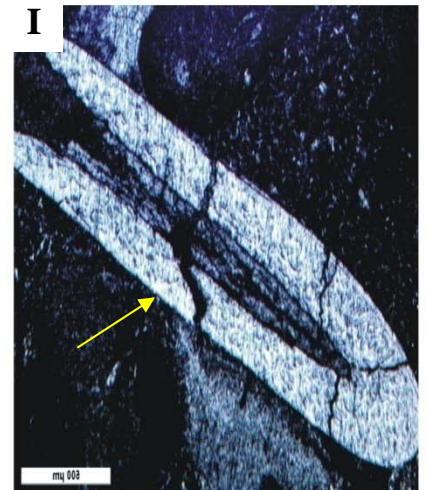
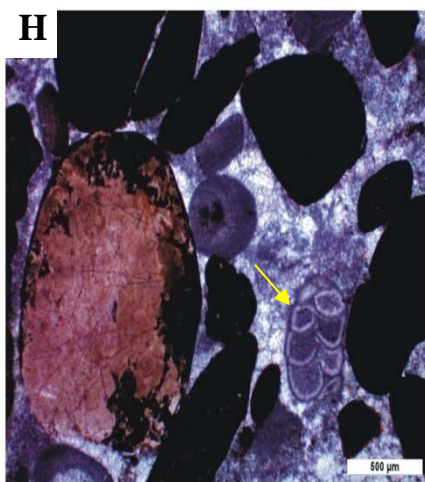
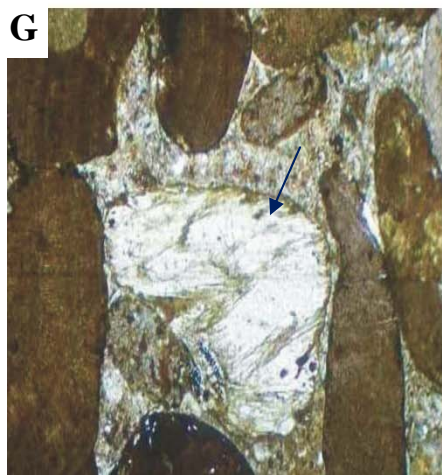
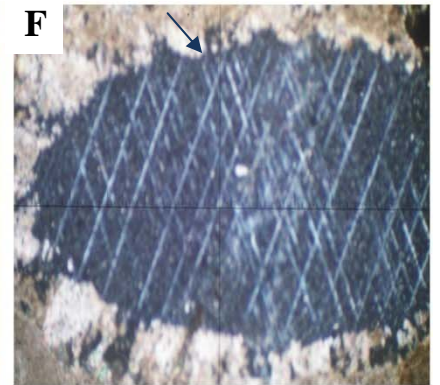
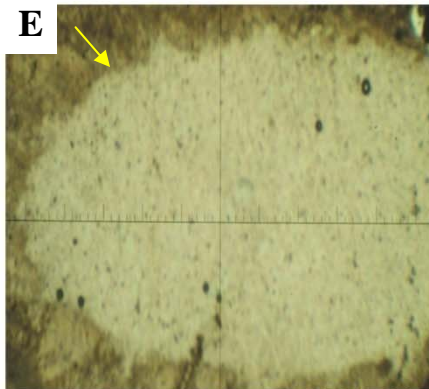
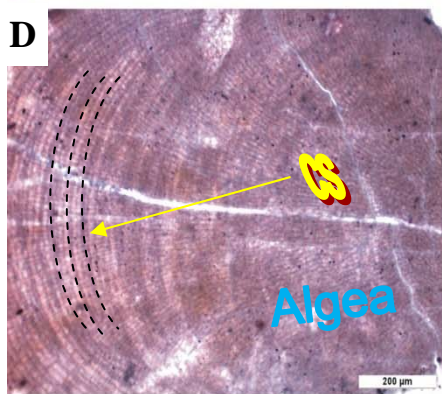
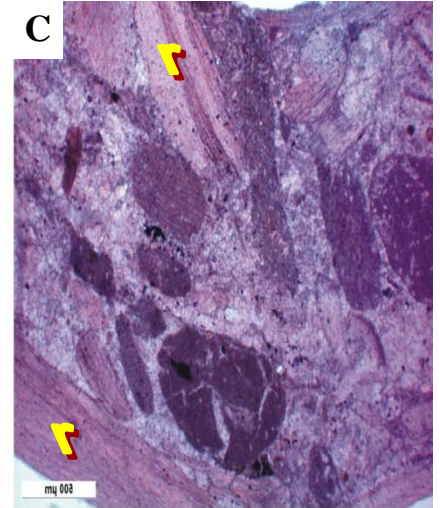
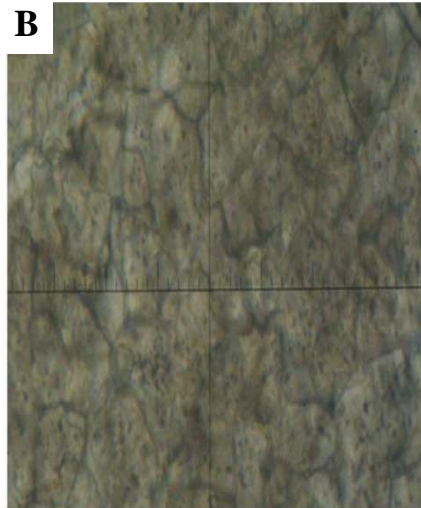
Plate (4-1-F): The same last Plate showing the optical behavior of echinoderm (↑) as a single crystal of calcite, (20X), XPL.

Plate (4-1-G): Shell fragment (↑), sample no. (BN5/3), (20X), PPL.

Plate (4-1-H): Biserial Foraminifera (↑), sample no. (BN6/2), (10X), PPL.

Plate (4-1-I): Sponge specules (↑), sample no. (BN6/4), reflected light,PPL.

Plate (4-1)



## Plate (4-2)

Plate (4-2-A): Photomicrograph showing partially replacement (pr) of fossils (Algae), by iron oxides, sample no. (BN6/3), (5X), PPL.

Plate (4-2-B): Photomicrograph showing completely replacement (cr) of fossils (Algae) by iron oxides, sample no. (BN2/5), PPL.

Plate (4-2-C): Photomicrograph showing iron oxides occurrence as coated(cd) of grains, sample no.(BN4/1),PPL.

Plate (4-2-D): Photomicrograph showing iron oxides occurrence as filled of pores inside fossils (intragranular) (↑), sample no. (BN2/7), PPL.

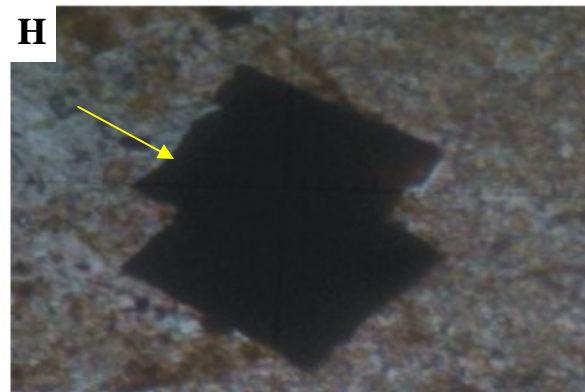
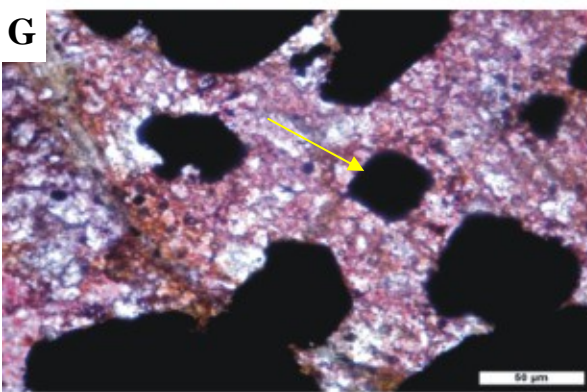
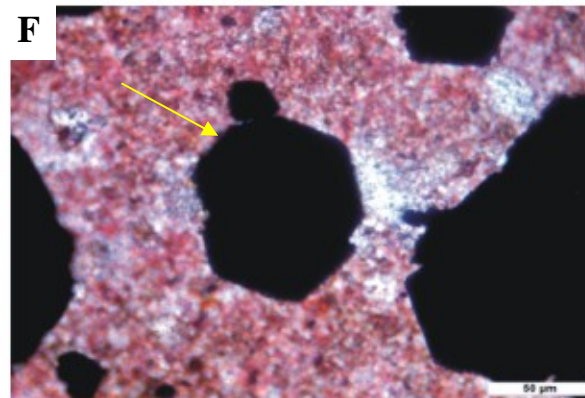
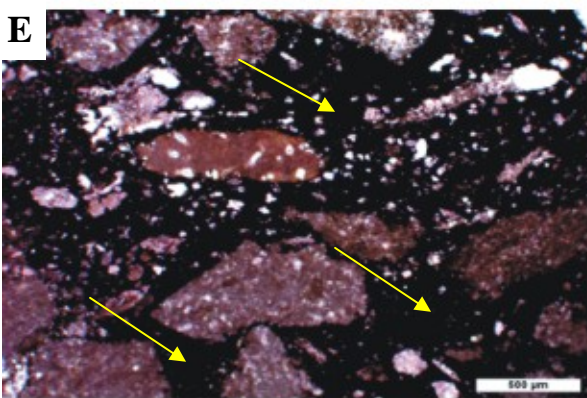
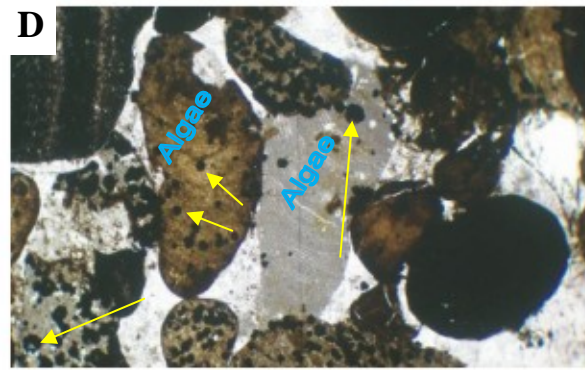
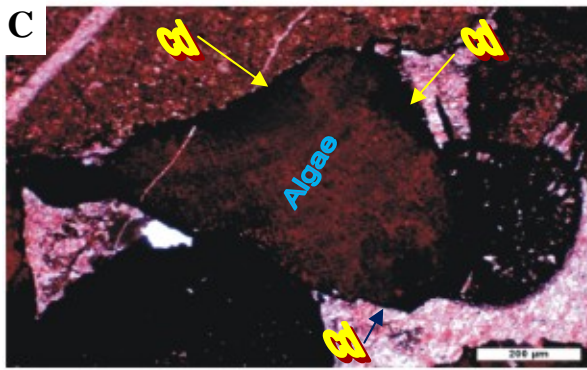
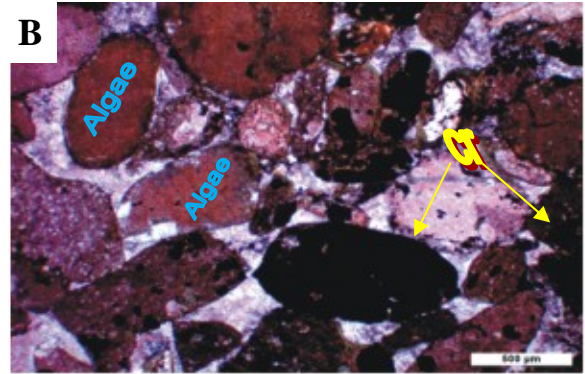
Plate (4-2-E): Photomicrograph showing iron oxides occurrence filled pores between grains (intergranular) (↑), sample no. (BN6/5), PPL.

Plate (4-2-F): Photomicrograph showing presence of iron minerals as hexagonal euhedral crystals (↑), sample no. (BN1/5), PPL.

Plate (4-2-G): Photomicrograph showing presence of iron minerals as cubic euhedral crystals (↑), sample no. (BN1/5), PPL.

Plate (4-2-H): Photomicrograph showing presence of iron minerals as twin cubic euhedral crystals (↑), sample no. (BN5/5), (40X), PPL.

Plate (4-2)



## Plate (4-3)

Plate (4-3-A): Photomicrograph showing the presence of glauconite(Gl) inside fossils (Algae), sample no. (BN9/1), (20X), PPL.

Plate (4-3-B): The same as Plate (3-5-A) but under XPL.

Plate (4-3-C): Photomicrograph showing the presence of glauconite(Gl ) inside fossils (Algae), sample no. (BN8/3), (10X), PPL.

Plate (4-3-D): Photomicrograph showing six-sided prismatic crystal of apatite (Ap), sample no. (BN3/1), (20X), PPL.

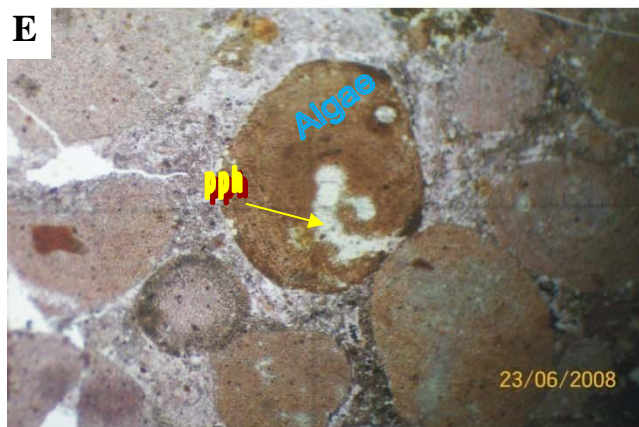
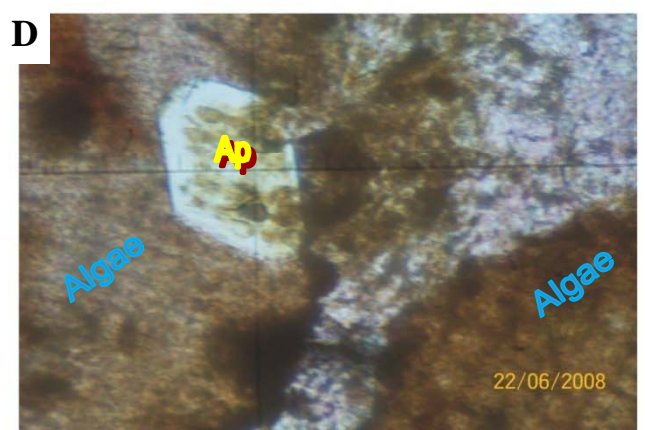
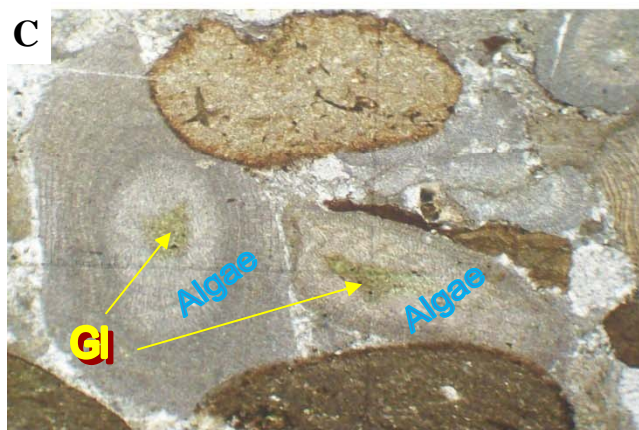
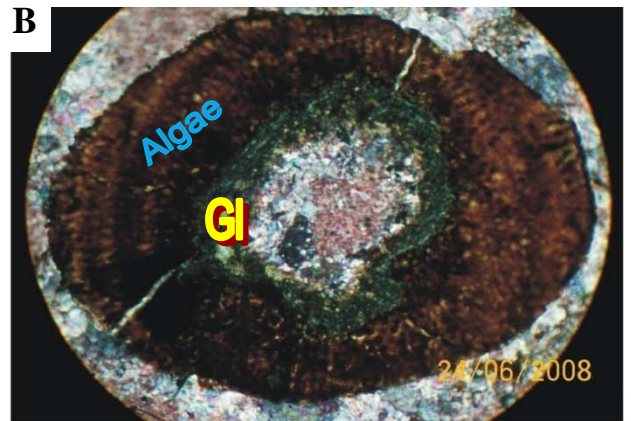
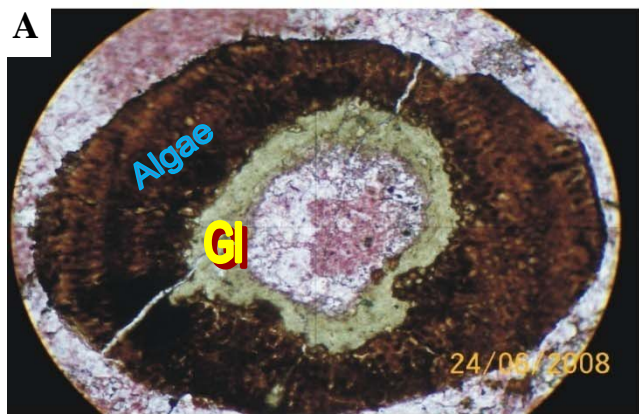
Plate (4-3-E): Photomicrograph showing partial phosphatization (pph) of fossils (Algae), sample no. (BN3/1), (10X), PPL.

Plate (4-3-F): The same as Plate (3-5-E) but under XPL.

Plate (4-3-G): Photomicrograph showing complete phosphatisation (cph) of fossils (Algae), sample no. (BN8/4), (5X), PPL.

Plate (4-5-H): The same as Plate (3-5-G) but under XPL.

Plate (4-3)



## Plate (4-4)

Plate (4-4-A): Photomicrograph showing chamosite (ch) as outer rim of completely impregnated fossils by iron oxides, sample no. (BN1/4), PPL.

Plate (4-4-B): Photomicrograph showing chamosite (ch) as outer rim of completely impregnated fossils by iron oxides, sample no. (BN9/1), (20X), PPL.

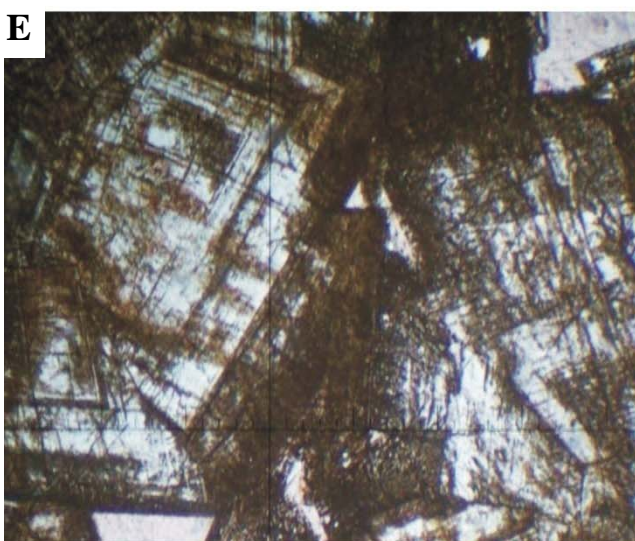
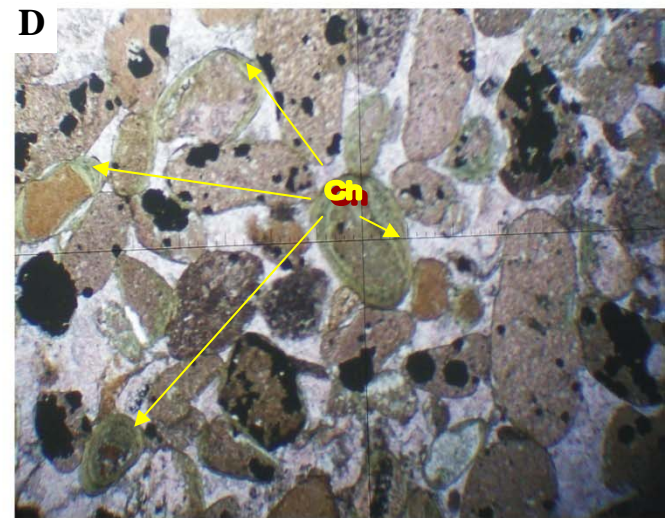
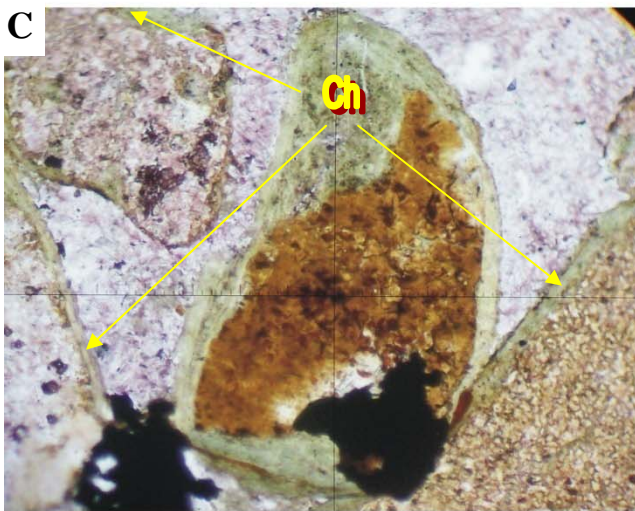
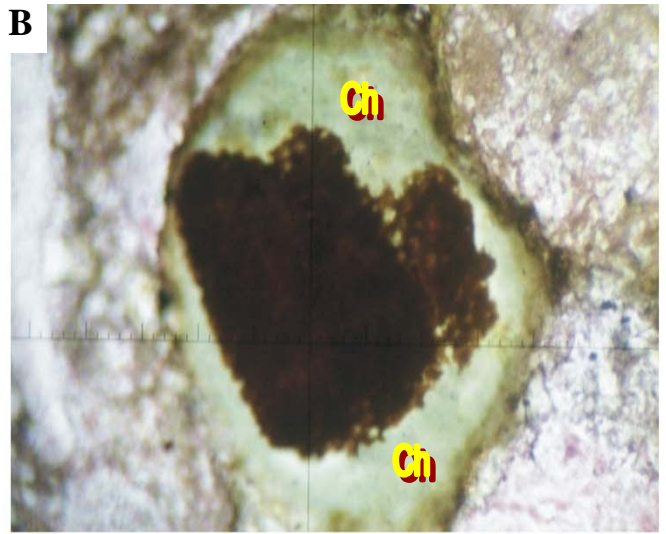
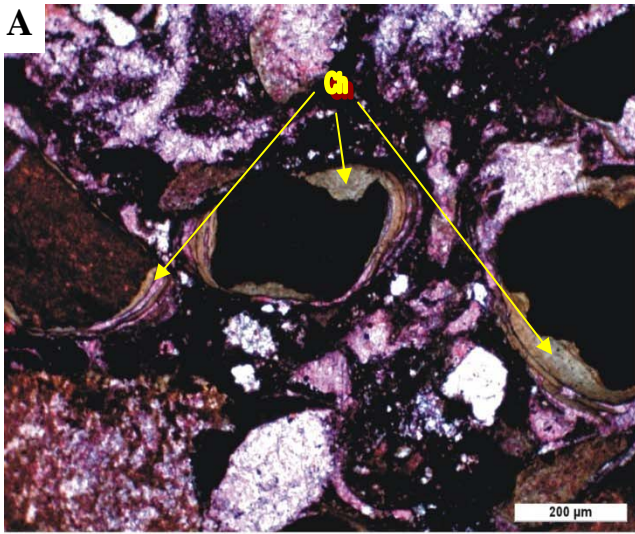
Plate (4-4-C): Photomicrograph showing chamosite (ch) as outer rim of partially impregnated fossils by iron oxides, sample no. (BN8/2), (20X), PPL.

Plate (4-4-D): Photomicrograph showing chamosite (ch) around fossils not affected by iron oxides replacement, sample no. (BN2/3), (5X), PPL.

Plate (4-4-E): Photomicrograph showing siderite rhomb grains and the brown stains along cleavage, sample no. (BN5/2), (40X), PPL.

Plate (4-4-F): The same as Plate (3-7-E) but under XPL.

Plate (4-4)



## Plate (4-5)

Plate (4-5-A): Photomicrograph showing euhedral quartz ( Q )replaced parts of fossils (Algae), sample no. (BN1/2), PPL.

Plate (4-5-B): Photomicrograph showing euhedral quartz ( Q ) replaced parts of fossils (algae) ,sample no.(BN6/2),PPL.

Plate (4-5-C): Photomicrograph showing euhedral quartz ( Q ) replaced parts of fossils (Algae) ,sample no.(BN10/1),PPL.

Plate (4-5-D): The same as Plate (3-4-C) but under XPL.

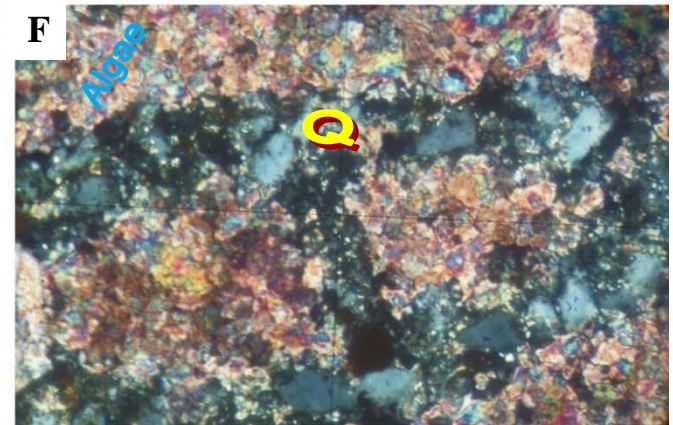
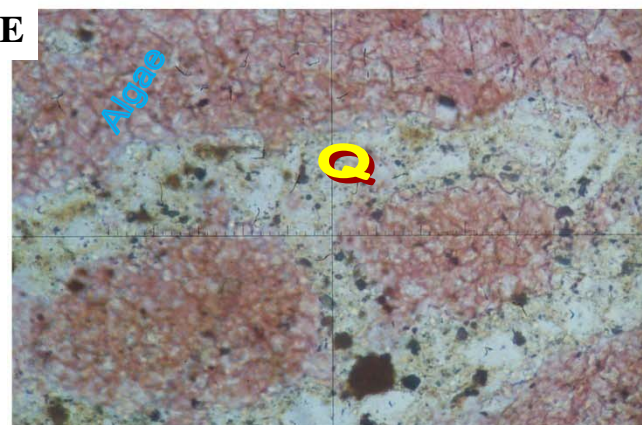
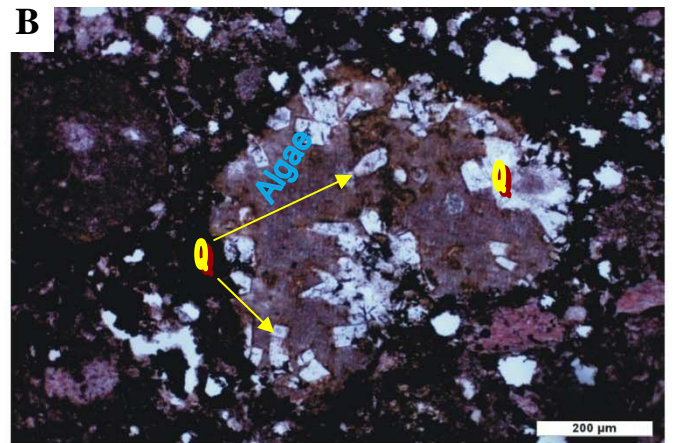
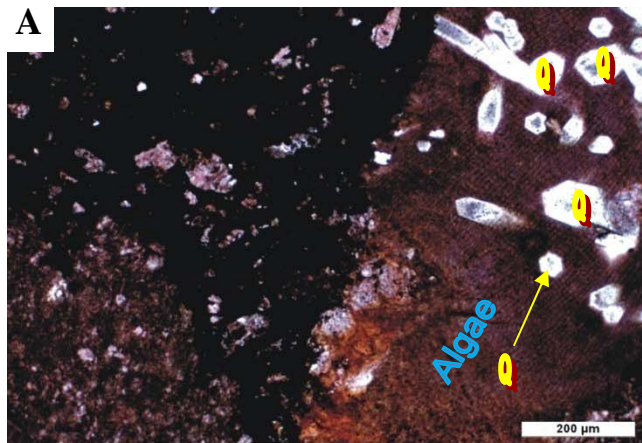
Plate (4-5-E): Photomicrograph showing anhedral quartz ( Q ) replaced parts of fossils (Algae) ,sample no.(BN3/1),(40x),PPL.

Plate (4-5-F): As the same of Plate (3-4-E) but under XPL .

Plate (4-5-G): Photomicrograph showing chalcedony (ch) replaced parts of fossils (Algae), sample no. (BN4/1), (40x), PPL.

Plate (4-5-H): The same as Plate (3-4-G) but under XPL.

Plate (4-5)



## Plate (4-6)

Plate (4-6-A): Photomicrograph showing the spary calcite cement (cc) filled pore spaces between grains sample no. (BN5/5), PPL.

Plate (4-6-B): Photomicrograph showing the spary calcite cement (cc) filled pore spaces between grains, sample no. (BN1/3), PPL.

Plate (4-6-C): Photomicrograph showing the neomorphism(n) feature, sample no. (BN10/2), PPL.

Plate (4-6-D): Photomicrograph showing the highly neomorphism (n) in overlying country rocks of IRS, sample no. (BN1/8).

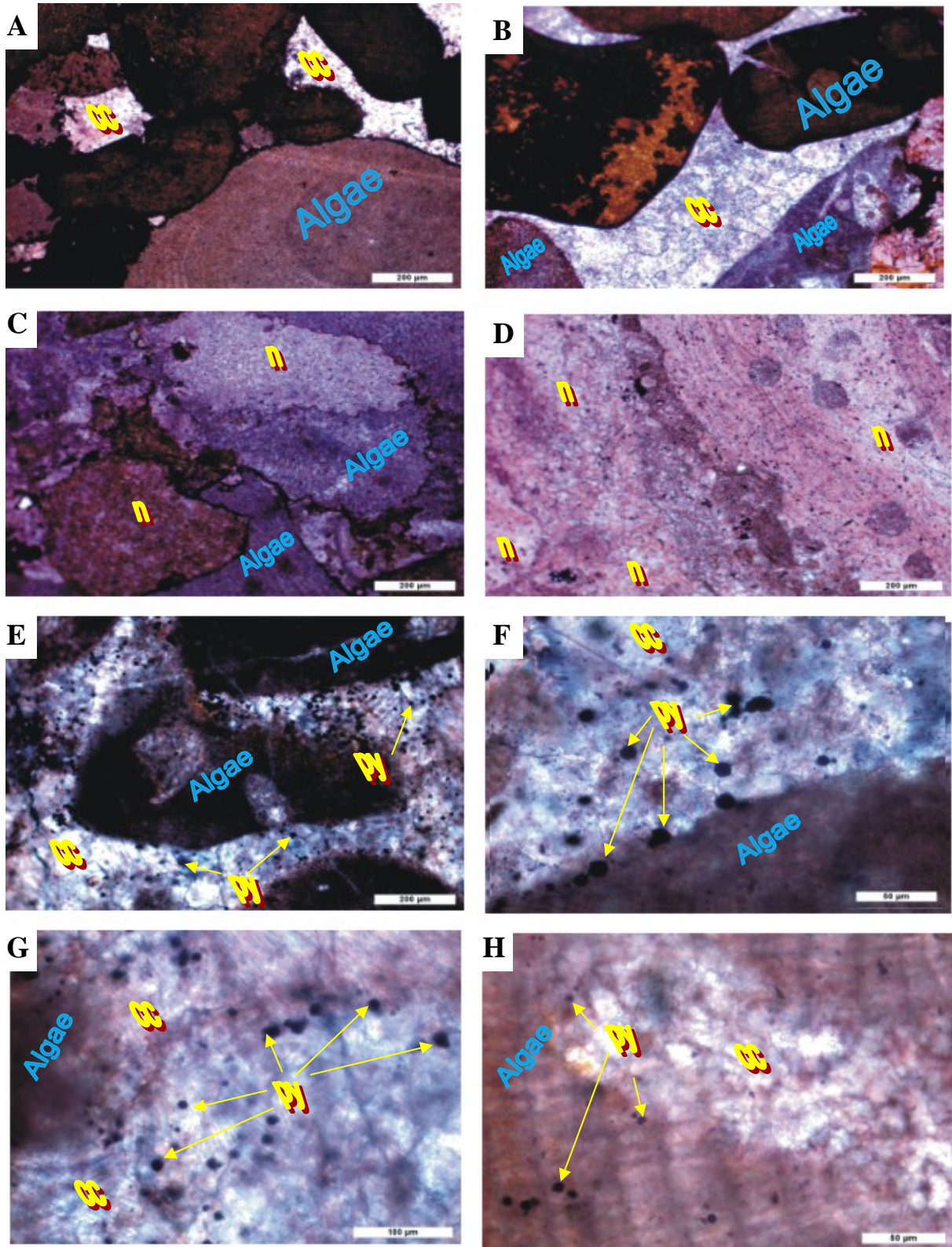
Plate (4-6-E): Photomicrograph showing pyrite (py) crystals float in spary calcite cement (cc), sample no. (BN5/2), PPL.

Plate (4-6-F): Photomicrograph showing pyrite (py) crystals released from skeletal of fossils(Algae) to spary calcite cement(cc) by the effect of neomorphism , higher magnification than previous Plate , (BN5/2), PPL.

Plate (4-6-G): As the same of previous Plate in another site, sample no. (BN5/2), PPL.

Plate (4-6-H): Photomicrograph showing pyrite (py) crystals released from inside fossils(Algae) to spary calcite cement (cc) by the effect of neomorphism, high magnification, sample no. (BN6/4).

Plate (4-6)



## Plate (4-7)

Plate (4-7-A): Photomicrograph showing the dolomitization (Do) feature observed in some of IRS samples, sample no. (BN5/1), (20X), PPL.

Plate (4-7-B): Photomicrograph showing rhombs of dolomite (D) crystals associated with quartz, sample no. (BN10/1), PPL.

Plate (4-7-C): The same as Plate (3-6-B) but under XPL.

Plate (4-7-D): Photomicrograph showing dedolomitized calcite (dc) cement due to dedolomitization phenomenon, sample no. (BN9/1), PPL.

Plate (4-7-E): Photomicrograph showing the mechanical compaction feature, sample no. (BN2/7), PPL.

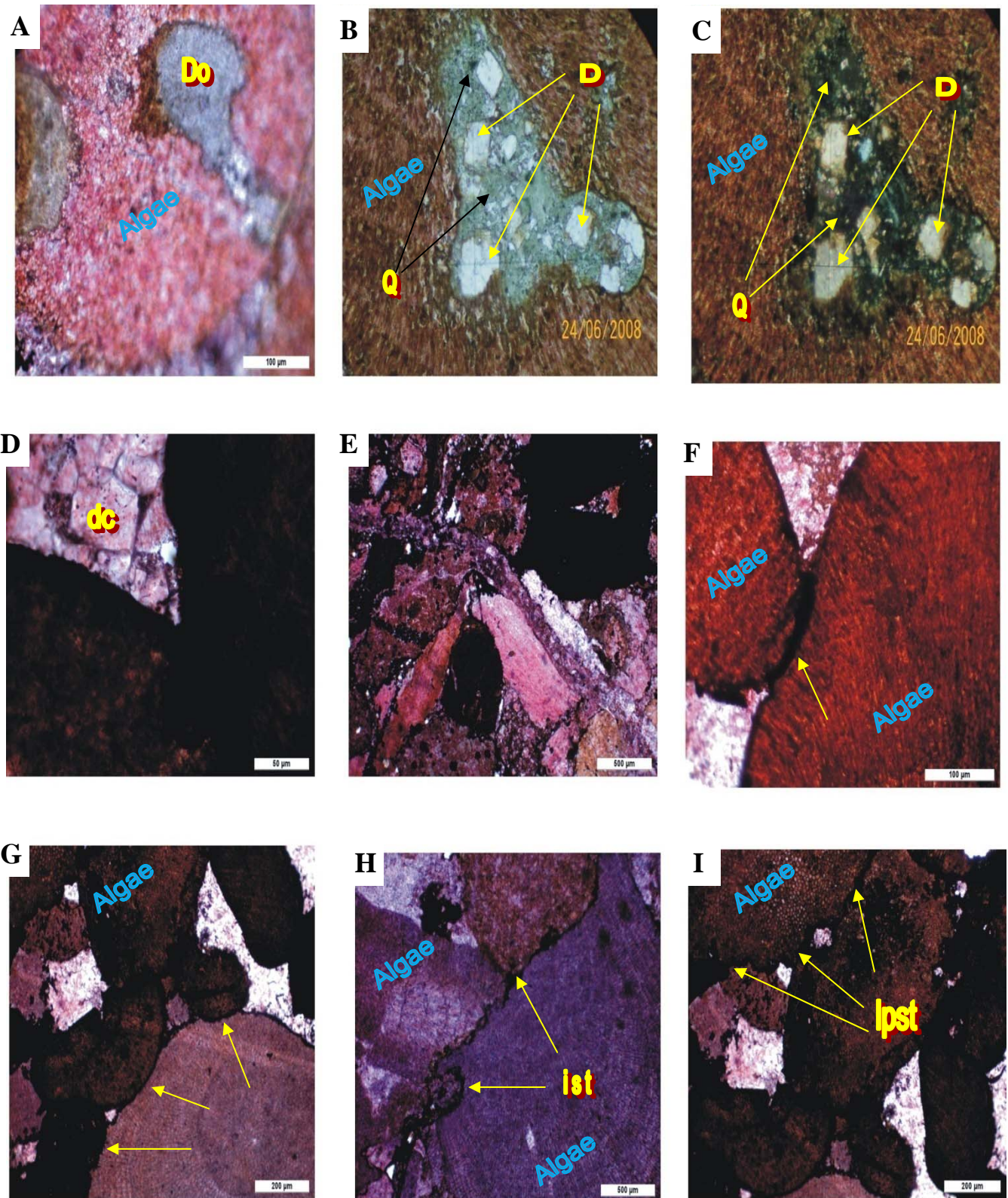
Plate (4-7-F): Photomicrograph showing the surface contact ( $\uparrow$ ) between grains which vary from point and planar, sample no. (BN4/1), PPL.

Plate (4-7-G): Photomicrograph showing the sutured and corroded grain margins ( $\uparrow$ ) due to compaction and dissolution, sample no. (BN6/4), PPL.

Plate (4-7-H): Photomicrograph showing irregular stylolite (ist) phenomenon in IRS samples, sample no. (BN4/2), PPL.

Plate (4-7-I): Photomicrograph showing low peaks amplitude stylolite (lpst) phenomenon in IRS samples, sample no. (BN7), PPL.

Plate (4-7)



## Plate (4-8)

Plate (3-8-A): At very low magnification, nearly all IRS samples show many rounded or irregular shaped biogenic carbonate, the iron content causes their varieties being brown, sample no.(BN5/4) ,(5X),polished thin section ,transmitted light,PPL.

Plate (4-8-B): Framboidal texture of pyrite (fpy), sample no ( BN1/4), reflected light ,PPL.

Plate (4-8-C):Pseudomorphs of hematite after framboidal pyrite(htp), sample no.(BN5/5),reflected light , PPL.

Plate (4-8-D): Disseminated pyrite (dpy), sample no. (BN9/1), reflected light, PPL.

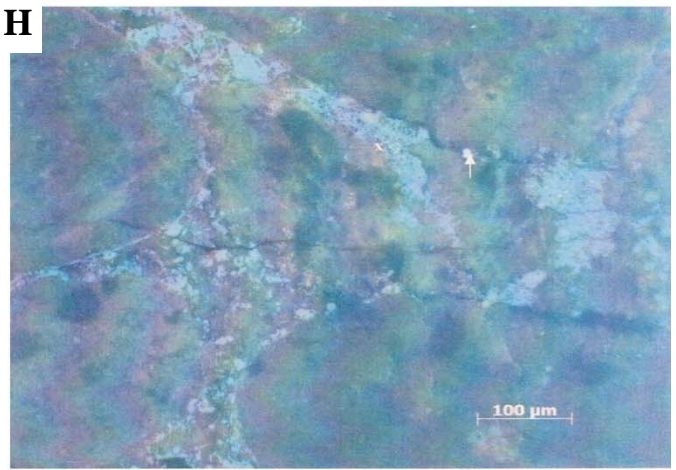
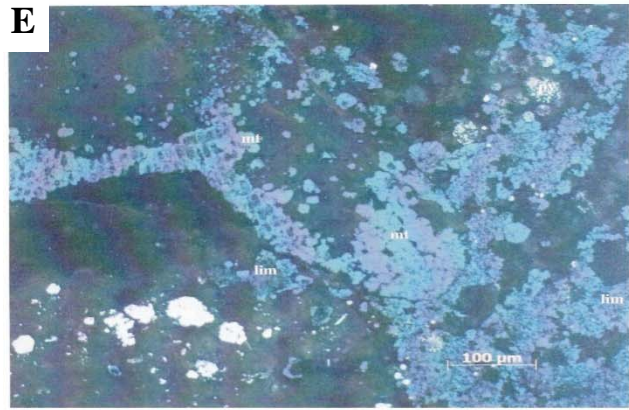
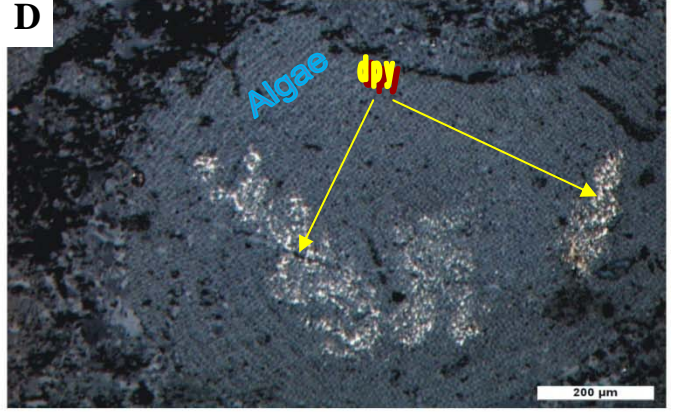
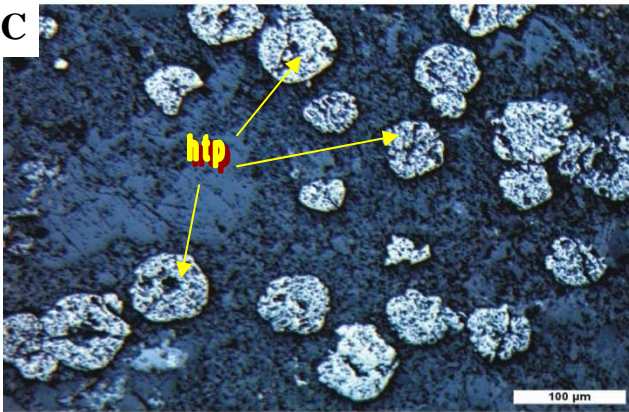
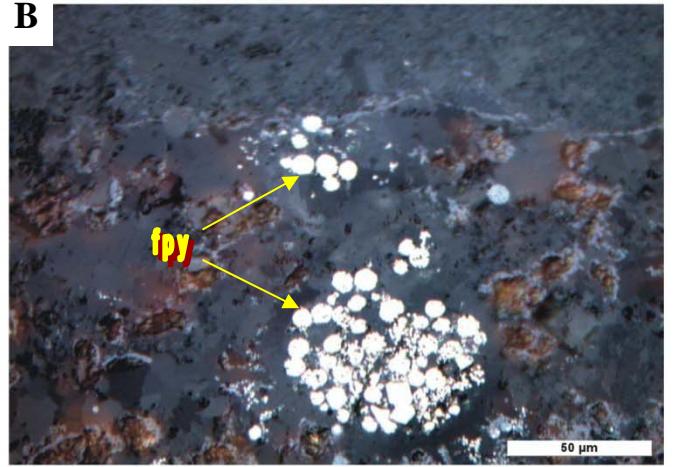
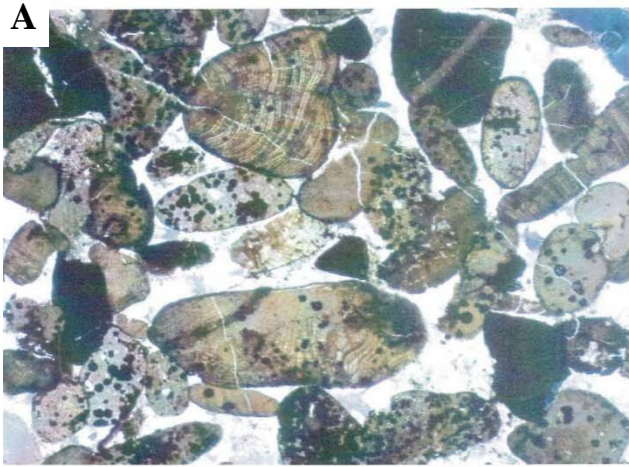
Plate (4-8-E): Photomicrograph shows the presence of magnetite (mt) and of pyrite (py) besides there is limonite (lim). All are embedded in carbonates,sample no.(BN1/4), polished thin section, reflected light ,oil immersion.

Plate (4-8-F): Photomicrograph exhibits the presence of arsenopyrite ,sample no . (BN8/2), reflected light,PPL.

Plate (4-8-G): Photomicrograph showing the biogenic carbonate,the contours and holes of biogenic structures are rimmed by limonite(bluish ,red internal reflections),the rounded structures are cemented by carbonate,sample no.(BN2/4),polished thin section ,reflected light , oil immersion.

Plate (4-8-H): The rounded bioclasts are of iron bearing carbonate with varying yellowish or greenish internal reflections, they are cemented or rimmed by limonite(bluish grey )and carbonate, Rutile (↑) and spars framboids(X) of pyrite, Sample no. (BN2/5), polished thin section,reflected light,oil immersion.

Plate (4-8)



## Plate (4-9)

Plate (4-9-A): The interstices between hematite rich fragment (left) and two biogenic pebbles (yellowish, top and right) are filled by calcite (cc) and some limonite (lim). The pebble on the right is rimmed by limonite and contains idiomorphic magnetite (x), sample no. (BN2/8), polished thin section, reflected light, oil immersion.

Plate (4-9-B): Embedded in a groundmass of iron bearing carbonates, an aggregate of former idiomorphic pyrites transformed to limonite (lim). Besides, there are small relicts of pyrite framboids (↑), sample no. (BN5/2), polished thin section, reflected light, oil immersion.

Plate (4-9-C): The bioclasts may be rich in limonite (a) or they almost contain no limonite (b), sample no. (BN5/3), polished thin section, reflected light, oil immersion.

Plate (4-9-D): Relicts of pyrite (white) embedded in goethite (grey), sample no. (BN5/3), reflected light, PPL.

Plate (4-9-E): Significant content of magnetite (mt), together with hematite (pale bluish), it is as aggregates that probably are pseudomorphs after framboids of pyrite. There are also fragments of calcite (cc), cemented by limonite (bluish, reddish internal reflections), sample no. (BN5/4), polished thin section, reflected light, oil immersion.

Plate (4-9-F): Pseudomorphs of magnetite (pmt) after framboids of pyrites, sample no. (BN5/4), reflected light, PPL.

Plate (4-9-G): The more frequent yellowish bioclasts are rimmed by hematite and limonite; besides, there are bioclasts that contain much hematite (a), at the interstices occurs calcite (cc), limonite (lim) is less frequent, sample no. (BN6/4), polished thin section, reflected light, oil immersion.

Plate (4-9-H): Most of bioclasts (bc) are moderately impregnated by hematite, the interstices are filled by calcite (cc) or by hematite (he); magnetite (mt) is also present, the magnetite in the photograph is not intergrown with the adjacent Carbonate (x), sample no. (BN6/5), polished thin section, reflected light, oil immersion.



## Plate (4-10)

Plate (4-10-A): Bioclasts with lower iron content embedding idiomorphic quartz (IQ) (authigenic). Pseudomorph hematite after framboidal pyrite (hfp) is present, sample no. (BN10/1), reflected light, PPL.

Plate (4-10-B): Several fragments of the bioclasts rich in limonite (bluish) and the carbonates can be recognized (ca), traces with pseudomorphs of hematite after framboidal pyrite (x) are visible as well as rutile (↑), sample no. (BN10/1), polished thin section, reflected light, oil immersion.

Plate (4-10-C): Simple sedimentary structure as alternating carbonate layers of hematite rich (hr) and hematite poor (hr), sample no. (BN3/4), reflected light, PPL.

Plate (4-10-D): Fragments of iron bearing bioclasts (bc) show low content of hematite (bright bluish). Along fissures and at interstices a rather closely packed hematite (he) is present. The texture is cut by a veinlet of pure calcite (cc), sample no. (BN10/3), polished thin section, reflected light, oil immersion.

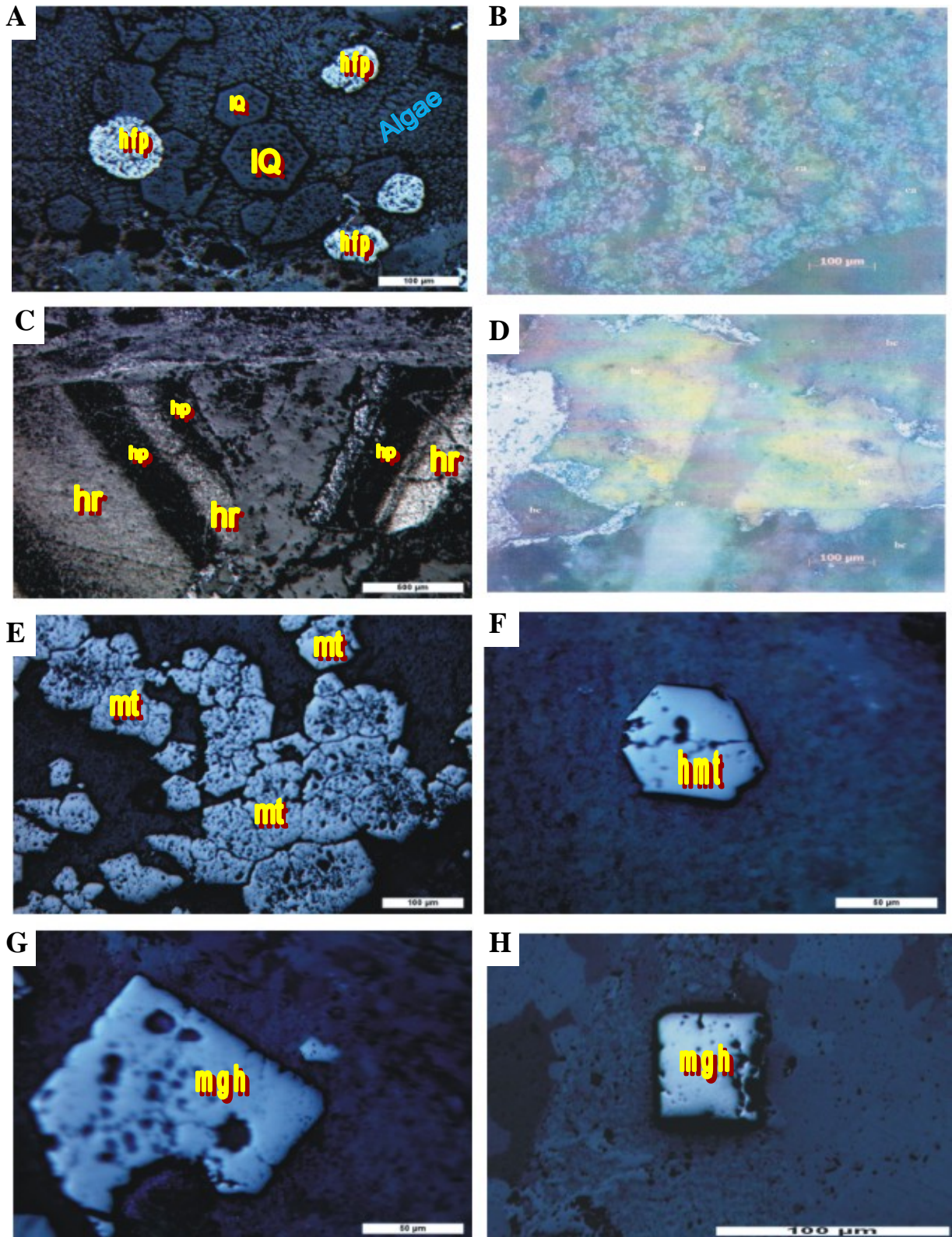
Plate (4-10-E): Photomicrograph showing high content of magnetite (mt) present in some of the IRS samples, sample no. (BN2/7), reflected light, PPL.

Plate (4-10-F): Photomicrograph showing the presence of euhedral hexagonal pseudomorph magnetite after hematite (hmt), sample no. (BN1/6), reflected light, PPL.

Plate (4-10-G): Photomicrograph showing the presence of euhedral cubic pseudomorph maghemite (mgh) after magnetite, sample no. (BN1/5), reflected light, PPL.

Plate (4-10-H): Photomicrograph showing the presence of euhedral cubic pseudomorph maghemite (mgh) after magnetite, sample no. (BN1/6), reflected light, PPL.

Plate (4-10)



## Plate (4-11)

Plate (4-11-A): BSE image showing replacement rim texture of pyrite (white) by goethite (pale grey), sample no. (BN10/1).

Plate (4-11-B): BSE image showing zonal texture, the growth zonation takes place by gradual alteration of pyrite with goethite usually from outside inwards, sample no. (BN5/2).

Plate (4-11-C): Photomicrograph showing inclusions (relicts) of pyrite inside goethite, sample no. (BN9/2), reflected light, PPL.

Plate (4-11-D): Photomicrograph showing idiomorphic texture of magnetite, sample no. (BN1/5), reflected light, PPL.

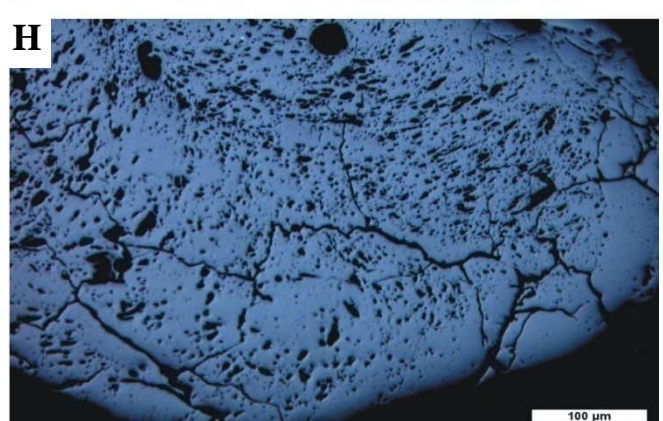
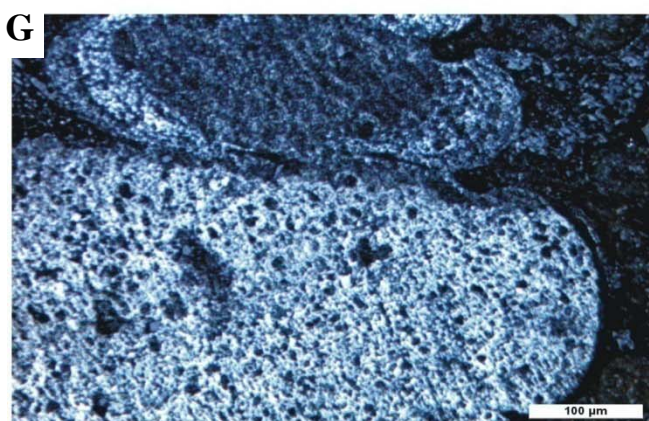
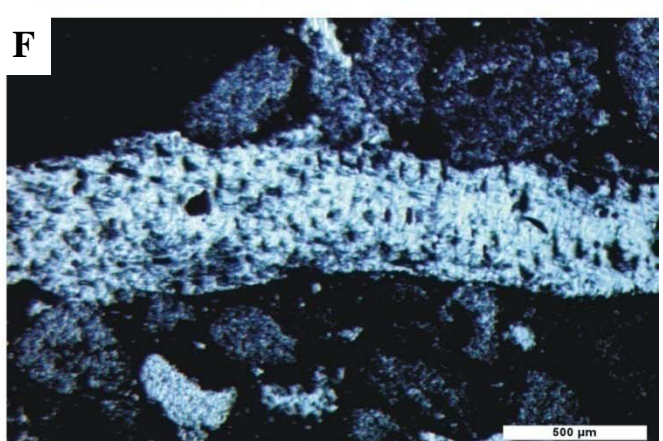
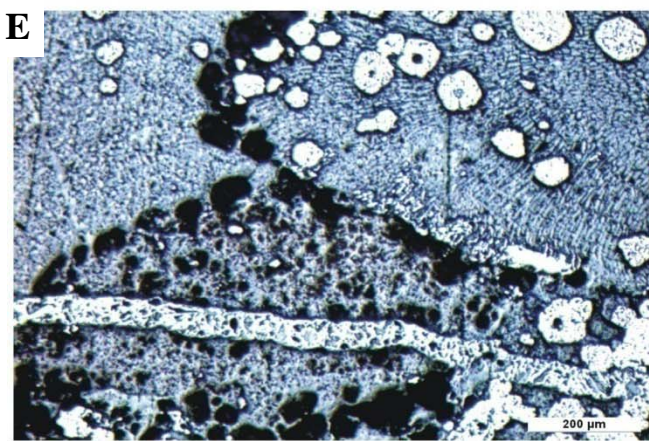
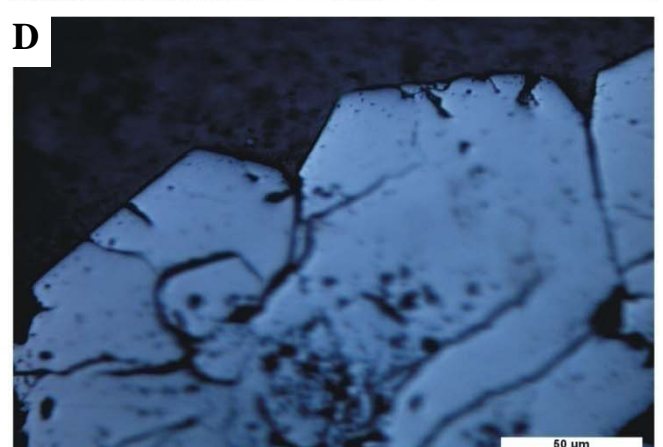
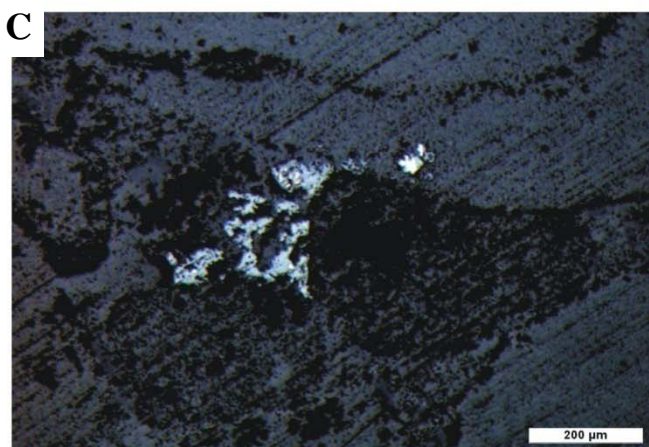
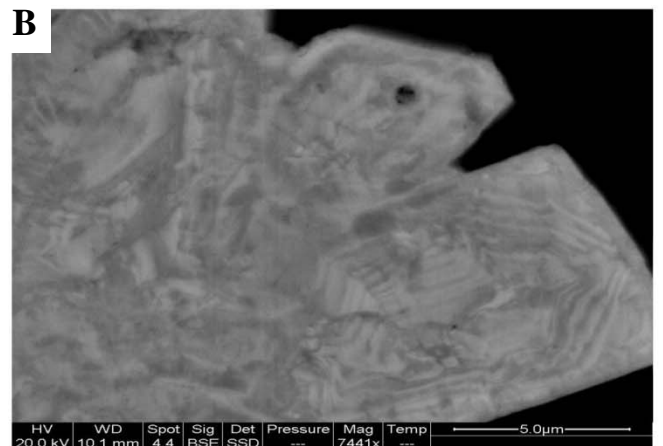
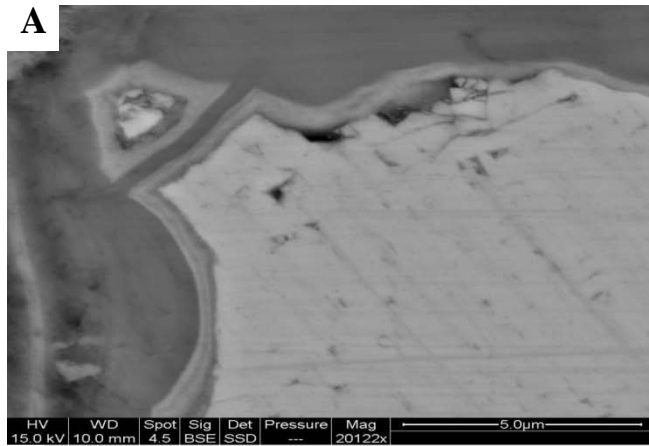
Plate (4-11-E): Photomicrograph showing vein texture of goethite, sample no. (BN9/3), reflected light, PPL.

Plate (4-11-F): Photomicrograph showing vein texture of hematite, sample no. (BN9/3), reflected light, PPL.

Plate (4-11-G): Photomicrograph showing porous texture of hematite, sample no. (BN10/3), reflected light, PPL.

Plate (4-11-H): Photomicrograph showing porous texture of hematite, sample no. (BN5/4), reflected light, PPL.

Plate (4-11)



## Plate (4-12)

Plate (4-12-A): BSE image showing oolitic texture of chamosite , sample no. (BN1/4).

Plate (4-12-B): BSE image showing boxwork texture of hematite, sample no. (BN2/7).

Plate (4-12-C): BSE image showing microplates of hematite grains filled veinlets , sample no. (BN6/5).

Plate (4-12-D): BSE image showing microplates of hematite grains filled veinlets , sample no. (BN8/5).

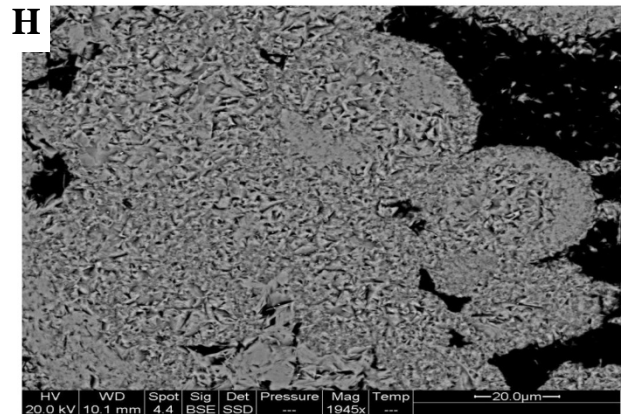
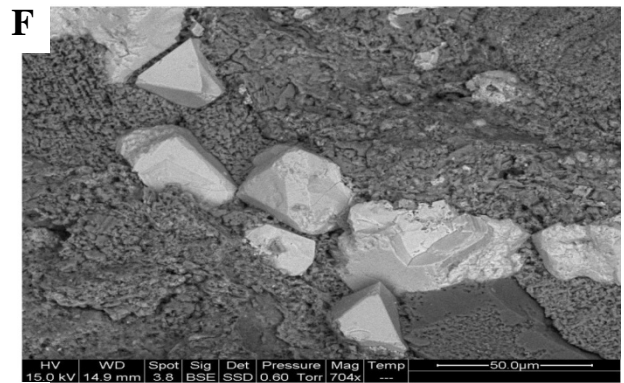
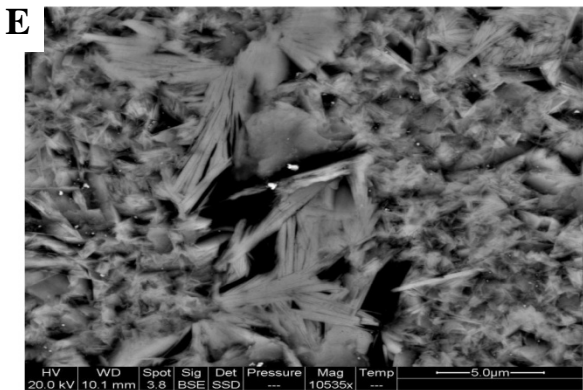
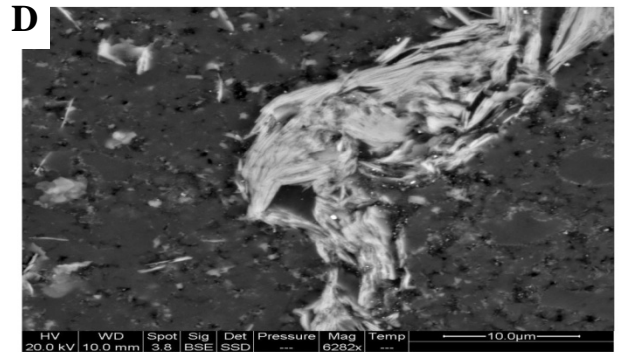
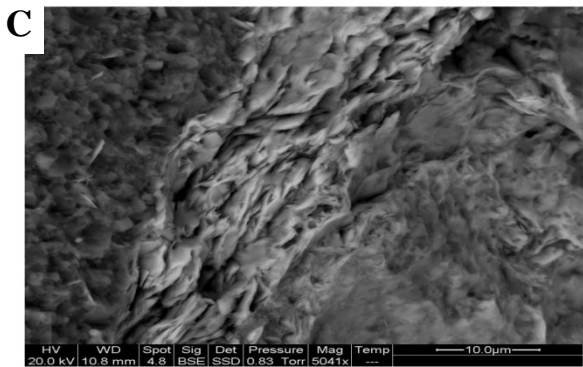
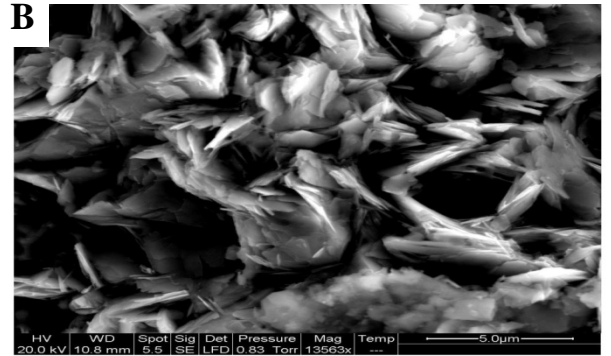
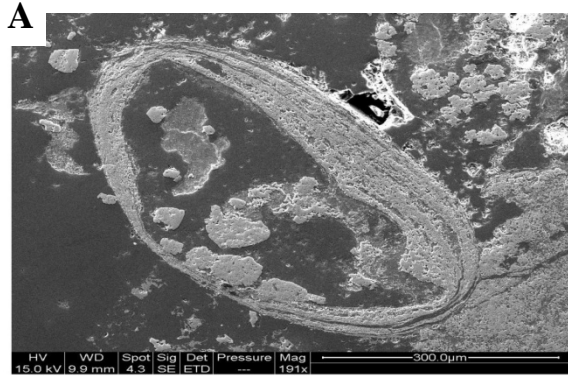
Plate (4-12-E): BSE image showing microplates of hematite grains filled pore space sample no. (BN7).

Plate (4-12-F): BSE image showing the euhedricity of magnetite crystals, sample no. (BN2/7).

Plate (4-12-G): BSE image showing magnetite frambooids after pyrite frambooids , sample no. (BN5/4).

Plate (4-12-H): BSE image showing goethite frambooids after pyrite frambooids , sample no. (BN6/5).

Plate (4-12)



# *Chapter Five*

# *Geochemistry*

## 5-1 Preface:

The geochemical characteristic of Benavi IRS have been investigated through the analyses of (28) samples comprising the whole IRS body. These analyses were carried out at the State Company for Geological Survey and Mining (GEOSURV) for chemical analyses according to the procedures adopted by this company ( $\text{SiO}_2$ , FeO & L.O.I by wet chemical analysis,  $\text{Na}_2\text{O}$  &  $\text{K}_2\text{O}$  by flame photometer type/Gallen Kamp,  $\text{Al}_2\text{O}_3$  &  $\text{TiO}_2$  by auto-analyzer Type/Technicon,  $\text{P}_2\text{O}_5$  by spectrophotometer Type/Labomed-WC ), while the trace elements and  $\text{Fe}_2\text{O}_3$  &  $\text{MgO}$  were analyzed by Atomic Absorption Type/PYE UNICON, SP 2900.

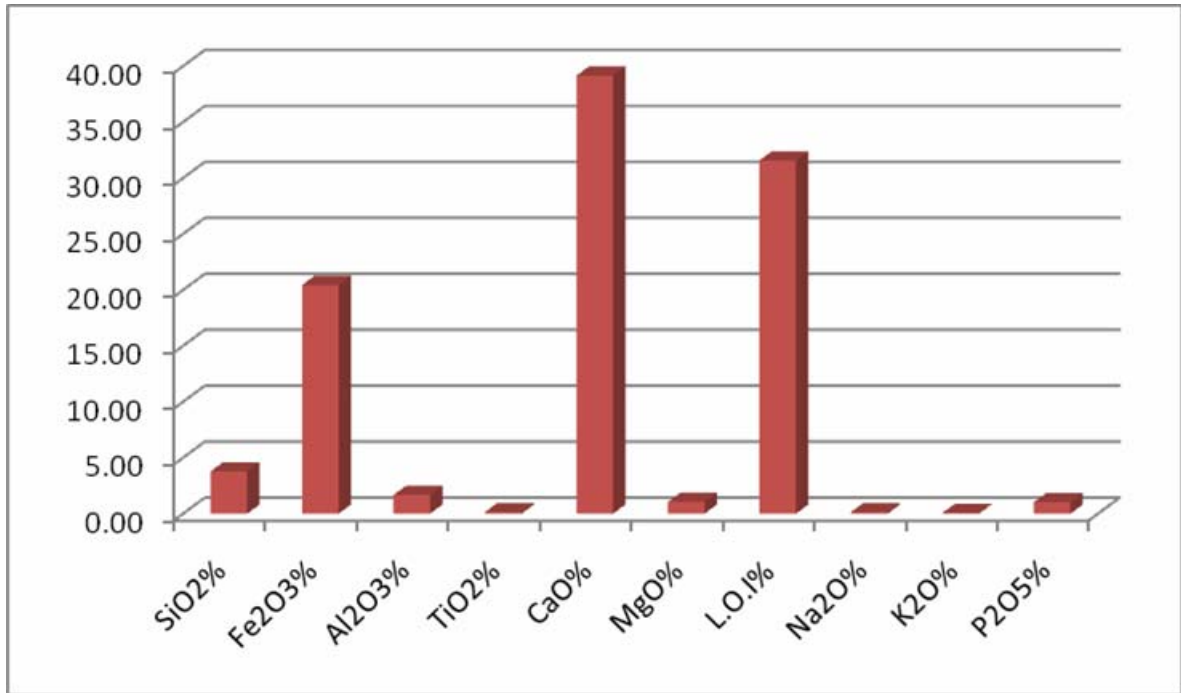
The results for the major oxides analyses in (wt %) and the trace elements in (ppm) are given in (Appendix 5-A and B respectively), whereas the average of these analyses are shown in ( Fig. 5-1). The results for the samples BN1, BN2, BN5 and BN6 sections are also shown in (Fig.5-2) to illustrate the horizontal and vertical variations of elements throughout Benavi IRS.

(11) Samples were selected from the previous (28) samples, where the powder of each sample divided to two homogenous portions, one for GEOSURV Lab. with the rest of (28) and another portion was sent to SOCIETE NATIONAL INDUSTRIELLE ET MINIERE' (SNIM) IN MOURITANIA for chemical analyses. The results are listed in (Appendix 5- C).

Both results (GEOSURV & SNIM) were statistically treated separately to compare and check for best accuracy in the interpretation. Sometimes there is little difference in range and average between them due to the number of samples (SNIM=11 whereas GEOSURV=28). In general there was noticeable convergence between them.

Frequency histograms were drawn to determine the style distribution of elements in Benavi IRS. Minimum, maximum and average values for major and trace elements were measured, as well as, three statistical methods were utilized for analyzing data collected from the bulk chemical analyses which are: correlation, factor and cluster analyses.

A



B

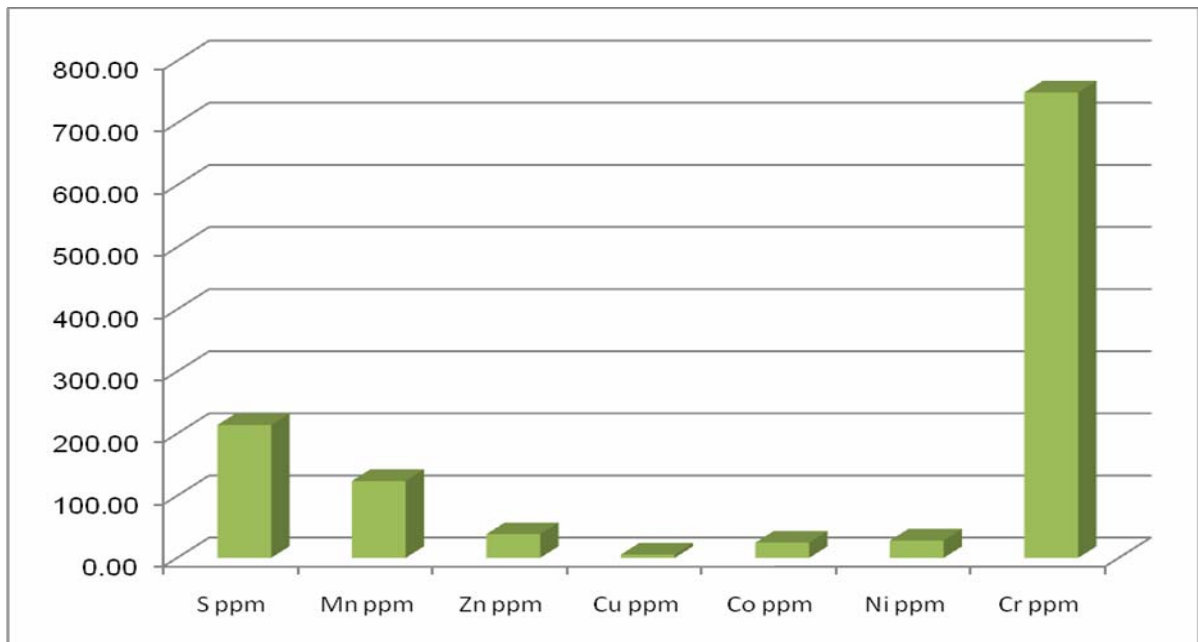
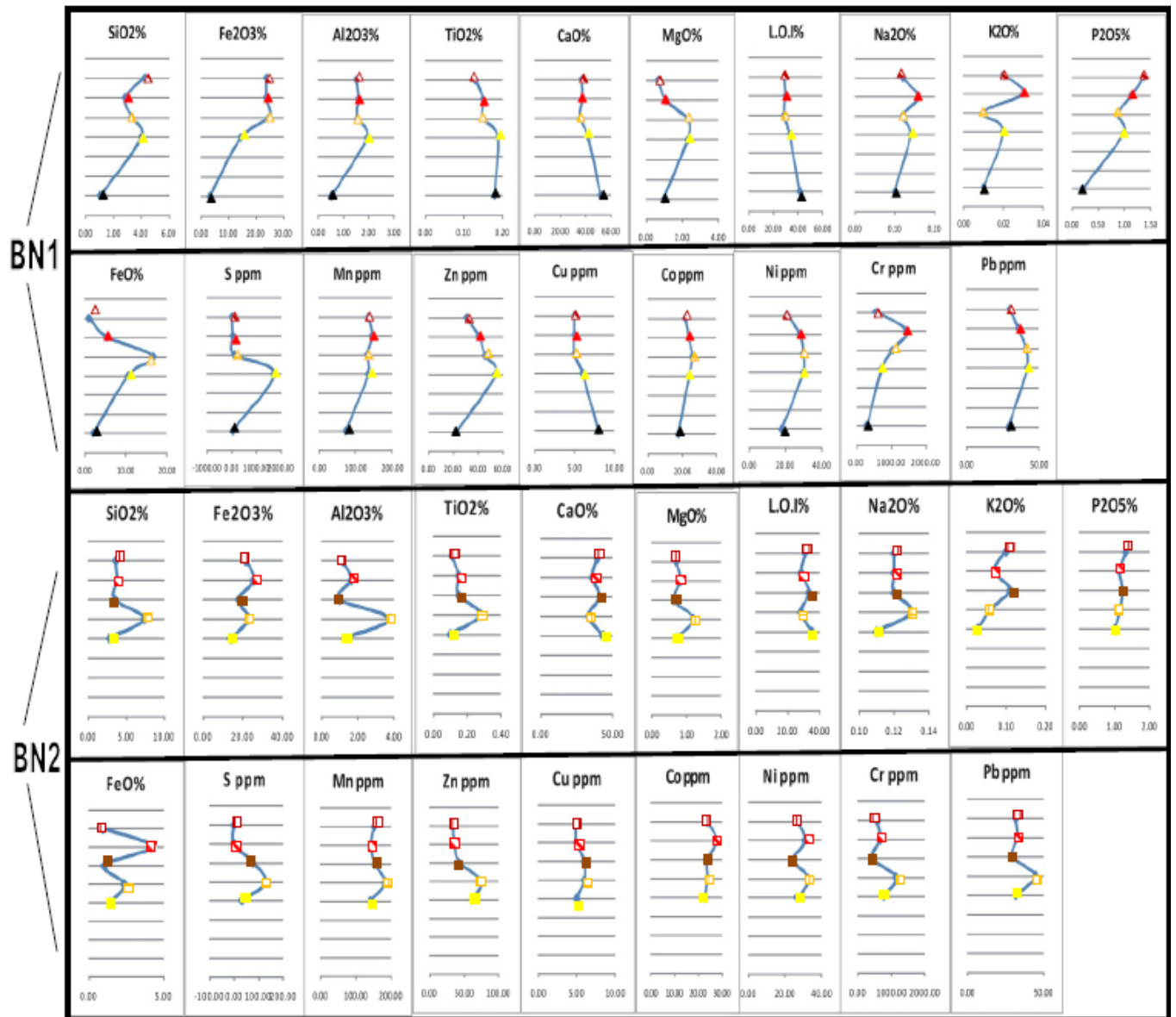


Figure (5-1): Bar charts for the average of the concentrations of: A- major oxides (%), and B-trace elements (ppm) of Benavi IRS .



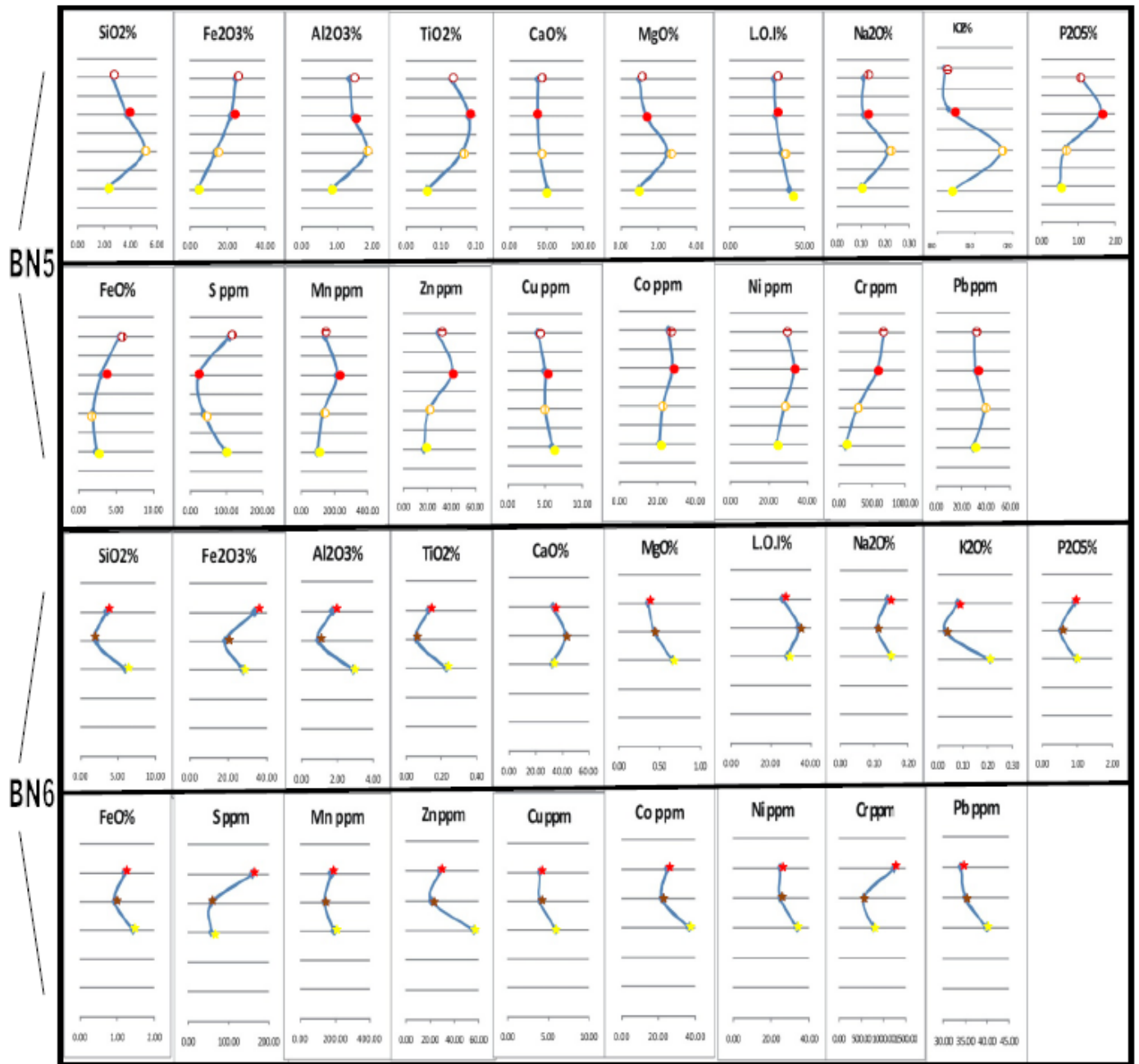
Legend:

- |       |   |       |   |
|-------|---|-------|---|
| BN1/7 | ▲ | BN2/8 | □ |
| BN1/6 | ▲ | BN2/7 | ◻ |
| BN1/5 | ▲ | BN2/6 | ■ |
| BN1/4 | ▲ | BN2/5 | □ |
| BN1/1 | ▲ | BN2/4 | ■ |

Where: X axis= the chemical concentration of the oxide (%) or element (ppm).

Yaxis= Sites of the samples in the sections (see real scale in appendix 2).

Figure (5-2): Shows the vertical variations of major and trace elements along: BN1, BN2, BN5 and BN6 sections of Benavi IRS.



Legend:

- |       |   |       |   |
|-------|---|-------|---|
| BN5/4 | ○ | BN6/5 | ★ |
| BN5/3 | ● | BN6/4 | ☆ |
| BN5/2 | ⊕ | BN6/3 | ✦ |
| BN5/1 | ● |       |   |

Where: X axis= the chemical concentration of the oxide (%) or element (ppm).

Y axis= Sites of the samples in the sections (see real scale in appendix 2).

Figure (5-2): continued.

## 5-2 Precision and accuracy of analysis:

There are many sources of mistakes in chemical analyses probably occurred in the: method of analysis, instruments and tools of analysis, preparation of the analyzed sample .....so on. Therefore, precision and accuracy are necessary to determine the range of these mistakes.

### 5-2-1 Precision:

It is the agreement of values among frequent readings for particular content from the sample. The accepted value was specified in confidence level measurement at 95%, it ranges between (5-25%), equation (5-1) according to Maxwell(1968). The precision is the confidence level at (63%) according to Stanton, 1966, equation(5-2), the accepted value at (63%) ranges between (5-15%), (Shaw, 1969).

One sample was selected and divided to three homogenous portions; each portion had been given different number for analysis. (Appendix 6 -A) shows the results of precision at the confidence level (95%) and (63%), all results mostly lie within accepted limited ranges.

$$P \% = 2SD/X * 100 \dots (95\% \text{ confidence}) \dots (\text{Maxwell, 1968}) \dots (5-1).$$

$$P \% = SD/X * 100 \dots (63\% \text{ confidence}) \dots (\text{Stanton, 1966}) \dots (5-2).$$

Where:  $SD = \sqrt{(x_1 - X)^2 + (x_2 - X)^2 + (x_3 - X)^2 / N}$

$x_1, x_2, x_3 \dots$  are the actual readings of analyses of the same sample.

N: the number of readings (number of analyses).

X: the average of readings for each element.

SD: standard deviation.

### 5-2-2 Accuracy:

It is the closeness of the results to reality, using international standards, these Standard materials are to be used for estimating the accuracy of the analysis of the various elements. In this study, the British Chemical Standard no.393 (BSC limestone) was used to estimate the accuracy (Appendix 6 -B).

### 5-3 Correlation coefficient:

Geochemical results of major and trace elements were statistically treated to show their chemical behavior and characteristics in Benavi IRS.

Correlation analysis is a statistical test to determine the linear association between the pairs of the data, ( $r$ ) is a value of the linear relationship between the data pairs which ranges from -1.0 to +1.0, the negative sign indicates negative correlation, positive sign to positive correlation and zero indicates no correlation (Aull, 2005).

Appendix (7) shows the correlation coefficients of major and trace elements of IRS samples. The following terms were used in this study to explain the type of relationship among different elements in IRS samples modified after Jawad (1980).

- Very strong : where ( $r$ ) between (0.99+/- to 0.75 +/-).
- Strong : where ( $r$ ) between (0.74+/- to 0.50 +/-).
- Moderate : where ( $r$ ) between (0.49+/- to 0.38 +/-).
- Weak : where ( $r$ ) between (0.37+/- to 0.0 +/-).

Where significant value of ( $r$ ) = 0.38 (Murdoch and Barnes, 1985).

### 5-4 Benavi IRS Geochemistry:

#### 5-4-1 Geochemistry of major elements:

##### 5-4-1-1 SiO<sub>2</sub>:

The concentration of SiO<sub>2</sub> in Benavi IRS ranges between (1.05-7.40%) with the average of (3.78%). This average is very low in comparison with the other iron-rich sediments abroad, and it is also lower than Hussainiyat and Gaara ironstones (Appendix 8).

The distribution style of SiO<sub>2</sub> is binary loom (Fig. 5-4-A) indicating that there are two sources for SiO<sub>2</sub> content in IRS: quartz and clay minerals (mainly from chamosite and kaolinite). This suggestion is supported by the mineralogical investigations and

petrographical observations (chapter 3 & 4), and by the very strong positive correlation between SiO<sub>2</sub> and Al<sub>2</sub>O<sub>3</sub> (r=0.90).

There is also a very strong positive correlation between SiO<sub>2</sub> and TiO<sub>2</sub> (r=0.80) attributed to the geochemical similarity of silica and titanium (Spears, 1961), and to the similarity in the geochemical behavior of Al<sub>2</sub>O<sub>3</sub> and TiO<sub>2</sub> through weathering processes (Al-Rubaii, 1997).

The positive moderate correlation of silica with Na<sub>2</sub>O (r=0.38), reflects evidence of the presence of Na and SiO<sub>2</sub> in clay minerals (Hirst, 1962) supported by EDS analysis (Ap.4- Fig.(3) -spectrum 5 ).

The strong negative correlation of SiO<sub>2</sub> with CaO (r= -0.58), is due to the growth of authigenic quartz and chalcedony as replacement material in the cavities which produced by dissolution of calcite (Plate 4-5 ).

The higher concentration of SiO<sub>2</sub> was observed in sample BN10/1 (7.36%); this agrees with petrographical observations and XRD analyses, which showed the presence of quartz in significant amount in this sample .

#### **5-4-1-2 Fe<sub>2</sub>O<sub>3</sub> & FeO:**

Abundance of Fe in sedimentary rocks is determined by various factors including provenance, pH & Eh conditions and extent of diagenetic alteration. The Fe content in sedimentary rocks is variable: clay, shale and greywacke (> 6% Fe), arkose (3% Fe), quartz-feldspathic sandstone (0.5% Fe) and carbonate rocks (0.5% Fe). The iron-rich sedimentary rocks defined as those containing (15% Fe) or more, these rocks commonly referred to as ironstones or iron formations (James, 1966). The general rule governing the mobilization and fixation of iron are those oxidizing and alkaline conditions promoting the precipitation of insoluble iron (Fe<sup>+3</sup> oxides / hydroxides); whereas acidic and reducing conditions promote the solution of ferrous compounds; the released iron readily precipitates as oxides/hydroxides as well as it substitutes for Mg & Al... in other minerals according to various prevalent conditions (Pendias, 1992).

Subsequently, the different mineralogical phases of Benavi IRS revealed that this deposit suffered from many changes in the geochemical environment caused the formation of these phases. SEM showed the presence of mineralized bacteria in this deposit (Fig.5-3) therefore bacteria may have also catalyzed the precipitation of part of iron oxides/hydroxides where many microorganisms can grow by oxidizing  $\text{Fe}^{+2}$  to  $\text{Fe}^{+3}$  (Newman and Kappler, 2004).

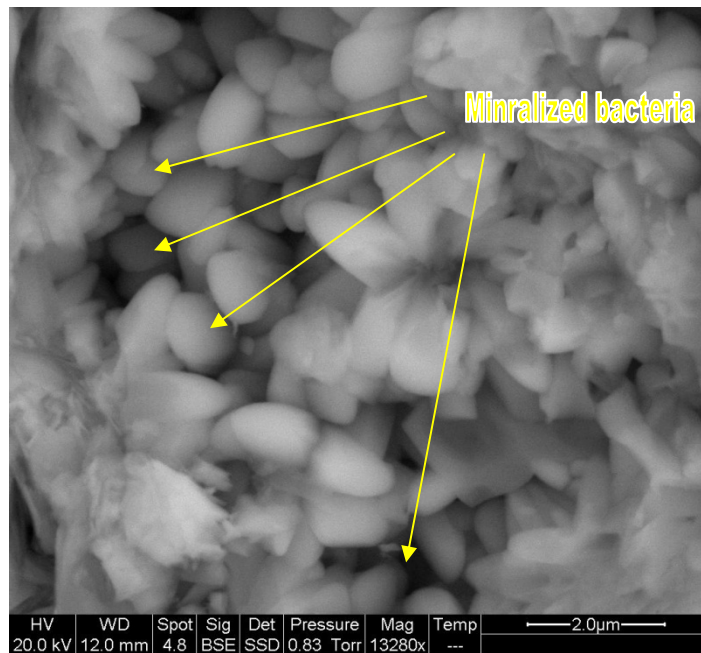


Figure (5-3): SEM view shows presence of mineralized bacteria in Benavi IRS.

The concentration of  $\text{Fe}_2\text{O}_3$  in IRS ranges (3.28-33.90%) with an average of (20.44%). The higher frequency in IRS samples is observed at the ranges (20-25%). The total iron of IRS is also measured (2.20-23.40 %) with average of (14.43%) .

Based on above and in comparison with other ironstones around the world, Benavi IRS can be considered as one of the low grades ironstones, and the iron content of Benavi IRS is lower than Gaara and Hussainiyat ironstones, too, (Appendix 8 ).

However, higher concentration of  $\text{Fe}_2\text{O}_3$  is observed at the upper parts of IRS outcrop, this is clearly shown in BN1, BN5 and BN6 (Fig. 5-2). There is a very strong negative correlation of  $\text{Fe}_2\text{O}_3$  with CaO ( $r = -0.92$ ) and L.O.I ( $r = -0.97$ ), this relationship supports the petrographical study, which showed the replacement of calcareous components by iron oxides / hydroxides minerals.

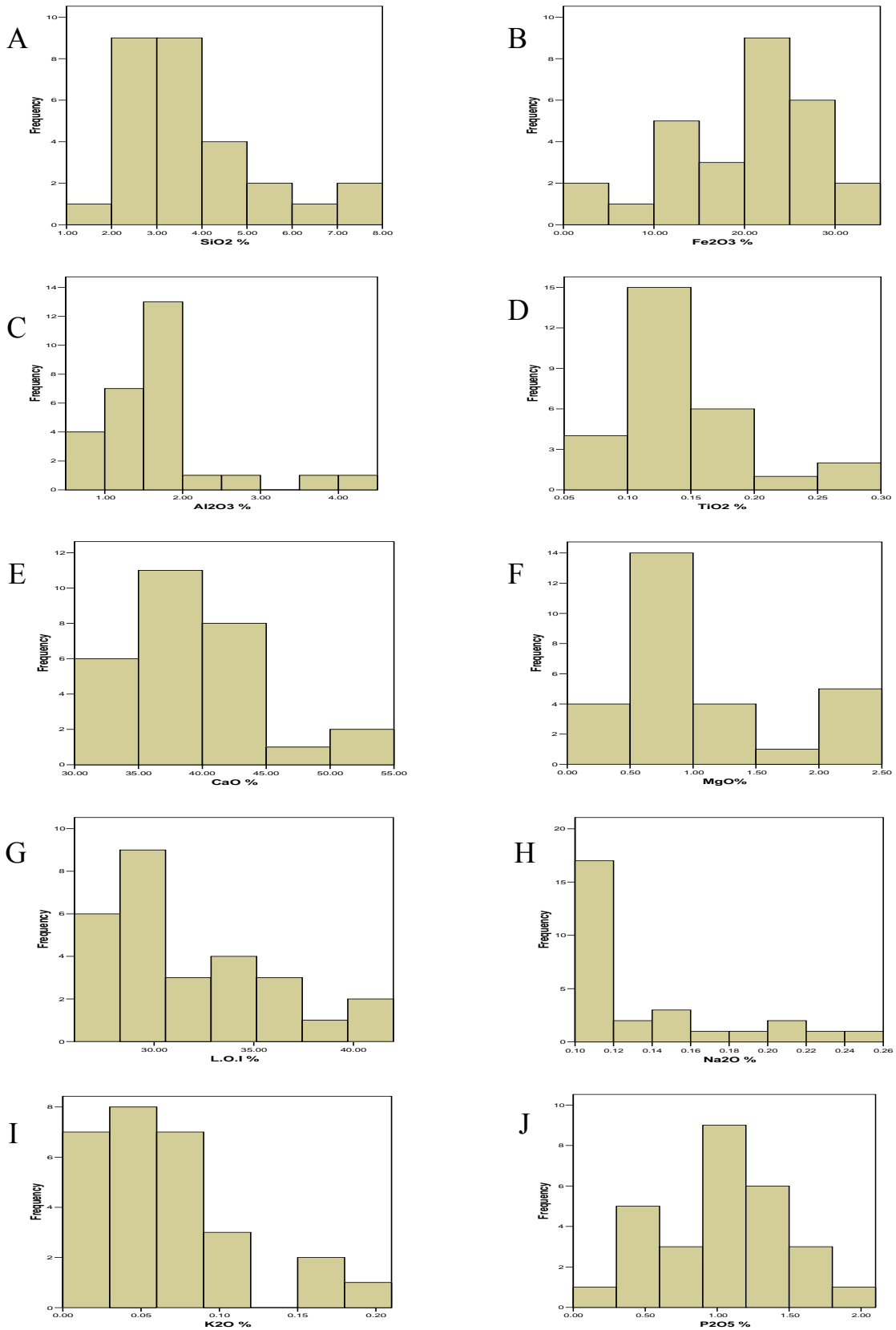


Figure (5-4): Histograms illustrating the distribution style of major oxides of Benavi IRS: A-SiO<sub>2</sub> %, B-Fe<sub>2</sub>O<sub>3</sub> %, C-Al<sub>2</sub>O<sub>3</sub> %, D-TiO<sub>2</sub> %, E-CaO %, F-MgO%, G-L.O.I %, H-Na<sub>2</sub>O %, I-K<sub>2</sub>O% and J-P<sub>2</sub>O<sub>5</sub> %.

Triple loom distribution style of  $\text{Fe}_2\text{O}_3$  (Fig 5-4-B ) refers to poly sources of iron content in IRS which are : iron oxides/hydroxides and other minerals such as, iron-bearing clay minerals present in IRS (chamosite ,glaucinite ), sulphides (pyrite , arsenopyrite) besides iron-rich carbonates minerals (siderite , ankerite).

FeO concentration is chemically measured, it ranges (0.71-16.65%) with average of (3.24%). The distribution style of FeO is also triple loom (Fig.5-6-A) indicating there are poly sources of  $\text{Fe}^{+2}$  in IRS. The first one is from chamosite and ankerite; this suggestion supported by the positively strong correlation of FeO with MgO ( $r=0.71$ ).

The second source is from pyrite supported by positively strong correlation of FeO with S ( $r= 0.55$ ). These positively relations in studied sections are clearly shown in (Fig.5-2).

The other sources of  $\text{Fe}^{+2}$  are from Magnetite, ferron calcite and siderite. All these minerals are present in IRS samples (chapter 3&4).

#### 5-4-1-3 $\text{Al}_2\text{O}_3$ :

$\text{Al}_2\text{O}_3$  content of Benavi IRS ranges between (0.53-4.13%) with the average of (1.67%). The higher frequency is observed at (1.97%). This content seems higher than sandy ironstones of Gaara ( Tobia , 1983) and lower than Hussainiyat ironstones (Yekta, 1981) , and it is also lower than most international ironstones(Appendix8) .

The very strong correlation between alumina and silica reflects that the main source of  $\text{Al}_2\text{O}_3$  in Benavi IRS is clay minerals (mainly kaolinite and chamosite as well as glaucinite in part).

The binary loom distribution style of  $\text{Al}_2\text{O}_3$  (Fig.5-4-C) revealed that there is another source for aluminum in IRS besides clay minerals which is probably goethite because XRD results showed there is substitution of  $\text{Fe}^{+3}$  by  $\text{Al}^{+3}$  in the lattice of goethite (Harder (1964) mentioned this possibility).

Regarding correlation coefficients,  $\text{Al}_2\text{O}_3$  has been chosen to represent clay minerals in order to understand the behavior of trace elements in IRS as clay minerals are the main resource for  $\text{Al}_2\text{O}_3$  in Benavi IRS. (Appendix 7) shows the positive relations of

Al<sub>2</sub>O<sub>3</sub> with trace elements. The positive moderate correlation with cobalt ( $r=0.45$ ) is due to the fact that most concentrations of cobalt in sediments attributed to the argillaceous fractions (Carr and Turekian, 1961).

#### 5-4-1-4 TiO<sub>2</sub>:

TiO<sub>2</sub> ranges (0.06-0.03%) with average of (0.15%). TiO<sub>2</sub> content of IRS is lower than Gaara and Hussainiyat ironstones and lower than many international ironstones as well as it is higher and close to others (Appendix 8).

The concentration of TiO<sub>2</sub> in kaolinite-rich soil is in the range (1-2%) (Jepson and Rowse, 1975), this percentage is similar to TiO<sub>2</sub> concentration of original igneous rocks (Bear, 1965). Weathering processes of these rocks produced kaolinite contain the same concentration of TiO<sub>2</sub> of the original rocks because in weathering titanium released as hydrous components Ti(OH)<sub>2</sub>, Ti(OH)<sub>4</sub> and redeposited as amorphous materials containing tiny crystals which grows to form anatase; the later relates to kaolinite by electrostatics bonds (Weaver, 1976). Therefore, there is very strong correlation of TiO<sub>2</sub> with Al<sub>2</sub>O<sub>3</sub> and SiO<sub>2</sub> ( $r=0.80$ ) and ( $r=0.84$ ) respectively; indicating that TiO<sub>2</sub> content in Benavi IRS may be attributed to kaolinite. Moreover, (Fig. 5-2) shows that TiO<sub>2</sub> adopts the same trend of SiO<sub>2</sub> and Al<sub>2</sub>O<sub>3</sub> in all IRS studied sections.

The distribution style of TiO<sub>2</sub> in Benavi IRS is Binary loom (Fig.5-4-D) indicating that there is another source of TiO<sub>2</sub> besides kaolinite as ore microscopic study showed the presence of rutile in sample no. BN10/1 (Plate 4-8-H) and the higher concentration of TiO<sub>2</sub> was in the same sample (Appendix 5-A). This is a good evidence that rutile is another source of TiO<sub>2</sub> in IRS.

#### 5-4-1-5 CaO:

Weight percentage of CaO is the highest one among the other major oxides in Benavi IRS, its range (32.48-51.83 %) with an average of (39.15%). This concentration is higher than CaO content of Gaara and Hussainiyat ironstones, and it is also higher than

most known international ironstones & iron formations. Though, there are only five international ironstones with CaO content close to Benavi IRS, these are :

Dolnilom ironstones in Bulgaria (15-54% CaO), Thosta-Beurgard ironstones in France (30-50% CaO), Kahlenberg ironstone in Germany (30.6% CaO), Nammen ironstones in Germany (33-36% CaO) and Camdag ironstones in Turkey (1.3-36.5% CaO) (Zitzmann, 1977), (Appendix 8).

The distribution style of CaO is binary loom (Fig. 5-4-E). The main source of CaO in Benavi IRS is from calcite; this suggestion supported by XRD, SEM analyses in addition to petrographical study which showed that calcite builds the framework constituents of studied samples (calcareous particle including algae, bioclasts and spary calcite cement). Another source of Ca is probably from phosphate minerals and Glaucinite where these minerals may contain Ca in their structures.

A very strong negative correlation of CaO with  $\text{Fe}_2\text{O}_3$  ( $r = -0.92$ ) attributed to the dissolution of calcite by slightly acidic solutions containing  $\text{Fe}^{+2}$  in the early diagenetic stage and iron oxides /hydroxides precipitation instead of calcareous dissolved parts causing replacement textures. There is also negative relation of CaO with  $\text{SiO}_2$ ,  $\text{P}_2\text{O}_5$  (Appendix 7) attributed to the silisification and phosphatization, respectively.

The strong negative correlation of CaO with  $\text{Al}_2\text{O}_3$  ( $r = -0.62$ ) revealed that clay minerals (kaolinite, chamosite and glauconite) increase when calcite constituents decrease due to dissolution; where they filled the cavities and pore spaces that produced by this dissolution. This may give interpretation for the negative relation of CaO with  $\text{TiO}_2$ ,  $\text{Na}_2\text{O}$  and  $\text{K}_2\text{O}$  due to their presence in the argillaceous fractions.

#### **5-4-1-6 MgO:**

It is in the range (0.36-2.45%) with an average of (1.05%); this average is relatively higher than Gaara and Hussainiyat ironstones, and it is also higher than many international ones with exception of Minette and Thuringia ironstones (Appendix 8).

The distribution style of MgO in Benavi IRS is binary loom (Fig.5-4-F) which yields evidence for two sources of Mg in the studied samples compiled with other evidences.

The main source of Mg in Benavi IRS is chamosite, this suggestion supported by the positive relations of MgO with: FeO, SiO<sub>2</sub> and Al<sub>2</sub>O<sub>3</sub> (Appendix 7). These relations may give indication to the conjugation between Mg and (FeO+SiO<sub>2</sub> + Al<sub>2</sub>O<sub>3</sub>) in one mineralogical phase which is mostly chamosite depending upon XRD, SEM, EDS(Figs:4-1&Ap.4-Fig.(1)-B) as well as petrographical study (Plate 4- 4 ) where all these techniques provided good evidences to widely distributed presence of chamosite in Benavi IRS. Although the dolomitization has been observed very limited in Benavi IRS (petrographically), but part of Mg concentration in IRS samples probably due to this process, as well as to scattered euhedral dolomite crystals that were observed present in some samples associated with quartz ( Plates: 4-7-A,B&C ).

XRD showed that calcite is impure (because substitutions of Mg<sup>+2</sup> and Fe<sup>+2</sup> in calcite crystals lattice) (Fig.3-5). XRD and SEM also confirmed presence of ankerite in Benavi IRS (Fig.3-9). Based on above the another source of Mg besides chamosite is from carbonates minerals containing Mg: (dolomite, impure calcite and ankerite ).

#### **5-4-1-7 L.O.I:**

(L.O.I) is in the range (26.02-41.76%) with an average of (31.57%), this average is higher than Gaara and Hussainiyat ironstones , and higher than many International ironstones(Appendix 8 ). Fig. (5-2) clearly shows that L.O.I percentage increases with increasing of CaO content in all IRS sections, as well as, there is very strong positive correlation between CaO and L.O.I ( $r=0.95$ ) . Conversely there is very strong negative correlation of L.O.I. with Fe<sub>2</sub>O<sub>3</sub> ( $r= -0.97$ ) in addition to other negative relations of L.O.I with Al<sub>2</sub>O<sub>3</sub>,SiO<sub>2</sub>,TiO<sub>2</sub>,Na<sub>2</sub>O ,K<sub>2</sub>O and P<sub>2</sub>O<sub>5</sub> (Appendix 7).

The statistical graph of L.O.I shows triple loom style type (Fig.5-4-G), this style with relations above revealed that L.O.I is produced mainly by decomposition of carbonate minerals, and also produced by: released adsorbed water, dehydration of limonite, dehydration or dehydroxlation of goethite and dehydroxlation of clay minerals, especially kaolinite. This suggestion is supported by TGA analyses, (Fig.3-10 and Table 3-2).

**5-4-1-8 Na<sub>2</sub>O:**

(Na<sub>2</sub>O) is in the range of (0.10-0.26%) with average of (0.14%), this percentages are normal in comparison with other ironstones (Appendix 8).

Billings (1978) mentioned that the percentage of (Na) in sediments lesser than its percentage in earth's crust (2.9%, Mason, 1982) attributed that to great dissolubility of Na through chemical weathering processes. Conversely (Fe) has great separation; therefore, the quantity of (Na) decreases in iron-rich sediments. Goldschmidt (1958) mentioned that sodium is present in clay minerals by adsorption, this is supported by EDS analysis where the concentration of (Na) was found (0.27 - 0.35 %) in the clays of IRS.

The distribution style of Na<sub>2</sub>O is triple loom (Fig.5-4-H) revealed poly sources of Na<sub>2</sub>O in IRS. The main source probably belongs to kaolinite because the later fixes sodium by surface adsorption (Goldschmidt, 1958) this suggestion supported by positive relations of Na<sub>2</sub>O with SiO<sub>2</sub> and Al<sub>2</sub>O<sub>3</sub> in Benavi IRS (Appendix 7) and also supported by EDS analysis (Ap.4-Fig. (14)-spectrum 3).

Na may also present in glauconite (Ap.4-Fig. (14)-spectrum 4) and in chamosite (Ap.4-Figs: (3) - spectrum 5 and (8) - spectrum 3). Goldschmidt (1958) also mentioned that there is a possibility of substitution of Ca by Na in the lattice of calcite crystals, this suggestion is supported by the negative relation of Na<sub>2</sub>O with CaO (Appendix 7).

**5-4-1-9 K<sub>2</sub>O:**

It ranges (0.01-0.21%) with an average of (0.06%); this average is close to the K<sub>2</sub>O content of Gaara and Hussainiyat ironstones, and it is also close to K<sub>2</sub>O content of most international ironstones (Appendix 8).

The distribution style of K<sub>2</sub>O is binary loom (Fig. 5-4-I). The modicum potassium in ironstones is attributed to its adsorption by manganese hydroxides that concentrated after iron deposition (Rankama & Sahama, 1950). However, the positive relations of K<sub>2</sub>O with SiO<sub>2</sub> and Al<sub>2</sub>O<sub>3</sub> in IRS indicate the conjugation of potassium with clay

minerals present in this deposits, where clays have good tendency for adsorbing cations and retaining them in an exchangeable state (Grim , 1968).

Petrographic study showed the presence of glauconite in some samples (Plate 4-3-A, B &C); therefore, some of  $K_2O$  in Benavi IRS may belongs to glauconite.

EDS analyses of spot area also showed the presence of K that is mostly related to glauconite (Ap.4-Fig.( 8)-spectrums:1,2 & 6 ).

Thus, the positive relations of  $K_2O$  with  $Na_2O$  , $SiO_2$  and  $Al_2O_3$  give evidence that The main source of K & Na in Benavi IRS is from clay minerals (Kaolinite , chamosite as well as glauconite ).

#### **5-4-1-10 $P_2O_5$ :**

Phosphates concentration in Benavi IRS is in the range (0.21-2.08%) with an average of (1.04 %). It is higher than Gaara and Hussainiyat ironstones and many international ironstones with exception with minette ores (Appendix 8 ).

The distribution style of  $P_2O_5$  is binary loom (Fig. 5-4-J). Correlation coefficient of  $P_2O_5$  is negatively strong with CaO ( $r= -0.58$ ). This negative relation is attributed to phosphatization where petrographic study showed the presence of partial or complete replacements in fossils by phosphates (Plates: 4-3-D,E,F,G&H ). Therefore, there is strong negative correlation of  $P_2O_5$  with L.O.I as the later relates with CaO.

(Matukhin et al, 1981) supposed that phosphates minerals adsorbed by iron hydroxides. Bergman and Savinova (1978) also mentioned that ( P) is collected as a result of adsorption by iron hydroxides, where the positively charged colloidal iron hydroxides adsorbed negative phosphates ion (Day, 1963 ; Borchert, 1960).

EDS elemental transverse in (Fig.5-5 ) shows increase in phosphates concentration in IRS besides iron oxides and raised the interpretation of why  $P_2O_5$  related positively to iron in Benavi IRS.

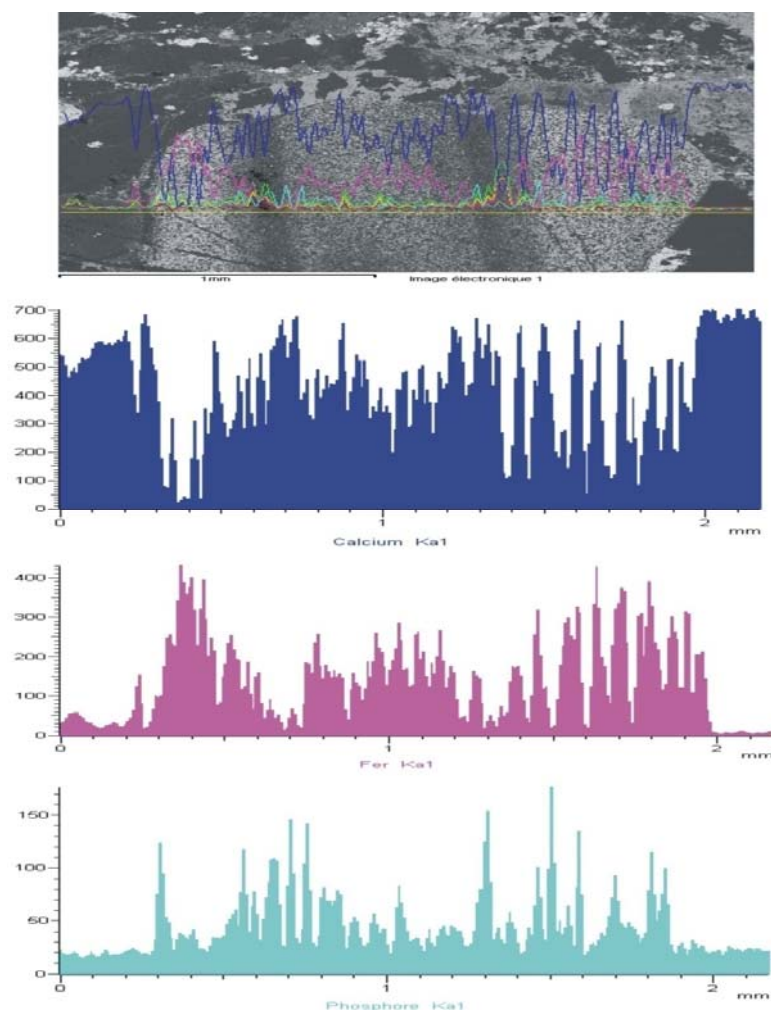


Figure (5- 5): EDS elemental transverse shows  $P_2O_5$  positively relates with iron oxides in Benavi IRS.

#### 5-4-2 Geochemistry of Trace elements:

The variations in concentrations of eight trace elements were studied. The vertical variations of these elements for the total samples in BN1, BN2, BN5 and BN6 sections are shown in (Fig.5-2).

In general, the trace elements of Benavi IRS samples are positively related to iron oxides / hydroxides and clay minerals due to their adsorption on the surfaces of these minerals. Sometimes negative relations were exhibited. Details are in the following:

##### 5-4-2-1 S:

Sulfur content ranges (0.0-1700 ppm) with an average of (214.12ppm). The concentration of sulfur in Benavi IRS is approximately lower than Gaara and Hussainiyat and many international types of ironstone (Appendix 8).

There is strong positive correlation of S with FeO ( $r= 0.55$ ) attributed to the presence of pyrite in Benavi IRS with significant amounts ( especially at the base of this deposits ) where chemical analyses showed that the highest quantities of S concentrations were found in samples: BN1 /4, BN2/8 and BN9/1, (1700 ppm, 1200 ppm, 1500 ppm, respectively ). These samples were selected from the bottom of IRS body. EDS confirmed the presence of pyrite in these samples, and also in other samples that site at the upper part of IRS like BN5/4, which contains high amount of hematite indicating the distribution of pyrite in all IRS body but in different amounts; reflecting the highly pyritization process effects in diagenetic history of Benavi IRS.

The distribution style of S is binary loom (Fig.5-6-B) indicating another source of S. According to (Matukhin et al, 1981), some of S in ironstones is probably derived from preserved organic materials containing sulfur. (Schwertmann et al,1977) also mentioned that sulphates adsorbed on the surfaces of oxides/hydroxides and react with Fe-OH bond to form complex components like behavior of phosphates; this link of sulphates with iron oxides is weaker than phosphates (Scott, 1986). Correlation coefficients also showed positive relations of S with MgO (Appendix 7); these relations are interpreted in term of the coexisting of pyrite with ankerite (Fig. 4-9 ) and chamosite ( Ap.4-Fig.(1)-B) in Benavi IRS.

#### **5-4-2-2 Mn:**

(Mn) content of Benavi IRS ranges (22-215ppm) with an average of (123.93ppm). Its concentration is higher than Gaara and relatively close to Hussainiyat ironstones, while it is very low in comparison with international ironstones. This is compared with the Mn content of the oolitic and limonitic ironstones of minette ores of Lorraine of range (4500-3900ppm) , the limonitic oolites of north Gottingen in Germany of average (1600ppm ) and the Pazde-Rio oolitic ironstones of range (400-4200 ppm), the low Mn content of Benavi IRS was probably due to the original low Mn content of source area (Yekta, 1981).

The distribution style of Mn is binary loom (Fig.5-6-C) indicating double sources for Mn in IRS (calcite & iron oxides).

The positive correlation of Mn with Fe in Benavi IRS is attributed to the geochemical similarity in the behavior of Mn and Fe (Krauskopf, 1979) where there is possibility in manganese transportation as coatings for iron oxides (Gibbs, 1973); there is also possibility for the replacement of  $\text{Fe}^{+2}$  by  $\text{Mn}^{+2}$  in iron oxides containing  $\text{Fe}^{+2}$  in their structures ; therefore, the negative relation of Mn with FeO in IRS samples may give an evidence to the replacement of  $\text{Fe}^{+2}$  by  $\text{Mn}^{+2}$  in magnetite . This suggestion is supported by ore microscopy observations which showed duller reflectivity of this mineral according to Ramdohr (1980) who mentioned that the duller reflectivity of magnetite denote the Mn content in this mineral.

The negative relationship of Mn with CaO probably indicates substitution of  $\text{Ca}^{+2}$  by  $\text{Mn}^{+2}$  under reducing sea water conditions (Bencini, and Allesandro, 1974).

The correlation coefficient of Mn with  $\text{SiO}_2$  and  $\text{Al}_2\text{O}_3$  indicates no relation between clay minerals and Manganese in Benavi IRS (Jawad, 1980).

#### **.5-4-2-3 Zn:**

(Zn) ranges between (17.0-75.0 ppm) with an average of (38.29ppm); this content is higher than Gaara and Hussainiyat, but it is lower than most international ironstones (Appendix 8). The distribution style of Zn in IRS appeared as binary loom (Fig.5-6-D).

The positive correlation coefficients of Zn with  $\text{Al}_2\text{O}_3$  &  $\text{SiO}_2$  (Appendix 7) give evidence to the relationship of Zinc with clay minerals (Till, 1971), where EDS analyses showed presence of ZN in clay minerals (chamosite) (Ap.4-Fig. (21)-A-spectrum 3).

The close relationship of Zinc with iron minerals is reflected by the positive relations with Co( $r= 0.37$ ) and Ni( $r= 0.41$ ) . Geochemically, the later elements are close to iron.

In addition to the soluble salts of Zinc formed through weathering processes are adsorbed and precipitated with iron hydroxides (Goldschmidt, 1958).

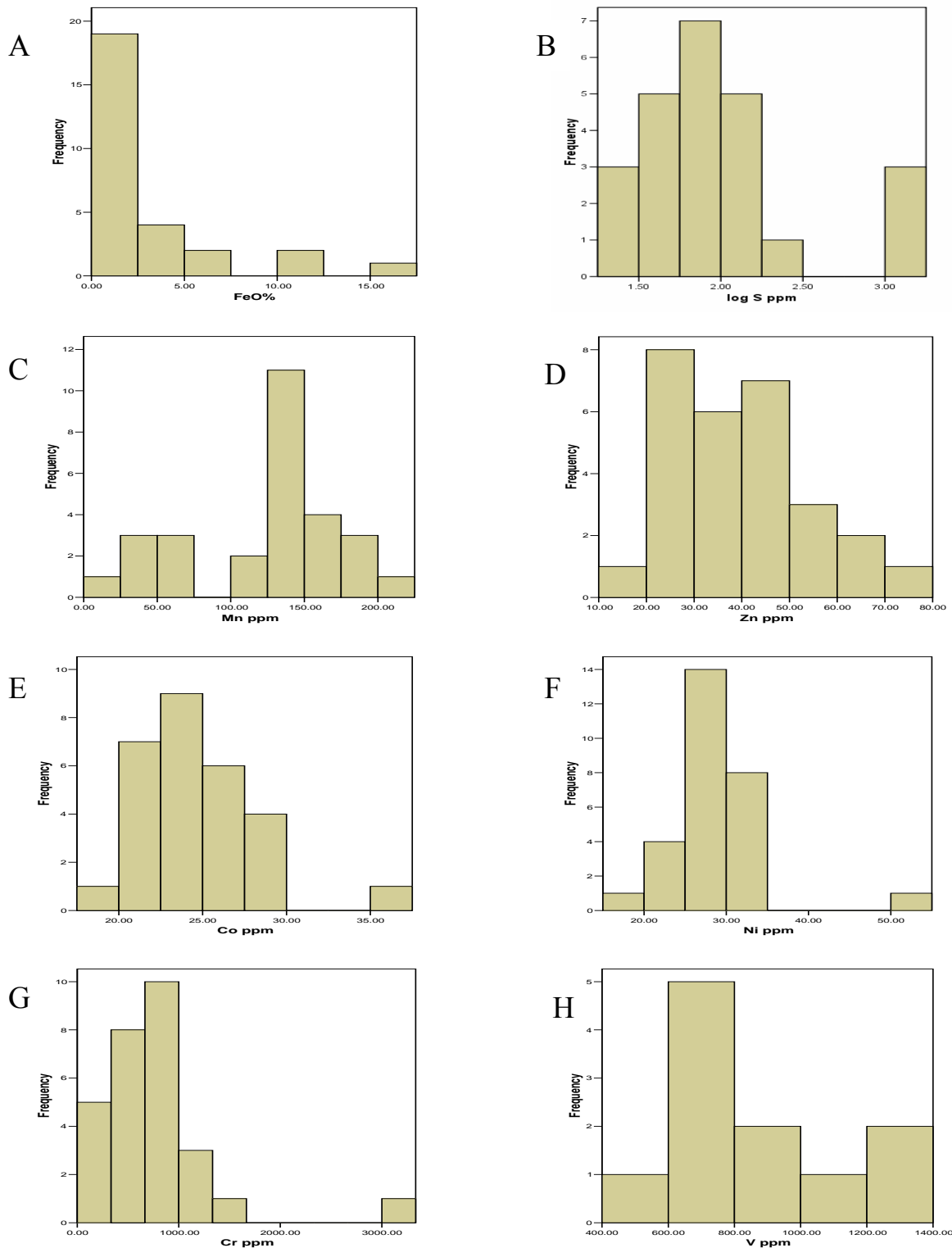


Figure (5-6): Histograms illustrating the distribution style of trace elements and FeO of Benavi IRS: A- FeO%, B- Log S ppm, C- Mn ppm, D- Zn ppm, E- Co ppm, F- Ni ppm, G- Cr ppm & H- V ppm.

**5-4-2-4 Co:**

Cobalt ranges between (18.0-37.0 ppm) with an average of (24.64ppm); this content is close to sandy ironstones of Gaara and to Hussainiyat ironstones, but it is lower than oolitic – pisolitic Gaara ironstones, and it is also lower than most international ironstones (Appendix 8 ).

The distribution style of cobalt is binary loom (Fig.5-6-E), where there is positive strong correlation of cobalt with:  $Fe_2O_3$  ( $r= 0.58$ ) and Ni ( $r= 0.3$ ) due to the similar geochemical behavior of iron, nickel, and cobalt as their radii are close ( $Fe= 1.27A^\circ$ ,  $Co= 1.26 A^\circ$  and  $Ni= 1.24 A^\circ$ ) (Goldschmidt, 1958). Also, cobalt associated with clay minerals supported by its positive relations with  $SiO_2$  and  $Al_2O_3$  (Hirst, 1962; Carr and Turekian, 1961).

**5-4-2-5 Ni:**

(Ni) content of Benavi IRS ranges between (18.0-53.0 ppm) with an average of (28.0 ppm); it is lower than Gaara, Hussainiyat and most international types ironstones (Appendix 8). In oxidate sediments such as, sedimentary iron ores, the concentrations of Ni & Co are generally low, mostly lower than the average of upper lithosphere (Goldschmidt, 1958).

The distribution style of nickle in Benavi IRS is binary loom (Fig.5-6-F); reflecting its relation with iron minerals and Kaolinite (Jawad, 1980). This suggestion is supported by positive relations of Ni with  $Fe_2O_3$ ,  $SiO_2$  and  $Al_2O_3$  (Appendix 7). According to (Koppelman and Dillard, 1977), (Ni) is one of elements adsorbed on the surface of clay particles like kaolinite and illite .

The highest concentrations of Ni in IRS are observed in samples containing higher amount of goethite such as: BN2/5, BN5/3, BN8/4 and BN10/1 (Appendix 5-A), in comparison with other samples (Mason, 1982).

Based on above ( Ni ) content of Benavi IRS may be attributed to the clay minerals (especially kaolinite ) and ironoxides/hydroxides (especially goethite ).

**5-4-2-6 Cr:**

It ranges between (75.0-3305 ppm) with an average of (749.46 ppm); this average is higher than Gaara , Hussainiyat and most known international ironstones (Appendix 8).

Chromium is a characteristic constituent of the ironstones, mainly lying in the range (10 – 400 ppm). Generally Aswan ironstone contains Cr about ( 230 ppm ), the ironstones of Wittmannsgereurth , Schmiedfeld and Thuringian basin are with content (400-600 ppm) (Mucke and Farshad, 2005). It is apparent that Benavi IRS has unique content of chromium among international ironstones.

The distribution style of Cr in Benavi IRS is binary loom (Fig.5-6-G). The positive moderate correlation coefficient of Cr with FeO ( $r=0.47$ ) and S( $r=0.42$ ) could be explained in terms of as an evidence that pyrite caused this unusual content (Houda et al, 2007) .

According to (Morse and Luther, 1999) , Cr can be reduced by biological and chemical means, and there are several studies on the methods and possible mechanisms of reduction of hexavalent chromium . Iron minerals are ubiquitous in nature and play a critical role in the geochemical cycling of trace elements where pyrite and other reactive iron sulfide minerals are important to sedimentary trace elements behavior.

Pyrite is the most common iron sulphide mineral at the earth surface appears as an interesting natural reductant to reduce  $Cr^{+6}$  to  $Cr^{+3}$  (Frederic et al, 2005), and also pyrite was found to act as an efficient  $Cr^{+6}$  reducing agent (Doyle et al, 2004). This study showed that chromium is related to clays( mostly chamosite) as the EDS analyses confirmed this association (Fig. 5-7 ), supported by positive relation of Cr with:  $SiO_2$  ,  $Al_2O_3$  , MgO and FeO as shown in (Appendix 7) .

According to (Shiraki and Matzat, 1978), chromium has the tendency to concentrate in clay minerals. Partially substitution of  $Al^{+3}$  in octahedron layer of kaolinite by  $Cr^{+3}$  may be present (Maximovic et al, 1981).

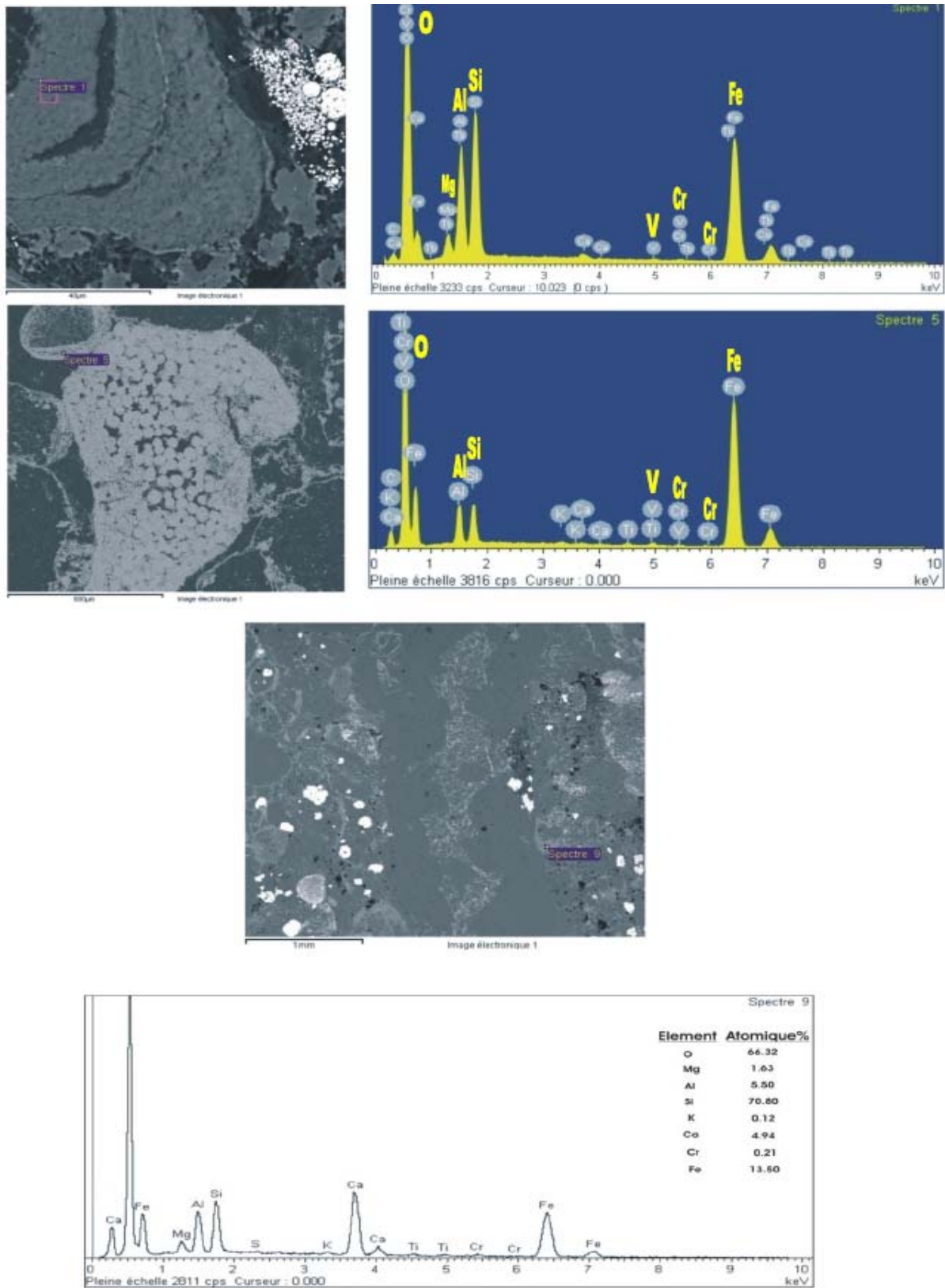


Figure (5-7): BSE image and EDS analyses showing chromium associated with clays (mostly with chamosite) in Benavi IRS .

**5-4-2-7As:**

EDS analyses showed the presence of arsenic in Benavi IRS where it is found in pyrite, goethite as well as arsenopyrite (Fig.5-8). According to Lazareva (2004), there are four major possible source of arsenic in sediments:

1-Francolite : Calcium phosphate or apatite can contain up to 1000 ppm of arsenic.

2-Sulfide minerals such as, pyrite and arsenopyrite : Prior studies of sulfide minerals in sediments revealed significant enrichment of arsenic in pyrite with concentrations as high as 11,200 and in pyrite framboids of up to 1000 ppm as a substitute element for sulfur in the FeS<sub>2</sub> structure. Therefore, sedimentary pyrite can be source of arsenic.

3-Clay and organic matter: Clays and organic substances can easily interact with heavy metals such as, arsenic via ion exchange or surface adsorption where they readily adsorb arsenic because they have very small particle size, which therefore result in a large surface area per unit volume and ability to adsorb arsenic.

4-Iron oxides/hydroxides: (As) adsorbed on to the extremely high surface area of precipitated iron oxides/hydroxides

More ever, arsenic may partially replaces phosphorous in apatite as  $As_5O_4PO_4$ , but this replacement is limited due to the larger ionic radius of (As) compare to ( P ) (Al-bassam, 2008, Personal communications).

EDS analyses in this work showed that the main sources of arsenic in Benavi IRS attributed to:

1-Pyrite: The concentration of arsenic is found in euhedral pyrite up to (1100 ppm), massive pyrite up to (5600ppm) and framboidal pyrite between (1600-2400ppm) (Fig 5-8 B, C and E, respectively).

2-Goethite: Arsenic has been found in goethite which produced by goethitization of pyrite. Its concentration in goethitized massive pyrite is ( 6700ppm) whereas in goethitized framboidal pyrite is (1500ppm ), (Figs. 5-8- D & F respectively ).

3-Arsenopyrite : Arsenic presence in the lower part of Benavi IRS is attributed to pyrite, goethite and arsenopyrite, where the later is only found in this part (Fig.5-8-A) .

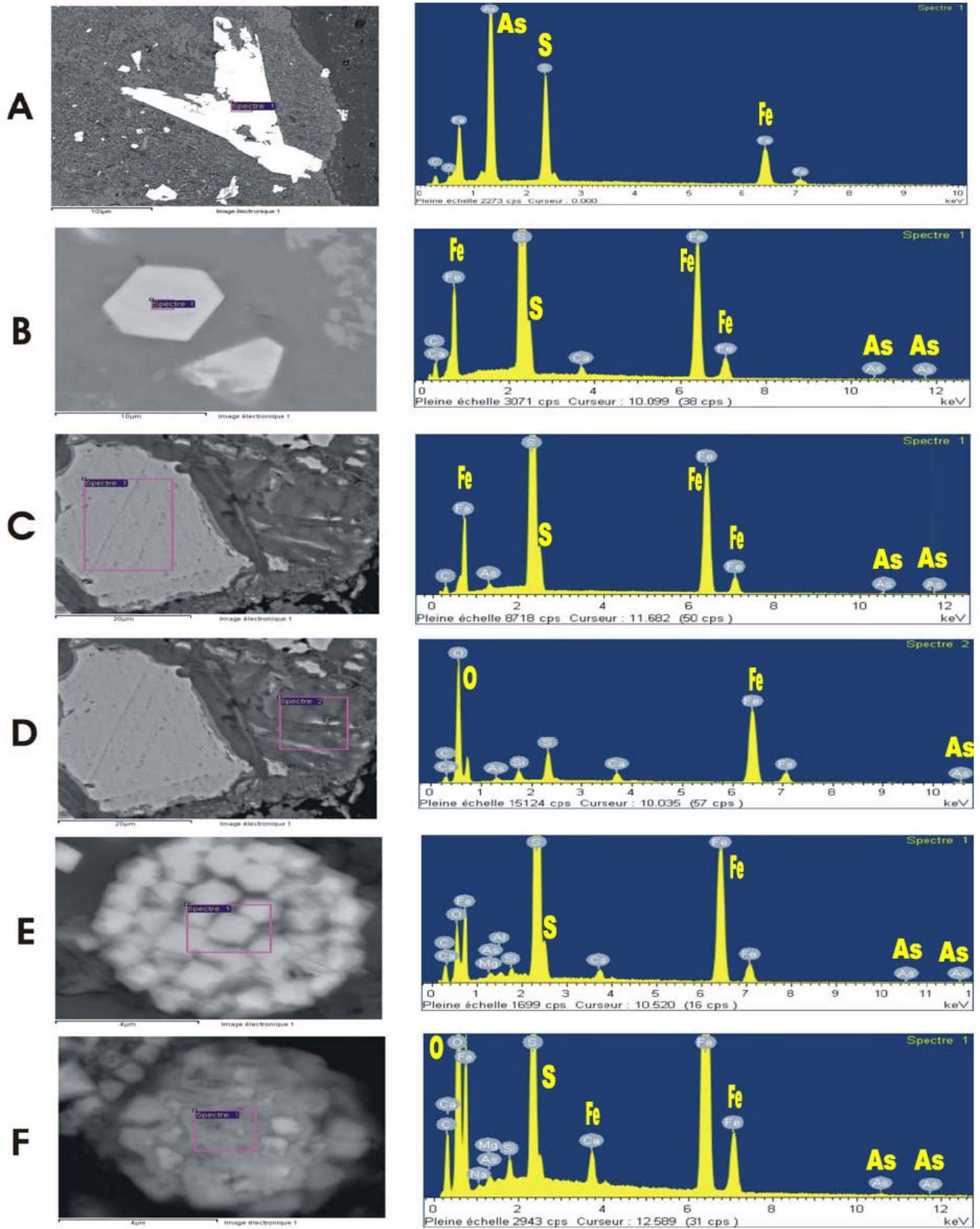


Figure (5-8): BSE images and EDS analyses showing arsenic content in: A-arsenopyrite, B-euhedral pyrite, C-massive pyrite, D-goethite (after goethitization of massive pyrite), E-framboidal pyrite and F-goethite (after goethitization of framboidal pyrite ).

**5-4-2-8 V:**

The presence of (V) in Benavi IRS is in significant concentrations; it ranges (400-1300ppm) with average of (800ppm), this concentration is higher than sandy ironstones of Gaara, Hussainiyat & most international ones, and it is slightly lower than oolitic & pisolitic ores of Gaara (Appendix 8).

The binary loom distribution style of vanadium (Fig.5-6-H) explains the conjugation of vanadium with clay minerals and iron oxides/hydroxides this suggestion is supported by the positive correlation of (V) with Fe, SiO<sub>2</sub> & Al<sub>2</sub>O<sub>3</sub> and it is also supported by EDS analyses which showed the presence of Vanadium in clay minerals (chamosite & kaolinite) and iron oxides/hydroxides (Fig. 5-9).

Vanadium relates with clay minerals through their formation (Rankama and Sahama, 1950) where there is possibility for V substitution with Al in clay minerals (Landergrén, 1978); this substitution probably occurred in clays of Benavi IRS because there is weak positively correlation of V with Al<sub>2</sub>O<sub>3</sub> where this substitution usually causes decreasing in positive relation with Al.

**5-4-3 Mn/Fe:**

Mn / Fe ratios of Benavi IRS samples are given in (Appendix 5-B), it varies between (0.0002-0.0035) with average of (0.0011), and this narrow variation indicating sedimentary origin (Koc & Bektas, 2003). The chemistry of iron and manganese are closely analogous. The main controls on the Fe & Mn phases present in solution for forming as precipitates are the Eh & pH of the solutions and the concentration of other ions present (Krauskopf, 1979). Manganese are more soluble under many conditions than iron ions, and ferrous ions are more readily oxidized than manganese ions, the greater mobility of Mn will lead to a greater tendency for Mn to move leaving behind an Fe-rich deposits (Maynard, 1983). Thus, inorganic processes should always lead to precipitation of iron before manganese from a solution containing both metals (Krauskopf, 1957).

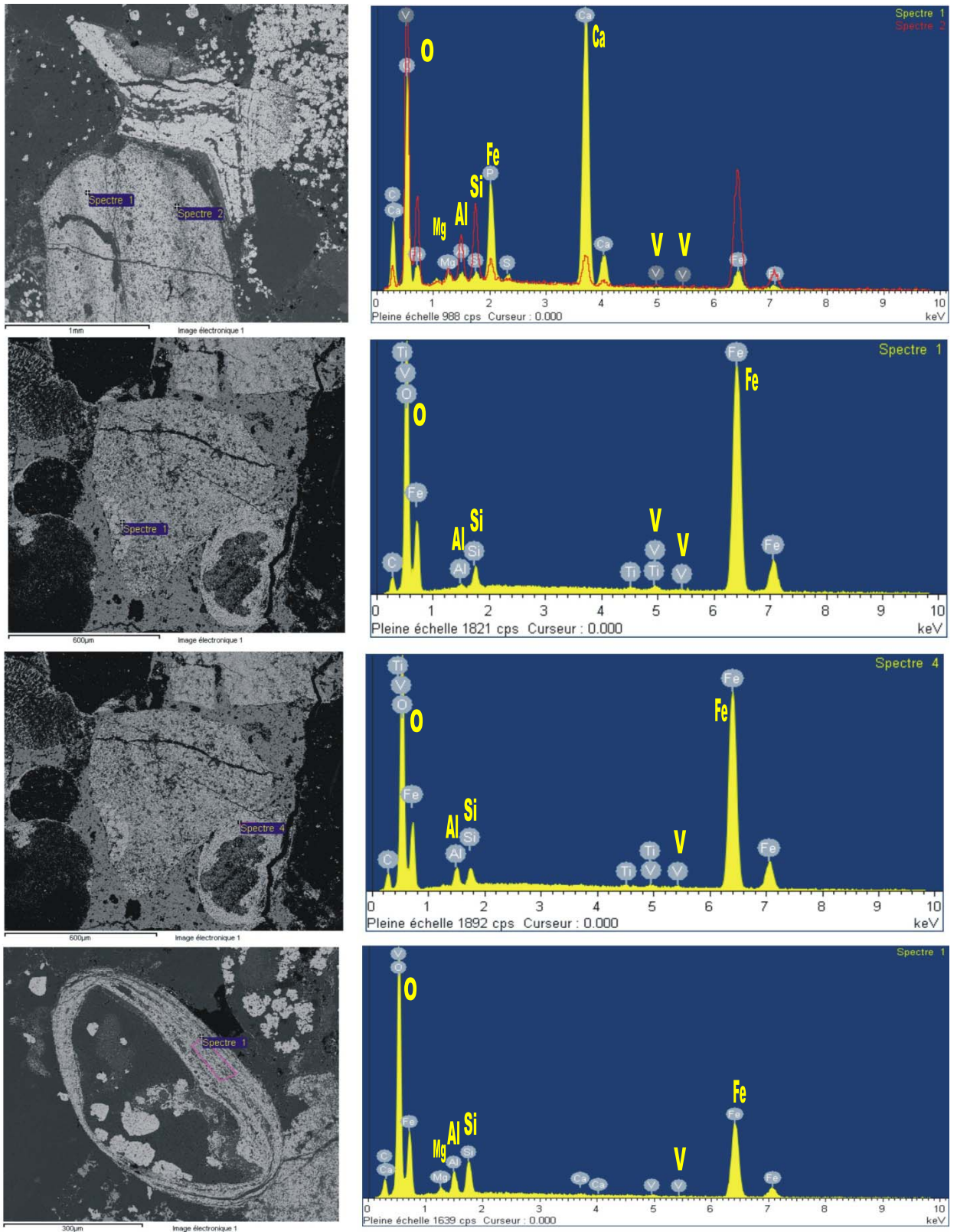


Figure (5-9): BSE images and EDS analyses showing Vanadium association with clay minerals and iron oxides/hydroxides.

According to (Lepp, 1963), Mn/Fe in sediments is about (0.022). The average of this ratio in igneous rocks is about (0.025), ( Lepp and Goldich, 1964).

In comparison with ratios mentioned above, the Mn/Fe values of Benavi IRS revealed high geochemical separation between iron and manganese in this deposit.

### 5-5 Factor analysis:

Statistical SPSS-12 program was used in this study for principle components analysis (factor analysis) to clarify and determine the important factors affecting the distribution style of chemical elements and predominant associations of these elements within group of geochemical variables (Davis, 1973).

This principle component analysis was carried out based on chemical analyses of twenty-eight samples. The significant value ( $r=0.38$ ) has been adopted in the interpretation, and any value less than 0.38 was neglected.

Five factors appeared and interpreted about (80.714%) of cumulative variance as shown in (Appendix 9-A); these factors are:

#### Factor (1):

It relates positively with:  $\text{Fe}_2\text{O}_3$  ,  $\text{Al}_2\text{O}_3$ ,  $\text{SiO}_2$ ,  $\text{TiO}_2$ ,  $\text{K}_2\text{O}$ ,  $\text{P}_2\text{O}_5$ ,  $\text{Co}$  and  $\text{Ni}$  , and negatively with  $\text{CaO}$  and L.O.I . This factor forms (34.106%) of total cumulative variance. It represents the initial dissolution of calcareous constituents of original rocks (algal-bioclastic –packstone ) and replacement processes that occurred simultaneously with dissolution or/and later of dissolution. These processes are: iron oxides/hydroxides replacement, silification, phosphatization .... (Chapter 4 ). This factor also expresses clay minerals occurrences in Benavi IRS. The very strong positive of this factor with  $\text{Fe}_2\text{O}_3$  is probably attributed to the oxidation of different mineralogical phases, which occurred mostly after Benavi IRS exposure .

**Factor (2):**

It forms (18.383%) of cumulative variance and relates positively with: FeO, MgO, SiO<sub>2</sub>, Al<sub>2</sub>O<sub>3</sub>, S, TiO<sub>2</sub>, Zn and Cr, and negatively with Fe<sub>2</sub>O<sub>3</sub>. This factor explains the effects of early diagenetic stage after burial which caused chamosite formation and pyritization in the whole Benavi IRS body and also gives evidence to chromium reduction by pyrite in this stage (Houda et al, 2007).

**Factor (3):**

It forms (14.033%) of cumulative variance and relates positively with SiO<sub>2</sub>, Al<sub>2</sub>O<sub>3</sub>, TiO<sub>2</sub>, Na<sub>2</sub>O, K<sub>2</sub>O and negatively with Fe<sub>2</sub>O<sub>3</sub> & Cr. This factor probably explains the effect of high alkaline conditions, which caused dissolved siliceous particle to redeposit as authigenic quartz which clearly observed under microscopes. These conditions also caused adsorption of Na<sub>2</sub>O by Kaolinite (Lorenz, 1969; Jepson, 1984).

This factor explains the continuity of clay mineral development because they have good tendency to adsorb K<sup>+</sup> (Goldshmidt, 1958), and also it may relate to glauconite formation, where normally there is negative relation between clay minerals and Ferric oxides (Al-Youzbaky, 1989).

**Factor (4):**

It forms (7.527%) of cumulative variance and relates positively with Ni and negatively with Na<sub>2</sub>O. This factor explains the presence of Ni in Benavi IRS which usually occurs in dispersed state in the rocks due to its ready substitution for Fe & Mg in silicates (Maynard, 1983). This factor also expresses the ability of Na to separate from iron in the weathering solution due to its high solubility (Lepp, 1975).

**Factor (5):**

It forms (6.665%) of cumulative variance, and relates strongly positive with manganese. This factor may explain the oxidation of manganese at high redox potential where Mn is usually soluble, except under strongly oxidizing conditions (Maynard, 1983).

### 5-6 Cluster analysis:

R-Mode cluster analysis has been carried out and shows three main clusters or groups (Appendix 9-B); comprise the components of all mineralogical phases of Benavi IRS. These groups are:

#### **Group A-(SiO<sub>2</sub>, Al<sub>2</sub>O<sub>3</sub>, TiO<sub>2</sub>, Na<sub>2</sub>O, K<sub>2</sub>O, MgO, P<sub>2</sub>O<sub>5</sub> and FeO):**

This group involves components of clay minerals, quartz and phosphates of the IRS samples. The presence of MgO with this group indicates very low dolomite content in IRS samples and supporting petrographical observation, XRD and the other techniques which showed that dolomitization is limited in Benavi IRS.

#### **Group B-( Fe<sub>2</sub>O<sub>3</sub>, Co, Ni):**

This group involves iron oxides and associated trace elements.

#### **Group C- (CaO, L.O.I):**

This group involves the coexisting of CaO and L.O.I in one group denoted to the calcite prevalent in studied samples.

Group A ( which includes clay minerals content of IRS) relates with groups ( B&C) by Zn link; this indicates that the relationship of zinc with both clay minerals and iron oxides minerals.

All groups are related together by Mn link, exhibits that manganese content is dispersed in all mineral phases.

This graph also shows that the biggest source of Fe<sup>+2</sup> is from chamosite, because FeO appeared in group A(associated with SiO<sub>2</sub>, Al<sub>2</sub>O<sub>3</sub> and MgO), and did not relate directly with S.

This graph also confirms the positively powerful relation of S and Cr.

### 5-7 Geochemical criteria in classification & genesis:

Depending upon some geochemical characteristics, Benavi IRS has been classified as ironstones, and it seems to be sedimentary in origin.

James(1992) showed that Phanerozoic ironstones can be distinguished from pre-Cambrian iron formations within  $[(\text{FeO}+\text{MnO})-\text{Fe}_2\text{O}_3-\text{SiO}_2]$  diagram, based on 131 analyses of ironstones and 129 analytical points of iron formations, distributed over all continents and originating from 17 countries and 43 localities, additionally Fig. (5-10) contains the proposed lines of James (1992) separating the two types of deposits (Mucke and Farshad, 2005).

It is clearly shown that Benavi IRS samples plot in the field of ironstones.

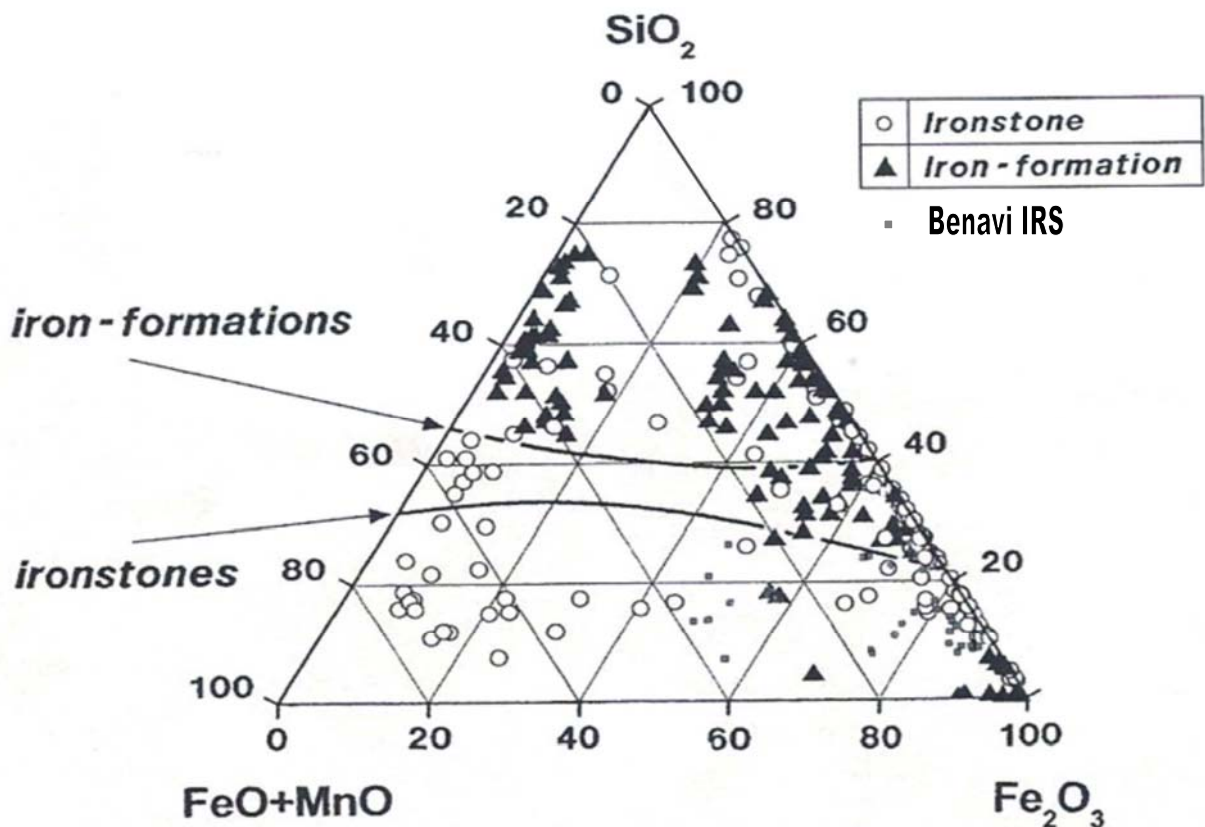


Figure (5-10): Shows Benavi IRS samples plot with analytical points of (131) samples of iron formations and (129) samples of ironstones expressed as  $[(\text{FeO}+\text{MnO})-\text{Fe}_2\text{O}_3-\text{SiO}_2]$  diagram including the lines separating the fields of iron formations from those of ironstones inferred by James, 1992, (in Mucke and Farshad, 2005).

As mentioned before, chromium is a characteristic constituent of the ironstones when the range lies between (10-400 ppm), the higher chromium content of IRS promotes to classify it as ironstones. Furthermore, in ironstones, the elements group (Zn+ Pb + Cu +Ni +Co) has in total a concentration which generally does not exceed (650ppm) (Mucke and Farshad, 2005); this case is also available in Benavi IRS samples where the total concentration of these elements group ranges between (106-108ppm) with average of (135.4 ppm).

The Al and Ti content of hydrothermal origin are generally too low in comparison to deposits of sedimentary origin (Koc and Bektas, 2003). The behavior of Al&Ti can be observed in Fig. (5-11) after (Crerar et al, 1982). Al and Ti of Gulocagi hydrothermal deposits are shown in this figure; Asilimbel shows similarity to the Gulocagi which is also hydrothermal (Koc and Bektas, 2003). Fig. (5-11) also shows the behavior of these elements in some sedimentary ironstones. As a result and based on the study of Al &Ti trend, it can be concluded that Benavi IRS is far from hydrothermal origin and closer to sedimentary origin.

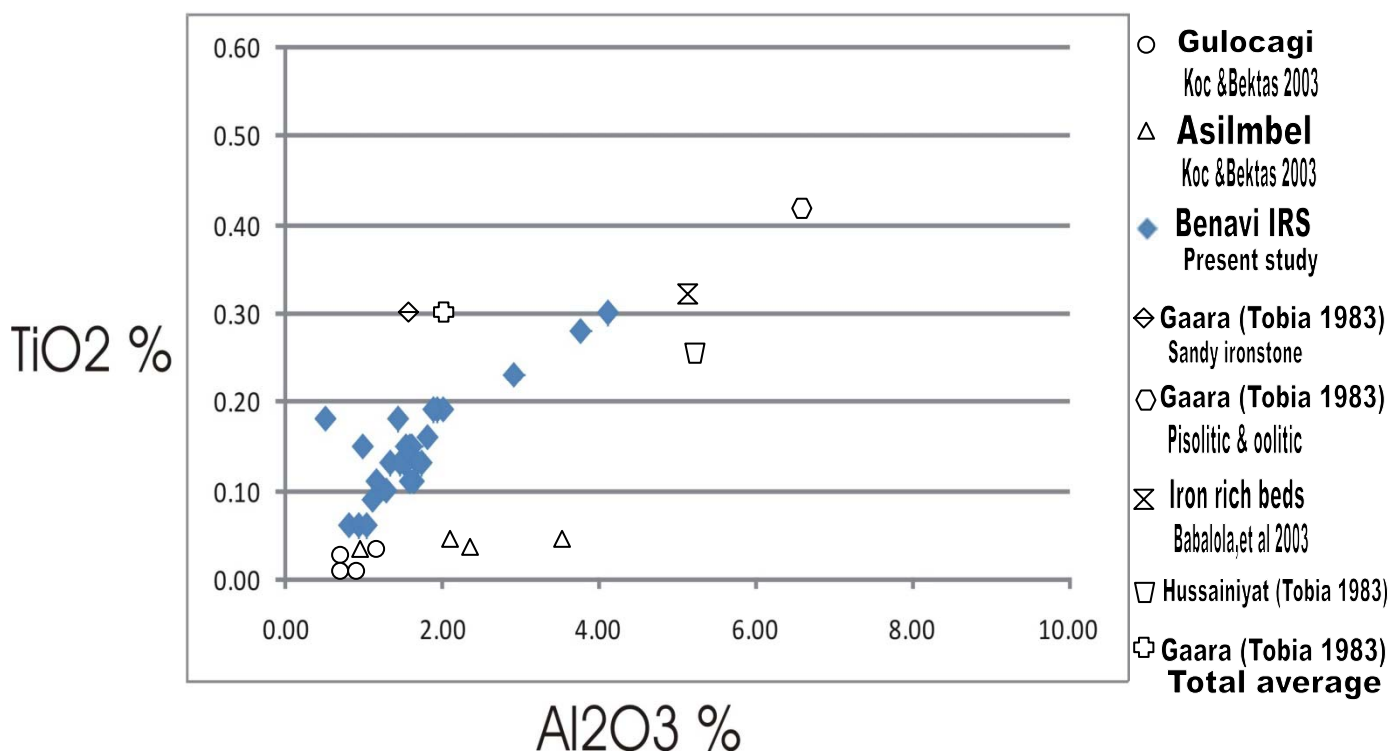


Figure (5-11): TiO<sub>2</sub>, Al<sub>2</sub>O<sub>3</sub> diagram of Benavi IRS(after Crerar et al, 1982). Gulocagi & Asilimbel hydrothermal ore samples (Koc and Bektas, 2003). Sedimentary ironstones: Garra & Hussainiyat (Tobia, 1983), and iron rich beds (Babalola et al, 2003).

The triangle of Zn-Ni-Co diagram (Choi & Hariya, 1992) has had important contribution in differentiation between sedimentary and hydrothermal types of mineralizations Fig.( 5-12 ). In this diagram; the location of Gulocagi and Asilimbel samples (hydrothermal in origin according to Koc & Bektas, 2003) are too far from Co and closer to Zn. Co mostly reflects sedimentary origin while Zn indicates hydrothermal origin (Crerar et al, 1982). Contrarily, this diagram also shows that the sedimentary ironstones are far from Zn.

In Fig. (5-12), Benavi IRS samples plot are closer to sedimentary ironstones locations in comparison with hydrothermal Gulocagi & Asilimbel sites, and then it seems closer to sedimentary origin.

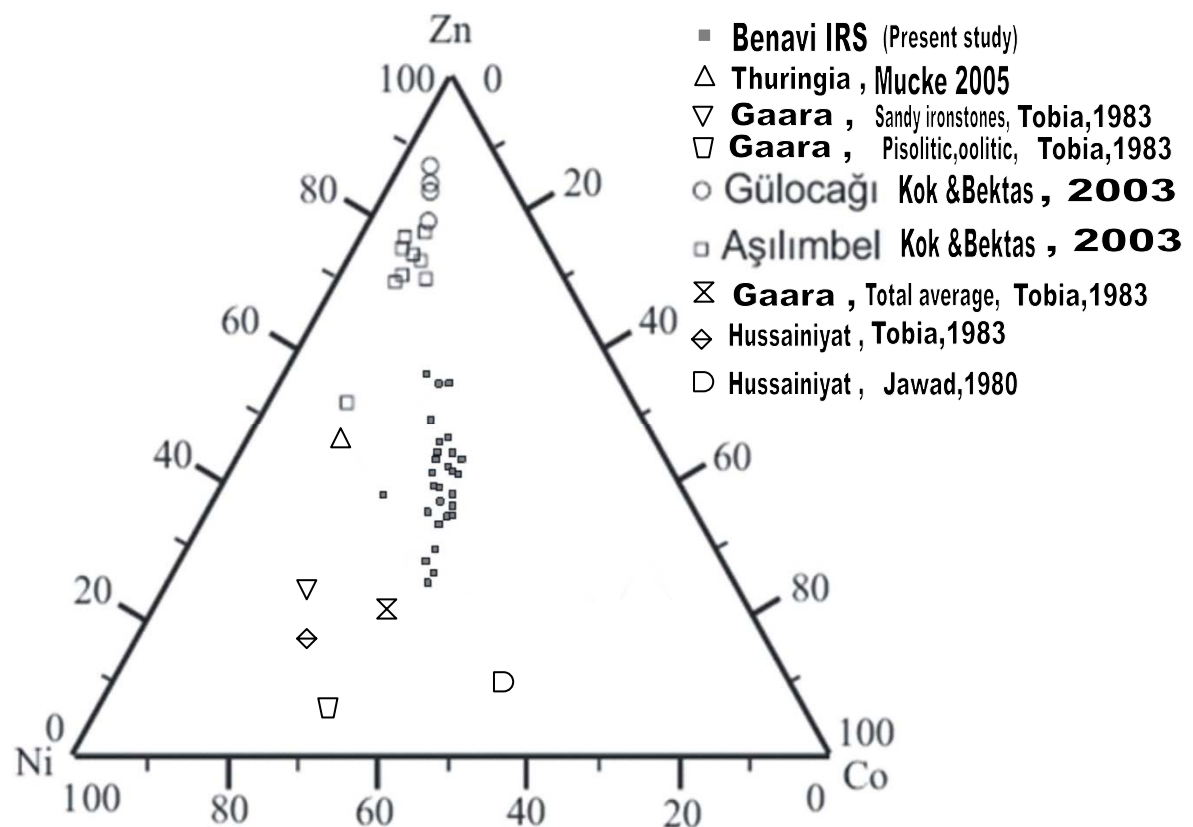


Figure (5-12): Zn-Ni-Co triangle diagram of Benavi IRS (after Choi & Hariya, 1992). Gulocagi and Asilimbel hydrothermal ore samples (Koc & Bektas, 2003). Sedimentary ironstones: Gaara, Hussainiyat (Tobia, 1983), Hussainiyat (Jawad, 1980) and Thuringia(Mucke and Farshad, 2005).

For further confirmation of genesis of Benavi IRS, the results of the present work compiled with the results of: Zaghoul et al, (1995) ; El Agami, (1996) and El Agami, (2000 ) that showed sedimentary origin for Mn-Fe ore of ( UM-Bogma / Egypt) where these results have been plotted on a bivariate plot (Si vs. Al wt%) after Crerar et al, (1982) .

The studied samples were plotted on this diagram too. This diagram showed that Benavi IRS is of diagenetic in origin Fig. (5-13).

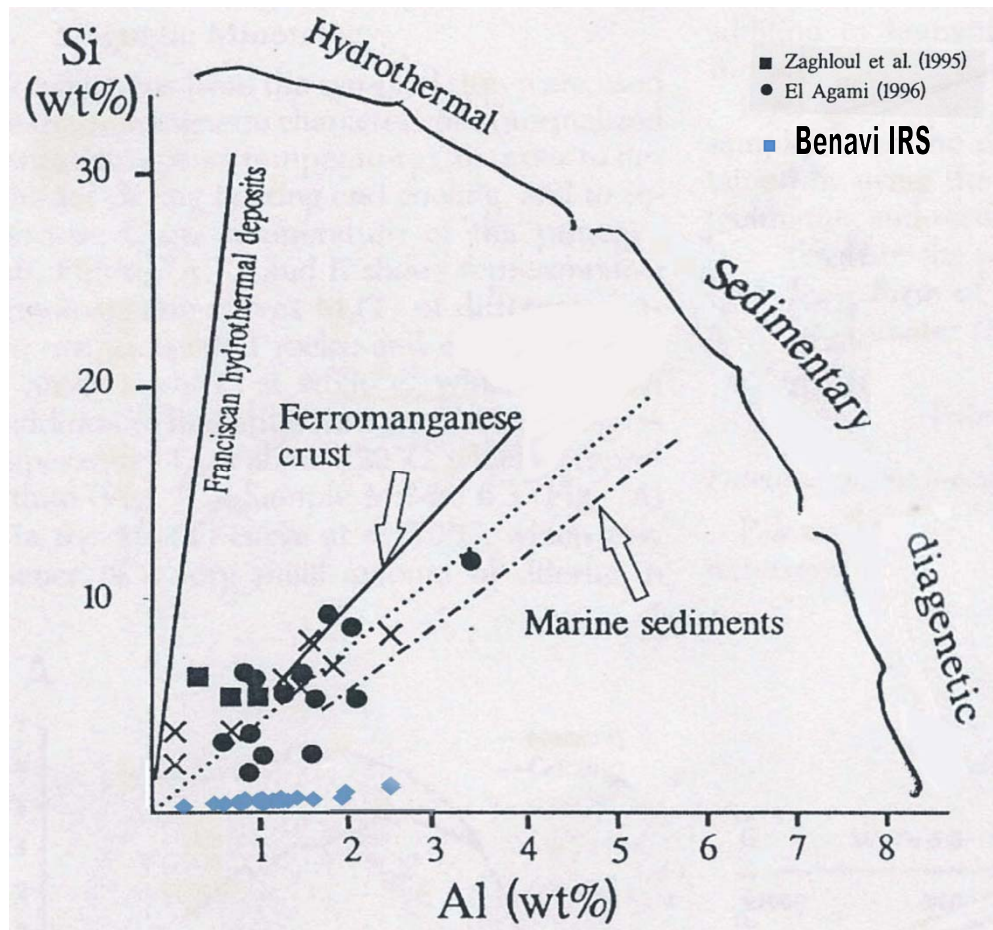


Figure (5-13): Si vs. Al diagram shows Benavi IRS samples plot in diagenetic field, [after Crerar et al, (1982) in El Agami, (2000 )].

### 5-8 Discussion:

The geochemical results of Benavi IRS samples appeared in accordance with the mineralogical investigation (chapter three). Also they explained the various diagenetic processes (chapter four) of this deposit.

In this study, it appears that the noticeable vegetation concentration along the outcrop of Benavi IRS extension observed throughout the field work is attributed to the unusual content of iron in this deposit in comparison with the underlying and overlying country rocks.

According to the geochemical analyses of studied samples, the sedimentary diagenetic origin of this deposit has been confirmed, where iron contents of carbonate sediments are commonly increased during diagenesis (Maynard, 1983). The very strong negative relationship between calcium and iron attributed to the replacement of calcareous constituents by iron minerals suggests a diagenetic origin of Benavi IRS (Babalola et al, 2003). Therefore, Benavi IRS can be considered as epigenetic ores formed by the diagenetic replacement of carbonate rocks (Selley, 2007).

The negative relations of CaO with SiO<sub>2</sub>, Al<sub>2</sub>O<sub>3</sub>, P<sub>2</sub>O<sub>5</sub>, Co, Ni, Zn ... also reflects the high effects of diagenetic processes in these deposits and support the petrographical study of this thesis. The ferruginization probably occurred by descending solutions that caused dissolution, migration and precipitation of various elements depending on prevailing Eh/pH conditions. The ferruginization appeared to be an important phenomenon in the Cretaceous especially in late Cretaceous deposits in which Benavi IRS formed (Mücke and Farshad, 2005).

The relatively high concentrations of: Ti, Cr, P and Al support the sedimentary origin because the hydrothermal solutions originated from volcanic activities are poor in these elements (Tobia, 1983). Furthermore, there are no evidences for volcanic activities in Benavi IRS and the adjacent areas. The modicum of: Pb, Zn, Cu also indicates the sedimentary origin (James, 1966; Harder, 1964). High As in Pyrite of Benavi IRS is good evidence of the sedimentary origin too (Al-Bassam, 2008 personal communications).

Finding arsenopyrite in Benavi IRS is debatable, as there are many possibilities for the formation of this mineral in this area.

The large well formed crystals of arsenopyrite seem typical of hydrothermal origins and suggest some hot fluids probably had been involved (David Alderton, 2008 personal communication). But this suggestion may not appropriate with the case of Benavi area. There are other possibilities which probably more satisfied.

In acidic environments, the oxides surfaces are positively charged causing adsorption of anions (Cornell and Schwertman, 2003). The adsorbed arsenic may be mobilized with phosphate, these adsorbed anions may also be released upon reduction of iron oxides because the available surface area decreases, thus the reductive iron oxides has been suggested as a mechanism for arsenic oxyanions ( $\text{AsO}_4$ )<sup>-3</sup> and phosphates release (Pedersen, 2006). In Benavi IRS, probably this case occurred where this yield interpretation for phosphates occurrences in this deposits, and also for why phosphates observed associates with pyrite and arsenopyrite. The arsenic probably was more than enough to form As-rich pyrite and the access may form arsenopyrite at the reduction stage, and / or the arsenic might have been derived from pyrite crystals which undergone goethitization and combined with sulfur also from altered pyrite to form authogenic arsenopyrite crystals (Kettana, 2008, personal communication), where most of primary sulfides ores (pyrite) were altered to secondary ores (goethite) by influence of supergene solutions (Awadh et al, 2008). This suggestion supported by ore microscopy study and SEM analyses which showed presence of arsenopyrite restricted geochemically to the richest samples in S and FeO, and mineralogically to the richest samples in pyrite.

*Chapter Six*

*Conclusions*

*&*

*Recommendations*

## 6-1 Conclusions:

Mineralogical, petrographical and geochemical studies of the Benavi IRS demonstrate the following conclusions:

1. Mineralogical analyses using instrumentation of: XRD, SEM, EDS, TGA and FTIR, showed that Benavi IRS samples are mainly composed of mineral assemblages including: carbonates (impure calcite, siderite, ankerite), iron oxides/hydroxides (hematite, goethite and/or limonite, magnetite), sulphides (pyrite, arsenopyrite), silicates (kaolinite, chamosite, glauconite, quartz) and apatite. Euhedral authigenic arsenopyrite crystals were found restricted at the lower part of Benavi IRS outcrop associated with pyrite, chamosite, phosphates and glauconite.
2. The main iron minerals are hematite and goethite. Hematite is mostly Al-poor type originated by dehydration of primary Al-poor goethite. Two types of goethite were found differ in crystallization and Al-content supported by wide range of decomposition temperature by TGA (263°C-350°C); besides the peaks shifts to higher  $2\theta$  angles indicating  $Al^{+3}$  substitution for  $Fe^{+3}$ . Al-rich goethite (secondary) produced by goethitization of: pyrite, siderite and chamosite under surface weathering circumstances after exposure of this deposit.
3. The main clay minerals of Benavi IRS are kaolinite and chamosite whereas glauconite is trace. Chamosite is formed from kaolinite where the later recrystallized or transformed to chamosite under reducing conditions in the availability of  $Mg^{+2}$  and presence of iron oxides.
4. Benavi IRS is related to algal-bioclastic- packstone host rocks which suffered from many diagenetic processes such as: iron oxides replacements, phosphatization, pyritization, neomorphism, silicification, cementation, and goethitization, in addition to mechanical and chemical compaction, with limited processes of dolomitization & dedolomitization.

5. Chamosite mostly occurs around impregnation fossils by iron oxides, this does confirm that chamosite growth is beyond iron oxides replacement after changing in initial redox conditions in diagenetic environment.
6. Ore microscopic study and BSE images showed that most ore textures are formed by replacement processes. These textures are: Rim, zonal, inclusions, vein, and idiomorphic. The porous texture is common and it is produced by dehydration of goethite. Oolitic textures and a boxwork texture of microplaty hematite grains are present. Euhedral magnetite crystals up to 50 $\mu$ m are also present.
7. Pyrite occurs in framboidal, massive and euhedral forms. It is unevenly distributed throughout Benavi IRS. The euhedral pyrite crystals are produced by the evolution of framboidal textures where the main steps for this evolution have been recognized by BSE images. Pseudomorph goethite and magnetite framboids are common in Benavi IRS; they formed by oxidation of original pyrite framboidal textures.
8. Fe<sub>2</sub>O<sub>3</sub> concentration ranges between (3.28-33.90%) with the average of (20.44%); therefore, this deposit can be considered as one of the low-grade ironstones. Benavi IRS also characterized by high concentration of (CaO, L.O.I, P<sub>2</sub>O<sub>5</sub>, MgO, Cr, V) and low concentration of (Ni, Cu, Zn, Mn, S, TiO<sub>2</sub>, Al<sub>2</sub>O<sub>3</sub>, SiO<sub>2</sub>); in comparison with Gaara, Hussainiyat and most of international ironstones.
9. The very strong negative correlation between CaO and Fe<sub>2</sub>O<sub>3</sub> attributed to the replacement of calcareous constituents by iron minerals and suggests a diagenetic origin of this deposit, which can be considered as epigenetic ore formed by the diagenetic replacement of carbonate rocks. Furthermore, the negative relations of CaO with SiO<sub>2</sub>, Al<sub>2</sub>O<sub>3</sub>, P<sub>2</sub>O<sub>5</sub>, Co, Ni, and Zn revealed the high effect of diagenetic processes on Benavi IRS.
10. EDS showed high arsenic in pyrite of Benavi IRS, where the arsenic concentration in: euhedral pyrite up to (1100ppm), massive pyrite

- (5600ppm) and framboidal pyrite between (1600-2400ppm). Goethite produced by goethitization of pyrite characterized by unusual As content.
11. Factor analyses showed 5 factors interpreted about (80.714%) of cumulative variance. Factors 1 and 2 are the main; where Factor 1 relates positively with:  $\text{Fe}_2\text{O}_3$ ,  $\text{Al}_2\text{O}_3$ ,  $\text{SiO}_2$ ,  $\text{TiO}_2$ ,  $\text{K}_2\text{O}$ ,  $\text{P}_2\text{O}_5$ , Co, Ni and negatively with: CaO & L.O.I and explains the initial dissolution of calcareous components of the original rocks and replacement processes occurred simultaneously and/or later of this dissolution by slightly acidic solutions rich in iron; whereas Factor 2 relates positively with FeO, MgO,  $\text{SiO}_2$ ,  $\text{Al}_2\text{O}_3$ , S,  $\text{TiO}_2$ , Zn, Cr and negatively with  $\text{Fe}_2\text{O}_3$ , which explains the effect of the reduction stage caused chamosite formation and pyritisation in the whole IRS body.
  12. R-mode cluster analyses showed three groups represent the components of all mineralogical phases of Benavi IRS. Group A: ( $\text{SiO}_2$ ,  $\text{Al}_2\text{O}_3$ ,  $\text{TiO}_2$ ,  $\text{Na}_2\text{O}$ ,  $\text{K}_2\text{O}$ , MgO,  $\text{P}_2\text{O}_5$ , FeO ), which collects the components of clay minerals, phosphates and quartz. Group B: ( $\text{Fe}_2\text{O}_3$ , Co, Ni) collects iron oxides and associated trace elements. Group C: ( CaO, L.O.I ) this group denote to calcite predominant in studied samples. Zn relates with group A&B by individual link due to the adsorption of zinc by clay and iron oxides. Mn link relates with all group because it is dispersed in all phases.
  13. The discrimination diagrams based on major ( $\text{TiO}_2$  vs.  $\text{Al}_2\text{O}_3$ ), and trace (Zn-Ni-Co) elements, showed the sedimentary origin corroborated by: high As in pyrite, narrow variations in Mn/Fe, the modicums of Zn,Pb,Cu and high content of: Cr,  $\text{P}_2\text{O}_5$ . Furthermore, a bivariate plot of (Si vs. Al ) suggests that Benavi IRS is of diagenetic in origin.
  14. Benavi IRS is one of phanerozoic ironstones based on Cr content, [Zn+Pb+Cu+Ni+Co] and the discrimination diagram of [(FeO+MnO)- $\text{Fe}_2\text{O}_3$ - $\text{SiO}_2$ ]; therefore, the author suggest (Benavi ironstone) as official name for Benavi IRS as more appropriate.

**6-2 Recommendations:**

1. Dating by isotopic methods is suggested to be applied to demonstrate the chronology the formation of the different mineralogical phases.
2. Trenches every 500m are suggested to determine the contact between overlying and underlying country rocks and to calculate the true thickness of this deposits.
3. Digging exploration bore holes in the area to study subsurface mineralization, and also to determine the continuity of this deposit with depth for reserve calculations purposes.
4. Further field investigations might be carried out as attempts to explore similar deposits in adjacent area.
5. Determine rare earth elements (REE) by Inductively Coupled Plasma –Mass Spectroscopy (ICP-MS) methods to better understand the genesis and source of iron.

# *References*

## *References*

---

- **Al-Ani,A.A.,2005**, Sedimentological studies of the Serikagni formation in Sinjar anticline, Unpubl.M.Sc. Thesis. Baghdad university, 133p.
- **Al-Bassam, K., 1972**, Reconnaissance mineralogical study of some lead – zinc deposits in northern and northeastern Iraq , Unpubl. M.Sc. Thesis , University of Wales, U.K., 55p.
- **Al-Bassam, K., 2004**, Minerogenic Map of Iraq (Scale 1: 1000000), 2<sup>nd</sup>. ed . GEOSURV, Iraq .
- **Ali,A.A,2007**, Sedimentology of Shiranish formation in selected areas from Northern Iraq, Unpubl.Ph.D.Thesis. Baghdad university,220p.
- **Al-Hasni,N.H.,1973**, Lithostratigraphy of Benavi area Northern Iraq, GEOSURV.Int.rep.no.671.
- **Alipour,S.,Cohen,D.R.,& Dunlop,A.C.,1995**, Seventeenth international exploration geochemical symposium Townsville ,15-19 may 1995.
- **Al-Rawi,D.,1978**, Structural and sedimentological evolution of the mesopeteman geosyncline (N-Iraq) , Annals de la societe geologique de Belgique,T.101,pp173-177.
- **Al-Rawi,D.,1975**, Field observations and some tectonic aspects of Benavia area , Amadia –Northern Iraq .Annals de la societe geologique de Belgique,T.98,pp 463-470.
- **Al-Rubaii,D.A.,1997**, Geochemistry and mineralogy of the karst bauxitic rocks in the western desert of Iraq, Unpubl.M.Sc. Thesis. Baghdad university,117p.
- **Al-Youzbaky,K.T.,1989**, Geochemical and mineralogical study of iron present with clay dposits in Gaara formation in western desert , Unpubl.M.Sc. thesis ,Mosul university ,186p.
- **Arai,Y. and Sparks,D.L.,2001**, ATR-FTIR spectroscopic investigation on phosphate adsorption mechanism at the ferrihydrite –water interface , J. of colloidal and interface science,V.241,pp317-326.
- **Aull,M.E.,2005**, Water quality indicators in watershed subbasins with multiple land uses, Unpubl.M.Sc. Thesis. Faculty of Worcester Polytechnic Institute.113p.
- **Awadh,S.M.,Habib,H.R, & Al-Bassam,K.S.,2008**, Upper Cretaceous carbonate hosted zinc-lead-barite deposits in Northern Thrust Zone , northern Iraq :petrography and geochemistry,Arab.J.Geosci.,V.1,pp75-85.
- **Babalola,L.O., Hussain,M. and Hariri,M.M.,2003**, Origin of iron- rich beds in the basal Wajid sandstone ,Abha-Khamis Mushayt area , Southwest Saudi Arabia, The Arabian J. for science and Engineering, V.28,no.1A,pp 3-24.
- **Bayliss,P. and Warne,S.,1972**, Differential thermal analyses of siderite- kaolinite mixtures , American mineralogist ,V.57,pp960-966.

## *References*

---

- **Bear,F.E.,1965**, Chemistry of the soil , 2<sup>nd</sup>. ed., Reinhold Publishing Corporation , N. Y.,515 p.
- **Bellen,R.C. Dunnington ,H.V.,Wetzel,R., and Morton,D.,1959**, Lexique stratigraphic Internat. Asie , Fasc.10, Iraq , Central national deal Recherches Scientifique,Paris,333p.
- **Bencini,A., and Allesandro,T., 1974**, Mn distribution in the Mesozoic carbonate rocks from lima valley , J. sed. petrol.,V.44,pp 774-782.
- **Bergman,I.A., and Savinova,Y.N.,1978**, Origin of Precambrian Iron Formations deduced from geochemistry of phosphorous and boron in rocks of Krivoy Rog Series , Geoch.Inter.,V.15,pp123-132.
- **Berner,R.A.,1970**, Sedimentary pyrite formation , Am.J.Sci.V.268, pp1-23.
- **Berner,R.A.,1984**, Sedimentary pyrite formation :An update ,Geochim. Cosmochim. Acta.,V.48, pp605-615.
- **Bhattacharrya, D.P., and Kakimoto,K.P.,1982**, Origin of ferriferous ooids ,an SEM study of ironstones ooids and Bauxite pisoids , J. Sed. Petrol. ,V.52,no.3,pp849-857.
- **Billings,G.K.,1978**, Sodium,11-K Abundance in sediments and common sedimentary rock types .In Wedepohl, K.H.1978 . Hand-Book of Geochemistry , Springer-Verlag Berlin,V.1,pp.1-3.
- **Blatt,H., Middleton,G. and Murray,R.,1972**, Origin of sedimentary rocks , Printice-Hall,Inc.,Englewood Cliffs,N. Y.,634p.
- **Borchert,H.,1960**, Genesis of marine sedimentary iron ores ,Trans.Ins. Min . Metall.,V.69,pp261-279.
- **Bottcher,M.E.,Gehlken,P.L.,and Vsdowski,E.,1992**, Infrared spectro -scopic investigations of the calcite –rhodochrosite and parts of the calcite magnesite minerals series , Contrib.Min.petro.,V 109 ,pp304-306.
- **Boukhtoyarov, I.S. and Yevlentyev, I.V., 1962**, On 1:200000 prospecting correlation of the area between the Greater Zab and Khabour Rivers, GEOSURV, Baghdad, Rep. no. 291, 36p.
- **Bricker, O.P.,1971**, Carbonate cements , Jhon Hopkins Press. Ltd. , London ,376p.
- **Brindely,G.W. and Brown,G., 1980**, Crystal structures of clay minerals and their x-ray identification , Mineralogical Society,295p.
- **Buday, T. and Vanecek, M., 1971**, Outlines of mineral occurrences of Iraq and general mineral investigation program for 1971-1990, GEOSURV, int. rep. no. 509 .
- **Buday ,T.,1980**, The regional geology of Iraq ,Stratigraphy and Paleogeography , Kassab ,I.I. and Jassim ,S.Z.,(eds), Dar Al-Kutib Publ. House ,Mosul,Iraq,445p.

## *References*

---

- **Buday T. and Jassim , S.Z., 1987**, The regional geology of Iraq, Tectonism ,magmatism and metamorphism , V. 2 , Geol.Surv.Min.Inv. Baghdad ,352p.
- **Carr,M.H.,and Turekian,K.K.,1961**, Geochemistry of cobalt , Geochim. Cosmochim. Acta,V. 23,pp 9-60.
- **Chaickin , S.I., 1970**, Report on the iron ore potentialities in Iraq and recommendation on the trend of further geological iron ore exploration , GEOSURV, int. rep. no. 548 .
- **Choi,J.H., and Hariya,Y.,1992**, Geochemistry and depositional environment of Mn oxide deposits in the Tokora belt Northeastern Hokkaida,Japan , Econ.Geol.,V.87,pp1265-1274.
- **Connor,D.J.,Sexton,B.A.,Smart,R.,2003**, Surface analyses methods in materials , Science,Springer-Verlag,Germany, 205p.
- **Cornell ,R.M. and Schwertman,U. 2003**, The iron oxides :Structures, properties,reactions,occurrences and uses , 2<sup>nd</sup> ed., Wily-VCH-Verlag GmbH&Co..
- **Crerar,H.D., Namson,M.S., Chyi,L., and Feigenson ,M.D. ,1982**, Manganiferous cherts of the Franciscan assemblage ,general geology, ancient and modern analogues and implications for hydrothermal convection at oceanic spreading centers, Econ.Geol.,V.77,pp519-540.
- **Curtis,C.D., and Spears,D.A.,1968**, The formation of sedimentary iron minerals, Econ. Geol. , V. 63,pp262-270.
- **Dabbagh,M.E.,2006**, Diagenesis of Jurassic Tuwaiq mountain limestone central Saudi Arabia , J.king saud.univ.,Riyadh,V.19,pp31-58 .
- **Davis, J. C., 1973**, Statistics and data analysis in geology, John Wiley and sons, Inc. New York, 463p.
- **Day,F.H.,1963**, The elements in nature , Harrap.London,372p.
- **De Groot,K.,1967**, Expermental de dolomitization texture , J. Sed. Petrol.,V 37 ,pp1216-1220.
- **Dickson,J.A.D.,1965**, A modified staining technique for carbonates in thin section , Nature,V.205, no.4971, p.587.
- **Doyle,C.S.,Kendelewicz,B.C., and Brown,G.E.,2004**, Soft X-Ray spectroscopic studies of the reaction of fractured pyrite surfaces with Cr<sup>+6</sup>-containing aqueous solutions .Geochim .Cosmochim .Acta., V.68,pp4287-4299.
- **Dubrawski,J.V.,Channon,A.L.,1989**, Examination of the siderite – magnesite mineral series by FTIR, Am. mineral.,V.74,pp187-190.
- **Dunham,R.J.,1962**, Classification of carbonate rocks according to depositional texture .In Ham,W.E.,(ed), classification of carbonate rocks, A symposium Am. Ass. Petrol. geologists , Memior 1, Talusa , Oklohoma,U.S.A,pp108-121.

## *References*

---

- **Edwards ,A.B.,1965**, Textures of the ore minerals , The Australian institute o mining and metallurgy , 242p.
- **El Agami,N.L.,1996**, Geology and radioactivity studies on the Paleozoic rock units in Sinai Peninsula , Egypt. Unpubl. Ph.D. Thesis. Mansoura univ.,302p.
- **El Agami,N.L.,2000**, Sedimentary origin of the Mn-Fe ore of Um Bogma ,Southwest Sinai , geochemical and paleomagnetic evidence , Econ. Geol. ,V.95,pp607-620.
- **Embry,A.F.,and Klován,J.E.,1971**, A late Devonian reef tract on northeastern Banks Island,Northwest Territories , Bull .Can .Petrol. Geol.V.19,pp730-781 .
- **Engelhardt,W.V.,1977**, The origin of sediments and sedimentary rocks, E.Schweizer bursche Verlag sbuch handing (Nagela U.ober miller),Stuttgart,359p.
- **Etabi, W., 1982**, Iron ore deposits and occurrences of Iraq, GEOSURV, int. rep. no. 1324 .
- **Evamy,B.D.,1967**, Dedolomitization and the evelopment of rhombohedral pores in limestones, J.Sed.Petrol.,V.37,1204-1215.
- **Folk,R.L.,1965**, Some aspects of recrystalization in ancient limestone, In:Pray,L.C.,and Murray,R.C.,(EDs.), Dolomitization and limestone diagenesis ,Spec.Publ.Soc.econ.Paleont.Mineral.13 ,Talusa,pp14-48.
- **Flügel,E.,1982**, Microfacies analysis of limestone, Springer-Verlag , Berlin ,633p.
- **Frederic,D., Mullet,M., Bernard,H., and Michot,L.,2005**, Pyrite oxidation by hexavalent chromium :solution species and surface chemistry , Environmental Science Technology,V.39 pp 8747-8751.
- **Frias,J.M.,Navaro,A. and Lunar,R.,1997**, First reference of pyrite framboids in a Hg-Sb mineralization : the valle del Azogue mineral deposits (SE Spain), Neues Jahrbuch fur min. Ab.,V 4 , pp175-184.
- **Friedman ,G.M.,1959**, Identification of carbonate minerals by staining methods, J. sed. Petrol., V.29, pp 87-97.
- **Frost,R.L. , Ding,Z. and Ruan,H.,2003**, Thermal analysis of goethite, Relevance to Australian Indigenous ART, J. of thermal analysis and calorimetry . V.71,no.3, pp783-797.
- **Gartner Von,H.R.,and Schellmann,w.,1965**, Rezente sedimente in Kustengebireich der Halbinsel Kaloum,Guinea , Mineral. Petrogr. Mitt.10, pp 349-367.
- **Geozavod (Yougoslavia) , 1981**, Geological investigation in Duri-Serguza lead-zinc deposit , N. Iraq , GEOSURV, int. rep. no. 1145 .
- **Gibbs,R.J.,1973**, Mechanism of trace metal transport in rivers , Science., V.180,pp.71-73.

## *References*

---

- **Gierth,E.,2008**, Microscopic studies of limestone samples from Mauritania, Unpubl.rept.Societe Nationale Industrielle et Miniere (SNIM), Mauritania ,17p.
- **Goldschmidt,V.M.,1958**,Geochemistry, Oxford univ.Press,London,730p.
- **Grim,R.E.,1968**, Clay mineralogy,Mc Graw-Hill Book Co.N. Y.,596p.
- **Gross,G.A.,1980**, A classification of iron formations based on depositional environments, Canadian Mineralogist,V.18,pp215-222.
- **Gultekin,A.H., 1998**, Geochemistry and origin of the Oligocene Binkilic Mn- deposit ,Trace Basin ,Turkey , J. of earth sciences ,V.7,pp11-23.
- **Hallsworth , C.R. and Knox,O.B.,1999**, Classification of sediments and sedimentary rocks , British geology survey , U.K.,research report number 99-03, 44p.
- **Hamza,N.M. and Isaac,E.A.,1971**, Geological survey of the area between Benavi village and Greater Zab river, NIMCO report ,SOM Library.Baghdad.
- **Harder,H.,1964**, The use of trace elements in distinguishing different genetic types of marine sedimentary iron ores .In :Genetic problems of ores, Inter.Geol.Cong.22 nd. New Delhi ,1964 pt.5,pp551-556.
- **Harder , H.,1978**, Synthesis of layer silicate minerals under natural conditions , J. of clay and clay minerals,V.26,no.1,pp65-72.
- **Herron,M.M., Abigail,M, and Gustavson ,G.,1997**, Dual-Range FTIR mineralogy and the analysis of sedimentary formations , Schlumberger-Doll research ,old quarry road ,Ridgefield. Best paper of 1997,ScA-9729.
- **Hirst.,D.M.,1962**, The geochemistry of modern sediments from the gulf paria –II,the location and distribution of trace elements , Geochim. Cosmochim .Acta,V.26,pp1147-1187.
- **Holand,H.D.,1999**, When did the earth's atmosphere become oxic?, Geochemical news, V.100, pp20-22.
- **Houda,Z.,Wang,Q,Wu,Y. and Xu,X.,2007**, Reduction remediation of hexavalent chromium by pyrite in the aqueous phase, J. of Applied Sciences , V.11, pp1522-1527.
- **Huang,C.K., and Kerr,P.K.,1980**, Infrared study of the carbonate minerals, American mineralogist,V.36,pp643-670.
- **James,H.L.,1966**, Chemistry of the iron – rich sedimentary rocks , U.S. Geol .Surv .Prof.Paper 440W,pp47-60.
- **James,H.L.,1992**, Precambrian iron formations:nature,origin and mineralogical evolution from sedimentation to metamorphism , In :Wolf, K.H., Chilingarian, G.V.(EDs),Diagenesis:III Developments in Sedimentology,V.47,pp543-589.
- **Jassim,S.Z., and Goff,J.C.,2006**, Geology of Iraq.Dolin,Parague and Moravian Museum , Brno,341p.

## *References*

---

- **Jawad,A.M.,1980**, Geochemistry and mineralogy of Ubaid formation in the western desert, Unpubl.M.Sc. Thesis. Baghdad university,227p.
- **Jepson,W.B., and Rowse,J.,1975**, The composition of kaolinite –An Electron Microscope Microprobe study , Clays and clay minerals ,V.23,pp 310-317.
- **Jepson,W.E.,1984**, Kaolins ,their properties and uses, Phi .Trans. R .Soc Londb .A.,V.311,pp411-432.
- **Johnson ,M.C.,Beard,L.B.,Klein,C.,Beukes,J.N. & Roden ,E., 2008**, Iron isotopes constrain biological and a biological processes in BIF genesis , Geochimica et cosmochimica ca Acta ,V.72,pp151-169.
- **Kampf ,N. and Schwertmann,U.,1983**, Goethite and hematite in a climosequence in southern Brazil and their application in classification of kaolinitic soils, Geoderma.,V.29,pp27-39.
- **Kerr,P.F.,1959**, Optical mineralogy ,(3<sup>rd</sup> Ed.),Mc Graw-Hill,N. Y.,442p.
- **Kholodov,V.N., and Butuzova,G.Y.,2004**, Problems of siderite formation and iron ore Epochs , Lithology and Mineral Recources, V. 39, no.5,pp389-411.
- **Kloss,W.S.,1974**, Differential thermal analysis ,application and results in mineralogy, Springer-Verlag Berlin.Heidelberg.Germany , 185p.
- **Kloss,W.S.,1986**, Thermal analysis in the geosciences, Jhon Wily & sons Inc.USA,814p.
- **Koc,S. , and Bektas,S., 2003**, Geochemical characteristics of Asilimbel and Gulocagi iron mineralizations ,Kaman –Kirsehir,central turkey, The Arabian J. for science and Engineering ,.V.28,no.2A,pp123-134.
- **Koppelman,M.H. and Dillard,J.G.,1977**, Astudy of the adsorption of Ni(II) and Cu(II) by clay minerals , Clays and Clay Minerals., V.25,pp457-462.
- **Krauskopf,K.B.,1957**, Separation of manganese from iron in sedimentary processes , Geochim. Cosmochim.Acta.,V.12,pp 61-68.
- **Krauskopf,K.B.,1979**, Introduction to geochemistry (2<sup>nd</sup> ed.),Mc Graw-Hill,N.Y.,617p.
- **Landergren,S.,1978**, Vanadium ,23-D,Abundance in rock forming minerals .In Wedepohl,K.H.,(ed).Hand book of Geochemistry , Springer-Verlag Berlin , V.2,pp 1-10.
- **Larsen,G. and Chilingar,G.V.,1979**, Diagenesis in sediments and sedimentary rocks, Elsevier, Amsterdam.579p.
- **Lazareva,O.2004**, Detaild geochemical and mineralogical analyses of naturally occurring arsenic in the Hawthorn group, Unpubl.M.Sc. Thesis. South Florida university,121p .
- **Lepp,H.,1963**, The relation of iron and manganese in sedimentary iron ores, Econ.Geol.,V.58,pp 515-526.

## *References*

---

- **Lepp,H. and Goldich ,S.S.,1964**, Origin of Precambrian Iron Formations, *Econ.Geol.*,V.59,pp 1030-1041.
- **Lepp , H., 1975**, *Geochemistry of Iron*, Halsted Press ,USA., 464p.
- **Listizin,A.P.,1972**, Sedimentation in the world ocean, *Spec .Publ .econ. Paleont .Miner.Tulsa*,218p.
- **Longman,M.W.,1980**, Carbonate diagenesis textures from nearsurface diagenetic environments, *Bull.Am.Ass.Petrol.Geol.*,V.64,pp461-487.
- **Lorenze,P.B.,1969**, Surface conductance and electrokinetic properties of kaolinite beds,*Clays and clay minerals*,V.17,pp223-231.
- **Love,L.G.,1965**, Micro-organic material with diagenetic pyrite from the lower proterozoic mount Isa shale and a carboniferous shale, *Yorkshire Geological Society* ,V.35,pp 187-201.
- **Love ,L.G.,Amstutz,G.C.,1966**, Review of microscopic pyrite from Devonian chattanoga shale and Rammelsberg Banderz.*Fortschritte der mineralogia* , V.43,pp277-309.
- **Mason,B.,1982**, *Principles of geochemistry*, 3<sup>rd</sup> ed. , ,Jhon Wiley and Sons ,Inc.N. Y.,329p.
- **Matukhin,R.G.,Menner,V.V. and Nuvareva , Y.U.,1981**, Iron ores in Devonian deposits of the October ReVution Island , *Severnaya Zemlya Archipelago .Lith. and Miner.Res*,V.16,pp 499-507.
- **Maximovic ,Z., White,J.L., and Logar ,M.,1981**, Chromium-bearing Dickite and chromium-bearing kaolinite ,Telsic,Yugoslavia, *Clays and Clay Minerals* .,V.29,no.3,pp213-218.
- **Maxwell,J.A.,1968**, *Rock and Minerals analysis*, Jhon Wiley and Sons, N. Y.,584p.
- **Maynard,J.B.1983**, *Geochemistry of sedimentary ore deposits*, Springer-Verlag, N. Y.,305p.
- **McCarthy , M.J. , 1955**, Final report on geology between the Zab and Khabour rivers, north of Amadia , *GEOSURV, int. rep. no. 266* .
- **Melnik,Y.P., 1982**, *Precambrian banded iron formations*, Elsevier Scientific Publishing Co.Amsterdam, 310p.
- **Merinero,R. , Lunar,R., Frias,J.M., Somoza,L. and Rio,V.D., 2008**, Iron oxyhydroxide and sulphide mineralization in hydrocarbon seep related carbonate submarine chimneys,Gulf of Cadiz (SW Iberian Peninsula), *Marine and PetroleumGeology*,V.25, pp706-713.
- **Mitchell,R.C.,1960**, Reconnaissance structural and tectonic studies of part of northern Iraq , *Internal .Geol.Congr.XXI*Session Proc.sect.18 Copenhagen.
- **Morse,J.W. and Luther,G.W.,1999**, Chemical influence on trace metal-sulphide interactions in an oxic sediments ,*Geochim .Cosmochim. Acta.*,V.63,pp3373-3378.

## *References*

---

- **Mucke,A. and Farshad,F.2005**, Whole rock and mineralogical composition of phanerozoic ooidal ironstones,comparison and differentiation of types and subtypes , Ore geology reviews .Elsevier Science B.V., V.26,pp227-262.
- **Murdoch,J. and Barnes,J.A., 1985**, Statistical Tables of science, engineering, management studies, 2<sup>nd</sup> ed. ,Macmillan , Oliver & Boyd Ltd.Edinburgh.
- **Neumann,T.,Rausch,N.,Leipe,T.,Dellwig,O.,Berner,Z.,and Bottcher, M.E .,2005**, Intense pyrite formation under low-sulfate conditions in the Achterwasser lagoon,SW Baltic sea,Geochim.et Cosmochim. Acta., V.69,no.14,pp3619-3630.
- **Newman,D.K., and Kappler,A., 2004**, Formation of Fe III minerals by Fe II –Oxidizing photoautotrophic bacteria, Geochim. et Cosmochim. Acta. ,V.68,no.6,pp 1217-1226.
- **Odin ,G.S., and Matter ,A.,1981**, Glauconite origin. Sedimentology, V . 28 , pp 611 -641.
- **Oldershaw,A.E. and Scoffin,T.P. 1967**, The source of ferron and non ferron calcite cements in the Halkin and Wenlock limestones, Geol.J.pp309-320.In Bricker, O.P.,1971. Carbonate cements . Jhon Hopkins Press. Ltd.,London,376p.
- **Ostrom,M.E.,1961**, Separation of clay minerals from carbonate rocks by using acid , J. of sed. Petrol. ,V.31.pp123-129.
- **Ostwald,J , and England B.M., 1977**, Notes on framboidal pyrite from Allandale New Sowth Wales ,Australia .Mineralium deposita,V. 12, pp111-116.
- **Ostwald,J , and England B.M., 1979**, The relationship between euhedral and framboidal pyrite in base metal sulphide ores .Mineral Magmatic,V.43,pp297-300.
- **Palau,A.T.,Garcia,J ,Barcelo,A.,Blas,M.P. and Martinez ,J.M. ,1997**, Structural modification of Sepiolite (natural magnesium silicates ) by thermal treatment:effect on the properties of polyurethane adhesives,Int.J.Adhesion and Adhesives ,V.17,pp111-119 .
- **Pedersen,H.D.2006**, The transformation of Fe(III) oxides catalysed by Fe(II) and the fate of arsenate during transformation and reduction of Fe(III) oxides, Unpubl. Ph.D. Thesis. Technical Univ. of Denemark,58p.
- **Pendias,H.1992**, Trace elements in soil and plants.2<sup>nd</sup> ed.,CRC. Press.Boca Raton.FL.
- **Pettijohn,F.J.,1975**, Sedimentary rocks, Harper &Row ,N. Y.,628p.
- **Qureshi,M.K., Masood,K.R. and Butt,G.A.,2005**, Lithofacies analysis of the lower cretaceous Lumshiwal formation,Kalla Chitta Range , northern Pakistan, Geol.Bull.Punjab. univ.,V.40,pp 1-19.

## *References*

---

- **Rankama,K., and Sahama,T.G., 1950**, Geochemistry, Univ. Chicago Press. Chicago , 912p.
- **Ramdohr,P., 1980**, The ore minerals and their intergrowth , Pergamon Press.,N. Y., 1202p.
- **Sawlowicz,Z.,1987**, Framboidal pyrite from the metamorphic Radzimowice Schists of Stara Cora , Poland.Mineralogia Polonica,V 18,pp57-67.
- **Sawlowicz,Z.,1993**, Pyrite framboids and their development :a new conceptual mechanism , Geologisch Rundschau ,V.82,pp148-156.
- **Schwertmann,U.,Fitzpatrick,R.W., & Le Rou,J.,1977**, Al-Substitution and Differential Disorder in Soil Hematites , Clays and clay Mins .,V .25 , pp 373-374.
- **Scott,K.M.,1986**, Elemental Partitioning in Mn-and Fe-Oxides derived from dolomitic shale –hosted Pb-Zn deposits , North West Queensland, Australia .Chemical Geology., V.57,pp 395-414.
- **Selley ,R.C.,2007**, Applied Sedimentology , (2 nd. Ed.).Academic Press. USA .543p.
- **Shaw ,D.M.,1969**, Evaluation of data , analytical error and related topics in geochemistry , In wedephol,K.H. (ed) ,Hand book of geochemistry , Springer – verlag.Berlin,V.I ,pp324-330.
- **Shiraki,K., and Matzat,E.,1978**, Cromium,24-G,behavior during weathering and alteration rocks, In Wedepohl,K.H.,(ed.).Handbook of Geochemistry , V.III ,Springer - Verlag Berlin.
- **Spears,D.A.,1961**, The major elements geochemistry of the Mansfield Marine Band in the Westphalian of Yorkshire , Geochim .Cosmochim. Acta .V.28,pp1679-1696.
- **Spry,P.G., and Gedlinske,B.L.,1987**, Tables for the determination of common opaque minerals , Economic Geology Publishing Co.New Haven.,52p.
- **Stanton,K.E.,1966**, Rapid methods of trace analysis for geochemical applications , Edward Arnold Corp., London,96p.
- **Stanton ,R.L.,1972**, Ore petrology , Mc Graw-Hill Book , U.S.A, 713 p.
- **Taylor,J.H.1949**, Petrology of the Northampton Sand Ironstone Formation , Mem.Geol.Surv.U.K.,111p.
- **Till,R.,1971**, Geochemical criteria for differentiating reef and non-reef carbonates , Bull.Amer.Assoc.Petrol.Geol.,V.55,pp 523-530.
- **Thorez,J., 1976**, Practical identification of clay minerals , Lellote (ed.), Belgium , 89 p.
- **Tobia,F.H.,1983**, Geochemistry and mineralogy of the iron ore deposits of Gaara formation in Iraqi western desert, Unpubl.M.Sc. Thesis. Baghdad university,156p.

## *References*

---

- **Trurnit,P.,1968**, Pressure solution phenomenon in detrital rocks , Sed. Geol., Amsterdam ,V.2,pp89-114.
- **Tucker,M.E.,1981**, Sedimentary petrology ,an introduction , Blackwell Scientific Publications ,Oxford,252p.
- **Vanecek,M.,1970**, Short report on the field trip to northern Iraq in July and August 1970, GEOSURV, Baghdad, Rep. no. 399, 4 p.
- **Vandermal,H.W. , and Beutelsparcher,H.1976**, Atlas of Infrared Spectroscopy of minerals , Elsevier-Amsterdam .376p.
- **Vaughan,D.J.,and Craig , J.R.,1981**, Ore microscopy and ore petrology, Jhon Wiley & Sons.Inc.,U.S.A.,406p.
- **Weaver,C.E.,1976**, The nature of TiO<sub>2</sub> in Kaolinite , Clays and Clay Minerals ,V.24,pp 215-218.
- **Wetzel,R.,1950**, Stratigraphic of the Amadia region,MPC report,NIMCO Library .no.TR/RW12,Baghdad.
- **Wilkin ,R.T.and Barnes ,H.L.,1997**, Formation processes of framboidal pyrite, Geochimica cosmochimica Acta,V.61,no.2,pp323-339.
- **Wright ,E.L., and Schwarcz,H.P.,1996**, Infrared and isotopic evidence for diagenesis of bone apatite and D.S.Pilas , Guatemala .J. of Archaeological science , V 23 ,pp933-944.
- **Zaghloul,Z.M., Elshahat,A., Kora,M., and AbuShabana ,M.,1995**, Modes of occurrence ,geochemistry and origin of Mn-Fe deposits of Um Bogma west central Sinai , Egypt .J. of Environmental Sciences, Egypt,V.9,pp29-59.
- **Zitzmann,A.,1977**, The iron ore deposits of Europe and adjacent areas , Hannover,418p.
- **Yan,J., Munnecke,A., Steubert,T., Carlson,E.H., and Xiao,Y., 2005**, Marine sepiolite in middle permian carbonates of south china , J. of sedimentary research ,V.75, no.3, pp 328-338.
- **Yekta,S.A.,1981**, Ironstone sedimentation in western desert Iraq, Unpubl. M.Sc . Thesis,university of wales,256p.
- **Young ,T.P., and Taylor,W.E.,1989**, Phanerozoic ironstones , an introduction, Geological Sociaty Special publication no. 46,pp ix-xxv.

# *Appendices*

## Appendix 1



### CERTIFICATE

Mr. Ali Taha YASSIN has worked for two months in the Research Materials Centre, a research centre of the Alès School of Mines, in France, from October 28 to December 27, 2008. I was his supervisor

His research project about an iron ore concentration located in the north of Iraq was successfully improved by these two months work. He spent his time here in fine petrographical and mineralogical investigation on some samples from Iraq. To conclude this project, Mr. YASSIN has made a remarkable analytical work, taking in account the results obtained from many analytical techniques, as ore microscope, Scanning electron Microscope with Energy Dispersive X-Ray Spectrometry, Thermal analysis and IRFT to get a large and precise sight of the mineralogy. These mineralogy and petrography studies enabled him to propose a logical model to explain the behaviour of iron in the deposit showing his technical and scientific capacities.

Mr. YASSIN shows a high scientific level and a very good capacity to learn new techniques he needed, by a good bibliographic method, and a large curiosity for all scientific topics. He shows a great tenacity and an outstanding working capacity, both in intellectual and practical things. By his personal qualities, he has found among members of the research centre all the help he needed to improve his project.

It was a pleasure to work with him.



MINISTÈRE DE L'ÉCONOMIE  
DES FINANCES ET DE L'INDUSTRIE

École des Mines d'Alès 6, avenue de Clavières 30319 ALES cedex FRANCE - Téléphone +33 (0)4 66 78 50 00 - Fax +33 (0)4 66 78 50 34  
Site EERIE parc scientifique Georges Besse 30035 NIMES cedex 1 FRANCE - Téléphone +33 (0)4 66 38 70 00 - Fax +33 (0)4 66 84 05 06  
Hélioparc 2, avenue Pierre Angot 64053 PAU cedex 9 FRANCE - Téléphone +33 (0)5 59 30 54 25 - Fax +33 (0)5 59 30 63 68

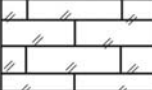
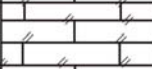
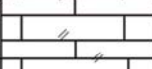
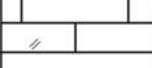
## Appendix 2

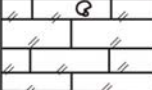
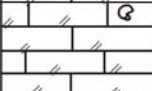
Section No. :BN1 Map No. :91/520 Total Thickness :30.0 Scale : 1:100					Location		
					UTM		DMS
					X	356 185	43 22 42.9
					Y	4122870	37 14 28.6
Z	1580	1580					
Age	Fn.	Th.(m.)	Sample	Lithology	Description		
Upper Cretaceous	Hadiena	4.20	BN1/8		Limestone, light grey, medium tough to tough, contain macro fossils, medium bedded, brecciated.		
		1.80	BN1/7		Calcareous Ironstone, vary colour, yellow, red, grey, black, reddish brown medium tough to tough, with high amount of hematitic grains, angular, subangular, semirounded and oval in shape, up to 3.0 mm in diameter, the weathered surface is yellow mottled with reddish brown as well as the grains of hematite are very clear in distinct habit, brecciated		
		1.50	BN1/6		Calcareous Ironstone,black,reddish brown mottled with black, yellow, red, tough, contain subangular hematitic grains with macro fossils, veinlets filled with Ironoxides and secondary calcite crystals, brecciated.		
		1.50	BN1/5		Calcareous Ironstone,black, dark grey, greenish grey, more reddish upward mottled with yellowish green, tough, the weathered surface is light yellowish brown, grains of hematite increase upward		
		1.50	BN1/4		Calcareous Ironstone,black, dark grey, greenish grey, more reddish upward mottled with yellowish green, tough, the weathered surface is light yellowish brown, grains of hematite increase upward		
		2.0	BN1/3		Limestone, dark greenish grey mottled with dark red and reddish brown tough, slightly ferruginous, contain Ironoxides grains in subangular to oval in shape, veinlets filled with secondary calcite crystals, brecciated.		
2.0	BN1/2		Limestone, light yellowish brown, yellow, slightly mottled with dark grey, medium tough to tough, slightly ferruginous, with macro fossils, veinlets filled with secondary calcite crystals and Iron oxides.				
2.50	BN1/1		Limestone, grey to yellowish grey, tough contain macro fossils, veinlets filled with secondary calcite crystals and slightly amount of Ironoxides brecciated.				
Upper Jurassic	Chia Gara	12.0	Non		Highly covered		
		1.0	BN1/1A		Limestone, dark grey, tough to medium tough, distorted.		

## Appendix 2

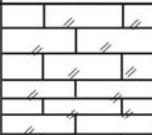
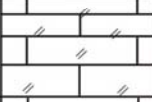
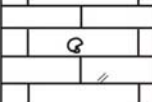
Section No. :BN 2 Map No. :91/520 Total Thickness :15.0 Scale : 1:100					Location		
					UTM		DMS
					X	256 077	43 22 38.6
					Y	4122846	37 14 27.7
Z	1600	1600					
Age	Fn.	Th.(m.)	Sample	Lithology	Description		
Upper Cretaceous	Hadiena	2.0	BN2/9	Q	Limestone, grey, medium tough thinly bedded, brecciated, with coarse crystalline secondary of secondary calcite crystals.		
		1.0	BN2/8	// // //	Calcareous Ironstone, vary colour yellow, red, reddish brown, black, grey, medium tough to tough, contain high amount of angular subangular and oval hematitic grains up to 3.0 mm in diameter, yellowish weathered surface mottled with reddish brown and black, hematitic grains are very clear in distinct habit.		
		1.0	BN2/7	// // //			
		1.0	BN2/6	// // // Q	Calcareous Ironstone, dark yellowish brown mottled with dark brown, green yellow, tough, with high amount of angular, subangular and oval hematitic fragments up to 3.0 mm diameter which increase upward with distinct clear habit, veinlets filled with Iron oxides		
		1.0	BN2/5	// // //	Calcareous Ironstone, yellow, light yellowish brown mottled with black and dark reddish stains, medium tough to tough, very tough in part, with coarse dark reddish grains up to 3.0 mm in diameter with oval in shape, veinlets filled with Iron oxide and secondary calcite crystals		
		1.0	BN2/4	// // //			
		2.0	BN2/3	// // // Q	Limestone, dark grey, mottled with black, medium tough, slightly ferruginous, veinlets filled with secondary calcite crystals, brecciated.		
		2.0	BN2/2	// // //			
Upper Jurassic	Chia Gara	3.0	Non	// // //	Covered		
		2.0	BN2/1	// // //	Limestone, dark grey, tough to very tough, recrystallized, veinlets filled with secondary calcite crystals		

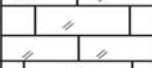
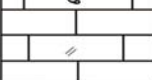
## Appendix 2

Section No. :BN3 Map No. :91/520 Total Thickness :4.50 Scale : 1:100					Location		
					UTM		DMS
					X	355 951	43 22 33.4
					Y	4122838	37 14 27.4
Z	1610	1610					
Age	Fn.	Th.(m.)	Sample	Lithology	Description		
Upper Cretaceous	Hadiena	1.5	BN3/4		Calcareous Ironstone, vary colaur, red, yellow, brown, reddish brown, black, medium tough to tough, contain high amount of hematitic fragments which have angular to sub angular and oval in shape, up to 4.0 mm in diameter veinlets filled with Ironoxides and secondary calcite crystals brecciated .		
		1.0	BN3/3				
		1.0	BN3/2		Ferruginous limestone, light yellowish brown, yellow, mottled with black stains, medium tough to tough, the interval (1.60-1.90), more yellow,is very tough, contain Iron fragments vary in shape and size, subangular to angular and oval in shape, up to 2mm in diameter, last 30cm with highly amount of hematitic fragments which increase upward, brecciated .		
		1.0	BN3/1				
					✂ Up and down of section is highly covered		

Section No. :BN 4 Map No. :91/520 Total Thickness :3.0 Scale : 1:100					Location		
					UTM		DMS
					X	355 882	43 22 30.7
					Y	4122 815	37 14 26.6
Z	1620	1620					
Age	Fn.	Th.(m.)	Sample	Lithology	Description		
Upper Cretaceous	Hadiena	1.50	BN4/2		Calcareous Ironstone, vary colorr cred, yellow, reddish brown, grey, black medium tough to tough, contain high amount of hematitic fragments in subangular, argular, semirounded and oval in shape, up to 3.0 mm. In diameter, Iron grains increase upward with macro fossil the weathered surface is very distinctive ,hematitic fragments appearance is very clear, veinlets filled with secondary calcite crystals and Ironoxides, breciated.		
		1.50	BN4/1				
					✂ Up and down of section is highly covered		

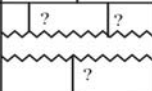
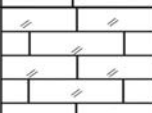
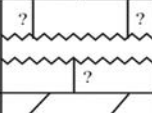
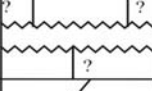
## Appendix 2

Section No. :BN5 Map No. :91/520 Total Thickness :8.60 Scale : 1:100					Location		
					UTM		DMS
					X	355 817	43 22 28.0
					Y	4122 869	37 14 28.4
		Z	1640	1640			
Age	Fn.	Th.(m.)	Sample	Lithology	Description		
Upper Cretaceous	Hadiena	2.0	BN5/5		Calcareous Ironstone, reddish brown, mottled with dark red, black, with yellowish stains, tough , hematitic grains are very clear with subangular to oval in shape, veinlets filled with secondary calcite crystals and Ironoxides fragments, brecciated, sharp cliff.		
		2.0	BN5/4		Calcareous Ironstone, light yellowish brown mottled with vary colour( red, yellow, grey, reddish brown ), hematitic grains in subangular to angular and oval in shape, up to more than 3.0 mm in diameter, distinct feature, more yellowish downward, veinlets filled with Ironoxides and calcite.		
		0.80	BN5/3				
		1.70	BN5/2		Calcareous Ironstone, yellow, light yellowish brown, tough, veinlets filled with siderite and secondary calcite crystals as well as Ironoxides, dark Iron fragments increase upward. Brecciated .		
		2.10	BN5/1		Limestone, dark grey, yellowish stains, more yellowish upward, tough, slightly ferruginous, up vienlets filled with secondary calcite crystals and Ironoxides.		

Section No. :BN6 Map No. :91/520 Total Thickness :13.20 Scale : 1:100					Location		
					UTM		DMS
					X	355 309	43 22 07.3
					Y	4122 904	37 14 29.2
		Z	1660	1660			
Age	Fn.	Th.(m.)	Sample	Lithology	Description		
Upper Cretaceous	Hadiena	2.0	BN6/5		Calcareous Ironstone, reddish brown to dark reddish brown, slightly mottled with white, yellow and black, tough, highly hematitic fine grains, brecciated .		
		1.50	BN6/4		Calcareous Ironstone, light yellowish brown mottled with white, red, yellow, dark reddish brown, black, more reddish upward, tough,Iron grains vary in shape and size ,oval, angular, subangular...), Weathered surface is more yellowish with distinct habit .		
		1.70	BN6/3		Calcareous Ironstone, pale yellowish brown mottled with red, yellow, dark reddish brown tough contain Iron fragment (oval in shape size up to 2mm in diameter) fine grained Iron fragments more than coarser.		
		2.0	BN6/2		Limestone, dark grey with yellowish stains, more yellowish upward, tough, slightly ferruginous, veinlets filled with Iron oxides, brecciated.		
		4.0	Non		Covered		
Upper Jurassic	Barsarin	2.0	BN6/1		Sandy dolostone, grey, very tough, recrystalized, brecciated.		

## Appendix 2

Section No. :BN7 Map No. :91/520 Total Thickness :2.50 Scale : 1:100					Location		
					UTM		DMS
					X	355 247	43 22 04.9
					Y	4122 859	37 14 27.7
					Z	1610	1610
Age	Fn.	Th.(m.)	Sample	Lithology	Description		
Upper Cretaceous	Hadiena	2.5	BN7		Calcareous Ironstone, vary colour, yellow, red, reddish brown, dark brown, tough, contain high amount of hematitic fragments with subangular to angular and oval in shape, up to 3.0mm in diameter, with macro fossils, weathered surface is light yellowish brown mottled with black and dark reddish brown and the hematitic fragments is very clear appearance, veinlets filled with secondary calcite crystals and Iron oxides, brecciated.		
							
							
							
					<b>X</b> Up and down of section is highly covered		

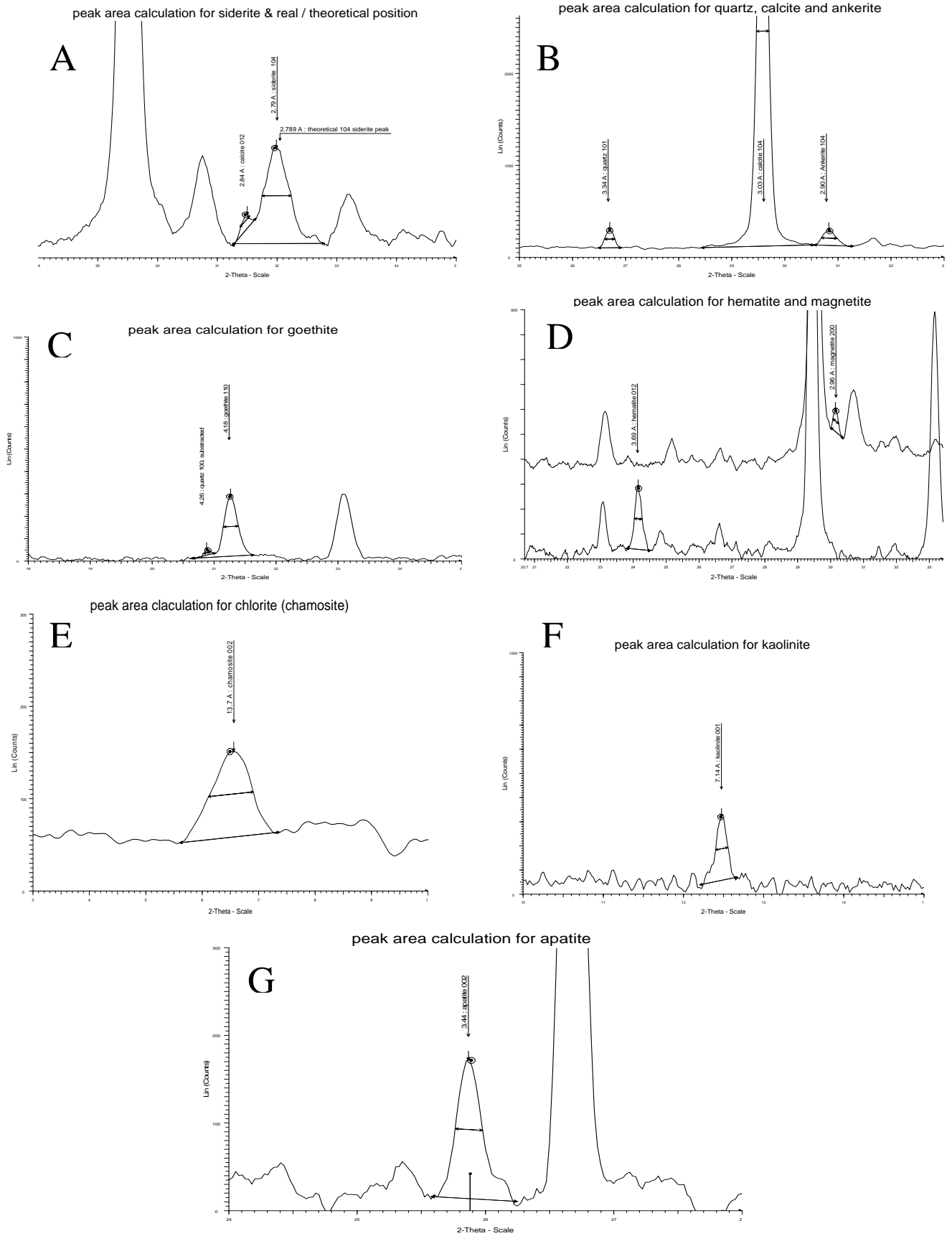
Section No. :BN8 Map No. :91/520 Total Thickness :44.0 Scale : 1:100					Location		
					UTM		DMS
					X	355 178	43 22 02.0
					Y	4122919	37 14 29.6
					Z	1580	1580
Age	Fn.	Th.(m.)	Sample	Lithology	Description		
Upper Cretaceous	Hadiena	3.0	BN8/6		Limestone, dark grey, very tough, recrystallized, brecciated.		
		6.0	Non		Covered		
		2.70	BN8/5		Calcareous Ironstone, vary colour, yellow, red, reddish brown, more reddish upward, more yellowish downward, medium tough to tough, contain high amount of Iron fragments with angular, subangular and oval in shape, up to 3.0 mm in diameter, weathered surface is yellow mottled with dark reddish brown, hematitic grains are very clear in distinct habit.		
		1.50	BN8/4		Calcareous Ironstone, light yellowish brown, yellow, mottled with black stains, medium tough to tough, wethered surface is yellow with black stains and slightly reddish brown stains, Iron grains increase upward, veinlets filled with Iron oxides and secondary calcite crystals.		
		1.50	BN8/3				
		1.30	BN8/2		Ferruginous limestone, black to dark greenish grey, tough, weathered surface is light yellowish brown, brecciated.		
Upper Jurassic	Barsarin	9.0	Non		Covered		
		2.0	BN8/1		Sandy dolostone, grey, very tough, recrystallized, brecciated.		
		16.0	Non		Covered		
		1.0	BN8/1A		Dolostone, grey, very tough dip (55-60) and strike (170-180)		

## Appendix 2

Section No. :BN9 Map No. : Total Thickness :5.90 Scale : 1:100					Location		
					UTM		DMS
					X	355 038	43 21 56.4
					Y	4122 828	37 14 26.3
					Z	1620	1620
Age	Fn.	Th.(m.)	Sample	Lithology	Description		
Upper Cretaceous	Hadiena	1.60	BN9/3		Calcareous Ironstone, dark reddish brown, mottled with yellow, red, brown, medium tough to tough, highly amount of fine hematitic grains, veinlets filled with Iron oxides and secondary calcite crystals, brecciated.		
		1.80	BN9/2		Calcareous Ironstone, dark yellowish grey, highly yellowish stains, tough contain higher amount of Iron fragments than the previous sample, more reddish upward, brecciated.		
		2.50	BN9/1		Calcareous Ironstone, black to dark greenish grey, slightly yellowish stains upward, tough, the weathered surface is light yellowish brown, contain Iron oxides fragments which increase upward, veinlets filled with secondary calcite crystals, brecciated.		
					✂ Up and down of section is highly covered		

Section No. :BN10 Map No. :91/520 Total Thickness :5.0 Scale : 1:100					Location		
					UTM		DMS
					X	354 866	43 21 49.4
					Y	4122 820	37 14 26.2
					Z	1600	1600
Age	Fn.	Th.(m.)	Sample	Lithology	Description		
Upper Cretaceous	Hadiena	1.50	BN10/3		Calcareous Ironstone, reddish brown, darker than previous sample, tough, contain highly amount of Iron fragments, finer grains of Iron more than coarser, veinlets filled with Iron oxide and secondary calcite crystals brecciated.		
		1.50	BN10/2		Calcareous Ironstone, reddish brown, more reddish upward mottled with yellow, dark grey, yellowish brown, medium tough to tough, cavernouse in part, contain high amount of angular and oval Iron fragments, coarse grains of Iron more than finer, up to 2.50 mm in diameter .		
		2.0	BN10/1		Calcareous Ironstone, yellowish green mottled with dark reddish brown and black, very tough, veinlets filled with Ironoxides and secondary calcite crystals, contain macro fossils, with colloidal texture, highly yellowish stains .		
					✂ Up and down of section is highly covered		

## Appendix 3



Appendix (3): Clarifying the procedure of peak area calculations for each mineral of Benavi IRS samples to determine the relative abundance of these minerals in this deposit.

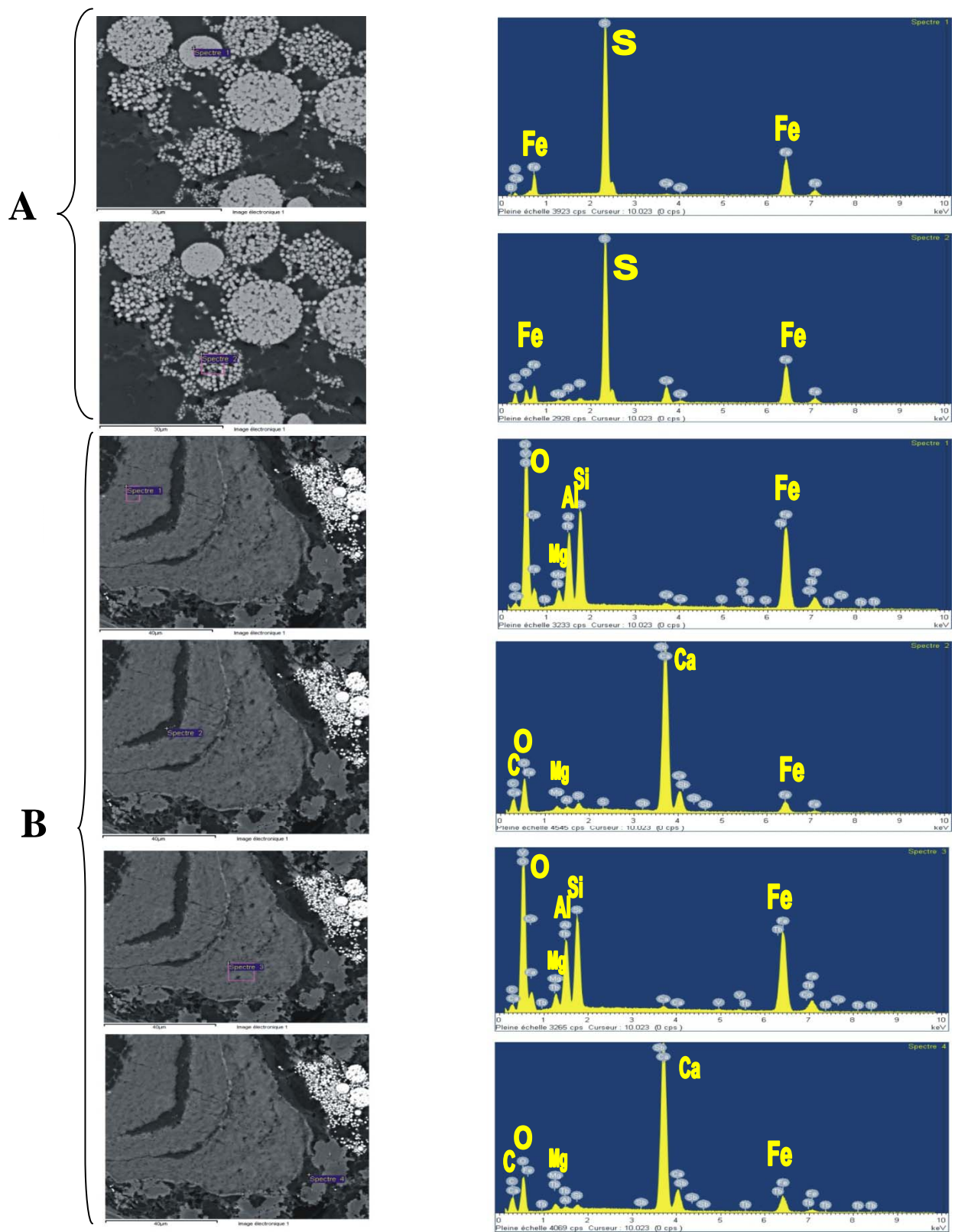


Figure (1): BSE images and EDS analysis of: A-Site 1 of sample BN1/4 and B-Site 2 of sample BN1/4 .

## Appendix 4

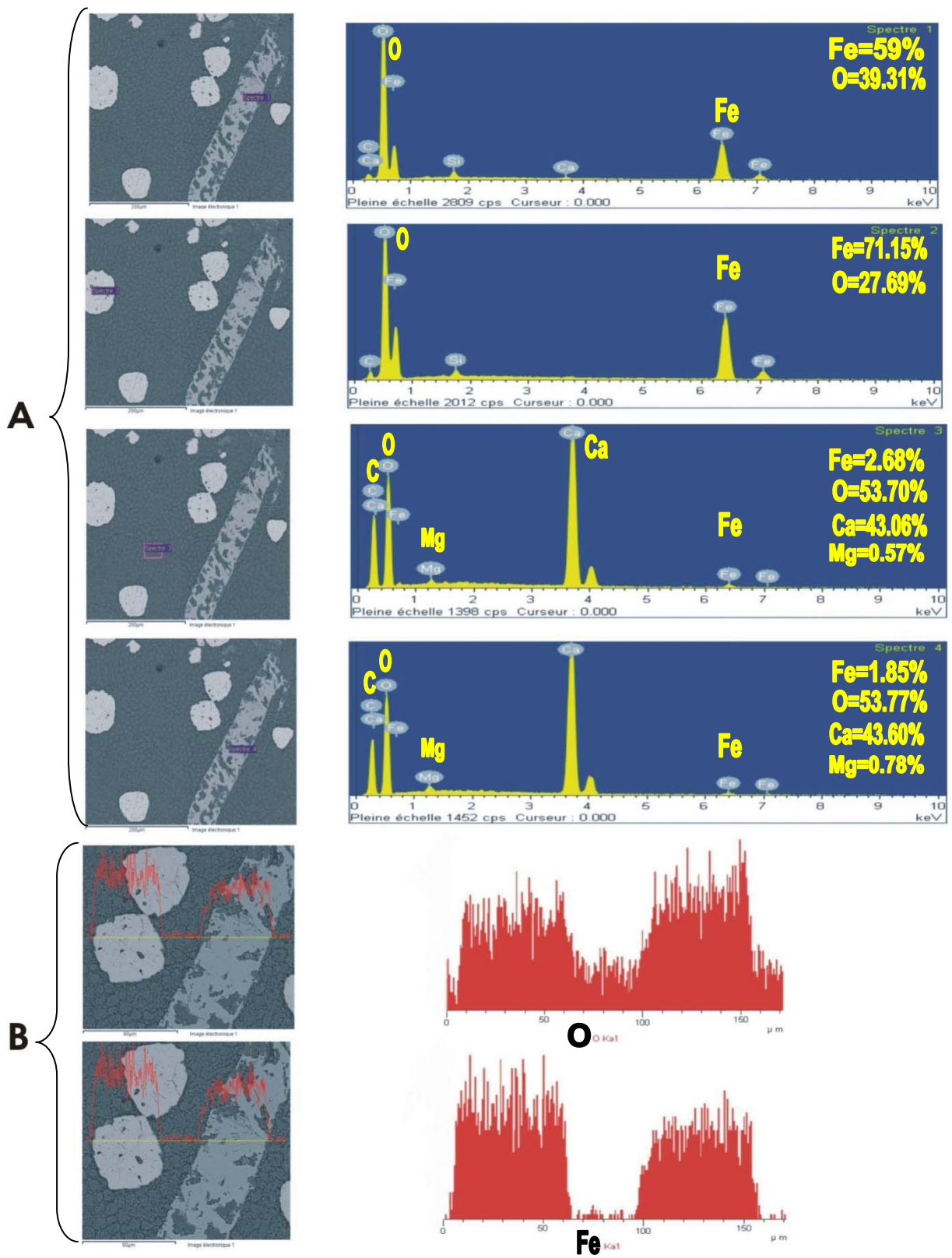


Figure (2): A-BSE images and EDS analysis of Site 1 of sample BN1/5.

B- Elemental transverse in site 2 of sample BN1/5.

## Appendix 4

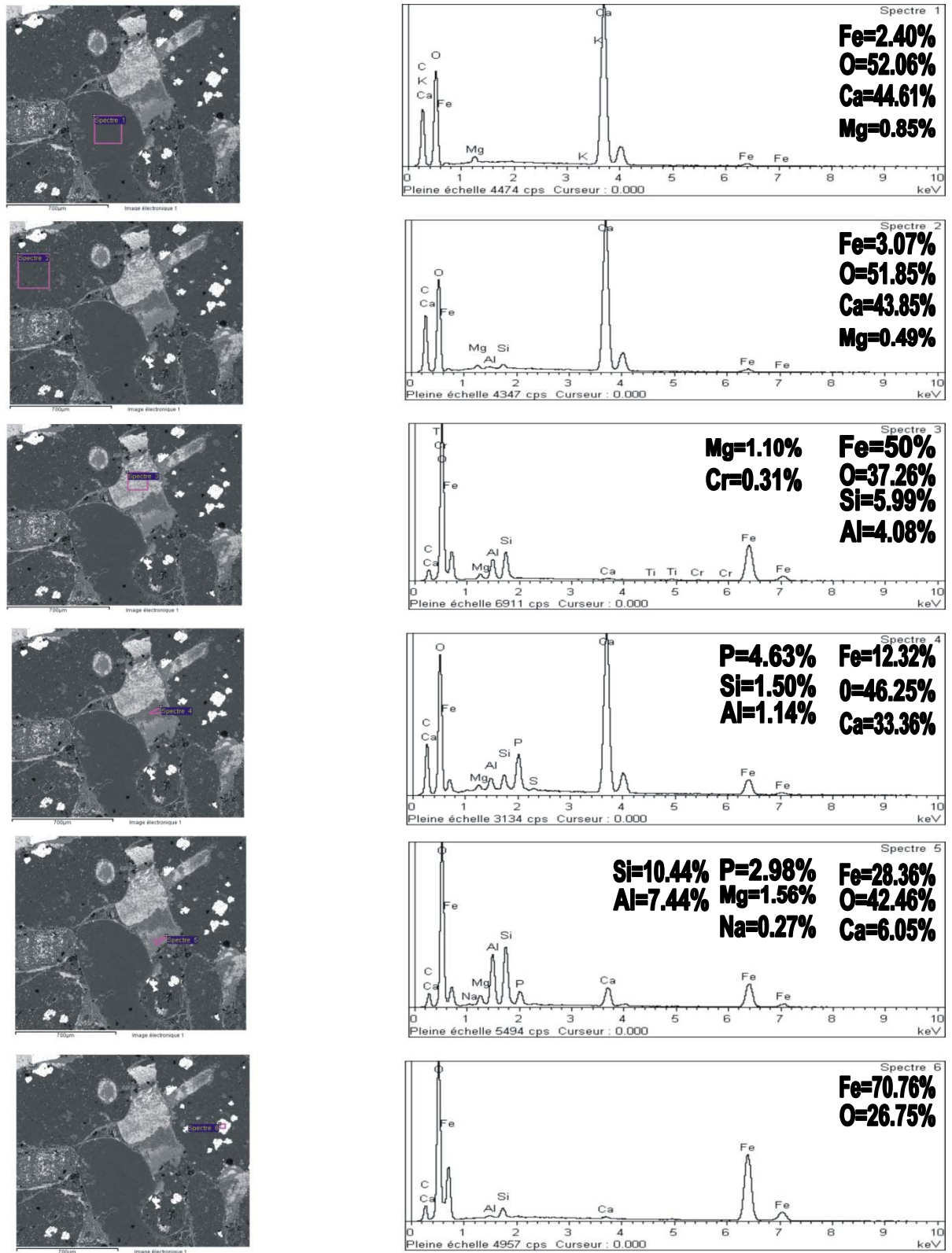


Figure (3): BSE images and EDS analysis of Site 1 of sample BN1/6.

## Appendix 4

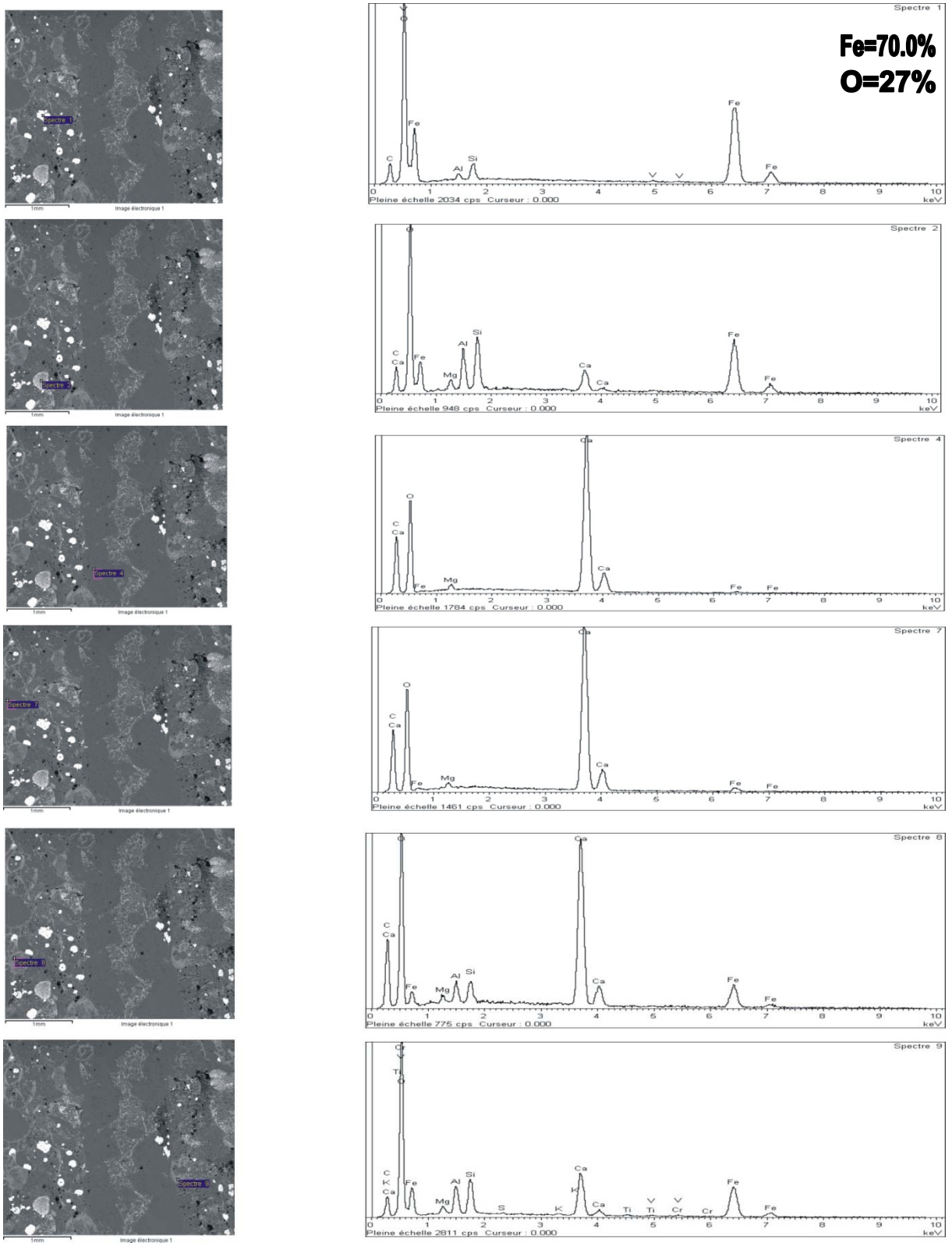


Figure (4): BSE images and EDS analysis of Site 2 of sample BN1/6.

## Appendix 4

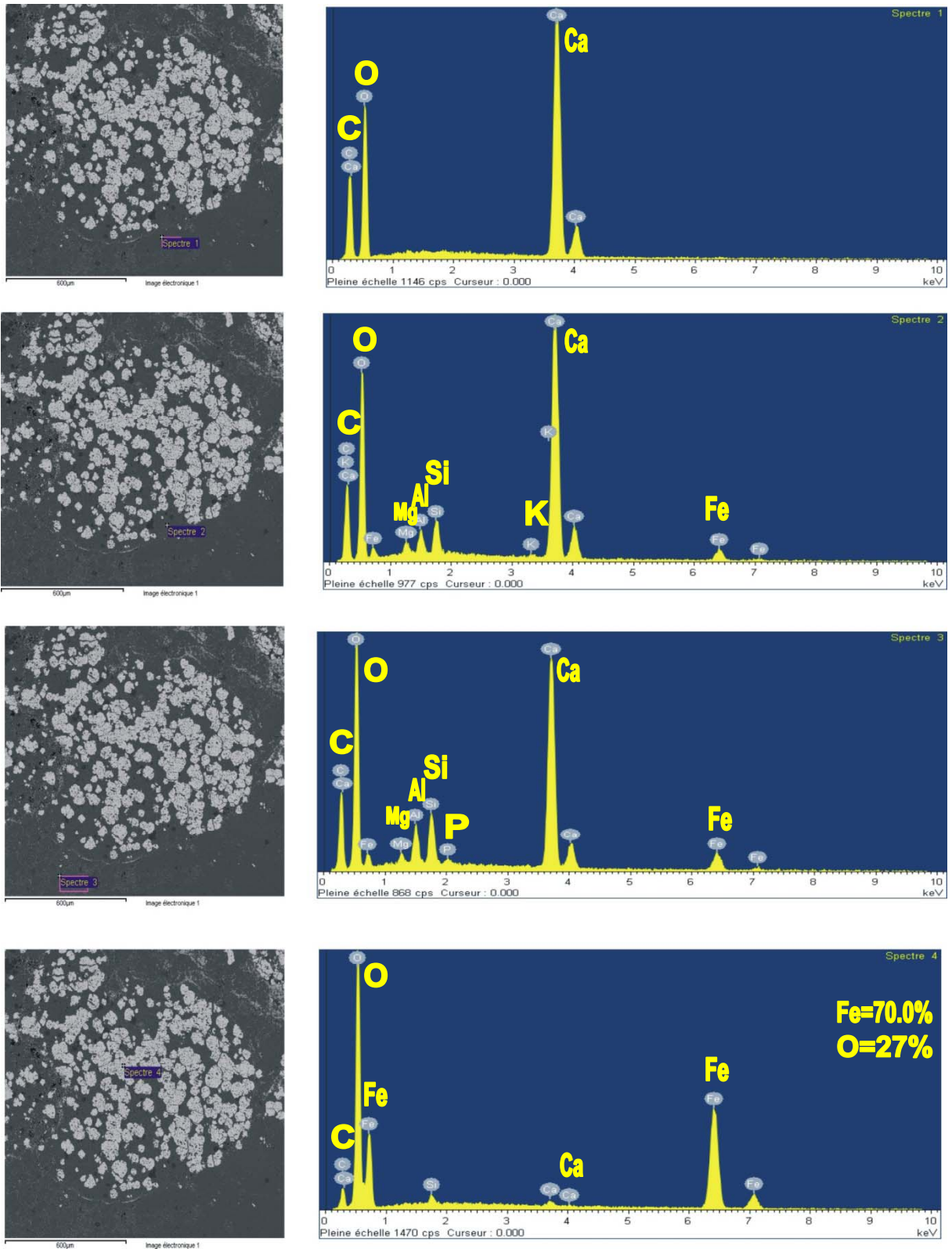


Figure (5): BSE images and EDS analysis of Site 1 of sample BN2/7.

## Appendix 4

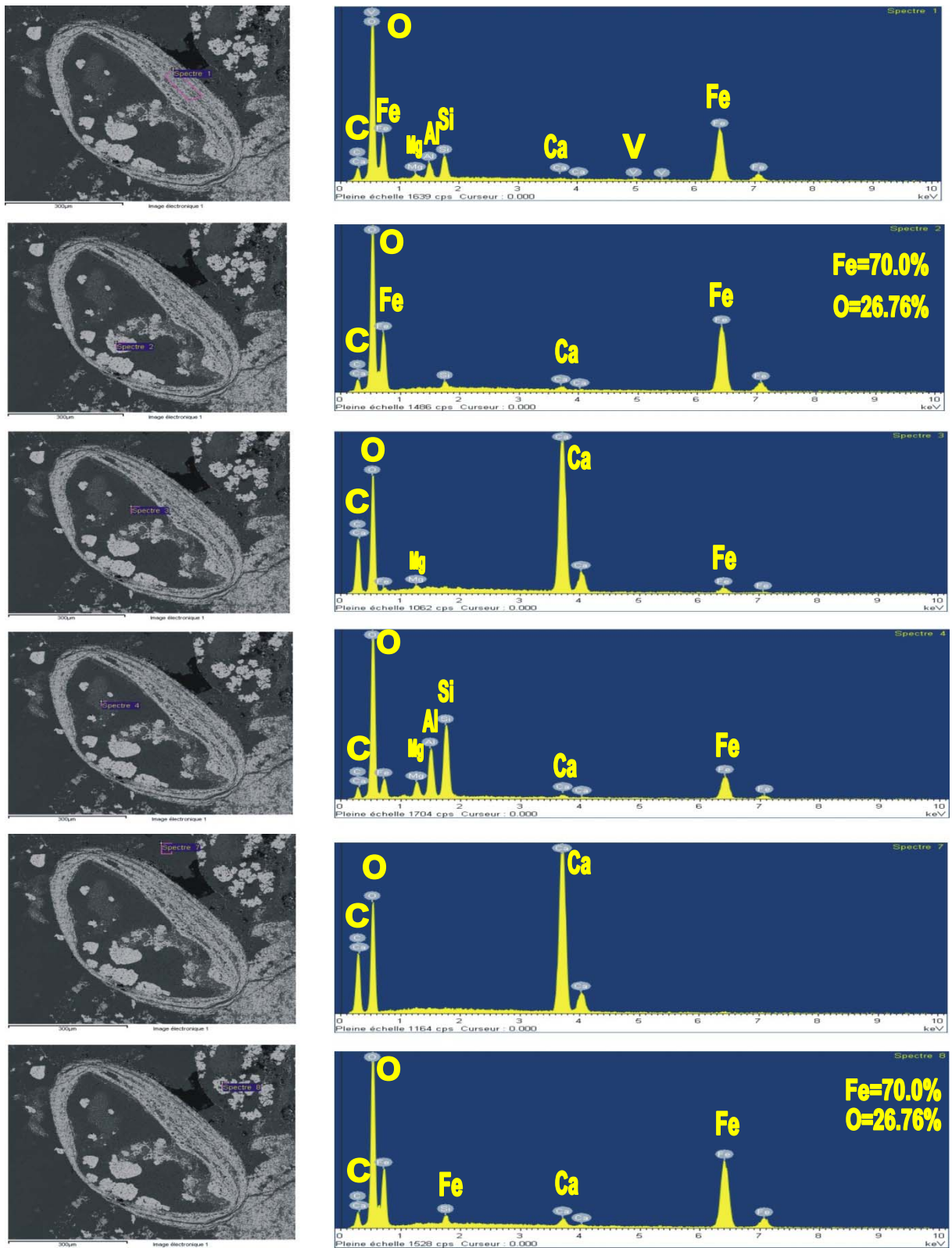


Figure (6): BSE images and EDS analysis of Site 2 of sample BN2/7.

## Appendix 4

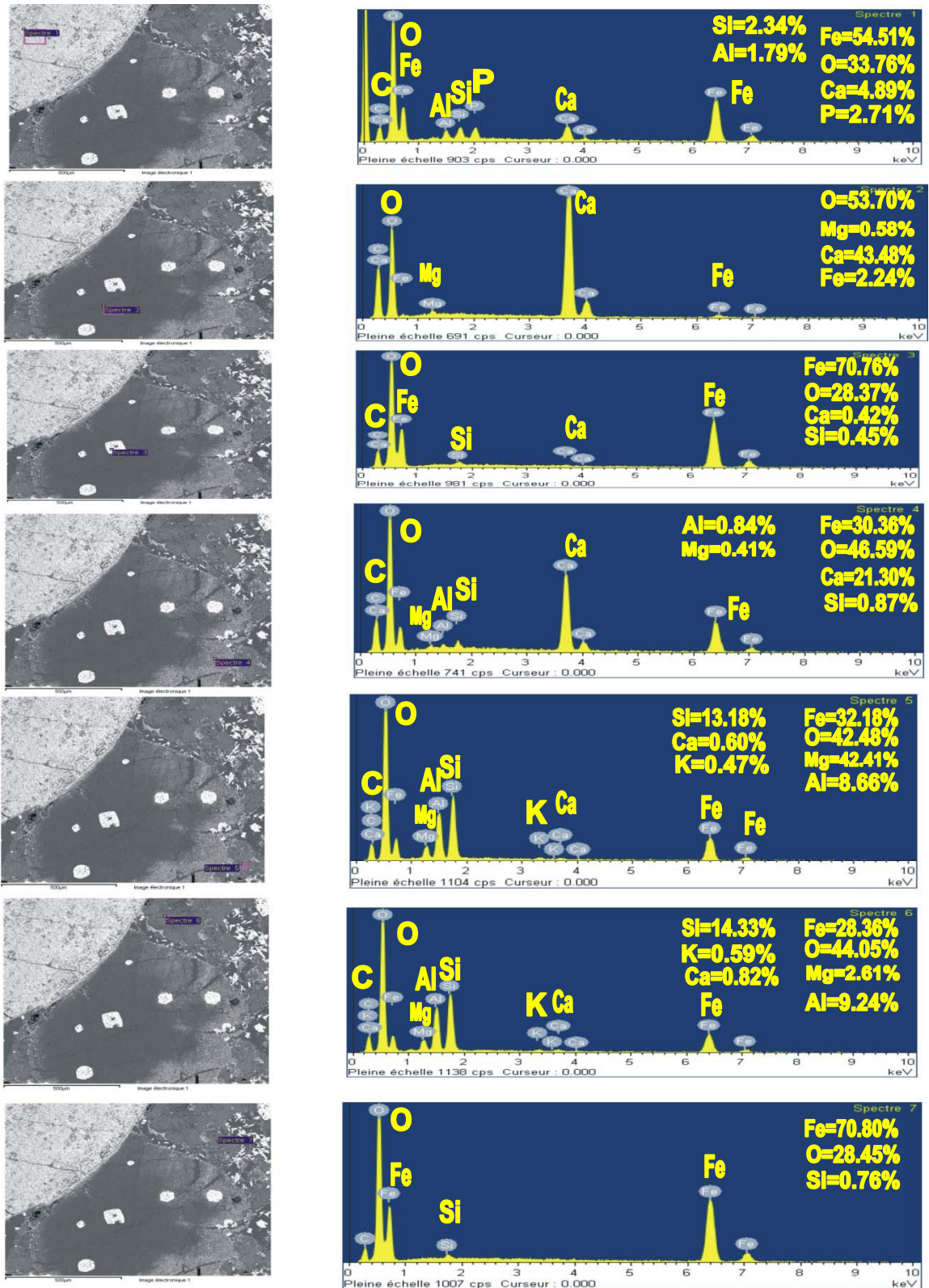


Figure (7): BSE images and EDS analysis of Site 3 of sample BN2/7.

## Appendix 4

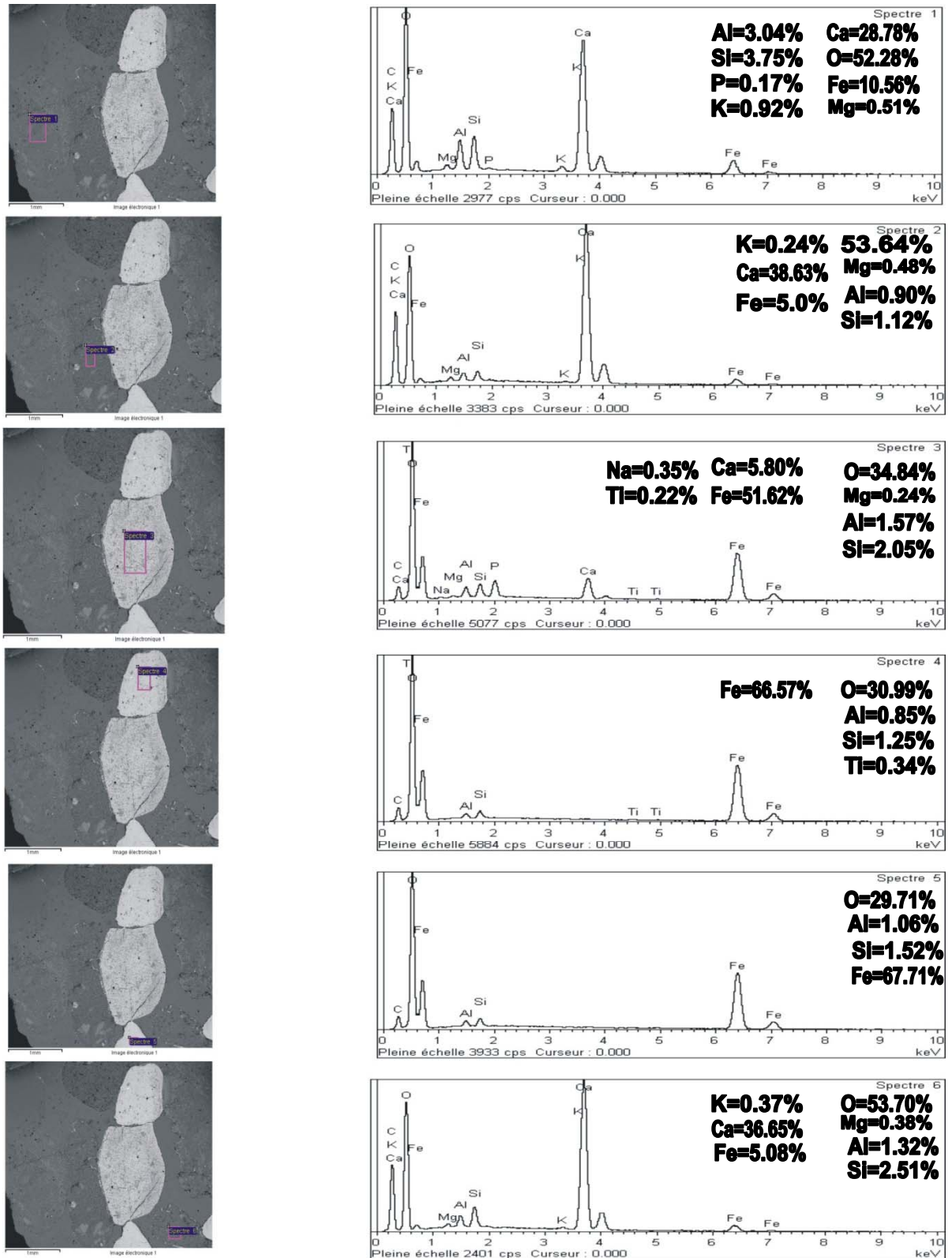


Figure (8): BSE images and EDS analysis of Site 1 (spectra 1-6) of sample BN3/4.

## Appendix 4

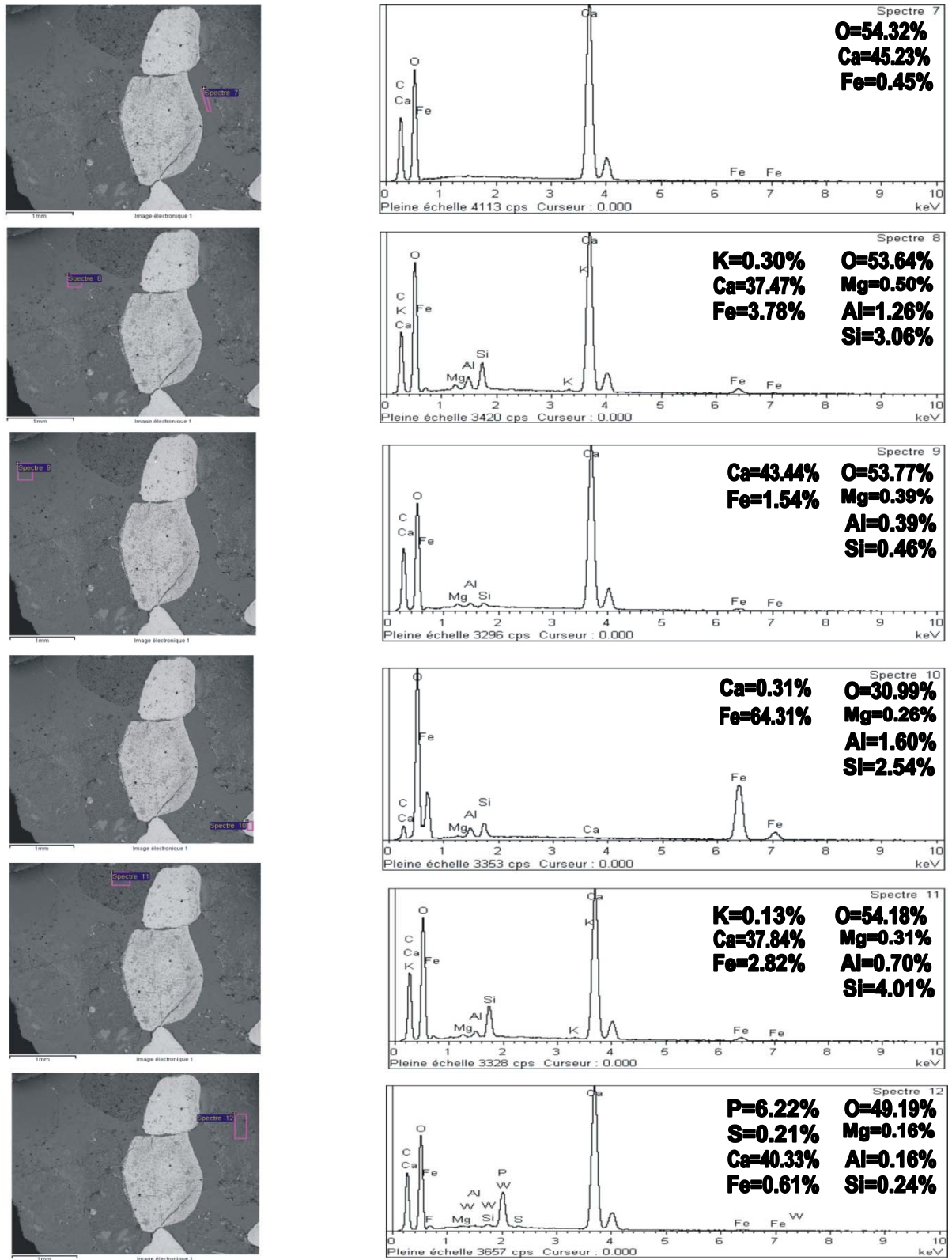


Figure (9): BSE images and EDS analysis of Site 1(spectra 7-12) of sample BN3/4.

## Appendix 4

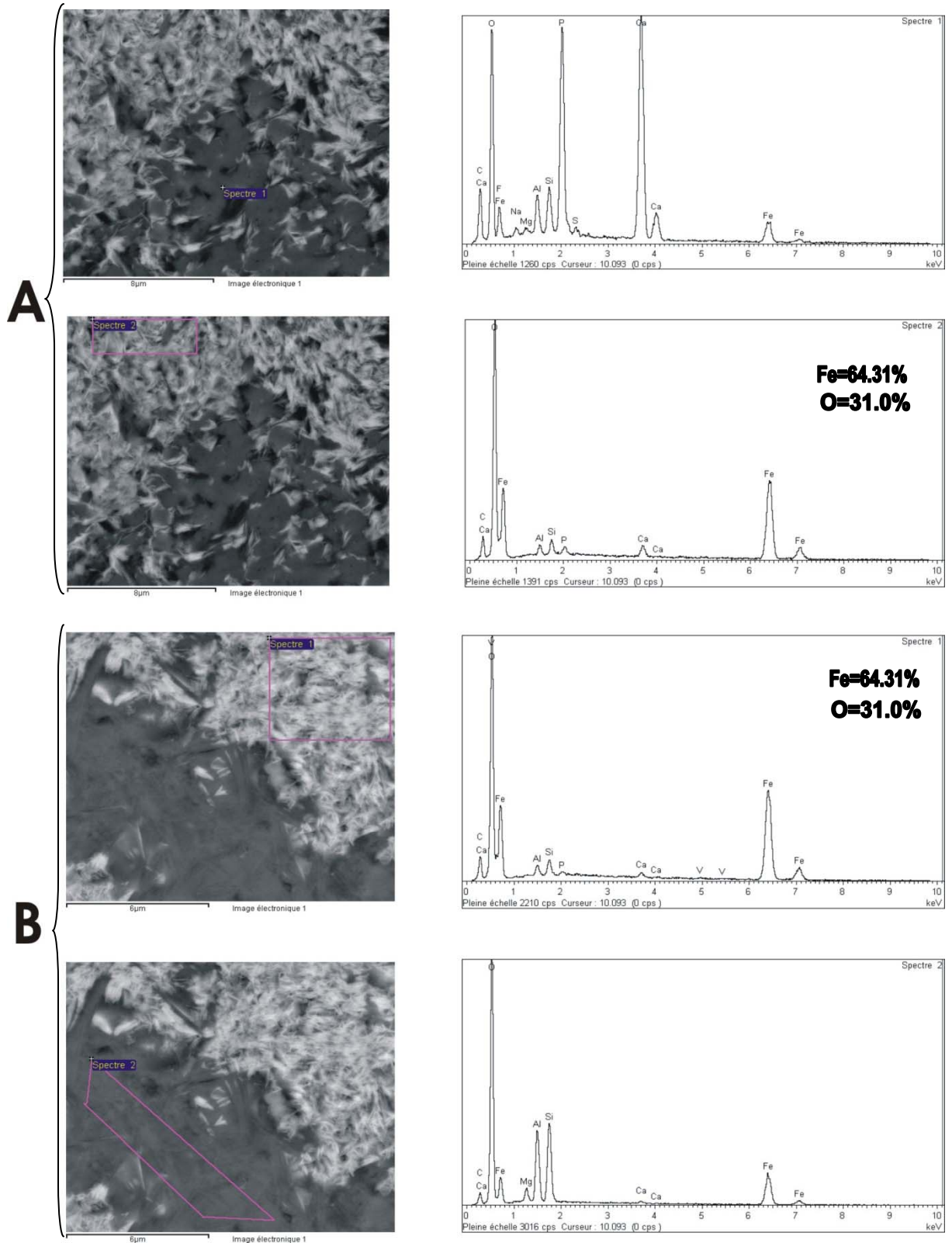


Figure (10):BSE images and EDS analysis of : A-Site 2 of sample BN3/4  
and B-Site 3 of sample BN3/4 .

## Appendix 4

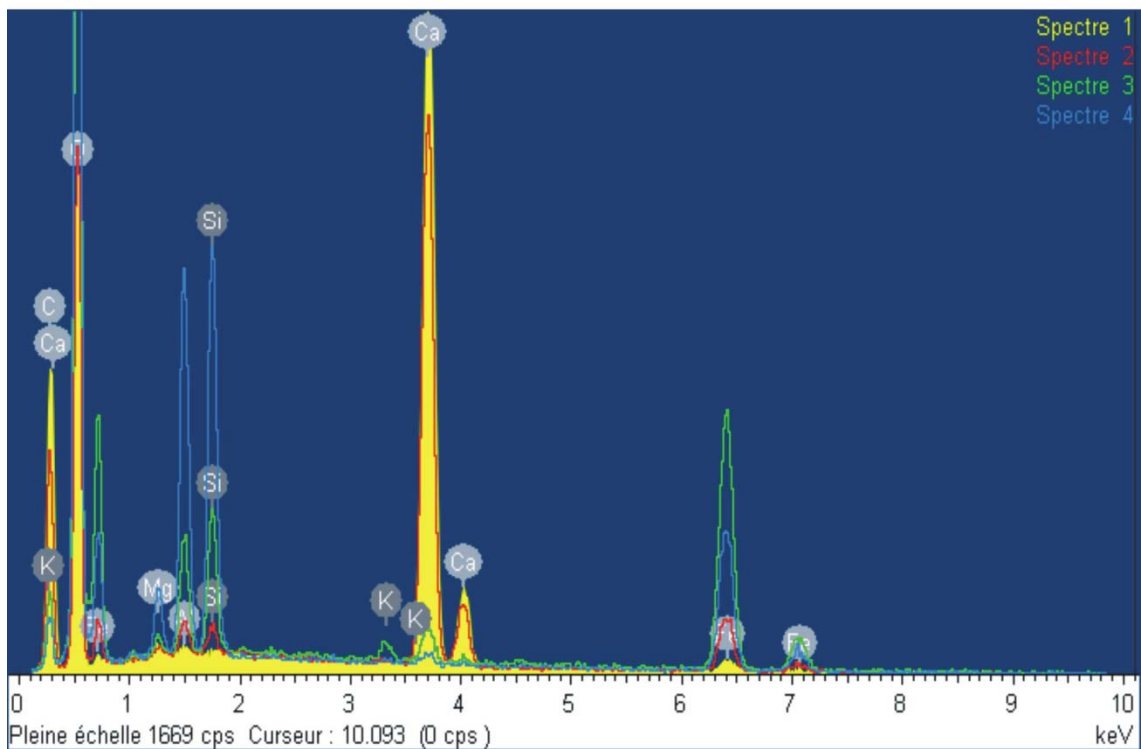
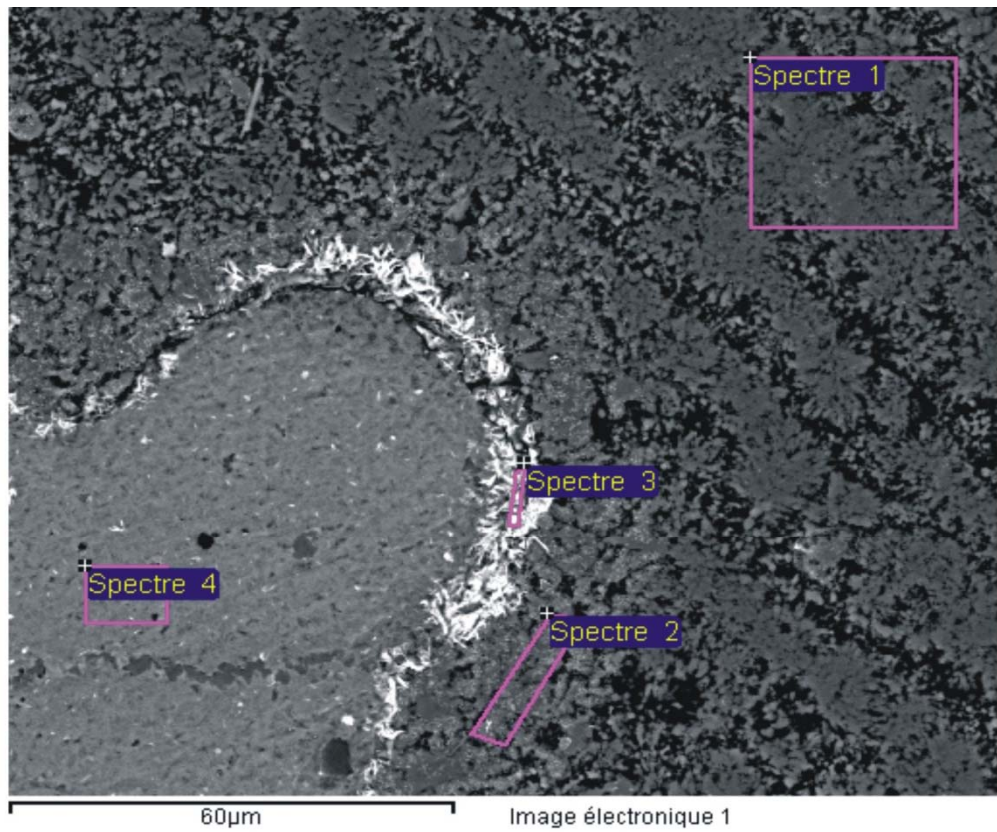


Figure (11): BSE images and EDS analysis of Site 4 of sample BN 3/4.

## Appendix 4

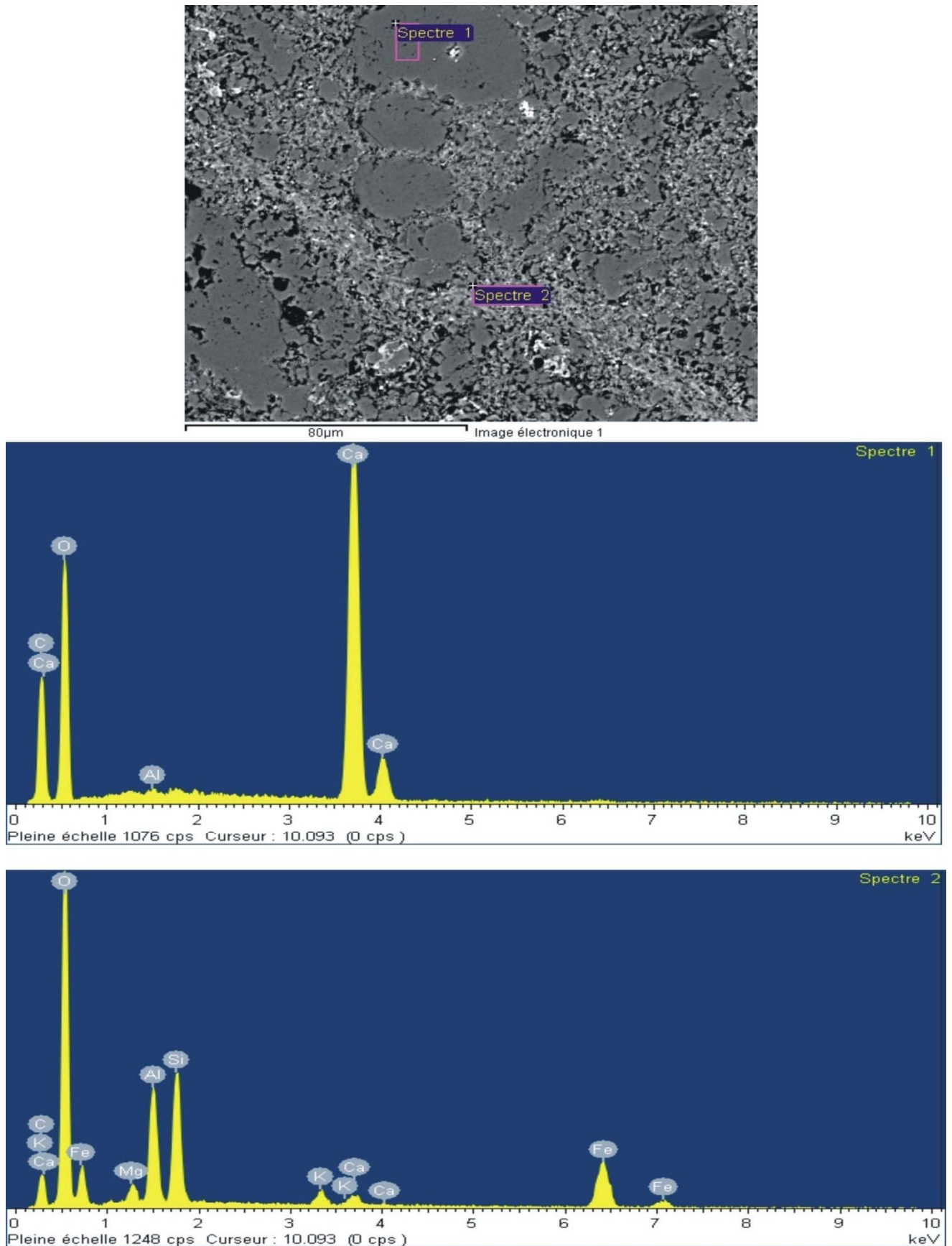


Figure (12): BSE images and EDS analysis of Site 5 of sample BN3/4.

## Appendix 4

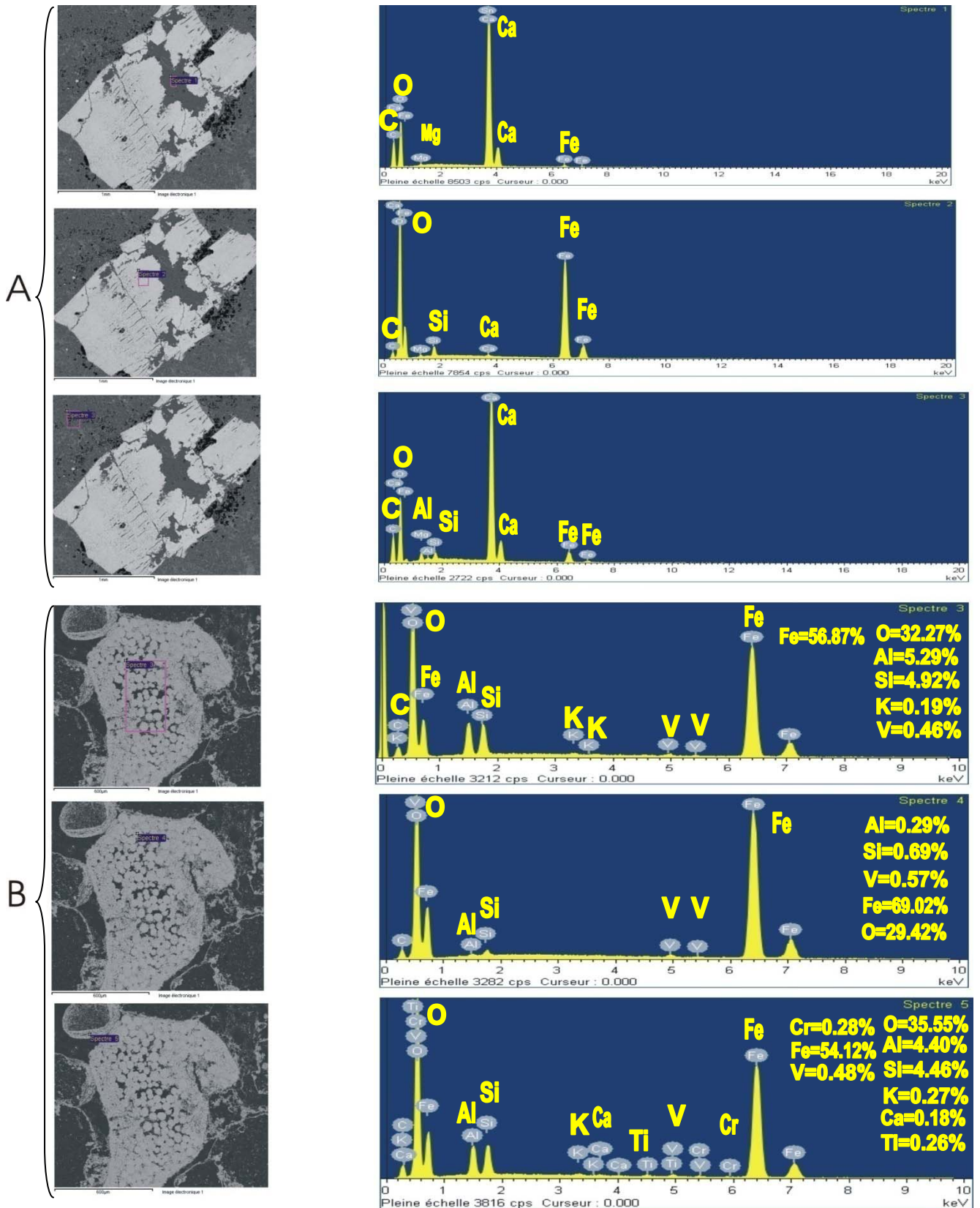


Figure (13): BSE images and EDS analysis of: A- Site 1 of sample BN5/2.  
 , B-Site 1 of sample BN6/5.

## Appendix 4

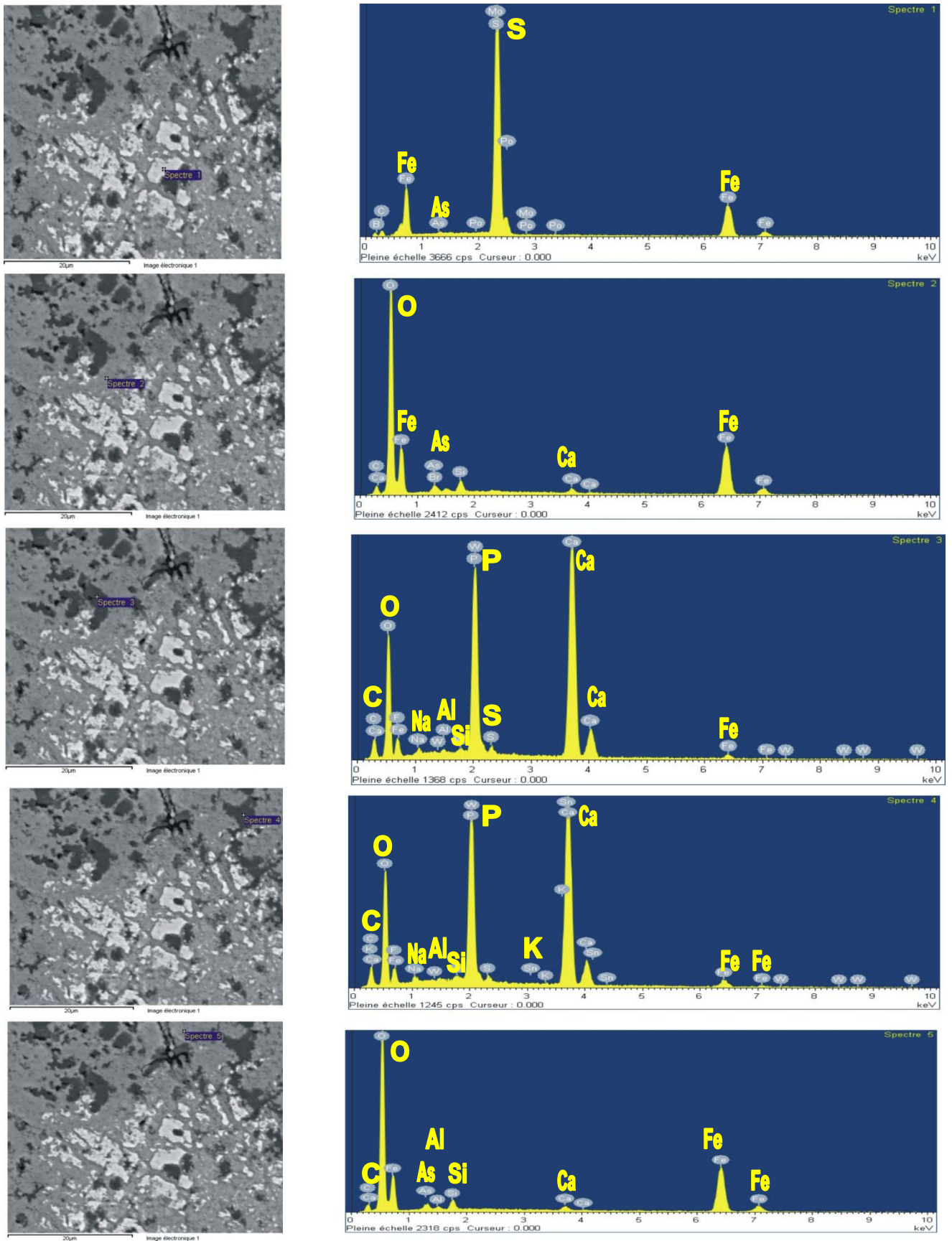


Figure (14): BSE images and EDS analysis of Site 1 of sample BN5/3.

## Appendix 4

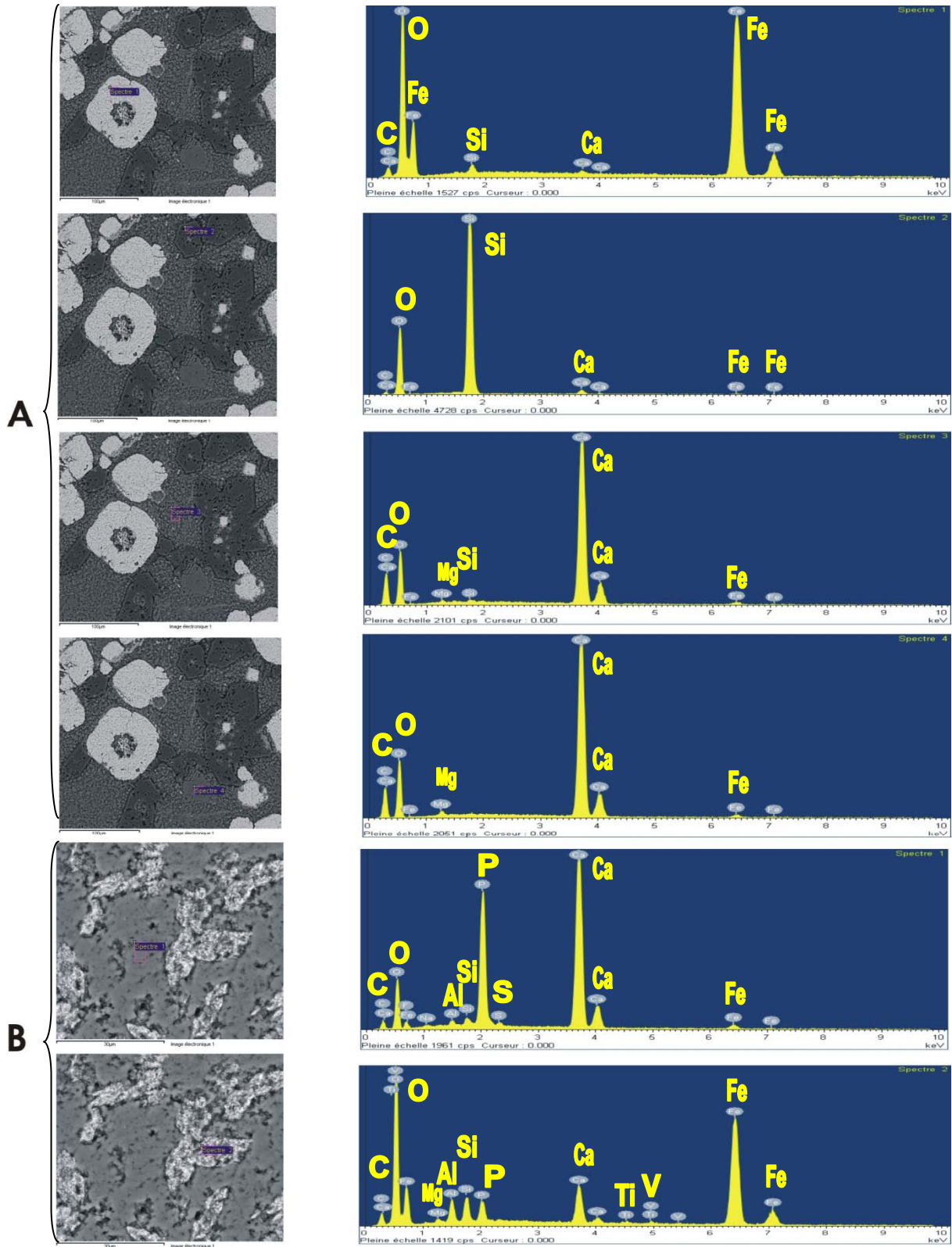


Figure (15): BSE images and EDS analysis of :A- Site 1 of sample BN5/4.,  
B-Site 2 of sample BN5/4.

## Appendix 4

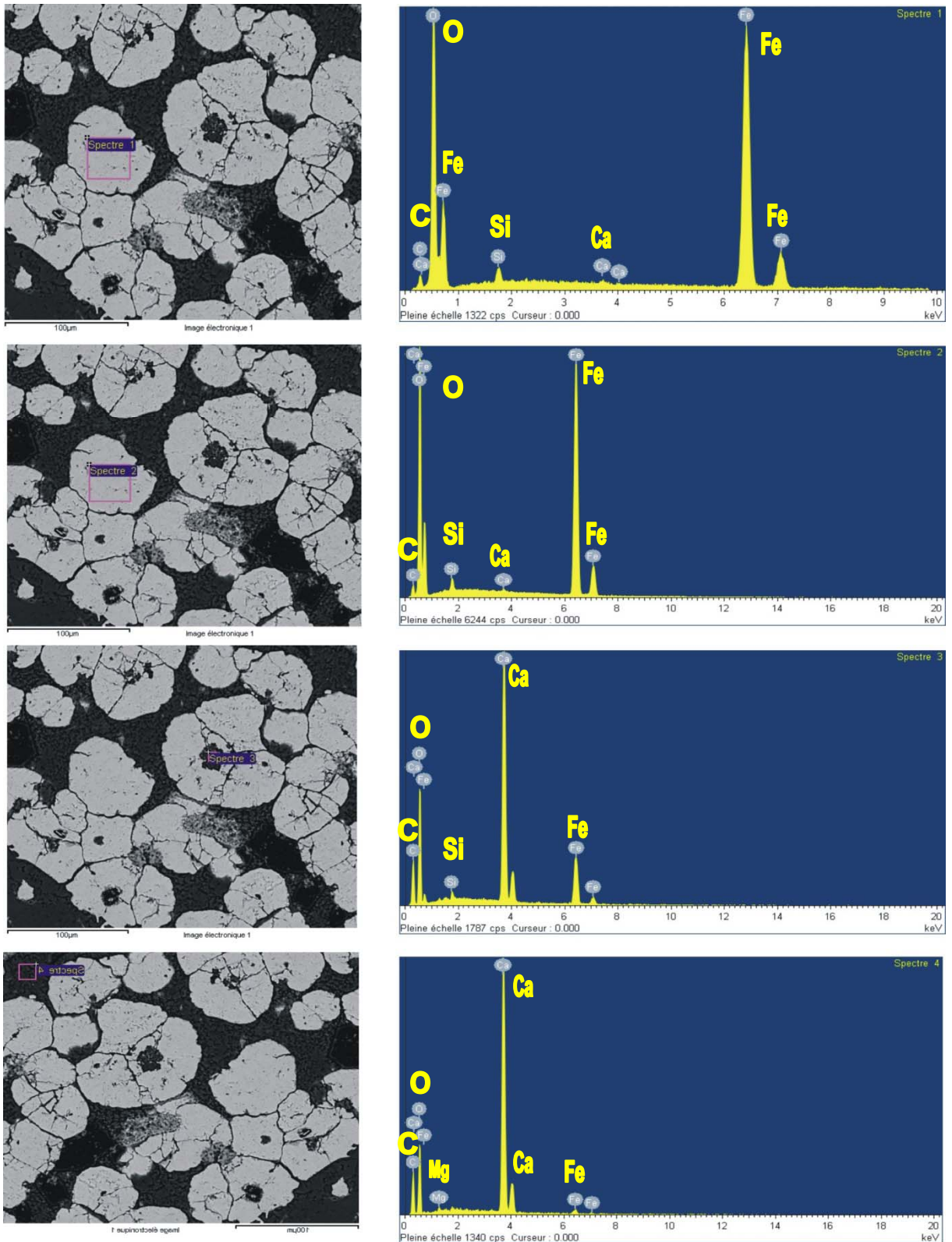


Figure (16): BSE images and EDS analysis of Site 3 of sample BN5/4.

## Appendix 4

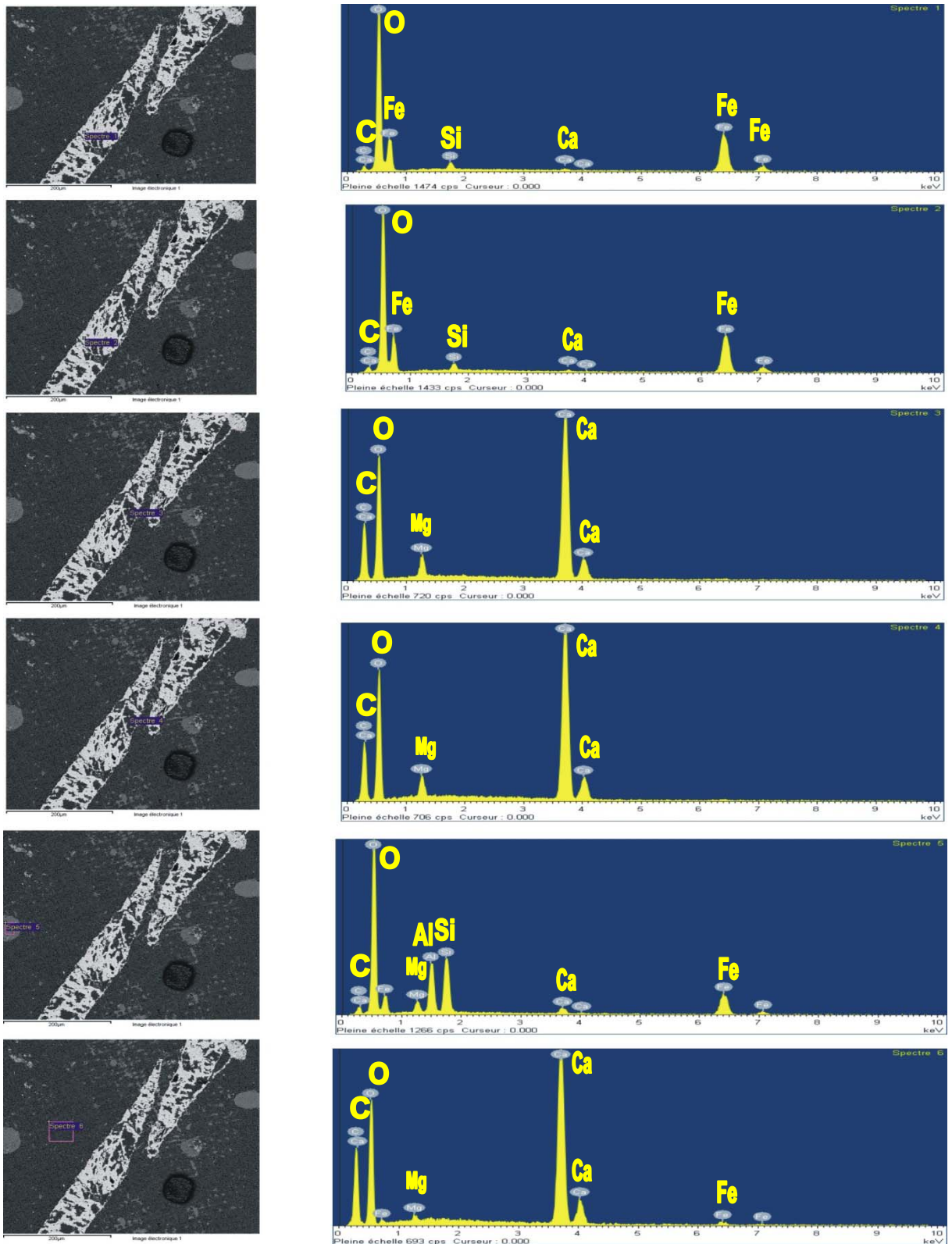


Figure (17): BSE images and EDS analysis of Site 1 of sample BN7.

## Appendix 4

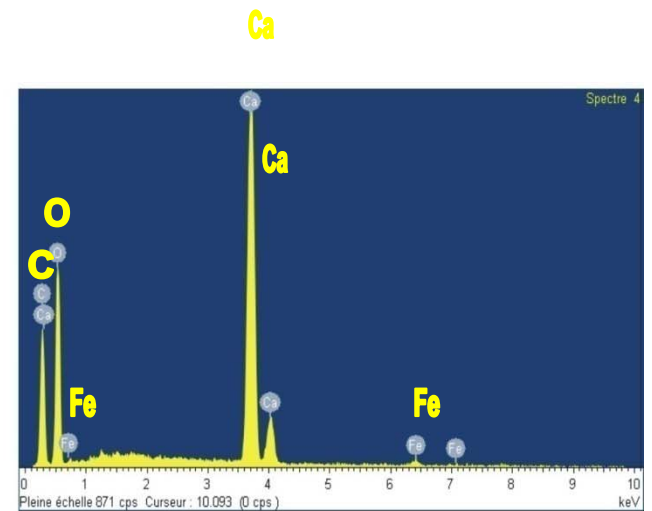
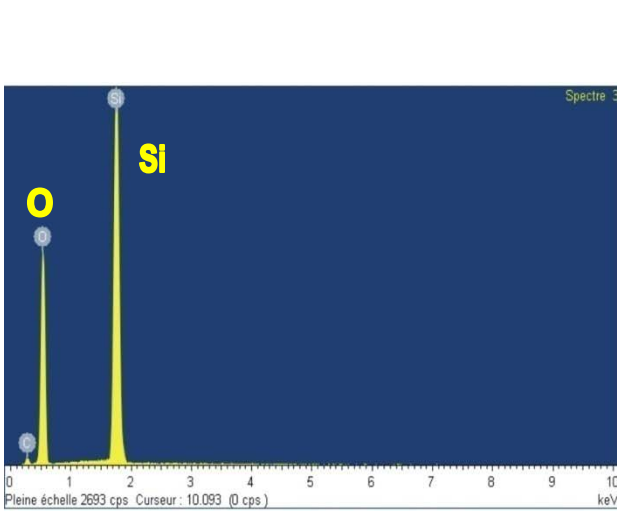
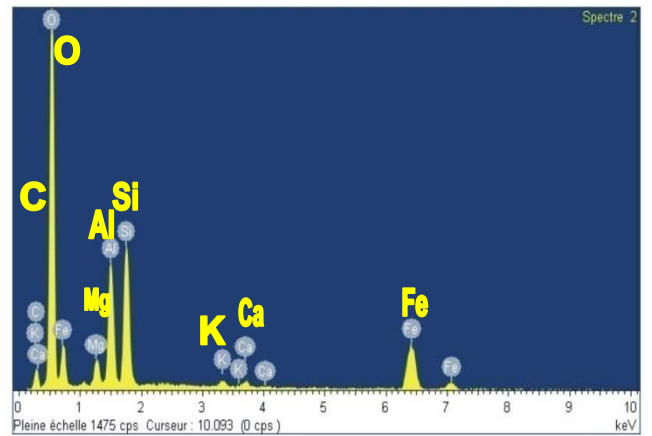
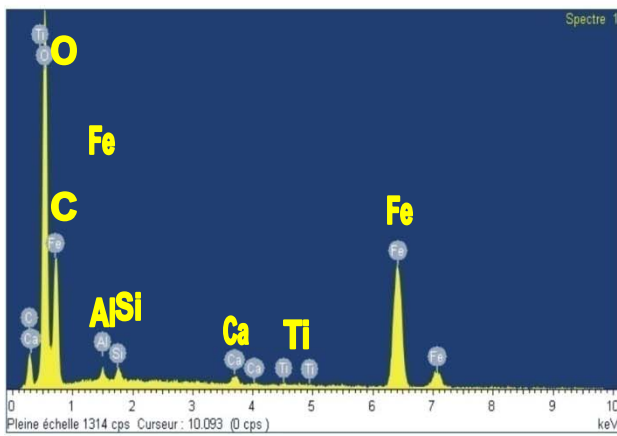
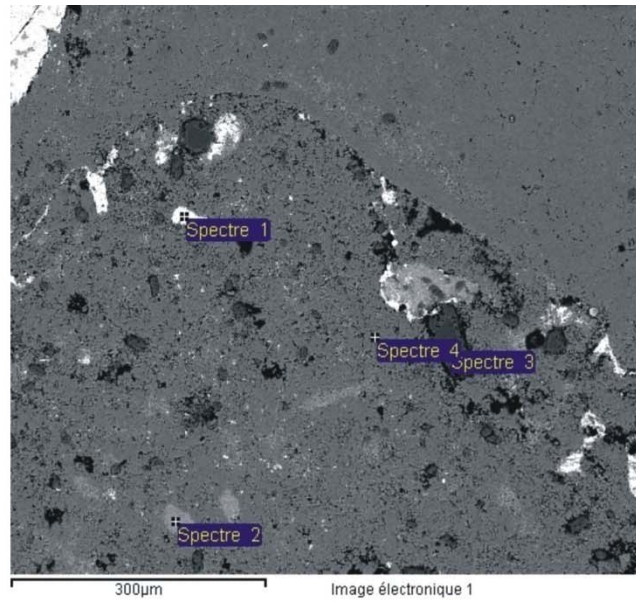


Figure (18): BSE images and EDS analysis of Site 1 of sample BN8/3.

## Appendix 4

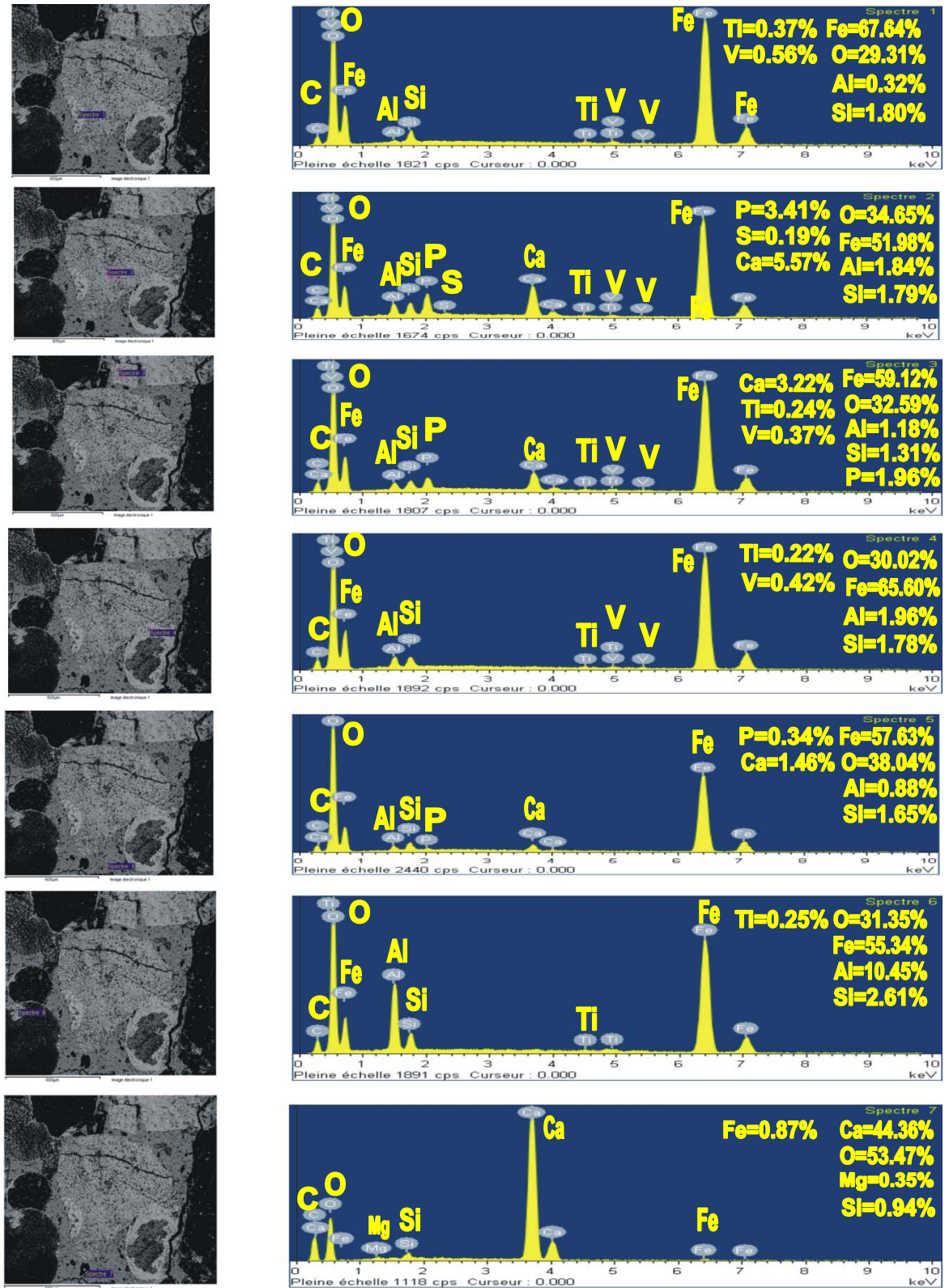


Figure (19): BSE images and EDS analysis of Site 1 of sample BN8/5.

## Appendix 4

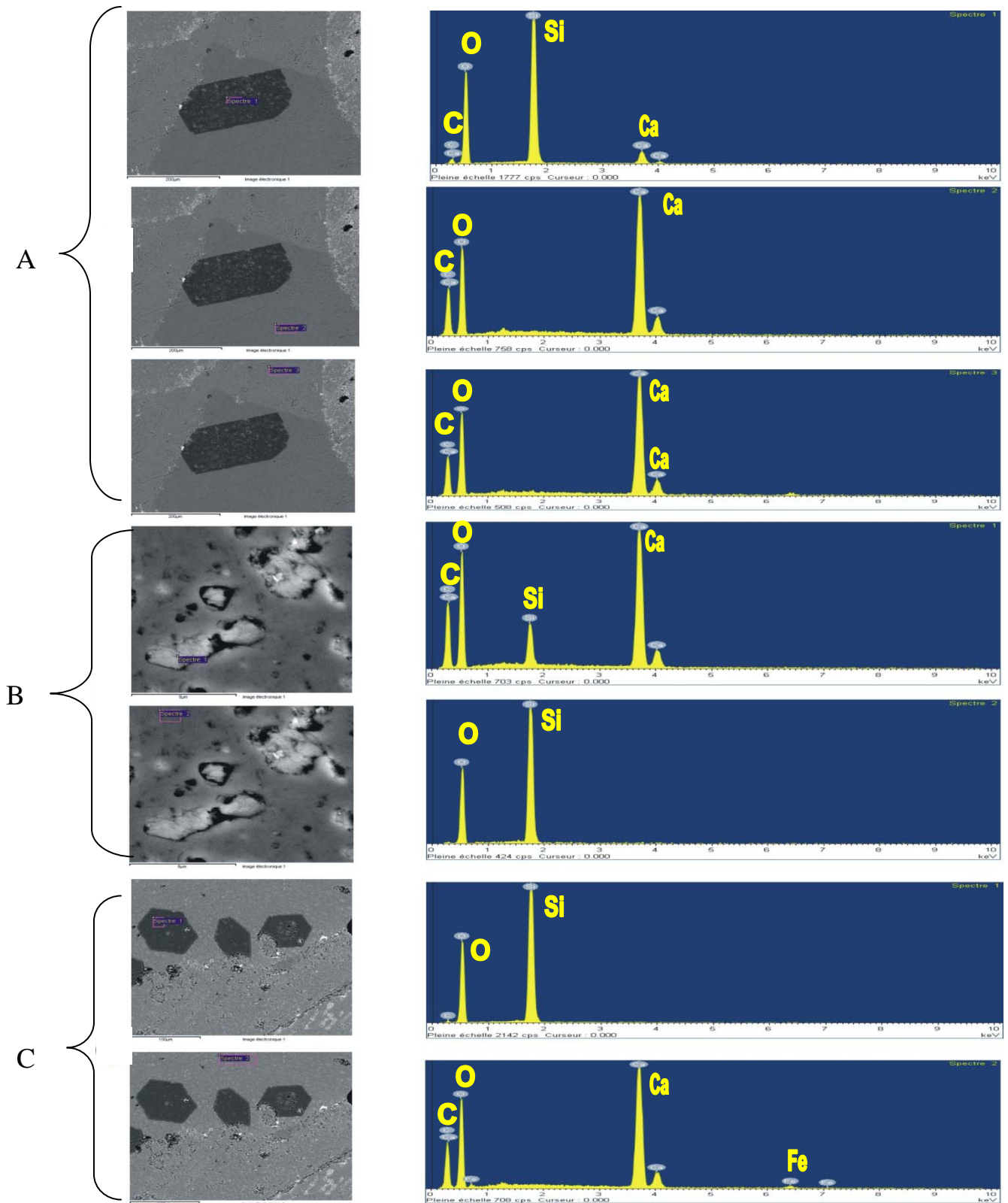


Figure (20): BSE images and EDS analysis of: A- Site 1 of sample BN9/2,  
, B- Site 2 of sample BN9/2 , C-Site 3 of sample BN9/2.

## Appendix 4

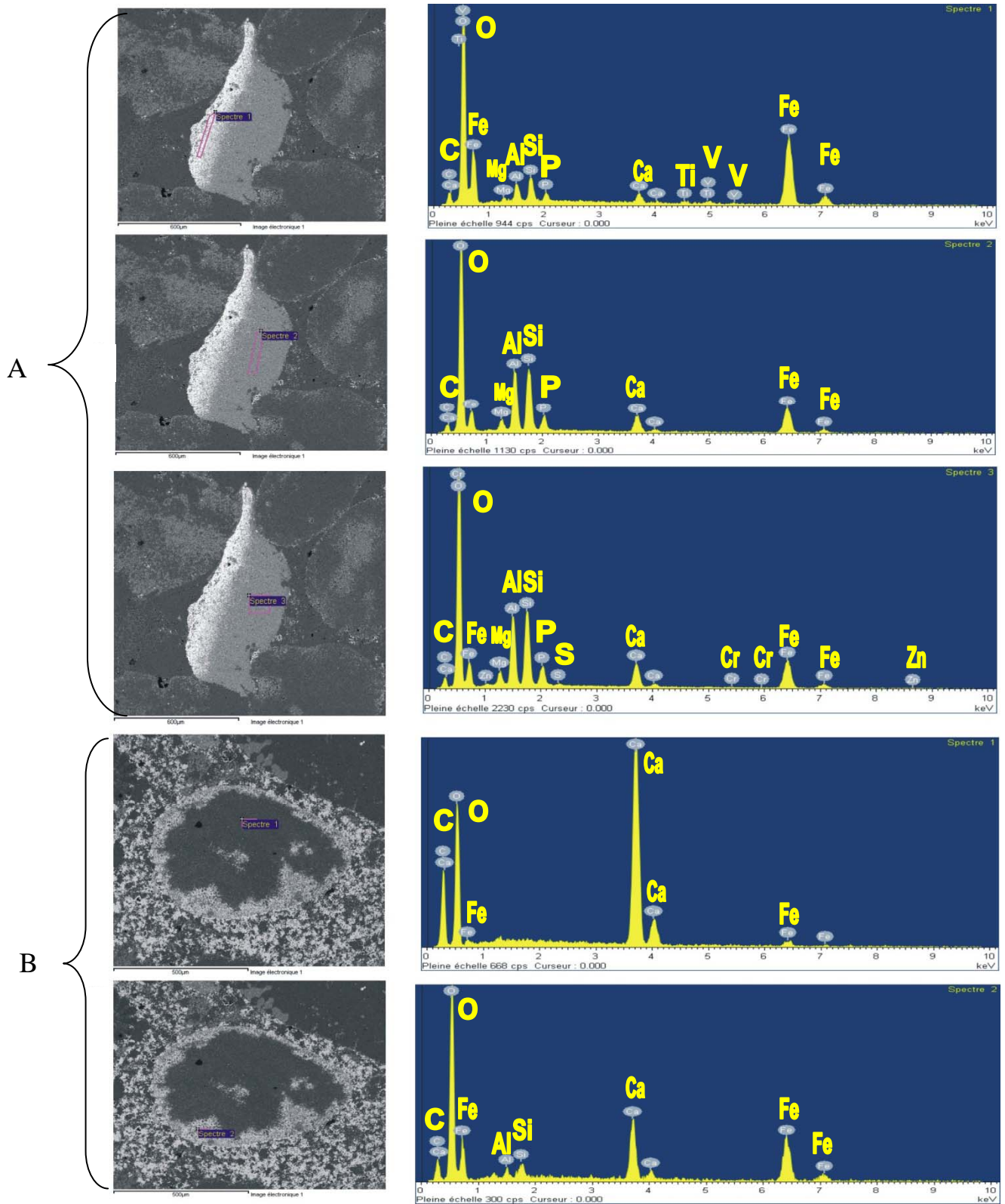


Figure (21): BSE images and EDS analysis of: A- Site 4 of sample BN9/2,  
B- Site 5 of sample BN9/2.

## Appendix 4

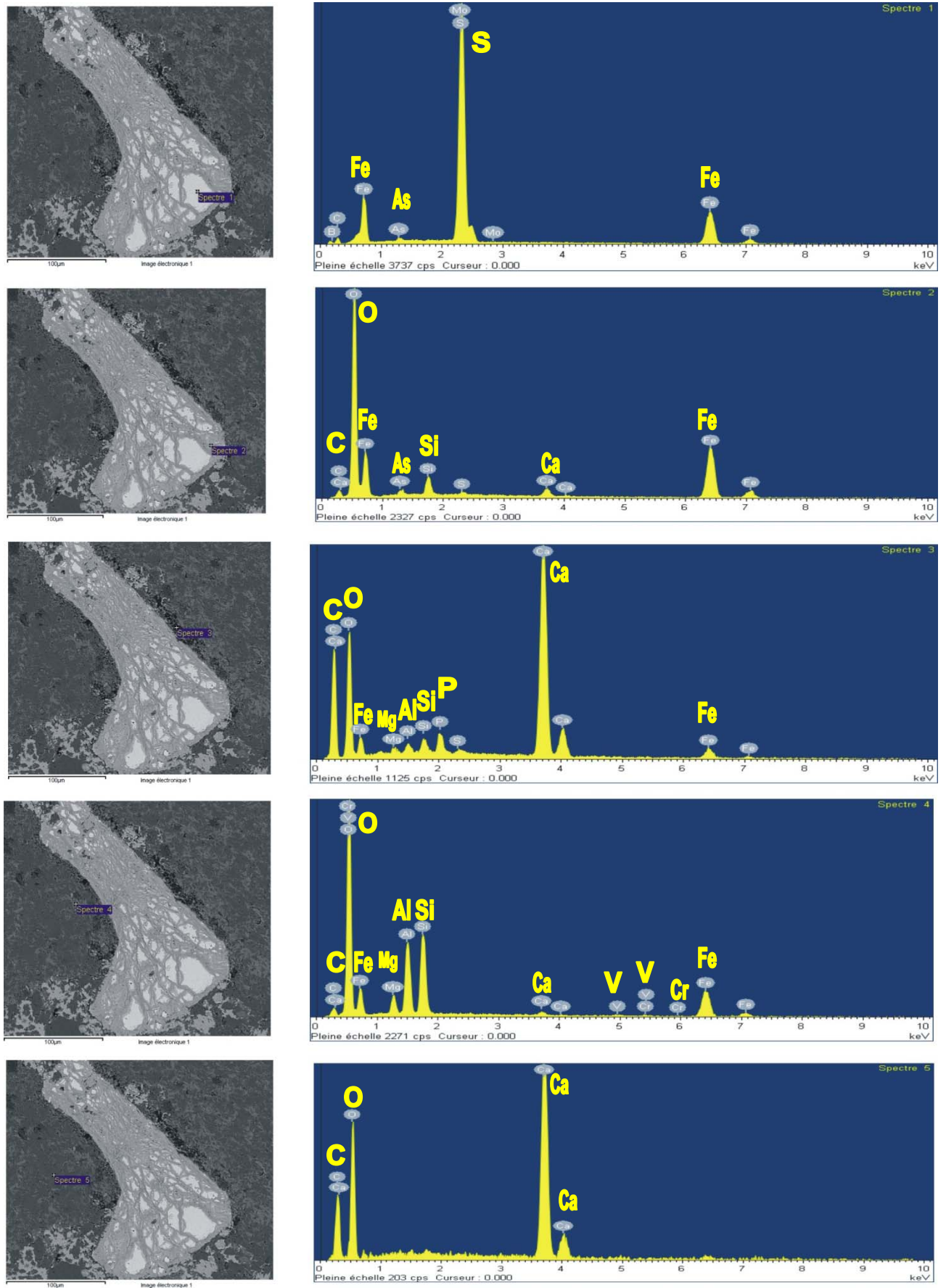


Figure (22): BSE images and EDS analysis of Site 1 of sample BN10/1.

## Appendix 5

	Sample	SiO2%	Fe %	Fe2O3%	FeO%	Al2O3%	TiO2%	CaO%	MgO%	L.O.I%	Na2O%	K2O%	P2O5%
1	BN1/1	1.05	2.20	3.28	2.01	0.53	0.18	51.83	0.98	41.76	0.10	0.01	0.21
2	BN1/4	4.02	10.30	14.65	10.57	1.94	0.19	42.33	2.30	33.30	0.14	0.02	0.99
3	BN1/5	3.30	17.43	24.90	16.65	1.56	0.15	35.92	2.35	29.12	0.12	0.01	0.88
4	BN1/6	2.84	17.00	23.90	5.38	1.60	0.15	37.51	1.10	30.14	0.16	0.03	1.13
5	BN1/7	4.24	17.00	24.00	1.00	1.53	0.13	36.96	0.67	29.11	0.12	0.02	1.37
6	BN2/4	2.76	10.00	14.00	1.43	1.29	0.10	43.68	0.72	35.48	0.11	0.03	1.01
7	BN2/5	7.40	16.00	22.80	2.36	3.78	0.28	33.60	1.20	28.45	0.13	0.06	1.16
8	BN2/6	3.48	13.00	17.90	1.00	0.99	0.15	41.21	0.64	33.70	0.12	0.11	1.23
9	BN2/7	3.82	18.06	25.80	4.16	1.63	0.15	36.14	0.83	28.73	0.12	0.07	1.15
10	BN2/8	3.60	15.20	21.70	0.93	1.16	0.11	39.54	0.71	31.18	0.12	0.10	1.33
11	BN3/2	4.50	9.00	12.25	1.93	2.03	0.19	42.00	2.20	35.40	0.22	0.17	0.40
12	BN3/4	4.08	20.10	28.70	1.65	1.60	0.14	34.92	0.50	26.16	0.26	0.07	1.60
13	BN4/1	3.98	18.13	25.90	1.07	1.56	0.13	36.68	0.48	28.55	0.12	0.07	1.31
14	BN5/1	2.27	3.00	4.06	2.36	0.83	0.06	50.38	0.92	40.16	0.10	0.04	0.50
15	BN5/2	5.02	10.00	13.60	1.93	1.82	0.16	40.93	2.45	35.00	0.21	0.17	0.64
16	BN5/3	3.74	15.30	21.80	3.01	1.44	0.18	37.52	1.34	30.72	0.11	0.03	1.61
17	BN5/4	2.68	17.10	24.40	5.52	1.35	0.13	37.87	0.98	29.83	0.11	0.02	1.07
18	BN6/3	6.02	20.00	27.80	1.43	2.93	0.23	32.48	0.66	28.26	0.15	0.21	0.96
19	BN6/4	2.00	12.11	18.20	0.93	0.94	0.06	42.56	0.44	34.01	0.11	0.03	0.53
20	BN6/5	3.48	23.40	33.90	1.20	1.75	0.13	33.04	0.36	26.02	0.14	0.08	0.93
21	BN7	2.32	14.00	19.60	1.34	1.13	0.09	42.00	0.59	32.08	0.13	0.06	1.23
22	BN8/2	2.80	4.40	6.22	4.33	1.04	0.06	48.05	1.50	39.22	0.12	0.02	0.57
23	BN8/4	5.92	14.10	20.10	0.92	1.89	0.19	37.52	0.65	29.64	0.12	0.04	2.08
24	BN8/5	3.38	22.00	31.20	1.13	1.69	0.13	34.16	0.52	26.96	0.20	0.08	1.63
25	BN9/1	3.90	10.00	13.85	11.00	1.46	0.13	40.66	2.35	36.69	0.10	0.02	0.47
26	BN9/3	2.92	21.00	29.80	1.91	1.65	0.11	35.00	0.55	26.62	0.12	0.03	1.25
27	BN10/1	7.36	14.10	20.10	2.84	4.13	0.30	34.26	1.06	29.81	0.19	0.09	0.84
28	BN10/3	2.96	20.00	28.00	0.71	1.60	0.11	37.52	0.47	27.86	0.11	0.05	0.97
	<b>Min.</b>	<b>1.05</b>	<b>2.20</b>	<b>3.28</b>	<b>0.71</b>	<b>0.53</b>	<b>0.06</b>	<b>32.48</b>	<b>0.36</b>	<b>26.02</b>	<b>0.10</b>	<b>0.01</b>	<b>0.21</b>
	<b>Max.</b>	<b>7.40</b>	<b>23.40</b>	<b>33.90</b>	<b>16.65</b>	<b>4.13</b>	<b>0.30</b>	<b>51.83</b>	<b>2.45</b>	<b>41.76</b>	<b>0.26</b>	<b>0.21</b>	<b>2.08</b>
	<b>Av.</b>	<b>3.78</b>	<b>14.43</b>	<b>20.44</b>	<b>3.24</b>	<b>1.67</b>	<b>0.15</b>	<b>39.15</b>	<b>1.05</b>	<b>31.57</b>	<b>0.14</b>	<b>0.06</b>	<b>1.04</b>

A- Bulk chemical analyses of major oxides (wt %) of Benavi IRS with Minimum (Min) Maximum (Max) and Average (Av.) values, (GEOSURV).

## Appendix 5

	Sample	S ppm	Mn ppm	Zn ppm	Co ppm	Ni ppm	Cr ppm	Mn/Fe
1	BN1/1	47.50	73.00	23.00	18.00	18.00	305.00	0.0032
2	BN1/4	1700.00	134.00	54.00	24.00	30.00	729.00	0.0013
3	BN1/5	107.60	131.00	46.00	26.00	30.00	1044.00	0.0008
4	BN1/6	44.30	145.00	41.00	24.00	28.00	1445.00	0.0009
5	BN1/7	20.60	135.00	31.00	22.00	21.00	570.00	0.0008
6	BN2/4	33.50	141.00	62.00	23.00	27.00	771.00	0.0014
7	BN2/5	131.80	184.00	75.00	24.00	33.00	1145.00	0.0012
8	BN2/6	79.00	154.00	44.00	24.00	25.00	455.00	0.0012
9	BN2/7	0.00	144.00	36.00	28.00	31.00	668.00	0.0008
10	BN2/8	0.00	152.00	34.00	24.00	27.00	577.00	0.0010
11	BN3/2	0.00	133.00	28.00	22.00	27.00	75.00	0.0016
12	BN3/4	0.00	154.00	37.00	24.00	25.00	627.00	0.0008
13	BN4/1	53.40	148.00	41.00	22.00	25.00	714.00	0.0008
14	BN5/1	95.90	100.00	17.00	21.00	24.00	99.00	0.0035
15	BN5/2	37.60	131.00	21.00	23.00	28.00	280.00	0.0014
16	BN5/3	23.30	215.00	41.00	28.00	33.00	578.00	0.0014
17	BN5/4	108.40	146.00	29.00	26.00	29.00	683.00	0.0009
18	BN6/3	57.10	194.00	56.00	37.00	34.00	775.00	0.0010
19	BN6/4	57.00	141.00	21.00	22.00	25.00	558.00	0.0011
20	BN6/5	160.20	180.00	28.00	25.00	25.00	1246.00	0.0008
21	BN7	103.70	118.00	25.00	22.00	23.00	599.00	0.0009
22	BN8/2	1200.00	38.00	36.00	22.00	22.00	92.00	0.0009
23	BN8/4	77.60	54.00	52.00	29.00	53.00	573.00	0.0004
24	BN8/5	22.40	43.00	40.00	25.00	30.00	809.00	0.0002
25	BN9/1	1500.00	65.00	61.00	24.00	25.00	3305.00	0.0007
26	BN9/3	67.00	36.00	32.00	27.00	27.00	799.00	0.0002
27	BN10/1	59.20	22.00	20.00	26.00	31.00	709.00	0.0002
28	BN10/3	208.30	159.00	41.00	28.00	28.00	755.00	0.0008
	<b>Min.</b>	<b>0.00</b>	<b>22.00</b>	<b>17.00</b>	<b>18.00</b>	<b>18.00</b>	<b>75.00</b>	<b>0.0002</b>
	<b>Max.</b>	<b>1700.00</b>	<b>215.00</b>	<b>75.00</b>	<b>37.00</b>	<b>53.00</b>	<b>3305.00</b>	<b>0.0035</b>
	<b>Av.</b>	<b>214.12</b>	<b>123.93</b>	<b>38.29</b>	<b>24.64</b>	<b>28.00</b>	<b>749.46</b>	<b>0.0011</b>

B- Bulk chemical analyses of some of trace elements in (ppm) and Mn /Fe ratios, of IRS with Minimum (Min), Maximum (Max) and Average (Av.) values, (GEOSURV).

	Fe %	FeO %	SiO2 %	Al2O3 %	CaO %	MgO %	P %	Na2O %	K2O %	TiO2 %	L.O.I %	S ppm	Mn ppm	V ppm	Mn/Fe
BN1/4	11.4	8.22	3.87	2.33	39.6	1.96	0.44	0.04	0.01	0.145	34.4	3300	170	700	0.001
BN2/4	10.9	0.74	2.63	1.5	42.35	0.63	0.48	0.03	0.015	0.08	35.8	400	170	770	0.002
BN2/5	17.3	1.54	7.58	4.06	31.2	1.04	0.68	0.04	0.06	0.24	29.1	400	250	1200	0.001
BN2/8	16.1	0.61	3.04	1.43	38.4	0.6	0.61	0.035	0.14	0.1	31.5	300	190	670	0.001
BN5/2	10.45	1.36	4.71	2.27	39.5	2.09	0.27	0.01	0.235	0.135	35.5	300	150	410	0.001
BN5/3	16.4	2.27	3.7	2.24	35.4	1.17	0.93	0.04	0.04	0.16	31.7	400	280	700	0.002
BN5/4	18.1	4.17	2.85	1.7	36.85	0.78	0.6	0.03	0.015	0.115	30.6	300	180	800	0.001
BN6/4	13.6	0.5	1.89	1.07	42.4	0.38	0.3	0.02	0.02	0.06	33.9	200	190	700	0.001
BN6/5	23.2	0.58	3.81	2.04	32.5	0.3	0.53	0.04	0.1	0.125	26.4	300	240	1250	0.001
BN10/1	15.3	2.08	8.02	4.37	32.7	0.8	0.48	0.17	0.12	0.28	30.4	600	200	810	0.001
BN10/3	21.3	0.67	3.3	1.72	34.4	0.42	0.56	0.03	0.06	0.11	27.9	200	200	1000	0.001
Min.	10.45	0.5	1.89	1.07	31.2	0.3	0.27	0.01	0.01	0.06	26.4	200	150	410	0.001
Max.	23.2	8.22	8.02	4.37	42.4	2.09	0.93	0.17	0.24	0.28	35.8	3300	280	1250	0.002
Av.	15.82	2.07	4.13	2.25	36.85	0.92	0.53	0.04	0.07	0.14	31.56	609.09	201.82	819.09	0.001

C- Bulk chemical analyses of major oxides (wt%) and trace elements ( ppm ) with Mn/Fe ratios of Benavi IRS, ( SNIM).

### Appendix 6

	SiO <sub>2</sub> %	Fe <sub>2</sub> O <sub>3</sub> %	Al <sub>2</sub> O <sub>3</sub> %	TiO <sub>2</sub> %	CaO%	MgO%	L.O.I%	Na <sub>2</sub> O%	K <sub>2</sub> O%	P <sub>2</sub> O <sub>5</sub> %
BN6/4	2.00	18.20	0.94	0.06	42.56	0.44	34.01	0.11	0.03	0.53
BN12	2.12	18.00	0.99	0.06	42.58	0.41	33.72	0.13	0.03	0.53
BN13	1.98	17.95	0.94	0.06	42.72	0.44	33.82	0.11	0.04	0.53
AV.	2.03	18.05	0.96	0.06	42.62	0.43	33.85	0.12	0.03	0.53
SD	0.06	0.08	0.02	0.00	0.07	0.01	0.11	0.01	0.00	0.02
<b>P 95%</b>	<b>6.08</b>	<b>0.83</b>	<b>3.48</b>	<b>0.00</b>	<b>0.31</b>	<b>6.09</b>	<b>0.66</b>	<b>14.96</b>	<b>26.19</b>	<b>8.74</b>
<b>P 63%</b>	<b>3.04</b>	<b>0.42</b>	<b>1.74</b>	<b>0.00</b>	<b>0.15</b>	<b>3.04</b>	<b>0.33</b>	<b>7.48</b>	<b>13.09</b>	<b>4.33</b>

	S ppm	Mn ppm	Zn ppm	Co ppm	Ni ppm	Cr ppm
BN6/4	57.00	141.00	21.00	22.00	25.00	558.00
BN12	61.00	151.00	25.00	23.00	24.00	480.00
BN13	60.30	155.00	28.00	24.00	25.00	532.00
AV.	59.43	149.00	24.67	23.00	24.67	523.33
SD	1.61	5.45	2.65	0.76	0.44	30.02
<b>P 95%</b>	<b>5.43</b>	<b>7.32</b>	<b>21.52</b>	<b>6.57</b>	<b>3.54</b>	<b>11.47</b>
<b>P 63%</b>	<b>2.72</b>	<b>3.66</b>	<b>10.76</b>	<b>3.29</b>	<b>1.77</b>	<b>5.74</b>

**A**

sample	SiO <sub>2</sub>	Al <sub>2</sub> O <sub>3</sub>	Fe <sub>2</sub> O <sub>3</sub>	CaO	MgO	K <sub>2</sub> O	MnO	L.O.I	TiO <sub>2</sub>	S
BSC □	0.70	0.12	0.045	55.4	0.15	0.02	0.010	43.4	0.009	0.007
BN11 Δ	0.77	0.19	0.03	55.16	0.15	0.02	0.01	43.13	0.01	0.01

**B**

A- Shows the precision (P) at confidence level of 95% (after Maxwell, 1968) and 63% (after Stanton, 1966 ).

B-Shows the Accuracy, compilation between geosurv analyses (Δ) and British Chemical Standard no. 393 (BSC) sample (□).

*Appendix 7*

---

	<i>SiO2</i>	<i>Fe</i>	<i>Fe2O3</i>	<i>FeO</i>	<i>Al2O3</i>	<i>TiO2</i>	<i>CaO</i>	<i>MgO</i>	<i>L.O.I</i>	<i>Na2O</i>	<i>K2O</i>	<i>P2O5</i>	<i>S</i>	<i>Mn</i>	<i>Zn</i>	<i>Co</i>	<i>Ni</i>	<i>Cr</i>
<b>SiO2</b>	<b>1.00</b>																	
<b>Fe</b>	0.25	<b>1.00</b>																
<b>Fe2O3</b>	0.24	<b>1.00</b>	<b>1.00</b>															
<b>FeO</b>	-0.06	-0.10	-0.10	<b>1.00</b>														
<b>Al2O3</b>	<b>0.90</b>	0.32	0.32	0.00	<b>1.00</b>													
<b>TiO2</b>	<b>0.80</b>	0.14	0.13	0.07	<b>0.84</b>	<b>1.00</b>												
<b>CaO</b>	<b>-0.58</b>	<b>-0.92</b>	<b>-0.92</b>	0.01	<b>-0.62</b>	<b>-0.44</b>	<b>1.00</b>											
<b>MgO</b>	0.16	<b>-0.44</b>	<b>-0.45</b>	<b>0.71</b>	0.11	0.23	0.23	<b>1.00</b>										
<b>L.O.I</b>	<b>-0.39</b>	<b>-0.97</b>	<b>-0.97</b>	0.10	<b>-0.44</b>	-0.26	<b>0.95</b>	<b>0.40</b>	<b>1.00</b>									
<b>Na2O</b>	<b>0.38</b>	0.22	0.21	-0.15	<b>0.38</b>	0.32	<b>-0.32</b>	0.15	-0.27	<b>1.00</b>								
<b>K2O</b>	<b>0.48</b>	0.16	0.14	<b>-0.38</b>	<b>0.39</b>	<b>0.35</b>	-0.28	0.04	-0.14	<b>0.55</b>	<b>1.00</b>							
<b>P2O5</b>	0.28	<b>0.62</b>	<b>0.62</b>	-0.24	0.13	0.11	<b>-0.58</b>	<b>-0.45</b>	<b>-0.69</b>	0.11	-0.06	<b>1.00</b>						
<b>S</b>	-0.03	<b>-0.35</b>	<b>-0.35</b>	<b>0.55</b>	-0.05	-0.08	0.28	<b>0.53</b>	<b>0.34</b>	-0.18	<b>-0.31</b>	-0.29	<b>1.00</b>					
<b>Mn</b>	0.05	<b>0.31</b>	<b>0.31</b>	-0.09	0.01	0.08	-0.27	-0.09	-0.28	-0.04	0.26	0.14	-0.26	<b>1.00</b>				
<b>Zn</b>	<b>0.39</b>	0.18	0.17	0.29	<b>0.32</b>	<b>0.33</b>	<b>-0.30</b>	0.15	-0.20	-0.17	-0.07	<b>0.30</b>	<b>0.33</b>	0.24	<b>1.00</b>			
<b>Co</b>	<b>0.46</b>	<b>0.58</b>	<b>0.56</b>	0.03	<b>0.45</b>	<b>0.36</b>	<b>-0.65</b>	-0.14	<b>-0.57</b>	0.03	<b>0.37</b>	<b>0.39</b>	-0.10	0.24	<b>0.37</b>	<b>1.00</b>		
<b>Ni</b>	<b>0.58</b>	0.27	0.27	0.03	<b>0.44</b>	<b>0.45</b>	<b>-0.44</b>	0.01	<b>-0.38</b>	0.05	0.13	<b>0.56</b>	-0.10	-0.01	<b>0.41</b>	<b>0.63</b>	<b>1.00</b>	
<b>Cr</b>	0.11	0.24	0.24	<b>0.47</b>	0.15	0.09	<b>-0.32</b>	0.22	-0.17	-0.17	-0.23	-0.03	<b>0.42</b>	-0.04	<b>0.50</b>	0.15	0.04	<b>1.00</b>

(r = 0.38)

Correlation coefficients of major and trace elements of Benavi IRS.

**Appendix 8**

	<b>A</b>	<b>B</b>	<b>C</b>	<b>D</b>	<b>E</b>	<b>F</b>	<b>G</b>	<b>H</b>	<b>I</b>	<b>J</b>	<b>K</b>	<b>L</b>	<b>M</b>	<b>N</b>	<b>O</b>	<b>P</b>	<b>IRS</b>
<b>SiO<sub>2</sub> %</b>	46.8	15.6	55.2	24.7	25	21.8	27.5	71.5	48.5	50.6	50.5	16.4	3-13	11.0	9-11	4.2-20	3.78
<b>Fe<sub>2</sub>O<sub>3</sub> %</b>	50.8	41.37	35.95	37.8	41.61	22.7	42.5	15.0	18.9	30.6	39.01	17.7Fe	24.4Fe	18.23Fe	13-15	18-41Fe	20.44
<b>Al<sub>2</sub>O<sub>3</sub> %</b>	0.25	8.75	1.59	18.2	4.6	10.7	7.1	4.85	14.2	5.52	1.855	-	-	3-4	1.5-2	3.5-11	1.67
<b>CaO %</b>	0.8	2.40	1.3	-	4.85	12.2	3.20	2.3	2.07	3.188	1.463	15.5	30-50	30.6	33-36	1.3-36	39.15
<b>MgO %</b>	0.02	2.91	0.1	-	2.1	3.6	0.16	0.4	1.7	0.087	0.096	-	-	-	-	-	1.05
<b>TiO<sub>2</sub> %</b>	0.05	0.75	0.3	1.5	-	0.53	0.43	0.33	-	0.251	0.3	-	-	-	0.1 Ti	-	0.15
<b>Na<sub>2</sub>O %</b>	0.05	0.20	0.02	-	-	0.08	0.01	0.5	0.7	0.035	0.02	-	-	-	-	-	0.14
<b>K<sub>2</sub>O %</b>	-	0.07	0.06	0.07	-	0.09	0.02	0.07	0.549	0.05	0.065	-	-	-	-	-	0.06
<b>P<sub>2</sub>O<sub>5</sub> %</b>	0.12	1.02	0.41	-	1.88	-	0.45	0.1	-	0.46	0.432	-	-	0.28 P	0.19 P	0.28 P	1.04
<b>SO<sub>3</sub> %</b>	0.17	-	1.27	-	-	-	6.6	-	-	<0.07	0.123	-	-	-	-	-	-
<b>L.O.I %</b>	0.35	19.9	4.25	-	7.7	-	11.63	5	11	8.11	5.06	-	-	-	-	-	31.57
<b>S ppm</b>	-	-	-	-	0.07	-	-	-	-	-	-	-	-	-	0.14	0.11-0.2	214.12
<b>Mn ppm</b>	-	-	49	98	-	1600	47	-	131	187	55	-	-	1600	0.11	7000-1200	123.9
<b>Pb ppm</b>	-	17	7	66	-	-	22	-	15	13	8	-	-	-	-	-	<50
<b>Cr ppm</b>	-	440	356	-	-	240	265	-	310	193	336	-	-	-	-	-	749.46
<b>Cu ppm</b>	-	51	17	54	-	-	23	-	728	32	17	-	-	-	-	-	5.42
<b>Co ppm</b>	-	43	15	22	-	200	84	-	182	17	25	-	-	-	-	-	22.64
<b>Ni ppm</b>	-	208	46	77	-	200	150	-	143	96	56	-	-	-	-	-	28
<b>V ppm</b>	-	745	290	-	-	500	850	28	434	489	355	-	-	-	0.33	-	800
<b>Zn ppm</b>	-	201	19	-	-	-	16	7.3	22	29	19.1	-	-	-	-	-	38.29

**A:**Siliceous and calcareous red iron ores /Germany/ James,1966. **B:**Thuringia ironstones /Germany /Mucke ,et al 2005. **C:** Sandy ironstones / Gaara /Iraq/Tobia,1983. **D:**Oolitic and pisolitic ores /Hussainiyat/Iraq/Yakta,1981. **E:**Oolitic limonitic(goethitic)ironstones/minette ores /Verte / Lorrain/James , 1966 . **F:**Chamositic ironstones /Gottingen/Germany/ James ,1966. **G:**Oolitic and pisolitic ironstones/Gaara/Iraq/Tobia,1983. **H:**Iron rich beds/Abha Khamis area/Saudi Arabia/Babalola,etal ,2003. **I:**Hussainiyat ironstones/Iraq/Jawad,1980. **J:** Hussainiyat ironstones /Iraq/Tobia,1983. **K:**Total average of Gaara ironstones/Iraq /Tobia,1983. **L:**Dolnilom ironstones/marine sedimentary/Bulgaria/Zitzmann,1978. **M:**Thost\A-Beauregard ironstones/marine sedimentary/France/Zitzmann,1978. **N:**Kahlenberg ironstones/Germany/ Zitzmann ,1978. **O:**Nammen ironstones/marine sedimentary/Germany/Zitzmann,1978. **P:**Camdag ironstones /Turkey/ Zitzmann,1978. **IRS:**Benavi ironstone(present study).

## Appendix 9

variables	Factors				
	1	2	3	4	5
SiO2%	.757	.372	-.399	.171	-.036
Fe2O3%	.774	-.307	-.403	-.335	-.114
FeO%	-.139	.750	-.327	-.264	-.063
Al2O3%	.740	.369	.376	.026	-.114
TiO2%	.622	.424	.435	.127	.023
CaO%	-.926	.038	.200	.264	.119
MgO%	-.219	.797	.258	-.215	.053
L.O.I%	-.850	.252	.320	.232	.164
Na2O%	.367	-.058	.581	-.404	-.327
K2O%	.423	-.123	.674	-.205	.300
P2O5%	.633	-.312	-.376	.311	-.164
S ppm	-.316	.724	-.220	-.022	-.087
Mn ppm	.286	-.180	-.108	-.297	.815
Zn ppm	.401	.534	-.373	.219	.325
Co ppm	.742	.085	-.147	.127	.225
Ni ppm	.641	.206	-.046	.581	-.016
Cr ppm	.161	.553	-.512	-.300	-.077

Extraction Method: Principal Component Analysis.  
5 components extracted.

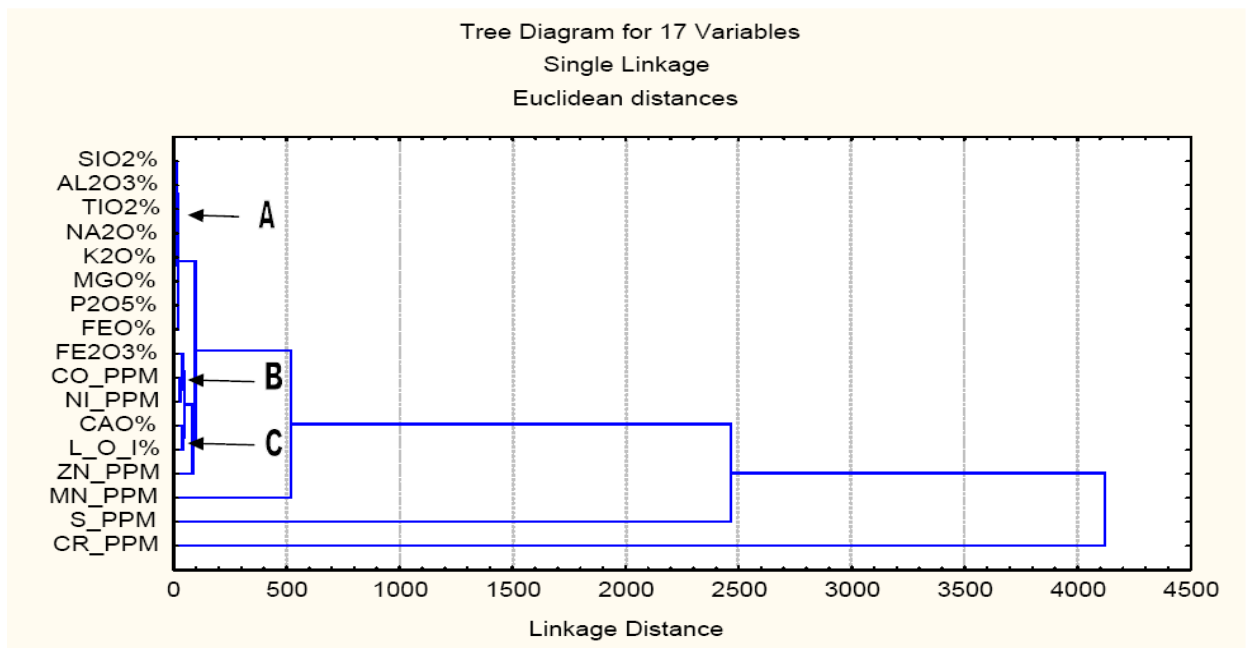
A

### Total Variance Explained

Component	Initial Eigenvalues			Extraction Sums of Squared Loadings		
	Total	% of Variance	Cumulative %	Total	% of Variance	Cumulative %
1	5.798	34.106	34.106	5.798	34.106	34.106
2	3.125	18.383	52.489	3.125	18.383	52.489
3	2.386	14.033	66.521	2.386	14.033	66.521
4	1.280	7.527	74.049	1.280	7.527	74.049
5	1.133	6.665	80.714	1.133	6.665	80.714
6	.805	4.737	85.451			
7	.677	3.983	89.434			
8	.645	3.795	93.229			
9	.387	2.278	95.507			
10	.236	1.386	96.893			
11	.184	1.083	97.976			
12	.154	.903	98.880			
13	.089	.525	99.405			
14	.068	.397	99.802			
15	.026	.152	99.954			
16	.007	.040	99.994			
17	.001	.006	100.000			

Extraction Method: Principal Component Analysis.

B



A: Factor analyses results based on chemical analyses of (28) samples of Benavi IRS by using SPSS-12 program.

B: A: Shows R-Mode cluster analysis of Benavi IRS samples.



وزارة التعليم العالي و البحث العلمي  
جامعة بغداد  
كلية العلوم

# معدنية و بتروغرافية و جيوكيميائية الترسبات الغنية بالحديد في منطقة بنافي / شمال العراق

رسالة مقدمة الى  
كلية العلوم - جامعة بغداد

وهي جزء من متطلبات نيل درجة الماجستير في علوم الارض

تقدم بها  
**علي طه ياسين**  
بكالوريوس علوم 1995

بإشراف

أ.م.د. مظفر محمد محمود



(27&28)

تضمن البحث دراسة النواحي المعدنية و الصخرية و الجيوكيميائية للصخور الحديدية المنكشفة قرب قرية بناقي الواقعة على بعد (20) كم شمال مدينة العمادية في محافظة دهوك – شمال العراق ، ان السمك الحقيقي للمكشف السطحي لهذه الصخور يتراوح ما بين ( 2.5 ) الى ( 12.8 ) متراً ويمتد حوالي (2) كم طولاً باتجاه شرق – غرب ، و يتواجد ما بين التتابعات الجوراسية- الكريتاسية ضمن طبقات شديدة التكرس بفعل الحركات التكتونية الناتجة من الفالق الشمالي الزاحف.

تم جمع (48) نموذجاً موزعة على عشرة مقاطع تغطي امتداد هذا المكشف مع الصخور المحيطة به سفلياً و علوياً حيث كانت النمذجة نظامية حسب التغير باللون والصلابة والنسيج والمحتوى الحديدي .

لقد بينت الدراسة المعدنية باستخدام التقنيات ( FTIR ، TGA ، EDS ، SEM ، XRD ) بأن هذا الترسيب يتكون عموماً من المعادن الكربوناته (الكالسايت ، السدرايت ، الانكرايت) وأكاسيد وهيدروكسيدات الحديد (هيماتيت ، كوثايت ، لايمونايت ، مكنتايت ) وكبريتيدات الحديد (بايرايت ، ارسينوبايرايت ) والمعادن السيلكاتية (كاؤلينايت ، جاموسايت ، كلوكونايت ، كوارتز) و الأبتايت .

ان الكالسايت هو المعدن السائد في هذه الصخور وعادةً ما يكون شائب حيث يحتوي على المغنيسيوم و الحديد في بنيته البلورية. الهيماتيت و الكوثايت هما المعدنان الرئيسيان الحاملان للحديد اللذان يتواجدان بنسبٍ عالية نسبياً بالمقارنة مع المعادن الحديدية الاخرى المتواجدة في هذا الترسيب ، كما وبينت هذه الدراسة بأن اغلب الهيماتيت هو من نوع الفقير بالالمنيوم والذي قد يكون ناتج من تحول الكوثايت الاولي الفقير بالالمنيوم . كما يبدو ايضاً أن هناك نوعين من الكوثايت تختلف بمحتوى الالمنيوم ودرجة التبلور، حيث أن الكوثايت الغني بالالمنيوم هو ثانوي و ناتج من عمليات الاكسدة للبايرايت والسدرايت والجاموسايت التي حصلت تحت ظروف التجوية بعد عمليات الرفع التكتونية وبروز هذا الترسيب وانكشافه. ان الدراسة المعدنية بينت بان الكاؤلينات و الجاموسايت هي المعادن الطينية الرئيسية المنتشرة بهذا الترسيب ، اما الكلوكونايت فإنه نادر التواجد.

ان لهذه الدراسة السبق باكتشاف معدن الأرسينوبايرايت ولأول مرة في هذا الجزء من العراق ، حيث تم تمييزه بما لا يقبل الشك باستخدام تقنية EDS حيث يرتبط تواجده بالنطاق السفلي لهذا المكشف مترافقاً مع معادن الفوسفات والبايرايت والجاموسايت والكلوكونايت .

بينت الدراسة الصخرية لهذه النماذج بان الحديد مرتبط بسحنة الحجر الجيري المرصوص الغني بالطحالب الحمراء والفتات الحياتي والتي تعرضت للعديد من العمليات التحويرية ، كان ابرزها عمليات الاحلال المعدني الجزئي و الكلي وخصوصاً احلال المعادن الحديدية بدل المكونات الكلسية المذابة نتيجة المحاليل الحامضية الغنية بالحديد. وتتميز هذه السحنة الصخرية بشيوع ظواهر الفسفة والتشكل الجديد

وانتشار سطوح الاذابة ، با لاضافة الى شيوع بلورات الكوارتز الكاملة الاوجه الدالة على نشوءها الموضوعي ، كما بينت الدراسة الصخرية محدودية عملية الدلمتة بهذه الصخور.

ولقد أظهرت الدراسة البتروغرافية ايضاً انتشاراً واسعاً لمعدن الجاموسايت إذ يتواجد بشكل شائع جداً حول الحبيبات الهيكلية المشبعة بأكاسيد الحديد مما يعطي دلالة على تكون هذا المعدن بعد عمليات الأكسدة وتحت ظروف إختزالية في المراحل المبكرة من التاريخ التحويري لهذا الترسيب.

دراسة المجهر العاكس للضوء والمجهر الالكتروني الماسح بينت بان هذه الصخور مؤلفة من الفئات الحياتي والتي تختلف بمحتواها الحديدي ومُحاطة بمعادن اللايمونايت والكوثايت والهيمايت ، أما الفراغات البينية فتكون مملوءة بهذه المعادن بالاضافة الى الكالساييت. ان معدن الباييرايت يتواجد بأشكال متعددة كبلورات كاملة الأوجه او كتجمعات عنقودية واحياناً بهيئات كتليه ، كما اوضحت هذه الدراسة ان البلورات الكاملة الاوجه لمعدن الباييرايت ناتجة من التطور الحاصل على الانسجة العنقودية لهذا المعدن حيث ان المراحل الاساسية لهذا التطور تم تمييزها بصور المجهر الالكتروني الماسح.

اوضحت هذه الدراسة بأن اغلب انسجة الخامات في هذا الترسيب ناتجة من عمليات الاحلال والتي تشمل النسيج الحافي و النطاقي و المتضمن والعروقي و الايدومورفك ، وكذلك يتواجد النسيج المسامي بشكل شائع جداً وهو ناتج من عملية فقدان جزيئات الماء من معدن الكوثايت عند تحوله الى الهيمايت. كما لوحظ ايضاً النسيج السري ولكن بنطاق ضيق جداً. اما أنسجة العناقيد الكاذبة للكوثايت والمكتنايت فهي شائعة الوجود وناتجة من أكسدة أنسجة الباييرايت العنقودية. وأظهرت هذه الدراسة ايضاً شيوع بلورات المكتنايت الكاملة الأوجه في هذه الصخور.

تم في الدراسة الجيوكيميائية قياس تراكيز اكاسيد العناصر الاساسية (MgO, CaO),  $(S, Mn, Zn, Co, Ni, Cr)$  والاثرية  $(FeO, SiO_2, Al_2O_3, K_2O, Na_2O, P_2O_5, TiO_2, Fe_2O_3)$ , بالاضافة الى تحاليل EDS الكيمائية للعناصر الرئيسية والاثرية لمساحات نقطية مختارة بعناية لمعرفة التصرف الجيوكيميائي لتلك العناصر في هذا الترسيب حيث تمت الاستفادة من هذه الطريقة في قياس تراكيز الارسنك في المعادن المكونة لهذه الصخور كمحاولة للتعرف على أصل تشكل معدن الارسينوبايرايت .

ان محتوى الحديد يبين ان هذه الترسبات الحديدية واطئة الجودة. كما وتتميز هذه الترسبات بتراكيز عالية للعناصر  $(CaO, P_2O_5, MgO, Cr, V)$  مقارنةً بالصخور الحديدية للكعرة و الحسينيات ومعظم الصخور الحديدية العالمية ، اما أكاسيد الصوديوم والبوتاسيوم فهي ضمن المديات الطبيعية لتلك الصخور ، وتركيز الكوبلت مقارب الى تركيزه في صخور الكعرة والحسينيات واقل من الصخور الحديدية العالمية .

أثبتت هذه الدراسة وجود علاقة سالبة قوية ما بين اوكسيدي الكالسيوم و الحديد والتي تعزى الى إحلال المعادن الحديدية محل المكونات الكلسية ، لذا فإن هذه الصخور هي من الخامات المُتكونة بعد

الترسب والمُسمّاة ابيجنتيكُ اورز (epigenetic ores) حيثُ تكونت نتيجة الى عمليات الإحلال التحويرية للصخور الكربونائيه وهذا ما تؤيده ايضاً العلاقات السالبة لاوكسيد الكالسيوم مع (  $SiO_2, Al_2O_3, P_2O_5, Co, Ni, Zn$  ) والتي تعكس شدة التأثيرات التحويرية على هذه الصخور.

كما أظهرتُ الإستقصاءات الجيوكيميائية الادلة التي تبين و تؤكد الأصل الرسوبي لهذا الخام ، كتواجد البيرايت الغني بالأرسنيك ، قلة مُحتوى الرصاص و الزنك و النحاس ، المُحتوى العالي نسبياً للفوسفيت و المحتوى المميز للكروم. بالاضافة الى مُخطط التغيرات ما بين الالمنيوم والتيتانيوم. ناهيكَ عن نتائج التحليل العاملي في هذه الدراسة. والأكثر من ذلك كله فإن شكل التغيرات ما بين السليكا والالمنيوم يوضح جلياً الأصل الرسوبي التحويري لصخور بنافي الحديدية .

ان كلاً من المُخطط الجيوكيميائي المعتمد على [  $(FeO+MnO) - Fe_2O_3 - SiO_2$  ] و مجموع مُعدّل العناصر الاثرية (  $Zn+Pb+Cu+Ni+Co$  ) إضافةً الى المحتوى العالي للكروم تسمح بتصنيف صخور هذا الترسب ضمن مجموعة الصخور الحديدية الفينيروزوية تمييزاً لها عن الصخور الحديدية المُتكونة في عصور ما قبل الكامبري.